ANALYSIS OF THE PRENYLATED PROTEOME IN LIVING SYSTEMS: CONNECTING DOTS BETWEEN DISEASES AND THERAPEUTICS

A THESIS
SUBMITTED TO THE FACULTY OF
UNIVERSITY OF MINNESOTA
BY

CHARUTA CHANDRAKANT PALSULEDESAI

IN PARTIAL FULFILLMENT OF THE REQUIREMENTS
FOR THE DEGREE OF
DOCTOR OF PHILOSOPHY

ADVISER: PROF. MARK D. DISTEFANO

AUGUST 2015

Acknowledgements

I would like to take this opportunity to express my gratitude to all those who have been instrumental in the completion of my doctoral degree.

I would first like to thank my adviser Dr. Mark D. Distefano for his guidance throughout my graduate research career. I feel inspired by his scientific curiosity, enthusiasm and energy. He has provided me with honest feedback to make me a better scientist and I owe a great debt to him for helping me overcome some of my weaknesses. I appreciate that he gave me freedom to work at my own pace and learn from my mistakes. During individual meetings and group meetings, he shared with us how the academic research world works, politics behind it and given several pieces of advice. I have found his suggestions useful from time-to-time and I am sure they will be help me in the rest of my scientific career.

I am grateful for having wonderful colleagues in the Distefano lab who maintained a very friendly, helping and supportive environment in the lab and office. It would have been difficult to get through the graduate school without the jolly conversations and scientific discussions we have had in office and group meetings. I am thankful to Amanda DeGraw, Dan Mullen, Joshua Ochocki and Jon Dozier for training me on the experimental techniques needed in various aspects of my research projects. Several of these Distefano group members

have become dear friends of mine, in a life outside of the lab. I have had great times hanging out with them.

I would like to thank my college teacher, Dr. Lakshmy Ravishankar, who instilled in me the passion for chemistry. She is the reason I chose to become a chemist and her encouragement is what helped me get into good educational institutions for my graduate studies. Over the last decade she has been a constant source of support and encouragement. I would also like to thank Prof. Bhisma K. Patel (IIT Guwahati, India), for his mentorship during my MS thesis project. He showed a lot of faith in me and guided me through a tough and interesting research project. I would like to thank other teachers in the Departments of Chemistry at the Vaze College (Mumbai, India) and IIT Guwahati, and Dr. Siva Murru for the training they all provided me.

I would like to thank my Mom and Dad, for having confidence in me and for supporting me to pursue the education of my choice. I would also like to thank my sister, brother-in-law, and my parents-in-law for their encouragement. I feel blessed to have gotten an unconditional love and support from my husband, Rohan, who is also my best friend. Even while being so away from him and the rest of my family and friends, he never let me feel lonely. Without his assuring presence in my life, I would not have been able to complete my masters and doctoral degrees.

Finally I owe heartfelt thanks to all my friends in Minneapolis. They made my time here memorable and a lot of fun. The time I had hanging out with them helped me forget all the stress of grad school life and provided me with energy to get all the work done in the lab. I particularly would like to mention my friends: Chandru Ramasubramanian, Naveen Rondla, Jon Dozier, Veronica Diaz-Rodriguez, Ravindra Khedkar, Ameya Kirtane, Maya Raghunandan, Satyajeet Jadhav, Sanika Joshi, Gargee Lad, Shreyas Bhaban and Kanchan Kulkarni. Some of the things I will always cherish include: Energizing bike rides with Ravindra; de-stressing comfort food with Maya; coffee breaks with Chandru and Veronica; countless number of dinners with Ameya, Ravindra, Satya, Sanika and Gargee; and enthusiasm and willingness of them all to be guinea pigs for my baking experiments.

Dedication

This thesis is dedicated to my parents and my husband…

Abstract

Protein prenylation is a ubiquitous post-translational modification, involving attachment of an isoprenoid near the C-terminus of certain proteins. It plays a critical role in mediating membrane localization and protein-protein interactions. Inhibition of prenylation has been extensively studied for developing therapeutics against several types of cancers, and more recently against neurodegenerative disorders and parasitic diseases. However, their limited success in clinical trials indicates that much still remains unknown regarding the enzymology of protein prenylation. In this dissertation, our efforts to develop methods for quantification and identification of the prenylated proteome are described. We first demonstrate that the alkyne-functionalized isoprenoids metabolically label prenylated proteins, and allow for subsequent derivatization via “click” reaction. Next, we coupled metabolic labeling and differential gel electrophoresis to detect and identify proteins showing altered levels of prenylation in response to prenylation inhibitor. Additionally, we utilized metabolic labeling and the “click” reaction on intact cells to enable imaging and flow cytometry-based quantification of the prenylated proteome. Finally, we developed methods for profiling of prenylated proteome and detection of site of prenylation via mass spectrometry. Our results indicate that these methods should be applicable for elucidating the connection of protein prenylation and its inhibition with the neurodegenerative diseases and cancers.

Table of Contents

List of Tables..... xiii

List of Figures..... xv

Chapter 1 Protein prenylation.....1

1.1. Protein prenylation.....1

1.2. Mechanism of protein prenylation.....5

1.3. Peptide substrate specificity.....10

1.4. Isoprenoid analogs.....12

1.5. Analysis of the prenylated proteome.....17

1.6. Inhibition and therapeutic applications.....22

1.7. Biotechnological applications.....26

1.8. Current status of research on protein prenylation.....29

Chapter 2 Alkyne-modified analogs as chemical reporters of protein prenylation 31

2.1. Introduction.....31

2.2. Research objectives.....35

2.3. Results and discussion.....35

2.3.1. Evaluation of C10Alk and C15Alk for metabolic labeling of prenylated proteins.....35

2.3.2. Incorporation of C10Alk and C15Alk into prenylated proteins in the absence of an inhibitor of isoprenoid biosynthesis 38
2.3.3. Identification of prenylated proteins from HeLa cells via 2D electrophoresis and tandem mass spectrometry 40
2.4. Conclusions 43
2.5. Methods 43
2.5.1. Cell treatments and lysis 45
2.5.2. In-gel fluorescence analysis 45
2.5.3. Two-dimensional gel electrophoresis 46
2.5.4. MS analysis of protein spots 47
2.5.5. Database searching and protein identification 47
2.6. Acknowledgements 48
Chapter 3 Identification of prenylated protein in response to a farnesyltransferase inhibitor using differential gel electrophoresis 49
3.1. Introduction 49
3.2. Results 55
3.2.1. Overview of combining metabolic labeling with 2D-DIGE 55
3.2.2. 2D-DIGE visualizes effects of FTI treatment on C15Alk-labeled prenylome 57

3.2.3. Triton X-114 fractionation of prenylated and non-prenylated proteins prior to DIGE....64
3.2.4. GNAI-1 and GNAI-2 are potential novel prenylated proteins....67
3.3. Discussion....77
3.4. Conclusion....80
3.5. Methods....81
Chemicals and reagents....81
3.5.1. Cell culture and metabolic labeling....82
3.5.2. Triton X-114 fractionation....82
3.5.3. Click reactions....83
3.5.4. 2D gel electrophoresis....84
3.5.5. DeCyder analysis....85
3.5.6. Spot excision and in-gel tryptic digestion....85
3.5.7. MS analysis of protein spots and database search....85
3.5.8. Synthesis of 5-FAM-DVIIKNNLKDCGLF (2) and Ds-GCGLF (4)....86
3.5.9. Enzymatic farnesylation of peptide 2....89
3.5.10. Continuous fluorescence assay....89
3.6. Acknowledgements....90
Chapter 4 Imaging and quantification of the prenylated proteome....92
4.1. Introduction....92

4.2. Research objectives 99
4.3. Results and discussion 99
4.3.1. Characterization of C15Alk substrate 99
4.3.2. Cellular labeling and visualization of prenylated proteins 104
4.3.3. Quantitative analysis of prenylated protein levels using flow cytometry of whole cells 107
4.3.4. Optimizing conditions for metabolic labeling 111
4.3.5. Extension of flow cytometry method to other cell types 126
4.3.6. Effects of prenylation inhibitors on the extent of labeling 130
4.3.7. Measurement of prenylation levels in a cellular model of compromised autophagy 133
4.4. Conclusions 134
4.5. Methods 136
Materials 136
4.5.1. General cell culture 137
4.5.2. Imaging Prenylated Proteins 137
4.5.3. Quantifying the Prenylome 138
4.5.4. In-gel fluorescence 140
4.5.5. In-gel fluorescence densitometry 141
4.5.6. Primary Astrocyte Preparation 141

4.5.7. Kinetic Constant Measurement 143
4.5.8. Western Blot Analysis 144
4.5.9. TAMRA-PEG-N_3 synthesis 145
4.5.10. Farnesyl alkyne synthesis 145
4.6. Acknowledgements 146
Chapter 5 Comparative study of alkyne-modified isoprenoids as chemical reporters of protein prenylation 147
5.1. Introduction 147
5.2. Research objective 150
5.3. Results and discussion 151
5.3.1. In-gel fluorescence analysis of labeling caused by various alkyne-modified isoprenoid analogs 151
5.3.2. Proteomic profiling of COS-7 cells labeled with C15Alk-OPP and 7hp-FPP 159
5.4. Summary 165
5.5. Future direction 166
5.6. Methods 167
5.6.1. Synthesis of biotin-PC-N_3 168
5.6.2. Monitoring photocleavage of biotin-PC-N_3 by HPLC 169
5.6.3. In-gel fluorescence analysis 169

5.6.4. Enrichment of prenylated proteins 170
5.6.5. MS/MS analysis of tryptic peptides 172
5.7. Acknowledgements 181
Chapter 6 Aldehyde-modified isoprenoid analogs as chemical reporters of protein prenylation 182
6.1. Introduction 182
6.2. Research objectives 186
6.3. Results and discussion 186
6.3.1. In-gel fluorescence analysis 186
6.3.2. Identification of HeLa cell proteins labeled by FAPP 191
6.3.3. Identification of prenylated proteins from mouse brain tissue 194
6.3.4. Catch-and-release strategy: Proof-of-concept experiments 197
6.3.5. Catch-and-release of FAPP-bound proteins in HeLa cells 202
6.4. Summary 205
6.5. Future direction 205
6.6. Methods 207
6.6.1. Synthesis of aminooxy-modified agarose resin 207
6.6.2. Synthesis of SSPRTQSPQNCSIM (III) 208
6.6.3. Prenylation of III with FAPP and conjugation to II 208
6.6.4. *In-vitro* prenylation of HeLa cell proteins with FAPP 209

6.6.5. In-gel fluorescence analysis 210
6.6.6. Pull-down of aldehyde-tagged proteins using aminooxy-modified agarose resin.....211
6.6.7. Catch-and-release of aldehyde-tagged proteins or peptides.....211
6.6.8. LC-MS/MS analysis 212
6.6.9. SEQUEST Database search 213
6.7. Acknowledgements 213
Bibliography 215

List of Tables

Table 2.1. Summary of proteins identified via proteomic analysis with C10Alk probe 41

Table 3.1. List of protein spots used for protein identification from the 2D-DIGE gel comparing C15Alk labeling of HeLa cells in presence or absence of an FTI (Analysis without Triton X-114 fractionation).....63

Table 3.2. List of identified proteins containing a possible C-terminal prenylation motif. 72

Table 3.3. Migration pattern and 3D spot view (from DIA analysis) of the spots used for protein identification from the 2D-DIGE gel comparing C15Alk labeling of HeLa cells in presence or absence of an FTI (Analysis without Triton X-114 fractionation). 73

Table 3.4. List of protein spots used for protein identification from the 2D-DIGE gel comparing C15Alk labeling of HeLa cells in presence or absence of an FTI (Analysis with Triton X-114 fractionation).....75

Table 4.1. Kinetic constants for the rPFTase-catalyzed reaction of FPP and analogues with Ds-GCVLS peptide. 100

Table 5.1. Summary of profiling of prenylated proteins labeled by C15Alk-OPP and 7hp-FPP. 162

Table 5.2. A complete list of prenylated proteins identified in the proteomic profiling of COS-7 cells labeled with C15Alk-OPP 173

Table 5.3. A complete list of prenylated proteins identified during proteomic profiling of COS-7 cells labeled with 7hp-FPP.....176

Table 6.1. List of prenylated proteins identified from the three replicates of proteomic analyses of HeLa cell proteins labeled with FAPP. 193

Table 6.2. List of prenylated protein identified from mouse brain sample subjected to in vitro prenylation with FAPP and then pull-down with aminooxy-modified agarose resin.....195

List of Figures

Figure 1.1. A. Structures of 1 (farnesyl diphosphate, FPP) and 2 (geranylgeranyl diphosphate, GGPP). B. Reactions catalyzed by prenyltransferase enzymes. 3

Figure 1.2. Three-step prenylation processing of proteins.. 4

Figure 1.3. Structures of isoprenoid analogs used to probe mechanism of prenyltransferase enzymes. 8

Figure 1.4. Crystal structures of prenyltransferase enzymes. 8

Figure 1.5. Key features of catalysis by protein farnesyltransferase. 9

Figure 1.6. Isoprenoid analogs used to study structure, mechanism and isoprenoid substrate specificity of FTase and GGTase-I....16

Figure 1.7. Chemical proteomic strategy for analysis of the prenylated proteome. 20

Figure 1.8. Structures of isoprenoid analog used to analyze prenylated proteome. 20

Figure 1.9. Structures of FTIs and GGTI investigated in clinical trials against cancer or HGPS. 24

Figure 2.1. Cu(I)-catalyzed click reaction between and alkyne and an azide. 34

Figure 2.2. Structures of alkyne-modified isoprenoid analogs 34

Figure 2.3. Scheme showing workflow for in-gel fluorescence analysis. 37

Figure 2.4. Analysis of labeled proteins in crude HeLa cell lysates by Cu(I)-catalyzed click chemistry. 37
Figure 2.5. Analysis of labeling in absence of lovastatin.. 39
Figure 2.6. In-gel fluorescence analysis of prenylated proteins from HeLa cells after 2D electrophoretic separation. 39
Figure 3.1. An overview of protein prenylation. 51
Figure 3.2. An overview of the strategy of combining metabolic labeling with DIGE. 52
Figure 3.3. 2D-DIGE analysis shows that when identical samples are reacted with Cy3-N3 and Cy5-N3 and run together on a 2D gel, the corresponding Cy3- and Cy5-labeled spots co-migrate on the gel. 57
Figure 3.4. Representative gel showing 2D DIGE analysis of samples from FTI-treated HeLa cells. 59
Figure 3.5. Merged 2D-DIGE image of proteins from HeLa cells treated with 50 μM C15Alk in absence or presence of 10 μM FTI. 59
Figure 3.6. Migration pattern and 3D view of representative spots from metabolic labeling and 2D DIGE analysis of prenylated proteins. 62
Figure 3.7. Spot maps showing protein spots excised for digestion and mass spectrometric protein identification.. 65
Figure 3.8. DIGE of Triton X-114 fractionated FTI-treated HeLa cells. 66

Figure 3.9. Structure of dansyl-GCGLF. 69

Figure 3.10. Continuous fluorescence assay carried out using a peptide concentration range of 0.2-25 μM, 10 μM FPP and 100 nM rPFTase.....69

Figure 3.11. Analysis of the farnesylation of a C-terminal peptide derived from GNAI-2.....71

Figure 3.12. Left: HPLC analysis of purified peptide 2 showed 94.5% purity. Right: ESI-MS analysis showed presence of expected peptide. 88

Figure 3.13. Left: HPLC analysis of purified peptide 4 showed 98.5% purity. Right: ESI-MS analysis showed presence of expected peptide.. 88

Figure 4.1. Workflow for metabolic incorporation of alkyne-modified isoprenoid analog and subsequent derivatization to a fluorophore for monitoring the global prenylome. 98

Figure 4.2. Fluorescence-based enzyme assay for prenylation using varying concentrations of FPP and C15Alk-OPP.....100

Figure 4.3. Incorporation of C10Alk and C15Alk into H-Ras in COS-1 cells.....103

Figure 4.4. Densitometry analysis of western blot bands in Figure 3.3 using ImageJ.....103

Figure 4.5. Imaging of prenylated proteins in mammalian cells with confocal microscopy indicates C15Alk-labeled proteins localize in ER. 106

Figure 4.6. Establishing reaction conditions to label the prenylome in cells.....109

Figure 4.7. Control experiments utilizing a non-reactable farnesyl alkyne analog demonstrate no background labeling. 110
Figure 4.8. Flow cytometry analysis indicates concentration dependent increase in the incorporation of C15Alk. 112
Figure 4.9. In-gel fluorescence analysis demonstrates effects of lovastatin pre-treatment on incorporation of C15Alk at various concentrations. 113
Figure 4.10. Farnesol and geranylgeraniol do not decrease incorporation of 25 or 50 μM C1Alk in HeLa cells.. 117
Figure 4.11. Farnesol and mevalonolactone do not decrease the incorporation of 25 or 50 μM C1Alk in HeLa cells. 118
Figure 4.12. Incorporation of C15-DH-Alk in HeLa cells is independent of lovastatin treatment. 120
Figure 4.13. Flow cytometry and in-gel fluorescence analysis show that farnesol and geranylgeraniol significantly compete away C15Alk labeling. 122
Figure 4.14. 10-50 μM FOH and GGOH significantly compete away labeling caused by 10 μM C15Alk, particularly in 25 kDa region. 123
Figure 4.15. Incorporation kinetics of 10 μM C15Alk in HeLa cells studied by flow cytometry and in-gel fluorescence analysis. 124
Figure 4.16. Extent and pattern of incorporation of C15Alk-OH and C15Alk-OPP in HeLa cells is similar.. 125

Figure 4.17. Extension of our method to other cell lines. 128

Figure 4.18. Metabolic labeling of prenylated proteins with C15Alk and subsequent click reaction and flow cytometry analysis can be extended to cell lines other than HeLa cells. 129

Figure 4.19. Quantitation of the effects of prenyltransferase inhibitors on the metabolic incorporation of C15Alk. 132

Figure 4.20. In a cellular model of compromised autophagy, a surrogate for studying aging disorders, the levels of prenylated proteins are increased over normal control levels. 135

Figure 5.1. Structure of FPP with C1, C3 and C7 positions indicated by corresponding numbers. 152

Figure 5.2. Structures of alkyne-modified isoprenoid analogs used in this study. 152

Figure 5.3. Labeling of HeLa cells with C10Alk and C15Alk. 154

Figure 5.4. In-gel fluorescence analysis indicates differences in the labeling of HeLa cells with various alkyne-modified isoprenoids. 157

Figure 5.5. In-gel fluorescence analysis indicates differences in labeling of HeLa cells with various alkyne-modified isoprenoids. 158

Figure 5.6. Structure and photocleavage reaction of biotin-PC-N_3. 161

Figure 5.7. Photocleavage of biotin-PC-N3 monitored by the disappearance of its peak in HPLC analysis upon irradiation of 365 nm light. 161
Figure 5.8. Structures of C15Alk-OPP and 7hp-FPP. 162
Figure 6.1. Structures of farnesyl aldehyde diphosphate (i), formylbenzoyl-oxy geranyl diphosphate (ii), and 2-aminooxy-*N*,*N*,*N*-trimethylethylaminium iodide (iii). 189
Figure 6.2. In-gel fluorescence analysis of HeLa cells proteins prenylated with FAPP in an *in vitro* reaction. 189
Figure 6.3. Workflow describing enrichment of aldehyde-tagged prenylated proteins using aminooxy-modified agarose resin. 190
Figure 6.4. Venn diagram showing overlap of prenylated proteins identified in three independent experimental replicates. 190
Figure 6.5. Workflow showing our catch-and-release strategy for identification of prenylated proteins and detection of the site of modification. 196
Figure 6.6. Detection of a synthetic prenylated peptide using a SEQUEST database search algorithm. 201
Figure 6.7. Detection of C-terminal prenylated peptide from GNG12 (Uniprot ID: Q9UBI6) using SEQUEST database search algorithm. 204

Chapter 1 Protein prenylation

1.1. Protein prenylation

Protein prenylation was first discovered in fungi in 1978,[1] and almost 10 years later, the first prenylated protein in mammalian cells, farnesylated Lamin B, was detected.[2, 3] Since then, this modification has been studied extensively due to its importance for the proper cellular activity of numerous proteins. Protein prenylation is an irreversible covalent post-translational modification found in all eukaryotic cells, comprising of farnesylation and geranylgeranylation. Three prenyltransferase enzymes catalyze this modification. Farnesyltransferase (FTase) and geranylgeranyltransferase type 1 (GGTase-I) catalyze attachment of a single farnesyl (15 carbon), or geranylgeranyl (20 carbon) isoprenoid group, respectively, to a cysteine residue located in a C-terminal consensus sequence commonly known as “CaaX box” (Figure 1.1), where “C” is cysteine, “a” generally represents an aliphatic amino acid and the “X” residue is largely responsible for determining which isoprenoid is attached to the protein target.[4] Geranylgeranyltransferase type 2 (GGTase-II or Rab geranylgeranyltransferase)

catalyzes the addition of two geranylgeranyl groups to two cysteine residues in sequences such as CXC, CCXX close to the C-terminus of Rab proteins (Figure 1.1).[4]

Proteins prenylated with FTase and GGTase-I typically undergo two additional processing steps.[5] First, the C-terminal aaX tripeptide is cleaved from the newly prenylated CaaX protein by an endoprotease, either Ras-converting enzyme 1 (Rce1p) or Ste24p (Figure 1.2). This is followed by methylation of the prenylcysteine residue at the new C-terminus by isoprenylcysteine carboxylmethyltransferase (Icmt, Figure 1.2). This three-step process increases protein hydrophobicity, and often leads to plasma membrane association.[5] However, it is been noted that prenylation alone is not sufficient to cause stable membrane association.[6] Either the presence of a polybasic domain upstream of the CaaX box (as found in K-Ras4B, for example) or additional lipid modification such as palmitoylation at one or two cysteine residues (such as in H-Ras), supports more stable membrane localization of prenylated proteins (Figure 1.2).

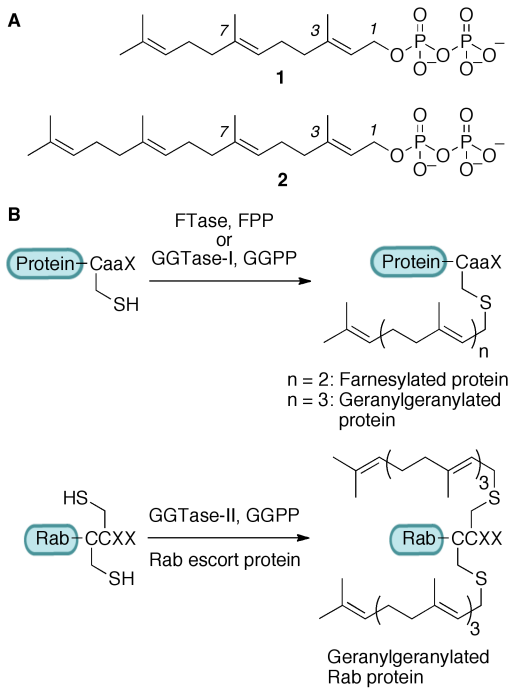

Figure 1.1. A. Structures of 1 (farnesyl diphosphate, FPP) and 2 (geranylgeranyl diphosphate, GGPP). B. Reactions catalyzed by prenyltransferase enzymes.

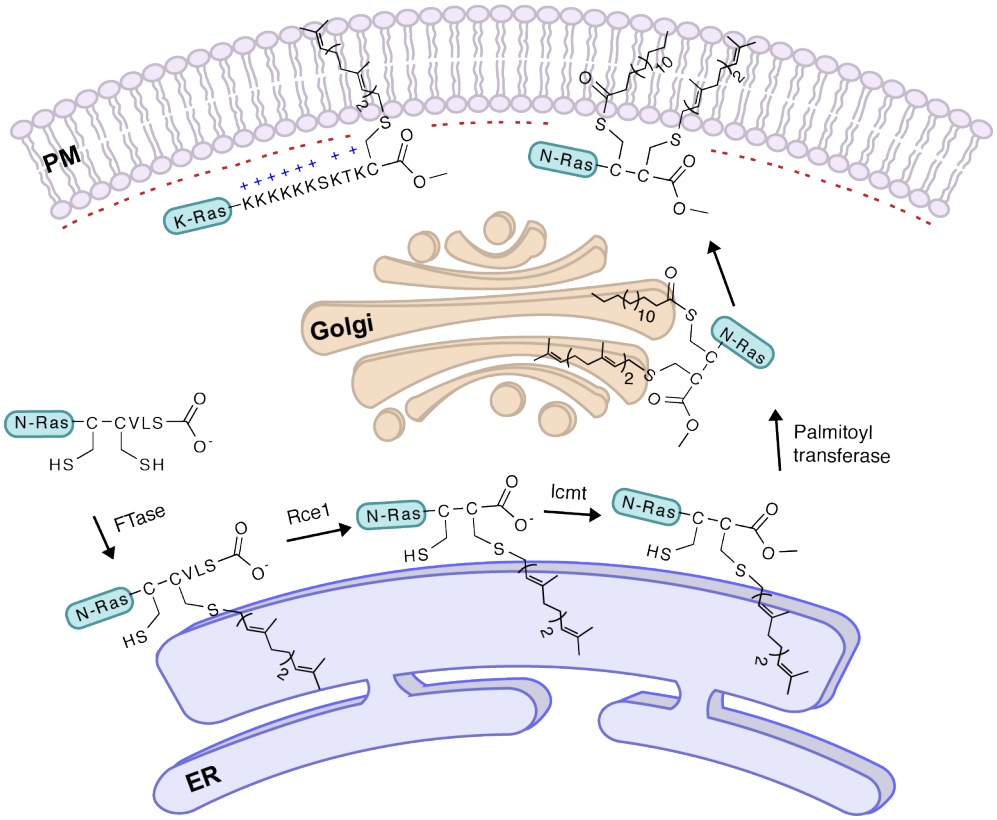

Figure 1.2. Three-step prenylation processing of proteins. Proteins undergo farnesylation, proteolytic cleavage of aaX residues, followed by carboxymethylation and then get localized at the plasma membrane. Some proteins, shown here N-Ras, undergo palmitoylation and then localize to plasma membrane, while other proteins, shown here K-Ras, have a polybasic sequence upstream of the "CaaX box" facilitating membrane localization.

1.2. Mechanism of protein prenylation

Protein prenylation is catalyzed by three distinct prenyltransferase enzymes that all exist as heterodimers and have very similar topologies (Figure 1.4A and B). While FTase and GGTase-I share a common α-subunit, the α-subunit of rat GGTase-II has only 22% sequence similarity to the rat FTase α-subunit.[7] In rat-derived enzymes, the β-subunit of FTase is only 25% and 32% identical to that of GGTase-I and GGTase-II, respectively.[8] The reaction catalyzed by GGTase-II requires an additional, escort protein, for activity. Most mechanistic analyses have focused on farnesylation with a more limited number of studies probing geranylgeranylation. Early kinetic analysis demonstrated that farnesylation proceeds via an ordered mechanism in which FPP binds first.[9, 10] After binary complex formation occurs, the CaaX-box containing substrate binds and C-S bond formation occurs. At that point, a new FPP molecule binds while the farnesylated protein remains bound followed by product dissociation either prior to, or concerted with, binding of a new CaaX-box substrate protein. All of these intermediates have been observed crystallographically, providing a clear view of the events occurring during catalysis; interestingly, minimal differences in the protein conformation are observed in these different structures.[11] Single turnover kinetic experiments and calculations suggest that a conformational change in the enzyme occurs prior to C-S bond formation although no evidence for this has

been noted in any of the crystal structures solved to date.[12, 13] Stereochemical analysis of the enzymatic process using deuterated isotopomers of FPP (**3**) revealed that the reaction proceeds with clean inversion of configuration of stereochemistry at C-1 of the isoprenoid[14, 15] suggesting that attack of the sulfur nucleophile is concerted with departure of the diphosphate leaving group. Work with isoprenoid analogs incorporating electron withdrawing fluorine substituents (**4**) provides evidence that the transition state involves some carbocationic character[16] although analogues including **5** designed to trap such intermediates failed to do so.[17] Kinetic isotope effect measurements with both ^{2}H- and ^{13}C-isotopomers suggest a transition state that involves participation of the incoming sulfur nucleophile with significant development of positive charge at C-1 of the isoprenoid (Figure 1.5A-C);[18-20] QM/MM computational experiments are in accord with this as no evidence for a discrete carbocationic species was observed.[21] For efficient catalysis, kinetic experiments indicate that the enzyme activates the sulfur nucleophile as a Zn-thiolate.[22, 23] Such a species is consistent with what has been observed crystallographically as well as via EXAFS spectroscopy.[24]

The enzymology of GGTase-I is similar to that FTase. The enzyme proceeds via an ordered sequential kinetic mechanism[25] and the reaction proceeds with inversion of stereochemistry at the C-1 position of the isoprenoid.[26] Interestingly, GGTase-I does not require Mg^{2+} for catalysis due to the presence of

a lysine residue in the active site which assists with the departure of the diphosphate leaving group in lieu of the divalent metal.[27] The overall structure of GGTase-I[8] is very similar to that of FTase although the former has a deeper isoprenoid binding pocket to accommodate the larger substrate.[28] The process catalyzed by GGTase-II is more complex since it involves participation of an additional escort protein, Rab Escort protein (REP),[29] that both recruits the substrate proteins and traffics them following prenylation.[29, 30] Typically two cysteine residues (CC or CXC) are prenylated in a processive fashion. Several crystal structures of these enzymes have been reported.[31, 32] Unlike FTase and GGTase-I, GGTase-II has a more extended binding site for the protein target and interacts with the latter over a larger surface rendering short peptides inefficient as substrates. Finally, it should be noted that while the majority of the above enzymological studies have been carried out *in vitro*, the situation may be more complex *in vivo*. For example, recent work suggests that some Ras-like proteins may associate with putative chaperone proteins prior to prenylation; hence the true substrates of prenyltransferases *in vivo* may be protein complexes instead of simply the polypeptide substrate alone.[33] This remains an active area of inquiry.

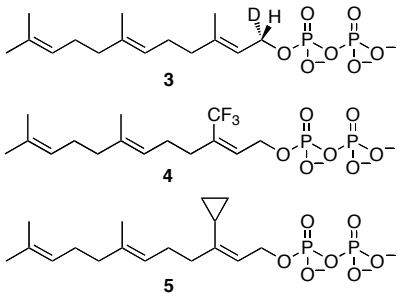

Figure 1.3. Structures of isoprenoid analogs used to probe mechanism of prenyltransferase enzymes.

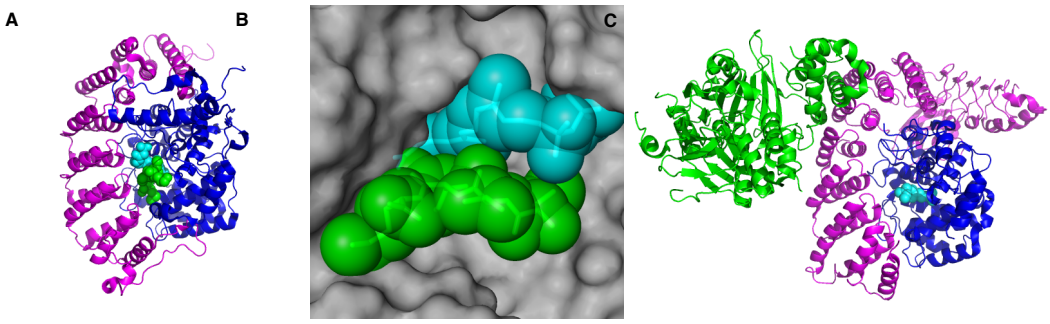

Figure 1.4. Crystal structures of prenyltransferase enzymes. A. Crystal structure of FTase in complex with a non-hydrolyzable FPP analog and a peptide substrate based on KRas-4B (PDB 1D8D). Magenta: α-subunit, blue: β-subunit, cyan: isoprenoid analog, green: CaaX peptide. B. Binding pocket of FPP showing interaction of protein and isoprenoid substrates over large surface area. Gray: Space-fill structure of β-subunit of FTase, cyan: isoprenoid analog, green: CaaX peptide. C. Crystal structure of GGTase-II in complex with Rab escort protein and FPP (PDB 1LTX). Magenta: GGTase-II α-subunit, blue: GGTase-II β-subunit, green: Rab escort protein, cyan: FPP.

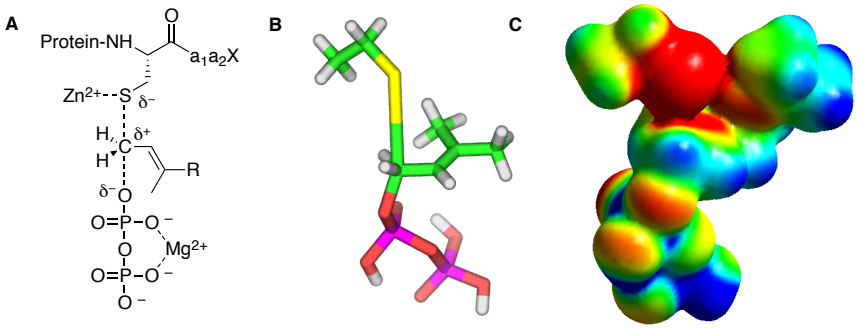

Figure 1.5. Key features of catalysis by protein farnesyltransferase. A. Schematic representation of transition state showing thiol activation by Zn^{2+}, diphosphate stabilization by Mg^{2+} and partial bonding to leaving group and incoming nucleophile (adapted from Reference 23). B. Structural model for transition state based on kinetic isotope effect measurements and DFT calculations. The model reaction used for computation (shown in these images) employed ethane thiol and dimethylallyl diphosphate. C. Electrostatic potential map of transition state based on the same model shown in Center. (Images B and C images adapted from Reference 24). Color scheme for B: Carbon (green), Hydrogen (white), Oxygen (red), Phosphorus (magenta) and Sulfur (yellow). Color scheme for C: Red represents more negative potential, blue represents less negative potential and green is intermediate.

1.3. Peptide substrate specificity

Early work with prenyltransferases suggested that the X residue in CaaX box determines whether the protein is farnesylated or geranylgeranylated and that CaaX sequences with the X residue being alanine, serine, methionine or glutamine are preferred by FTase whereas leucine, isoleucine and phenylalanine are preferred by GGTase-I. However, these enzymes do not manifest mutually exclusive substrate specificity.[34] Some of the examples of overlapping substrate specificity include K-Ras and Rho B proteins. The CVIM sequence from K-Ras protein is normally farnesylated in mammalian cells; however, it can be processed by GGTase-I when FTase is inhibited.[35] Rho B, which has a CKVL motif at C-terminus, is present in both farnesylated and geranylgeranylated forms in cells.[35]

The human protein database (SwissProt) indicates the presence of 756 unique proteins containing the Cxxx motif at their C-terminus.[36] Based on the available descriptions of sequence motifs recognized by prenyltransferase enzymes, Eisenhaber and co-workers developed an amino-acid sequence based predictors, the Prenylation Prediction Suite, and showed its utility by predicting which prenylated proteins would be preferentially affected in response to an enzyme-specific prenyltransferase inhibitor.[37, 38]

While that predictive algorithm has proven to be useful for inferring the prenylation status of non-annotated proteins, it was designed using a limited number of known prenylated proteins; importantly, it does not correctly predict the prenylation efficiency of numerous CaaX-box sequences.[39] Hence, expanding the training set should increase the accuracy of such bioinformatic methods. The process of testing a large number of sequences for activity against FTase has been possible since the enzyme accepts short peptides, including CaaX tetrapeptides, as substrates with affinity and reactivity comparable to full-length proteins.[40, 41] Fluorescence-based assays using dansylated peptides have been highly useful in this regard.[42, 43] Accordingly, several studies with small-scale and large-scale libraries of CaaX peptides have been conducted.[44, 45] In particular, Gibbs and co-workers utilized a library of 41 peptides with CaaL sequences and found that FTase efficiently processed a number of peptides having leucine at X position.[46] Fierke and colleagues screened a library of 80 peptides with CVaX sequences and interestingly found that substrate recognition is not limited to the nature of X residue.[47] They reported that FTase is sensitive to both the size and hydrophobicity of the residue at the a_2 position, and the nature of residue at X position affects the selectivity at the a_2 position. Later, the same group carried out an analysis of a library of small peptides representing the CaaX motif of 213 human proteins, and they observed that FTase could catalyze farnesylation of

several CaaX sequences that were not computationally predicted to be FTase substrates, with multiple turnover reactivity.[39] They also identified a large number of sequences that were processed with single turnover reactivity, and noted that at least two of these sequences corresponded to a known *in vivo* FTase substrate. This indicated that some of the single turnover *in vitro* peptide substrates could potentially be multiple turnover substrates in a cellular context.[48] Results from those studies have allowed for the development of improved bioinformatic programs, such as a FlexPepBind-based prediction protocol.[36]

Recently, Distefano and co-workers designed a method to synthesize solid-phase peptide libraries with free C-termini for studying the substrate specificity of prenyltransferase enzymes.[49] Using this method, they created libraries incorporating 760 peptides (based on CVaX and CCaX sequences) and screening of these libraries revealed numerous sequences that could be processed by mammalian FTase, including sequences occurring in genomes of bacteria and viruses.[50] This opens an exciting opportunity for therapeutic intervention against such proteins.

1.4. Isoprenoid analogs

A large number of isoprenoid analogs containing various functionalities have been synthesized to study a variety of aspects of the prenylation reaction and prenyltransferases (Figure 1.6). Before the crystal structure of FTase was solved,

photoaffinity probes such as compounds **6** through **9** were used extensively to probe the structural features of yeast and mammalian variants of FTase and GGTase-I.[25, 51-58] These analogs revealed the role of the β-subunit of FTase and GGTase-I in the recognition and binding of isoprenoid substrates as well as indicated differences between active site architecture of mammalian and yeast FTases. Later, similar experiments were also carried out with GGTase-II, which led to identification of proteins with which Rab5 interacts via the isoprenoid group.[59] Interestingly, it was noted that while **8** was accepted as a substrate by FTase, **9**, containing one more isoprenoid unit was a potent inhibitor of yeast FTase.[60, 61] Recently, a new photoactive isoprenoid probe containing a diazirine group (**10**) was reported whose size more closely approximates that of FPP. Peptides incorporating that photoactive isoprenoid were used in cross-linking studies of Icmt.[62] Phosphonate **11** and related analogues[63] have been particularly useful for crystallographic studies that have revealed that the isoprenoid binds in an extended conformation and that several active site residues undergo rearrangement upon isoprenoid binding compared to the unliganded enzyme.[64]

Recent studies with isoprenoid analogs have focused on investigating isoprenoid substrate specificity of prenyltransferase enzymes. Gibbs and co-workers synthesized a number of geometric isomers of all-*trans* FPP and GGPP (such as **12**). They found that while most of the analogs were substrates to mammalian

FTase, mammalian GGTase-I did not accept them as substrates. In fact, **12** was an inhibitor to GGTase-I, indicating more stringent specificity for the isoprenoid substrates for that enzyme.[65] Spielmann and co-workers have reported substantial plasticity in the binding site of FTase. For example, analog **13,** where all isoprene units were replaced with aryl groups, was an efficient FTase substrate.[66] They reported that the anilinogeranyl-based isoprenoid analogs **14** and **15**, which have 2–5 orders of magnitude less hydrophobicity compared to FPP, were substrates for FTase. Proteins modified with these analogs were processed by downstream enzymes Rce1 and Icmt; however, the resulting modified proteins were not biologically active, indicating the importance of increased hydrophobicity upon prenylation.[67] Additionally, they noted that some of the anilinogeranyl-based analogs, such as **16**, were substrates for FTase when a peptide based on K-Ras C-terminal sequence, dansyl-GCVIM, was used, but remarkably they were potent inhibitors of the enzyme when dansyl-GCVLS (IC_{50} of **16** was 3.0 nM), a sequence based on C-terminal of H-Ras, was used.[68]

A large number of analogs having substitutions at the 3- or 7-positions of FPP have been synthesized by Gibbs and co-workers. They concluded that subtle changes in the functionalities incorporated at these positions can lead to large and unexpected differences in incorporation efficiency. For example, they found that the 3-vinyl analog, **17**, was a slow FTase substrate in cells, whereas

the 3-allyl analog, **18**, was an FTase inhibitor.[69] During the screening of analogs against a library of eight CaaX sequences, 7-allyl analog, **19**, could farnesylate only the CVIM sequence, while **20** was an extremely efficient substrate to almost all the sequences in their library.[70] These subtle differences likely reflect the fact that the protein and isoprenoid substrates interact with each other over a large surface area when bound to FTase (Figure 1.4B); thus small perturbations in one of the substrate structures require compensatory changes in the other substrate to obtain optimal complementarity.

Waldmann and co-workers described the synthesis of fluorescent isoprenoid analogs based on NBD and BODIPY groups, and demonstrated the use of compound **21** in flow cytometry and imaging for analysis of uptake of these analogs in mammalian cells and zebrafish embryos.[71] Coumarin-, anthranilate-, and dansyl-functionalized analogues have also been prepared for both *in vitro* and cell-based assays.[72, 73] Finally, several types of FPP analogs have also been explored as FTase inhibitors; however, they were not as successful as other classes of FTIs possibly due to nonselective inhibition of other FPP utilizing enzymes and difficulty in designing cell penetrable analogs containing pyrophosphate group of FPP.[74, 75]

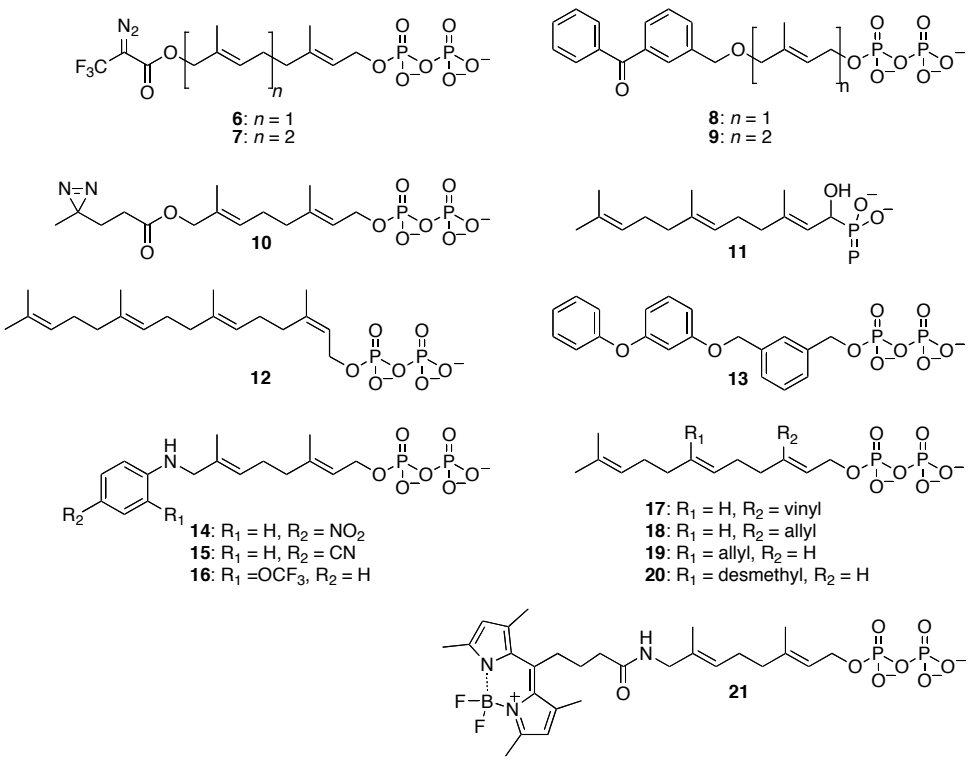

Figure 1.6. Isoprenoid analogs used to study structure, mechanism and isoprenoid substrate specificity of FTase and GGTase-I.

1.5. Analysis of the prenylated proteome

As noted above, there is considerable interest in identifying proteins that are prenylated in a cellular context in order to determine which prenyltransferase protein substrates have their prenylation status affected by FTIs. Chemical proteomic methods have been highly useful in this regard (Figure 1.7). In this approach, metabolic labeling of living cells is first carried out using isoprenoid analogs to tag prenylated proteins with a reporter group, such as an azide or alkyne. These tagged proteins are then functionalized using bioorthogonal reactions to install either a fluorophore for gel-based proteomic studies or a biotin moiety for enrichment of tagged proteins.

In 2004, Zhao and co-workers reported the first prenylomic study, wherein they employed azide-modified FPP analog **22** for the metabolic labeling of farnesylated proteins.[76] Chemoselective conjugation of labeled proteins to a biotinylated phosphine capture reagent using a Staudinger ligation reaction allowed for affinity purification and mass spectrometric identification of 18 farnesylated proteins. Tamanoi and co-workers incorporated an azide-modified analog of GGPP (**23**) into geranylgeranylated proteins, and subsequently installed a fluorophore via Cu(I)-catalyzed click reaction on the azide-labeled proteins.[77] They used pH fractionation coupled with narrow pH range 2D SDS-PAGE to achieve separation of low abundance geranylgeranylated proteins from

rest of the proteins in cells. LC-MS/MS analysis of some of the fluorescent protein spots led to identification of four substrates of GGTase-I and six substrates of GGTase-II. Berry et al. reported a method for detection and affinity purification of geranylgeranylated proteins utilizing an azide-modified GGPP analog and an alkyne capture reagent functionalized with a fluorophore as well as biotin.[78] Since alkyne-modified chemical reporters tend to give more sensitive and selective detection compared to their azido-counterparts, the Distefano and Hang groups used alkyne-functionalized isoprenoid analogs for analysis of the prenylome.[79, 80] DeGraw et al. reported two alkyne-modified analogs for metabolic labeling: **24**, which is a substrate for FTase,[81] and **25**, which is a substrate for both FTase and GGTase-I.[82] The authors derivatized the proteins labeled by **24** with a fluorophore via the Cu(I)-catalyzed click reaction and separated proteins on a 2D gel. Six prenylated proteins were identified upon MS analysis of some of the fluorescent protein spots. In another study, metabolic labeling with **25** was carried out in the presence and absence of a farnesyltransferase inhibitor. The two corresponding protein samples were then reacted with two spectrally orthogonal azide-functionalized dyes and mixed together.[83] This was followed by differential gel electrophoresis (DIGE) to facilitate visualization of several protein spots with altered levels of labeling in presence of an FTI. LC-MS/MS analysis of some of the protein spots identified 8

proteins with decreased amounts of labeling and 11 proteins with increased amounts of labeling in response to the FTI treatment.

In recent years, several reports indicated that intracellular human pathogens, which lack prenylation machinery, translocate several effector proteins containing CaaX-box motifs into host cell cytosol.[84-87] These proteins are prenylated using host cell prenyltransferase enzymes and later form membrane-bound organelles supporting replication of the pathogen.[85, 86] Hang and colleagues exploited analog **25** for investigating prenylation of a bacterial effector protein as well as immune effector proteins in host cells.[80, 88] They first detected intracellular prenylation of *Salmonella* T3SS effector protein SifA upon immunopurification and gel electrophoretic analysis of SifA metabolically labeled with **25** and conjugated to a fluorophore.[80] Later they carried out profiling of prenylated proteins in macrophages[88] using a Cu(I)-catalyzed click reaction of alkyne-tagged proteins with an azido-biotin reagent containing a chemically cleavable linker for enrichment and selective elution. Tandem mass spectrometric analysis of eluted proteins identified 17 prenylated proteins with high confidence, 5 proteins with medium confidence, and many other candidate isoprenoid-modified proteins. They also discovered isoform-specific farnesylation of zinc-finger antiviral protein (ZAP) and found that farnesylation of this protein was essential for increasing the antiviral activity of this immune effector protein.

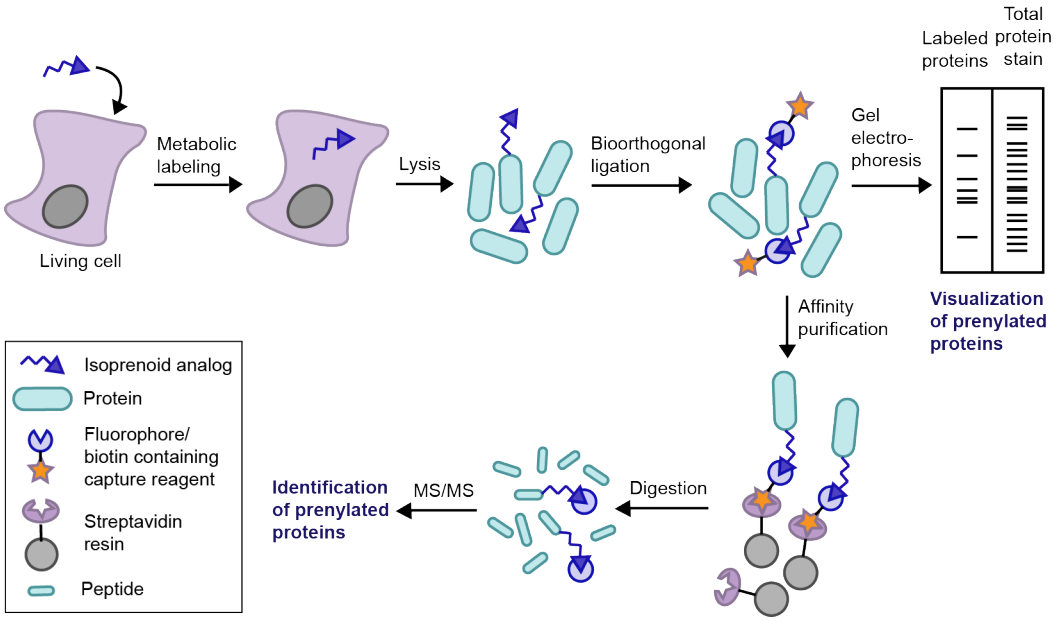

Figure 1.7. Chemical proteomic strategy for analysis of the prenylated proteome.

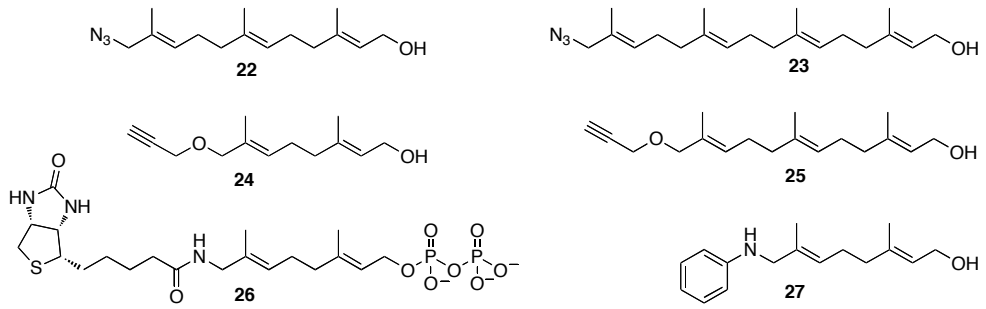

Figure 1.8. Structures of isoprenoid analog used to analyze prenylated proteome.

Alternative approaches of prenylome analysis by-pass the need for a bioorthogonal reaction. Alexandrov and colleagues employed a biotinylated isoprenoid, **26**, for *in vitro* prenylation of proteins using either *wt* GGTase-II or engineered FTase and GGTase-I, to allow for subsequent enrichment using streptavidin beads.[89] Using this approach they identified 42 Rab GTPases as GGTase-II substrates, and also quantitatively analyzed *ex vivo* effects of prenylation inhibitors in cell culture on the prenylation of these Rab GTPases. In a study carried out by Reuter and co-workers, anilinogeraniol, **27**, was used to tag the farnesylated proteome.[90] Proteins were separated on 2D gels and tagged proteins were detected by western blot using antibodies against the anilinogeranyl moiety. Effects of FTI treatments on labeling with **27** were also visualized using this approach.

Porcu et al. utilized a genomic method to globally analyze effects of FTIs on cellular activity.[91] They carried out differential labeling of cDNA with two fluorescent dyes by reverse RNA transcription of DNA isolated from FTI-treated or untreated yeast cells. Labeled cDNA were mixed together and hybridized with an array of 6,240 unique yeast ORFs. Expression levels of all the genes in the presence and absence of FTI treatment were quantified by comparing the fluorescence intensity of the two color panels. Utilizing this method, the authors

identified downstream effector proteins that get either up- or down-regulated as a result of FTI treatment.

1.6. Inhibition and therapeutic applications

The initial efforts to develop farnesyltransferase inhibitors (FTIs) targeted the inhibition of oncogenic Ras proteins. This was predicated on the occurrence of Ras mutations in more than 30% of human cancers, and the discovery that farnesylation of Ras proteins is essential for their proper cellular localization and signaling activity.[34, 92] Initially, FTIs were designed to be competitive inhibitors, either peptidomimetic compounds, isoprenoid analogs or bisubstrate analogs. Later, potent inhibitors were identified from library screening efforts.[93]

Preclinical studies of FTIs in cancer cell lines as well as animal models were highly successful leading to the advancement of four FTIs (Figure 1.9) into clinical trials starting in 2000.[35] While phase 1 and 2 studies were encouraging, this early stage success did not yield robust anticancer activity.[94] The four FTIs were evaluated in at least 75 clinical trials either as monotherapy or in combination with other anti-cancer drugs. The results were discouraging with >28% trials reporting no objective response and >36% studied showing very little (<15%) response.[35] One of the key reasons behind the failure of FTIs in clinical trials is the incorrect selection of patients enrolled in these studies.[35, 94] K-Ras protein, which is the most frequent isoform of oncogenic Ras proteins, was

reported to get geranylgeranylated and remain fully active when FTase activity is inhibited.[95, 96] And while it was known that K-Ras could escape FTI-mediated inhibition of FTase, phase III clinical trials were performed with patients having advanced or metastatic tumors harboring mutant K-Ras.[35] Recently, methods are being developed to predict patient populations that are likely to be susceptible to FTIs. Karp and co-workers developed a 2-gene expression assay to predict clinical outcome of tipifarnib (Figure 1.9) treatment administered to acute myeloid leukemia (AML) patients.[97] More clinical studies with patients who are predicted to be responsive to the FTI based on their gene expression profile could potentially identify FTI-based personalized anticancer therapies.

Since K-Ras can be geranylgeranylated and other geranylgeranylated proteins may also be involved in cancer, inhibitors of GGTase-I (GGTIs) have been evaluated as an alternative strategy to achieve anticancer therapies. Using structure-activity relationships, several GGTIs selectively inhibiting GGTase-I over FTase were developed. Only one of the GGTIs (Figure 1.9) entered phase I clinical trial in 2009 and that was discontinued due to lack of efficacy in patients.[34] Recently, experiments with a caged FTI demonstrated that such compounds may be useful for selective release of an FTI within a defined tissue location.[98]

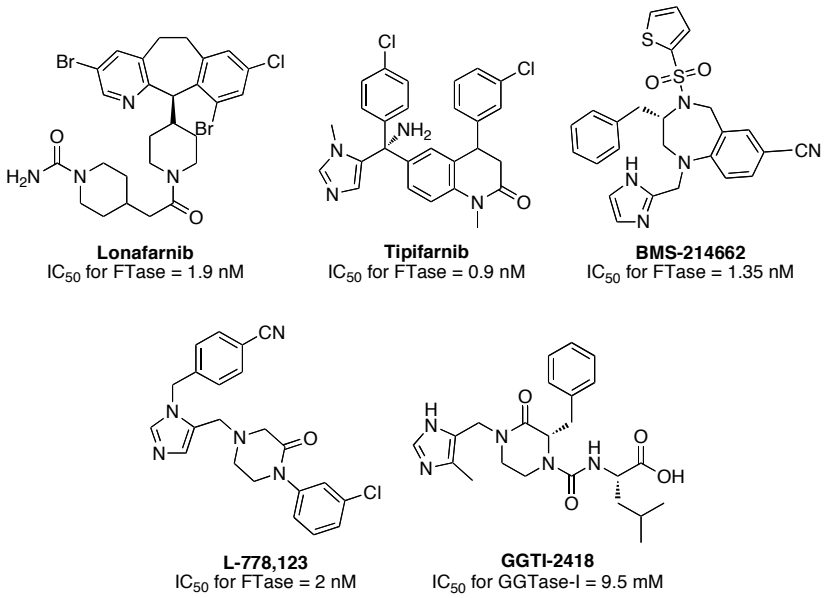

Figure 1.9. Structures of FTIs and GGTI investigated in clinical trials against cancer or HGPS.

The discovery that Hutchinson-Gilford Progeria Syndrome (HGPS) is caused, at least in part, by the accumulation of a farnesylated protein derived from a mutant form of farnesylated prelamin A, generated interest in using FTIs to treat HGPS.[34] Following *in vitro* and mouse model studies, two clinical trials using lonafarnib (Figure 1.9) as treatment for HGPS were undertaken.[99, 100] The first phase II clinical trial started in 2007 with 25 patients, where lonafarnib treatment for at least 2 years, was well received. It provided preliminary evidence that lonafarnib could potentially improve one or more disease measures related to HGPS.[101]. The other phase II clinical trial was initiated by Children's Hospital Boston in 2009, to test a combination lonafarnib and two other compounds for patients with progeria, and it is currently estimated to be completed in 2017.[102] The results of this study should help to design combination therapies to treat progeria with prenylation inhibitors.

The pathogenic parasites causing diseases such as malaria, African sleeping sickness, and Chagas disease have their own farnesyltransferase enzyme.[103] Inhibition of FTase severely affected the growth of these parasites, indicating FTIs as a useful treatment strategy.[103-105] Development of potent FTIs ($IC_{50} \geq 1$ nM) having up to 136-fold selectivity for the *Plasmodium falciparum* (malaria) FTase over the mammalian counterpart shows promise for potential uses of FTIs in treating parasitic diseases.[106] FTIs and GGTIs are also being

investigated for several other diseases including multiple sclerosis, osteoporosis, aging disorders and viral diseases such as hepatitis.[107-110]

1.7. Biotechnological applications

In recent years, the properties of FTase to specifically modify a single cysteine residue located at the C-terminal CaaX motif and to incorporate isoprenoid analogs containing bioorthogonal functionalities have been exploited for site-specific modifications of proteins. This has been possible since the presence of a CaaX-box at its C-terminus is sufficient to render almost any protein an efficient FTase substrate. Functionalization of the resulting proteins via bioorthogonal reactions provides a convenient methodology for preparing a wide of array of protein conjugates in a site-specific manner.

Both the Poulter and Distefano groups have used azide- and alkyne-functionalized FPP analogs in FTase-catalyzed reactions followed by click reactions or Staudinger ligations for immobilization of proteins (GFP or GST) onto solid surfaces such as glass slides or agarose resin.[111-114] Maynard and co-workers utilized a similar strategy for immobilization of mCherry protein tagged with **25** onto a patterned azide-functionalized surface created by microcontact printing.[115] A photochemical thiol-ene reaction between farnesylated recombinant proteins and surface-exposed thiols from functionalized surfaces was applied by Waldmann and co-workers for oriented and selective immobilization of functional

proteins (mCherry and Ypt1).[116] Recently, Poulter and co-workers achieved highly ordered, regioselective immobilization of the glutathione S-transferase enzyme and antibody-binding protein G to self-assembled monolayers on gold surfaces.[117] They further created sandwich antibody arrays of immobilized recombinant antibody-binding protein L for capturing antibodies for direct- and sandwich-type immunofluorescent detection of ligands in a microarray format.[118] In general, the prenylation-based immobilization strategy has several potential biomedical and biotechnology applications where oriented protein immobilization is required, such as protein arrays, and diagnostic applications based on immunoassays, Surfase Plasmon Resonance (SPR) or electrochemical methods.

A simple and efficient method for the derivatization and purification of recombinant proteins (such as YPT7, Rab7, GST) was developed by Alexandrov and co-workers using a fluorescent analog of FPP and phase partitioning.[119] Recently, Distefano and co-workers described the use of an aldehyde-functionalized FPP analog in conjunction with a hydrazide resin-based catch-and-release strategy to purify and functionalize proteins with groups like a fluorophore or PEG moiety.[120]

One important application of the prenylation-based labeling strategy is the formation of site-specific protein modifications such as protein-DNA conjugates, PEGylated proteins and dually labeled proteins.[121] Some of the protein-DNA

conjugates that have been synthesized using this method include a nanoscale sized defined tetrahedron architecture composed of four oligonucleotides and four GFP molecules, therapeutically relevant proteins GIP and HIV NC attached to oligonucleotides, as well as DNA-protein cross-links as DNA lesions to study DNA repair and replication.[121-123] Prenylation of a recombinant protein cilliary neurotrophic factor (CNTF) with an isoprenoid analog modified with an aldehyde group followed by oxime ligation-based catch-and-release yielded PEGylated CNTF, where attachment of the PEG group could potentially increase serum half-life of this biomedically important protein.[124] In another report, Rashidian et al. describe a multifunctional macromolecular protein self-assembly consisting of an antibody nanoring structure bearing a single chain anti-CD3 antibody as the targeting element, as well as a model cargo protein and a fluorophore. In that case, a trifunctional FPP analogue incorporating both aldehyde and alkyne functionality was used to create the key multifunctional fragment consisting of a cargo protein, fluorophore and protein dimerizer. This high-avidity "effector-antibody-fluorophore" conjugate was endocytosed into T-leukemia cells highlighting its potential use in developing protein-drug conjugates for therapeutic protein delivery and tracking.[125]

1.8. Current status of research on protein prenylation

Protein prenylation has emerged as an important post-translational modification responsible for the correct cellular localization, activity and protein-protein interactions of a number of signaling proteins. Over the past 25 years, a large number of isoprenoid analogs have been synthesized and employed to probe the structural and mechanistic features of the prenyltransferase enzymes. With the extensive studies using these analogs, peptide substrates as well as X-ray crystallographic analysis of the enzymes in complex with the substrates and product, the enzymology of prenyltransferases is now well understood. One of the early hypotheses in the field of prenylation was that prenyltransferase inhibitors could be used to suppress malignant activity of oncogenic Ras proteins. While those inhibitors gave early success in the laboratory, clinical trials proved less promising. Those results make it clear that much remains to be learned concerning the roles of prenylated proteins in living cells and this remains an intense area of current investigation. Several peptide library screening efforts, proteomic studies and yeast-based genomic experiments have provided preliminary results towards this end, however, completely defining the prenylated proteome is still an ongoing task; addressing this issue will be central for assessing which patients are the best candidates for treatment with prenylation inhibitors. More work also needs to be carried out to explore the potential of FTIs

and GGTIs for the treatment of other afflictions including progeria, multiple sclerosis, parasitic diseases, and bacterial and viral infections. Protein prenylation has also shown promise for site-specific modifications of proteins. While many interesting applications have been demonstrated in recent years, future work must focus on creating protein conjugates including antibody-drug conjugates, PEGylated proteins and other constructs that are directly applicable to therapeutic studies so that they can be evaluated in clinical contexts. Overall, these challenges suggest that investigation of protein prenylation and will remain an active and vibrant field of inquiry for some time to come.

Chapter 2 Alkyne-modified analogs as chemical reporters of protein prenylation

Reproduced in part with permission from Amanda J. DeGraw, Charuta Palsuledesai, Joshua D. Ochocki, Jonathan K. Dozier, Stepan Lenevich, Mohammad Rashidian, and Mark D. Distefano, Evaluation of alkyne-modified isoprenoids as chemical reporters of protein prenylation, *Chem. Biol. Drug Des.*, **2010**, *76*, 460-471. © John Wiley and Sons.

2.1. Introduction

The inhibition of protein farnesylation has been a target for disease intervention for the past two decades, and protein farnesyltransferase inhibitors (FTIs) have been evaluated as therapeutic agents for several medical problems. Despite copious amounts of research, much still remains unclear about protein prenylation and its inhibition. While decreases in the levels of a number of prenylated proteins have been shown to occur upon treatment with FTIs, direct evidence that these species, and not other undiscovered prenylated proteins, are relevant to the physiological effects of FTIs is severely lacking.[126, 127] Only a fraction of prenylated proteins have been observed experimentally despite the hundreds predicted by bioinformatics approaches.[37, 128] Clearly, comprehensive experimental techniques designed to study the posttranslational modification of proteins with isoprenoids by protein prenyltransferases are needed. Such

techniques would help provide a better understanding of the mechanism(s) of action of FTIs and GGTIs and could assist in the creation of more potent and selective compounds.

Recently, a relatively new technique known as chemical proteomics has been developed that allows post-translationally modified proteins to be selectively labeled or enriched for subsequent analysis.[129, 130] In this strategy, the proteins of interest are first labeled with a small chemical tag at the site of the modification. This can be carried out by exploiting the cell's own machinery to label the proteins in situ with a tagged substrate analog based on the posttranslational modification or by post-lysis modification by chemical or enzymatic means. The next step involves performing a bioorthogonal chemical ligation reaction with a capture/labeling reagent. A number of such reagents have been created bearing affinity labels (e.g., biotin, FLAG, etc.), reporter dyes, radiolabels, oligonucleotide tags, and stable isotope tags. The choice of capture chemistry depends on the downstream application with the most common being the 'click' reaction (Figure 2.1) and Staudinger ligation.[131]

In the prenylation field, Tamanoi, Zhang and coworkers explored the use of farnesyl azide in proteomics experiments as a surrogate for farnesyl diphosphate (FPP).[76] Growth of COS cells in the presence of azide-modified analog resulted in incorporation of these analogs into proteins. This was

established using a biotinylated phosphine capture reagent that reacted with the azide-labeled proteins via Staudinger ligation chemistry. Subsequent mass spectrometric analysis allowed them to identify a number of farnesylated proteins. In collaboration with Invitrogen, Corp., Tamanoi and coworkers followed up on this work and used an azide-containing analog of geranylgeranyl diphosphate (GGPP) to identify a number of geranylgeranylated proteins;[77] Berry et al. extended this approach to labeling in whole animals.[78] Other approaches for studying the 'prenylome' including the use of biotinylated substrates[132] and antibodies directed against isoprenoid analogs have also been employed[133]. The rapid rate of the Cu(I)-catalyzed click reaction has made it the method of choice for many proteomic profiling protocols. However, as noted by Cravatt and coworkers in related activity-based profiling experiments, background labeling does occur in the click reaction when the alkyne reagent is present in excess.[134] Significantly lower levels of non-specific reaction occur when the azide partner is employed in high concentration. Thus, for proteomic analysis of prenylated proteins, it would be advantageous to use isoprenoid analogs that incorporate alkyne functional groups so that subsequent labeling could be performed with the more selective azide-containing reagent present in excess.

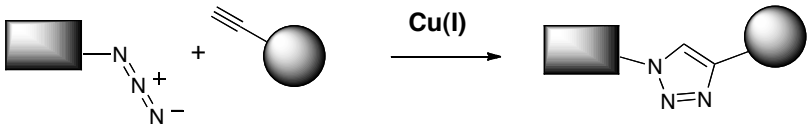

Figure 2.1. Cu(I)-catalyzed click reaction between and alkyne and an azide.

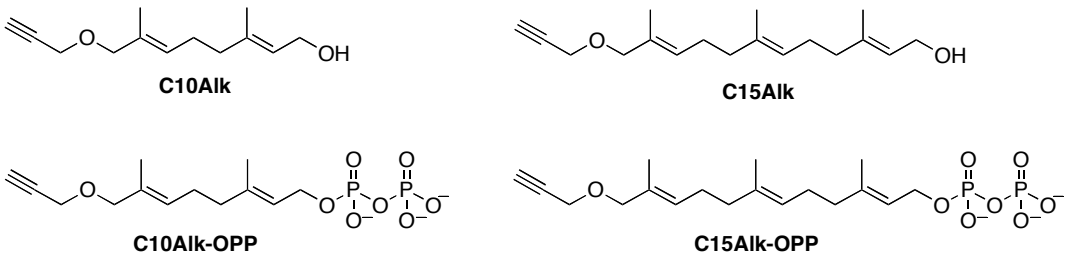

Figure 2.2. Structures of alkyne-modified isoprenoid analogs

In 2007, our group reported the synthesis of alkyne-containing analogs C10Alk-OPP[81] and C15Alk-OPP[82] (Figure 2.2) and demonstrated that C10Alk was an alternative substrate for FTase while C15Alk-OPP was an alternative substrate for both FTase and GGTase-I; related alkyne-containing analogs have also been reported by other groups[112, 135]. In light of their potentially greater specificity, we decided to investigate the utility of our alkyne-functionalized analogs for proteomics applications. Here, we explore the use of these probes as reporters of protein prenylation in the presence or absence of a HMG-CoA reductase inhibitor.

2.2. Research objectives

The goal of this study was to utilize alkyne-modified isoprenoid analogs for metabolic labeling of the prenylated proteins in mammalian cells, and subsequently use in-gel fluorescence analysis for evaluating the incorporation of these analogs.

2.3. Results and discussion

2.3.1. Evaluation of C10Alk and C15Alk for metabolic labeling of prenylated proteins

To examine the utility of alkyne-containing isoprenoid analogs, utilized an in-gel fluorescence strategy depicted in Figure 2.3. HeLa cells were treated with the

alcohol forms (unphosphorylated forms) of the C10Alk or the C15Alk probes (Figure 2.2) in the presence of lovastatin to suppress the production of endogenous FPP and GGPP for 24 h. The resulting cells were then lysed and treated with excess azido-fluorophore (TAMRA-azide, Figure 2.3) via the Cu(I)-catalyzed click reaction (Figure 2.1). Separation of the proteins was accomplished by SDS-PAGE, and the labeled proteins were visualized by in-gel fluorescence. The labeling of specific proteins in the crude cell lysate obtained with these compounds is shown in Figure 2.4. First, it should be noted that significant labeling was observed with both the probes indicating that alkyne-containing isoprenoid analogs are incorporated into proteins. While similar incorporation has been demonstrated before for related azide-based probes, this is the first reported example for the incorporation of alkyne-containing isoprenoid analogs in live cells; the fact that these molecules become incorporated indicates that the alcohols must be effectively phosphorylated to the corresponding diphosphates to convert them into substrates for the protein prenyltransferases. Remarkably, lysate not treated with isoprenoid analogs and reacted with excess TAMRA-azide shows virtually no background labeling.

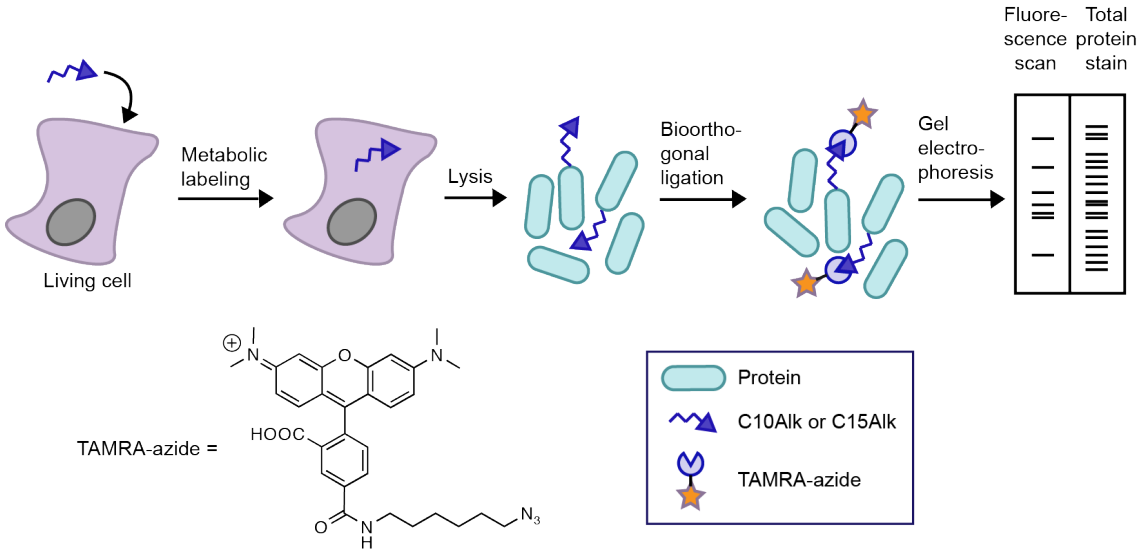

Figure 2.3. Scheme showing workflow for in-gel fluorescence analysis.

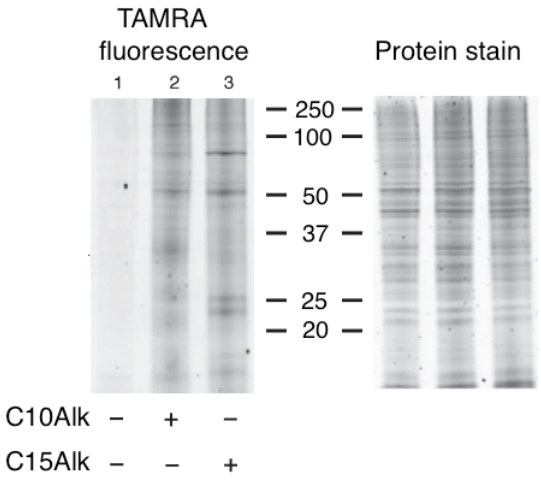

Figure 2.4. Analysis of labeled proteins in crude HeLa cell lysates by Cu(I)-catalyzed click chemistry. HeLa cells were treated with 50 μM C10Alk or C15Alk for 24 h. Cell were lysed and lysates were subjected to click reaction with 100 μM TAMRA-N_3. Proteins were separated on a 12% polyacrylamide and scanned for TAMRA fluorescence.

2.3.2. Incorporation of C10Alk and C15Alk into prenylated proteins in the absence of an inhibitor of isoprenoid biosynthesis

Proteomic experiments employing isoprenoid analogs have often been performed in the presence of lovastatin, an inhibitor of HMGCoA reductase. This reduces the level of endogenous FPP and hence increases the incorporation efficiency of the desired analogue. However, to use alkyne-based probes C10Alk and C15Alk to monitor real changes that occur in the presence of various inhibitors and drugs, it would be preferable to avoid the perturbing effects of simultaneous treatment with lovastatin. Accordingly, the effect of lovastatin on the incorporation of C10Alk and C15Alk was evaluated by growing HeLa cells in media containing the 50 μM of alkyne probes in the absence or presence of 25 μM of lovastatin. Cells were cultured, lysed, reacted with TAMRA-azide, analyzed by SDS-PAGE, and the results are presented in Figure 2.5. For C10Alk, comparison of lane 1 (without lovastatin) with lane 2 (with lovastatin) shows only a small increase in the labeling pattern. Similar results were observed with C15Alk (compare lanes 3 and 4). In total, these experiments suggest that both the alkyne-modified analogs can be efficiently incorporated even in the absence of lovastatin.

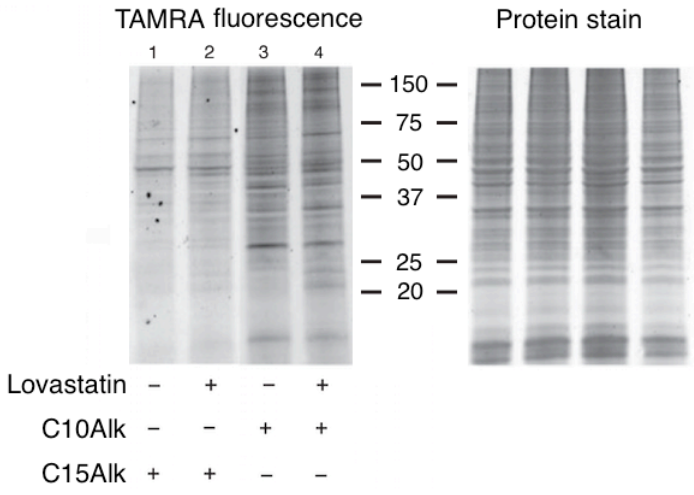

Figure 2.5. Analysis of labeling in absence of lovastatin. HeLa cells were treated with 50 μM C10Alk or C15Alk for 24 h. Cell were lysed and lysates were subjected to click reaction with 100 μM TAMRA-N_3. Proteins were separated on a 12% polyacrylamide and scanned for TAMRA fluorescence.

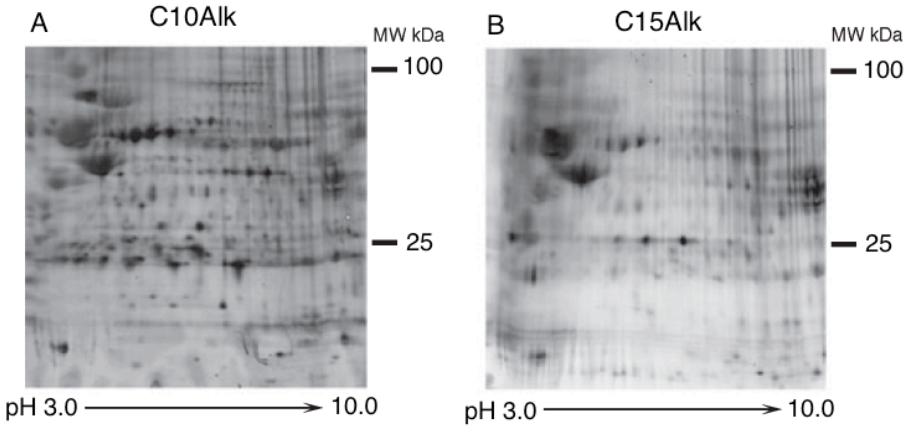

Figure 2.6. In-gel fluorescence analysis of prenylated proteins from HeLa cells after 2D electrophoretic separation: A: Two-dimensional gel of labeled proteins obtained from HeLa cells grown in the presence of C10Alk. B: Two-dimensional gel of labeled proteins obtained from HeLa cells grown in the presence of C15Alk.

2.3.3. Identification of prenylated proteins from HeLa cells via 2D electrophoresis and tandem mass spectrometry

While azide-based probes have been previously used to label and identify specific prenylated proteins, to date, alkyne-based isoprenoid analogs have not been employed for this purpose. Such studies provide a broad overview of the protein prenylome and a qualitative look as to which proteins are affected by prenyltransferase inhibitors. Thus, to examine the utility of these molecules for the profiling and identification of specific prenylated polypeptides, HeLa cells were grown in the presence of 50 μM C10Alk or 50 μM C15Alk for 24 h. After cell disruption in the presence of detergent, the resulting lysate was reacted with TAMRA-azide followed by fractionation by 2D electrophoresis and visualization of the labeled prenylated proteins by in-gel fluorescence scanning. Examination of the images from those gels (Figure 2.6) reveals a large number of labeled proteins of varying intensity.

To identify a subset of the labeled proteins, 20 spots from the 2D gel shown in Figure 2.6A were excised and subjected to in-gel tryptic digestion. Following concentration and desalting, the resulting peptides were then analyzed by LC-MS/MS to obtain peptide sequence information. From those 20 samples, seven proteins were identified (Table 2.1.) with a confidence level of >99%. Several additional proteins were identified at lower confidence levels.

Table 2.1. Summary of proteins identified via proteomic analysis with C10Alk probe

Protein	Accession number	C-terminal sequence	Number of peptides	Sequence coverage (%)
GNBP	gi 5729850 ref NP_006487.1	CGLY	3	7
Lamin B1	gi 5031877 ref NP_005564.1	CAIM	10	19
Rab 1B	gi 13569962 ref NP_112243.1	GGCC	8	38
Rab 2A	gi 4506365 ref NP_002856.1	GGCC	3	16
Rab 6A	gi 38679888 ref NP_942599.1	GCSC	4	24
Rab 7	gi 34147513 ref NP_004628.4	SCSC	3	15
Annexin A3	gi 4826643 ref NP_005130.1	CGGDD	6	19

Of the seven proteins identified here, one, GNBP, has not been previously labeled using azide-based probes, although it has been determined to be a *bona fide* FTase substrate based on an *in vitro* biochemical evaluation.[39] Five of the seven labeled proteins observed here have been previously detected in experiments employing azide-modified FPP and GGPP analogs. Interestingly, Lamin B1 was labeled with an analog of FPP, while the various Rab proteins were all detected with the larger GGPP-based. In contrast, in the experiment reported here, all of these proteins were visualized in cells treated with C10Alk. This may result from the phosphorylated form of the C10Alk acting as an alternative substrate for farnesyl- or geranylgeranyl synthase or GGTase-II (the enzyme that normally prenylates Rab proteins). The seventh protein identified here was Annexin A3. Interestingly, the closely related protein Annexin A2 was previously identified using the azide-modified FPP analog.[76] However, both of these proteins contain a non-canonical C-terminal sequence that has never been experimentally verified as a substrate for protein prenyltransferases. Moreover, recent results from experiments employing an antibody-based approach for the detection of prenylated proteins suggested that annexin proteins are not substrates for prenylation.[133] Evidently, more work is required to address this issue.

2.4. Conclusions

In an effort to develop improved probes that can be used for chemical proteomic experiments, alkyne-containing analogs of isoprenoid diphosphates C10Alk and C15Alk have been studied here. These analogs readily penetrate mammalian cells in culture and become incorporated into proteins that are normally prenylated. Derivatization via Cu(I)-catalyzed click reaction with a fluorescent azide reagent allows the proteins to be visualized and their relative levels to be analyzed. Two-dimensional electrophoretic separation of these labeled proteins followed by mass spectrometric analysis allowed several labeled proteins to be unambiguously identified. These results demonstrate the utility of alkyne-containing isoprenoid analogs for chemical proteomic applications and show that they complement the existing repertoire of probes developed to investigate the function of hydrophobic post-translational modifications.[136, 137]

2.5. Methods

Materials

Protease inhibitor cocktail and benzonase were purchased from Sigma Aldrich (St. Louis, MO, USA). ProteoExtract protein precipitation kit was obtained from Calbiochem (EMD Chemicals, Gibbstown, NJ, USA). TAMRA-azide was purchased from Invitrogen (Carlsbad, CA, USA). Detergent-compatible protein

assay reagents and Tris–HCl sodium dodecylsulfate polyacrylamide gel electrophoresis (SDS-PAGE) Protean II Ready gels were obtained from Bio-Rad (Hercules, CA, USA). Immobline Dry-Strips and ampholyte buffer were purchased from GE Healthcare (Piscataway, NJ, USA). One-dimensional gels were visualized using a BioRad FX Molecular Imager. Two-dimensional electrophoresis was performed using an Ettan IPGphor IEF apparatus and the resulting fluorescent spots visualized using a Typhoon 8610 scanner, both obtained from GE Healthcare. Fluorescent spots were picked using an Investigator ProPic instrument (Genomic Solutions, Ann Arbor, MI, USA). The Paradigm Platinum Peptide Nanotrap precolumn and Magic C18 AQ RP column were purchased from Michrom Bioresources (Auburn, CA, USA). LC–MS /MS analysis was performed using Paradigm 2D capillary LC system (Michrom Bioresources) interfaced with a linear ion trap spectrometer (LTQ, Thermo Scientific, Waltham, MA, USA). For data analysis, Sequest embedded in BioWorks Browser (v 3.3) was obtained from Thermo Scientific and Scaffold (v_2_00_03) was licensed from PROTEOME Software (Portland, OR, USA). Large-scale (1 L) growth of HeLa cell was performed by Biovest International Inc. / NCCC (Minneapolis, MN, USA). Compounds C0Alk and C15Alk were prepared as previously described.[81, 82]

2.5.1. Cell treatments and lysis

HeLa cells were routinely cultured in Dulbecco's modified Eagle's medium (DMEM) supplemented with 10% fetal bovine serum (FBS). For labeling experiments, cell media (40–50% confluence) were supplemented with 25 μM lovastatin, and 50 μM C10Alk or C15Alk. The cells were allowed to reach 80–90% confluence (approximately 24 h) and then washed with phosphate-buffered saline (PBS). Cells were then suspended in PBS, placed in 1.5-mL microcentrifuge tubes, and pelleted by centrifugation at 2000 x g, 4 °C, for 5 min. After discarding the supernatant, a PBS solution containing 0.10% SDS, 0.20% Triton X-100, protease inhibitor cocktail, benzonase, and 2.4 μM PMSF was added to the cell pellet. After vigorous vortexing, cell lysate was harvested by sonicating 4 times for 10 s each with 20 s intervals between sonication cycles. The concentration of protein in the lysate was determined using a detergent-compatible protein assay reagent kit.

2.5.2. In-gel fluorescence analysis

To 100 μg (0.83 mg/mL) of HeLa lysate protein was added 50 μM TAMRA-azide, 50 mM TCEP, and 100 μM tris[(1-benzyl-1H-1,2,3-triazol-4-yl)methyl] amine (TBTA). After vortexing, 1.0 mM $CuSO_4$ was added, and the reaction was allowed to proceed at RT for 1 h. Excess reagents were removed by protein precipitation with a ProteoExtract protein precipitation kit. Protein pellets were suspended in

1x Laemmli SDS-PAGE loading buffer and sonicated in a water bath for 20 min to insure dissolution. A 12% acrylamide gel was loaded with 15 μg of protein for in-gel fluorescence scanning and visualized on a BioRad FX Molecular Imager.

2.5.3. Two-dimensional gel electrophoresis

Two-dimensional gel electrophoresis was performed at the Center for Mass Spectrometry and Proteomics, University of Minnesota, Twin Cities using a standard procedure.[138] In brief, the protein pellet was resuspended in IPG running buffer [7.0 M urea, 2.0 M thiourea, 2.0% CHAPS, bromophenol blue, 0.50% (v/v) ampholyte buffer, 1.0% n-dodecyl β-*D*-maltoside, and 12 mM dithiothreitol (DTT)]. Samples containing 800 μg of protein were rehydrated into 18 cm pH 3–10 Immobline DryStrips overnight under low current and resolved in an Ettan IPGphor IEF apparatus per manufacturer's protocol. Strips were then equilibrated in SDS equilibration buffer (50 mM Tris, pH 8.8, 8.0 M urea, 30% glycerol (v/v), 4.0% SDS, 1.0% DTT) for 0.5 h and resolved on 8–16% Tris–HCl SDSPAGE Protean II Ready gels. TAMRA labeled proteins on the gel were visualized with Typhoon 8610 scanner using an excitation wavelength of 532 nm and a 580BP30 emission filter (580 nm). Gel images were imported into a Genomic Solutions Investigator Pro-Pic instrument for robotic excision and robotic trypsin digestion of excised spots. Tryptic peptides were then lyophilized and stored at -20 °C prior to subsequent use.

2.5.4. MS analysis of protein spots

LC-MS analysis was performed using a Michrom Bioresources Paradigm 2D capillary LC system interfaced with a linear ion trap spectrometer using a standard procedure.[138] Lyophilized tryptic peptides dissolved in water/CH_3CN/formic acid (95:5:0.1) were desalted and concentrated with a Paradigm Platinum Peptide Nanotrap (Michrom Bioresources) precolumn and eluted onto a Magic C18 AQ RP column at a flow rate of approximately 250 nL/min. A 60-min (10–40% CH_3CN) linear gradient was used to separate the peptides. The peptides were ionized with a voltage of 2.0 kV applied distally on the column and analyzed on the LTQ instrument set to positive polarity and data-dependent acquisition method (one survey MS scan followed by MS/MS (relative collision energy of 35%) on the four most abundant ions detected in the survey scan). Dynamic exclusion was employed for 30-second time intervals.

2.5.5. Database searching and protein identification

The MS/MS data were searched with Sequest embedded in Bio-Works Browser (v 3.3, Thermo Scientific) against the database of human, mouse, and rat [NCBI (http://www.ncbi.nlm.nih.gov)] nonredundant protein sequences, in addition to 179 common contaminant proteins (Thermo Scientific), for a total of 263 677 proteins. Fragment ion mass tolerance and parent ion tolerance were set at 1.00 Da. The search parameters were as follows: trypsin digestion, fixed

carbamidomethyl modification of cysteine, and variable oxidation of methionine, three missed trypsin cleavage sites allowed. The dta/out files generated by Bioworks were analyzed in Scaffold (v_2_00_03, PROTEOME Software) to validate MS/MS-based peptide and protein identifications. Peptide identifications were accepted if they could be established at >95.0% probability as specified by the Peptide Prophet algorithm. Protein identifications were accepted if they could be established at >99.0% probability by the Protein Prophet algorithm and contained at least three identified peptides.

2.6. Acknowledgements

I would like to thank the following people for their contribution to this work:

Amanda DeGraw (Department of Chemistry, University of Minnesota) - Optimized conditions for various steps involved in the in-gel fluorescence technique. Figure 2.4 Figure 2.6A were prepared using the data she acquired.

Joshua D. Ochocki (Department of Chemistry, University of Minnesota) - Cultured HeLa cells and treated them with C10Alk and C15Alk.

Todd W. Markowski (Center for Mass Spectrometry and Proteomics) - Ran 2D gels, performed spot excision, in-gel tryptic digestion, MS/MS analysis of proteomic samples.

Chapter 3 Identification of prenylated protein in response to a farnesyltransferase inhibitor using differential gel electrophoresis

[A combination of metabolic labeling and 2D-DIGE analysis in response to a farnesyltransferase inhibitor facilitates the discovery of new prenylated proteins, Charuta C. Palsuledesai, Joshua D. Ochocki, Todd W. Markowski and Mark D. Distefano, *Mol. BioSyst.*, **2014**, *10*, 1094-1103.] - Reproduced by permission of The Royal Society of Chemistry.

3.1. Introduction

Protein prenylation is a post-translational modification, involving covalent attachment of either a farnesyl (15 carbon) or a geranylgeranyl (20 carbon) isoprenoid to Cys residues close to the C-termini of certain proteins. Protein farnesyltransferase (FTase) and protein geranylgeranyltransferase type-I (GGTase-I) catalyze transfer of the corresponding isoprenoid to the Cys residue in the C-terminal CaaX-box motif of proteins (Figure 3.1A), where “C” indicates Cys, “a” is generally an aliphatic amino acid and “X” is a variable residue that roughly determines which isoprenoid becomes attached.[4] Geranylgeranyltransferase type-II (GGTase-II) catalyzes dual geranylgeranylation of Rab proteins possessing sequences with multiple Cys residues (such as CXC, CC), in the presence of Rab escort protein (REP) (Figure

3.1B).[4] There is considerable interest in the process of protein prenylation since prenylated proteins play key roles in the progression of many diseases ranging from cancer and viral infections to aging-related disorders.[34,35,110]

In an effort to detect and identify the prenylated proteome, several analogs of isoprenoid substrates, farnesyl diphosphate (FPP) and geranylgeranyl diphosphate (GGPP), have been synthesized and utilized. In chemical proteomic methods, prenylated proteins are first tagged with functionalized (alkyne,[79,80,88] azide,[76,77] biotin,[132] or anilinogeraniol[133]) isoprenoid analogs by exploiting the promiscuous substrate specificity of prenyltransferase enzymes. Detection of tagged prenylated proteins is achieved via either a bioorthogonal reaction (click reaction, Staudinger ligation) or affinity methods (streptavidin or antibody against anilinogeranyl). Once tagged, the proteins can be identified either by mass spectrometry or western blotting using antibodies against known prenylated proteins. This method has led to the detection and successful identification of a number of farnesylated as well as singly and dually geranylgeranylated proteins.[79-133] However, the number of prenylated proteins identified by these chemical proteomic methods is still much smaller compared to the predicted number of prenylated proteins (less than 100 prenylated proteins identified from several hundred predicted proteins)[139,88].

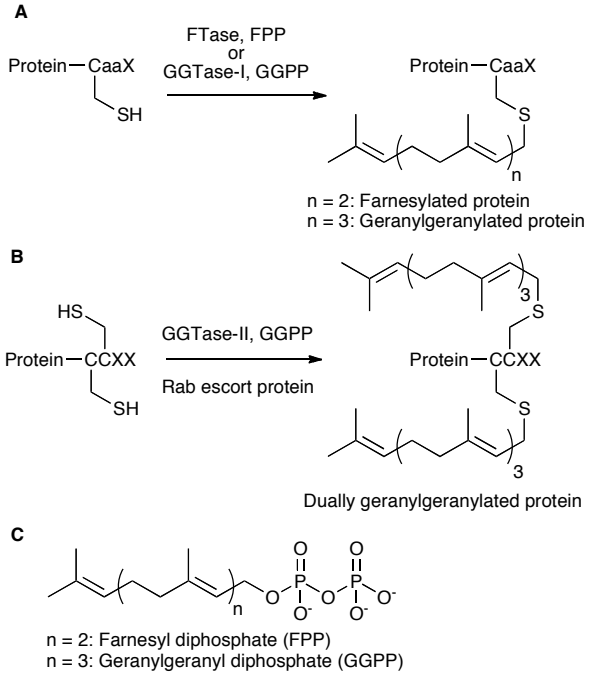

Figure 3.1. An overview of protein prenylation. (A) PFTase and GGTase-I catalyze covalent attachment of farnesyl and geranylgeranyl groups, respectively, to proteins with a CaaX motif. (B) GGTase-II catalyzes dual geranylgeranylation of Rab proteins (with CCXX or CXC motifs) in concert with Rab escort protein. (C) Structures of FPP and GGPP.

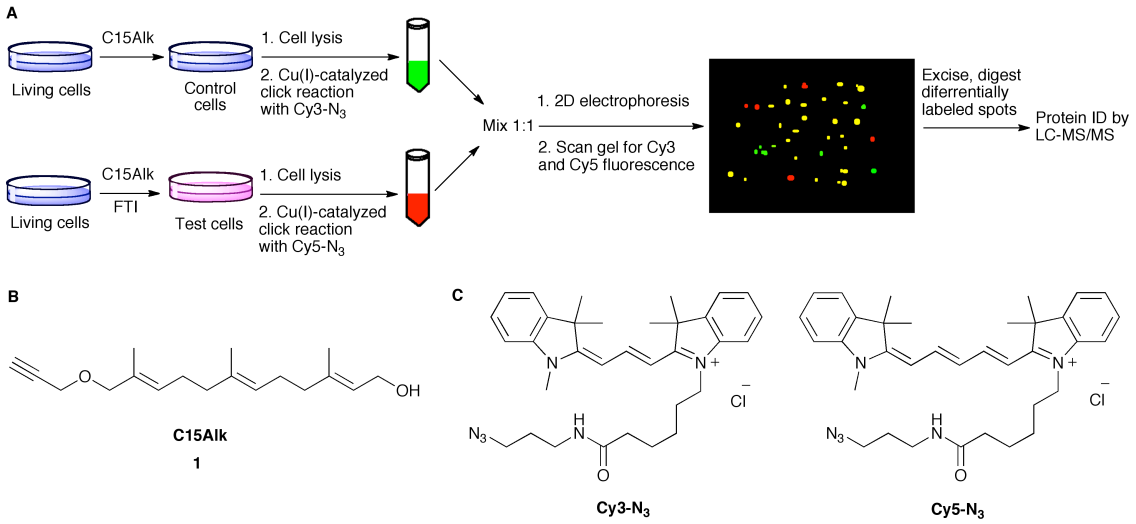

Figure 3.2. An overview of the strategy of combining metabolic labeling with DIGE. (A) Schematic showing metabolic labeling and DIGE workflow; (B) Structure of C15Alk, 1; (C) Structures of Cy3-N_3 and Cy5-N_3.

Several of the above mentioned studies describe efforts to characterize the effects of FTI treatment on the labeling of prenylated proteins with isoprenoid analogs, commonly employing 1D gel electrophoresis to visualize these effects.[79,80,76,132] However, the limited separation of proteins by 1D electrophoresis restricts the use of such a method to monitor changes in prenylation of individual proteins. Nguyen et al. used multidimensional protein identification technology (MudPIT), a mass spectrometry based method, and a ^{15}N-labeled internal standard to quantitate the *in vivo* effects of a GGTase-II inhibitor on prenylated proteins.[132] Onono et al. characterized effects induced by two different FTIs on the farnesylated proteome using 2D electrophoresis and subsequent western blotting.[133] While this latter method is useful for detecting overall changes in the farnesylated proteome using anilinogeraniol and antibodies specific for anilinogeranyl moiety, it requires antibodies against individual known farnesylated proteins to monitor changes in specific proteins. This makes it difficult to identify novel farnesylated proteins that might have altered levels of farnesylation in the presence of an FTI.

Based on the observation that alkyne-modified analogs manifest lower background labeling compared to azide-modified analogs,[134] we previously synthesized alkyne-modified isoprenoids, including C15Alk (**1**), and utilized them for visualizing differences in prenylated proteins in several cell lines, and changes

produced by FTI and an inhibitor of GGTase-I.[79] In that work, alkyne-tagged prenylated proteins were also fractionated using 2D gels and several labeled proteins were identified via mass spectrometry. Charron et al. also used this C15Alk analog for proteomic profiling of prenylation, wherein they identified several previously uncharacterized prenylated proteins along with numerous known prenylated proteins.[80,88] This C15Alk analog is of particular interest because it is accepted as a substrate by all three prenyltransferase enzymes.[79,80] Therefore, it provides a good way to metabolically label and monitor all the prenylated proteins within a cell. This is important considering several FTIs also possess some inhibitory activity against GGTase-I and/or GGTase-II and hence can produce effects beyond inhibition of farnesylation.

Here, we demonstrate the use of a C15Alk in gel-based quantitative proteomic method that combines a metabolic labeling strategy with differential gel electrophoresis (DIGE) to quantitatively characterize the effects of an FTI on the labeling of prenylated proteins. Use of DIGE combines the advantages of greater separation of proteins on a 2D gel and the ability to run and visualize two different samples together on a single gel. Using this strategy and subsequent mass spectrometry analysis, we report the identification of several prenylated proteins suggested to be undergoing changes in prenylation level upon treatment of an FTI. In an effort to validate those results, synthetic peptides derived from

the C-termini of GNAI-1 and GNAI-2 (proteins that have not previously been demonstrated to be prenylated) were prepared and used to confirm that they can be enzymatically prenylated by FTase.

3.2. Results

3.2.1. Overview of combining metabolic labeling with 2D-DIGE

To extend the use of our C15Alk analog for quantitative characterization of effects of FTIs on the prenylated proteome, a workflow was developed and summarized in Figure 3.2A. First, the prenylated proteins are metabolically labeled with C15Alk either in the presence or absence of an FTI. Then the alkyne-modified proteins from the two different samples are individually reacted with Cy3-N_3 or Cy5-N_3 via a Cu(I)-catalyzed click reaction and mixed in equal amounts. Finally, the proteins are separated by 2D gel electrophoresis, and differences in the labeling of proteins in the two samples are characterized by comparing fluorescence intensities of labeled proteins in Cy3 and Cy5 channels of a scanning densitometer.

While typically, Cy dyes used in DIGE are charge and mass-matched, size-matched azide-functionalized Cy dyes are not commercially available. There are two commercially available Cy3-N_3 and Cy5-N_3 dyes (Figure 3.2C), but there is a mass difference of 26 Da between them. Fortunately, Tsolakos et al. have reported that the mass difference of 26 Da between the two Cy dyes they used

did not produce detectable changes in the migration of the labeled proteins.[140] Therefore, we decided to use the commercially available dyes shown in Figure 3.2C in the DIGE experiments reported here. To verify this with the Cy3-N_3 and Cy5-N_3 dyes and to examine the utility of these dyes in the click reaction, HeLa cells were treated with 50 μM C15Alk (**1**) for 24 h in the presence of 25 μM lovastatin, to suppress endogenous production of FPP and GGPP and enhance C15Alk incorporation. Cells were lysed and the lysates were divided into two parts. These two different aliquots were reacted with either Cy3-N_3 or Cy5-N_3, respectively, under Cu(I)-catalyzed click reaction conditions. Equal amounts (based on protein concentration) of the Cy3- and Cy5-labeled proteins were mixed together and separated by 2D gel electrophoresis. Upon scanning the gel for Cy3 and Cy5 fluorescence, successful labeling was observed (Figure 3.3), which resembled our previously reported C15Alk labeling.[79] Analysis (DeCyder software, DIA module) of the Cy3 and Cy5 images showed that more than 96% of the spots had equal intensities in Cy3 and Cy5 channels (Figure 3.3), indicating that the two azide-based dye reagents react with equal efficiency. Also, visual inspection of the gel images did not reveal any differences in the migration of the labeled spots in the overlay image of the Cy3 and Cy5 channels. Overall, these experimental results indicate that proteins labeled with Cy3-N_3 and Cy5-N_3 via click reaction react with equal efficiency and co-migrate on 2D gels

suggesting that this DIGE strategy should be useful for quantifying differences in prenylated proteins resulting from various drug treatments. Note that in this and subsequent 2D-DIGE experiments, equal amounts of Cy3- and Cy5- labeled lysates were mixed together after estimating lysate protein concentration using standard protein assays. Minor differences in loading of the labeled samples as well as fluorescence characteristics of Cy3 and Cy5 get normalized in the Differential In-gel Analysis (DIA) module of the DeCyder software.

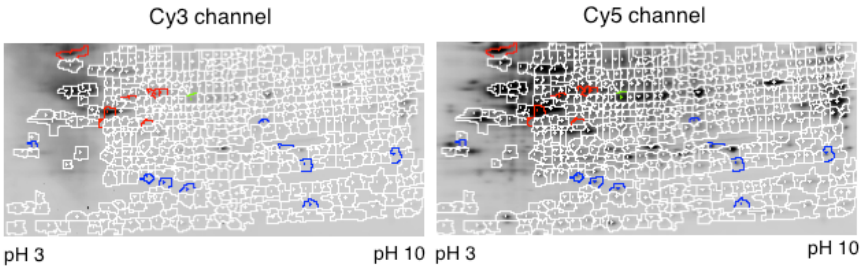

Figure 3.3. 2D-DIGE analysis shows that when identical samples (50 μM C15Alk-treated HeLa cells) are reacted with Cy3-N3 and Cy5-N3 and run together on a 2D gel, the corresponding Cy3- and Cy5-labeled spots co-migrate on the gel. >96% spots were found to have 1:1 ratio.

3.2.2. 2D-DIGE visualizes effects of FTI treatment on C15Alk-labeled prenylome

In order to assess the effects of FTI treatment on the labeling of prenylated proteins, HeLa cells were treated with 50 μM C15Alk in the presence or absence of 10 μM L-744,832, which is a commercially available potent FTase inhibitor.[141] FTI treatment under these conditions did not cause any noticeable toxicity to

HeLa cells, which is consistent with previous report.[142] Lysate of control cells (treated only with C15Alk) was reacted with Cy3-N_3, and lysate of the FTI-treated cells was reacted with Cy5-N_3. 2D-DIGE analysis of the mixed sample and subsequent DeCyder Differential In-gel Analysis detected 504 total spots of which 32 spots showed decreased labeling in the presence of the inhibitor while 23 spots showed an increase in labeling when the inhibitor was present (threshold of 2 model S.D). An overlay image of the fluorescence from the Cy3 and Cy5 channels is given in Figure 3.4 and Figure 3.5, while 3D views of spots showing differential labeling are shown in Figure 3.6 and Table 3.3. Two more replicates of this experiment were run using samples from new sets of cells and reversed labeling of samples with Cy3 and Cy5 dyes. DeCyder Biological Variation Analysis of these three replicates detected 394 spots in at least two of the three gels. 16 spots were detected to have decreased labeling and 17 spots with increased labeling in presence of FTI treatment, with T-test scores less than 0.05.

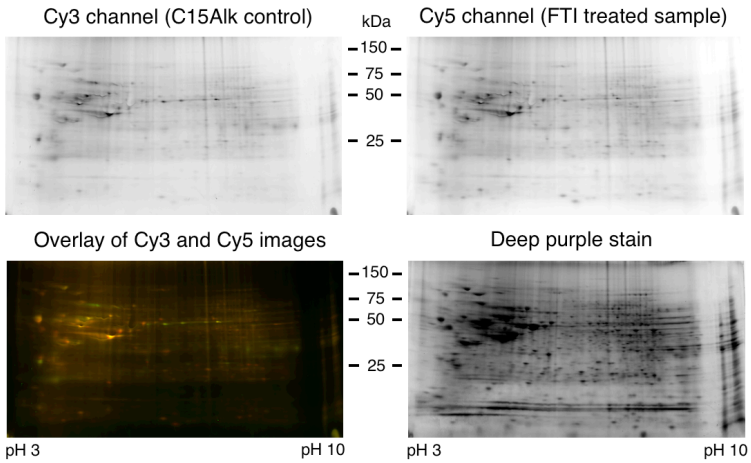

Figure 3.4. Representative gel showing 2D DIGE analysis of samples from FTI-treated HeLa cells. HeLa cells were treated with 50 μM 1 in presence or absence of 10 μM FTI. The lysate of FTI-treated cells was reacted with Cy5-azide while the C15-alkyne treated (control) was reacted with Cy3-azide. After mixing the samples, the proteins were first resolved using a pH 3-10 NL IPG strip and then with a 10-20% polyacrylamide gradient gel.

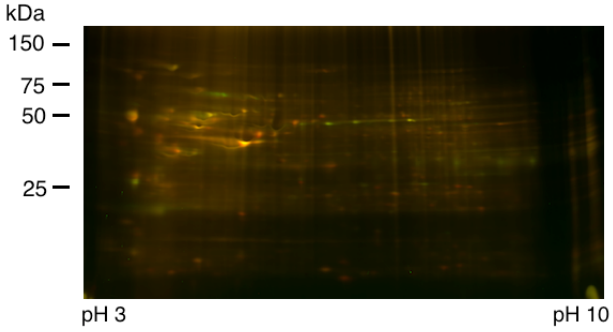

Figure 3.5. Merged 2D-DIGE image of proteins from HeLa cells treated with 50 μM C15Alk in absence (Green, reacted with Cy3-N_3) or presence of 10 μM FTI (Red, reacted with Cy5-N_3). Proteins were first resolved on a pH 3-10 NL IPG strip and then on a 10-20% polyacrylamide gradient gel.

We selected 12 most intense spots (7 with decreased labeling and 5 with increased labeling) from the first gel for excision (Figure 3.7A), tryptic digestion, and LC-MS/MS analysis. Most of these spots were detected in all the replicates of the gel and showed differential labeling with good T-test scores (Table 2.1). A total of 16 proteins containing potential prenylation motifs were identified from those spots and are listed in the Table 3.2. Most of the identified proteins (14) have been reported in previous studies,[88-132] whereas, HisRS and PACN-3, were not previously known or computationally predicted to be prenylated.[143] Interestingly, HisRS contains a LCIC sequence at the C-terminus, which could potentially be processed by GGTase-II. However, it is significantly bigger (57 kD) than Rab proteins (20-25 kDa) normally processed by GGTase-II. The C-terminus sequence of PACN-3 is CVGA, which is reported to be not a good substrate for FTase derived from yeast. In an *in vitro* screening of a peptide library based on CaaX sequences, Wang et al. observed that CVGA sequence was not an efficient substrate for yeast FTase.[49] *In vitro* as well as *in vivo* studies of CaaX variants of a yeast pheromone a-factor performed by Trueblood et al. indicated that a-factor-CVGA had a significant decrease in farnesylation compared to its wt CVIA counterpart.[144] Further studies are required to validate the prenylation status of HisRS and PACN-3 proteins. Unfortunately, we could not identify the C-terminal peptides of these proteins containing the modification

as a direct evidence of prenylation of these proteins, which is in accordance with the previous proteomic studies of protein prenylation. This could be due to the fact that the modified peptide is present in very small abundance and the fragmentation pattern of the modification on Cys is not precisely known. Additionally, many of the prenylated proteins have Lys and Arg residues in close proximity to the prenylated Cys, which results in very short C-terminal tryptic peptides.

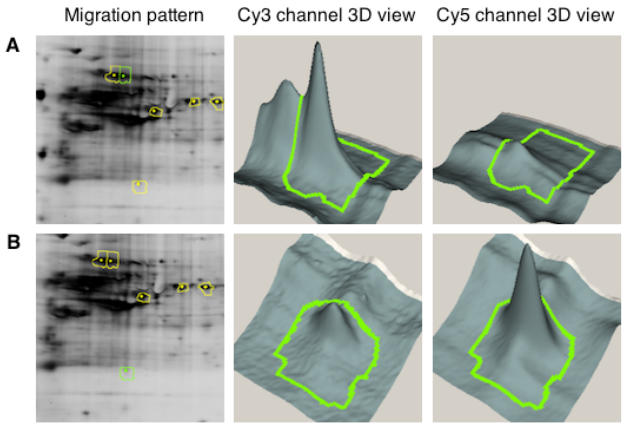

Figure 3.6. Migration pattern and 3D view of representative spots from metabolic labeling and 2D DIGE analysis of prenylated proteins. Left panel: Enlarged view of migration pattern in 2D gel for spots 91 and 473 (green) along with adjacent spots selected for excision and protein identification (yellow). Middle and right panels: 3D view of specified spots in the Cy3 and Cy5 channels, where x and y coordinates indicate the position of the spot on the gel and the z axis (vertical dimension) shows the fluorescence signal intensity in that channel. (A) Spot 91 shows decrease in C15Alk labeling (Cy3 channel) upon FTI treatment (Cy5 channel); (B). Spot 473 shows an increase in C15Alk labeling (Cy3 channel) upon FTI treatment (Cy5 channel).

Table 3.1. List of protein spots used for protein identification from the 2D-DIGE gel comparing C15Alk labeling of HeLa cells in presence or absence of an FTI (Analysis without Triton X-114 fractionation).

Spot number[a]	C15Alk+FTI/C15Alk Ratio in gel used for protein ID[b]	C15Alk+FTI/C15Alk Avg ratio from three gels[c]	T-test score[c]
91	-2.37	-1.97	0.0027
216	-1.53	-	-
265	1.97	1.27	0.33
362	-1.79	-1.71	0.014
414	2.39	2.57	0.0071
473	1.63	1.44	0.074
207	-2.09	-2	0.064
213	-2.77	-2.24	0.023
357	-1.57	-1.49	0.029
418	2.2	1.73	0.12
519	2.47	2.44	0.0000094
408	-1.78	-1.36	0.52

[a] Spot numbers are derived from the DIA analysis performed on the gel used for spot excision. [b] Ratios from DeCyder DIA analysis performed on the Cy3 and Cy5 images of the gel. [c] Values from DeCyder BVA analysis on three biological replicates of 2D-DIGE comparing C15-alkyne labeling in presence and absence of an FTI. A value is not provided for the spot that could not be detected in gels other than the one used for spot excision.

3.2.3. Triton X-114 fractionation of prenylated and non-prenylated proteins prior to DIGE

Many prenylated proteins are present in low abundance.[76] Therefore, it is desirable to enrich them to facilitate their detection via spectrometric methods. This can be achieved using Triton X-114 fractionation, which separates hydrophobic proteins from their more polar counterparts.[145] Previously, it has been established that addition of an isoprenoid increases protein hydrophobicity causing prenylated proteins to partition into the detergent phase.[84] Accordingly, HeLa cells were treated with C15Alk in the presence or absence of FTI, as described above. Cells were then lysed in Triton X-114 containing buffer and subjected to temperature dependent partitioning of the proteins into aqueous and detergent phases. Detergent phase-derived samples were used for click reactions with of Cy3-N_3 and Cy5-N_3 and subsequent separation of proteins via 2D gel electrophoresis.

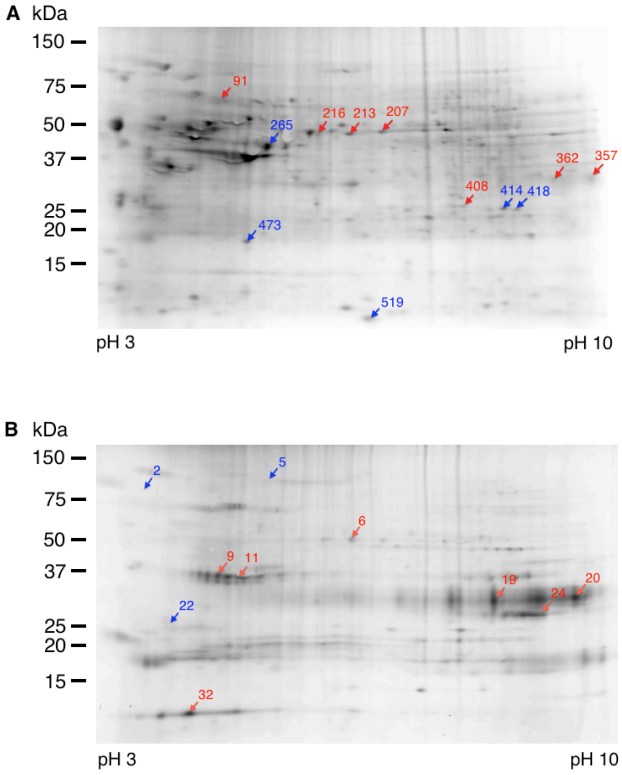

Figure 3.7. Spot maps showing protein spots excised for digestion and mass spectrometric protein identification. HeLa cells were treated with 50 μM 1 in presence or absence of 10 μM FTI. Blue and red arrows point to the spots whose intensities increased and decreased, respectively, in C15Alk labeling upon FTI treatment. (A) Gel image obtained from cell lysates subjected to click reaction and DIGE analysis without prior fractionation; (B) Gel image obtained from cell lysates that were first subjected to Triton X-114 fractionation followed by click reaction and DIGE analysis of the detergent-phase-derived samples.

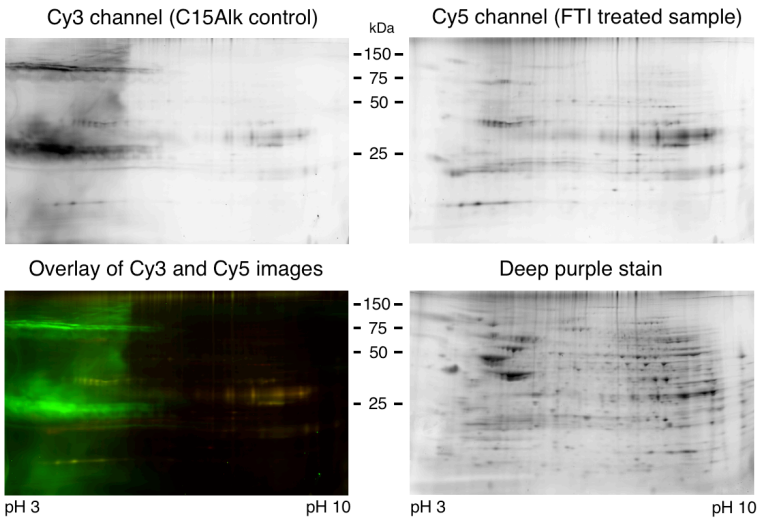

Figure 3.8. DIGE of Triton X-114 fractionated FTI-treated HeLa cells. HeLa cells were treated with 50 μM 1 in presence or absence of 10 μM FTI. Cell lysates were fractionated into aqueous and Triton X-114 phases. Triton X-114 phase of FTI treated cells was reacted with Cy3-N_3 and C15-alkyne treated Triton X-114 phase was reacted with Cy5-N_3. Proteins were first resolved on pH 3-10 NL IPG strip and then on 10-20% polyacrylamide gel.

Interestingly, the pattern of C15Alk-labeled and Triton X-114 fractionated protein (Figure 3.8) spots appeared different than the pattern obtained in the absence of fractionation (Figure 3.4), especially in 50-75 kDa region. DeCyder DIA analysis of Cy3 and Cy5 fluorescence images of the gel detected a total 208 spots, of which 45 spots showed decreases and 63 spots showed an increase in C15Alk labeling in presence of the FTI (threshold of 2 model S.D). We selected 10 spots (6 with decreased labeling and 4 with increased labeling) from this gel for excision (Figure 3.7B), tryptic digestion, and LC-MS/MS. This analysis identified 3 proteins containing potential prenylation motifs listed in

Table 3.2. Interestingly, the proteins GNAI-1 and GNAI-2 were identified for the first time in this study. These proteins have the CaaX-box sequence CGLF at their C-termini, which is computationally not predicted to be prenylated.[143] However, Hougland et al. reported that a short peptide based on this motif, Dansyl-TKCGLF, was accepted as a multiple turnover substrate by FTase.[39] Therefore, we decided to further study prenylation of CGLF motif-containing peptides.

3.2.4. GNAI-1 and GNAI-2 are potential novel prenylated proteins

In order to investigate whether the CGLF motif of GNAI-1 and GNAI-2 proteins can be enzymatically farnesylated, we first synthesized a short peptide, dansyl-GCGLF (Figure 3.9), to determine the kinetic parameters for farnesylation. Using

a previously established dansyl-based continuous fluorescence assay,[146,147] a time-dependent increase in fluorescence was observed suggesting that the peptide is an enzyme substrate. Kinetic analysis performed by varying the concentration of the peptide **2** yielded kinetic constants k_{cat} = 0.107 s^{-1} and K_m = 7.93 μM (Figure 3.10).

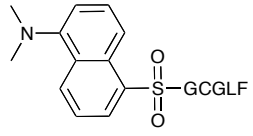

Dansyl-GCGLF
4

Figure 3.9. Structure of dansyl-GCGLF, 4.

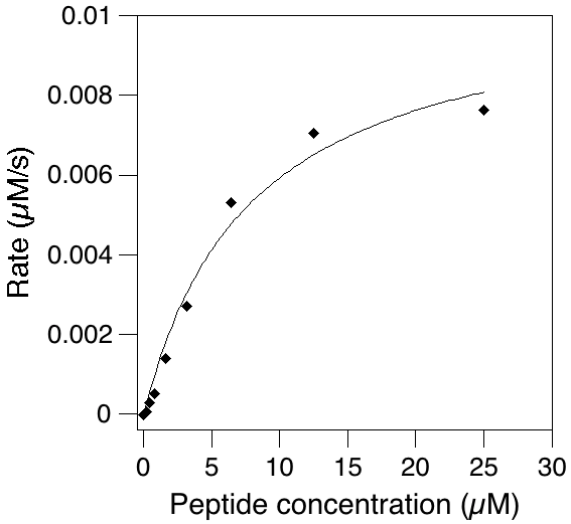

y = m1*x/(m2+x)		
	Value	**Error**
m1	0.010653	9.9177e-4
m2	7.9377	1.7691
Chi sq	1.3938e-6	NA
R	0.99085	NA

Figure 3.10. Continuous fluorescence assay carried out using a peptide concentration range of 0.2-25 μM, 10 μM FPP and 100 nM rPFTase.

Amino acid residues upstream of the CaaX-box are known to affect binding and reactivity in FTase-catalyzed reactions.[148] Therefore, we next synthesized a peptide containing 14 residues from the C-terminus of GNAI-1 and GNAI-2, **2** (Figure 3.11A). Having 10 residues upstream of the CaaX box, this peptide is a better mimic of GNAI-1 and GNAI-2, compared to the shorter peptide dansyl-GCGLF. Peptide **2** was subjected to *in-vitro* mammalian FTase-catalyzed farnesylation with FPP and the crude reaction mixture was analyzed by HPLC and LC-MS to probe for the presence of the farnesylated product. The presence of a new peak in the HPLC chromatogram at 65 min (Figure 3.11B) (with higher retention time in reverse-phase HPLC), indicated the formation of the farnesylated peptide **3**. This was confirmed by detection of ions at *m/z* = 718.70 and 1077.54 via LC-MS analysis (Figure 3.11C) that are consistent with the formation of **3**. Overall, the processing of peptide **2** by FTase suggests that mammalian FTase can accept GNAI-1 and GNAI-2 as substrates.

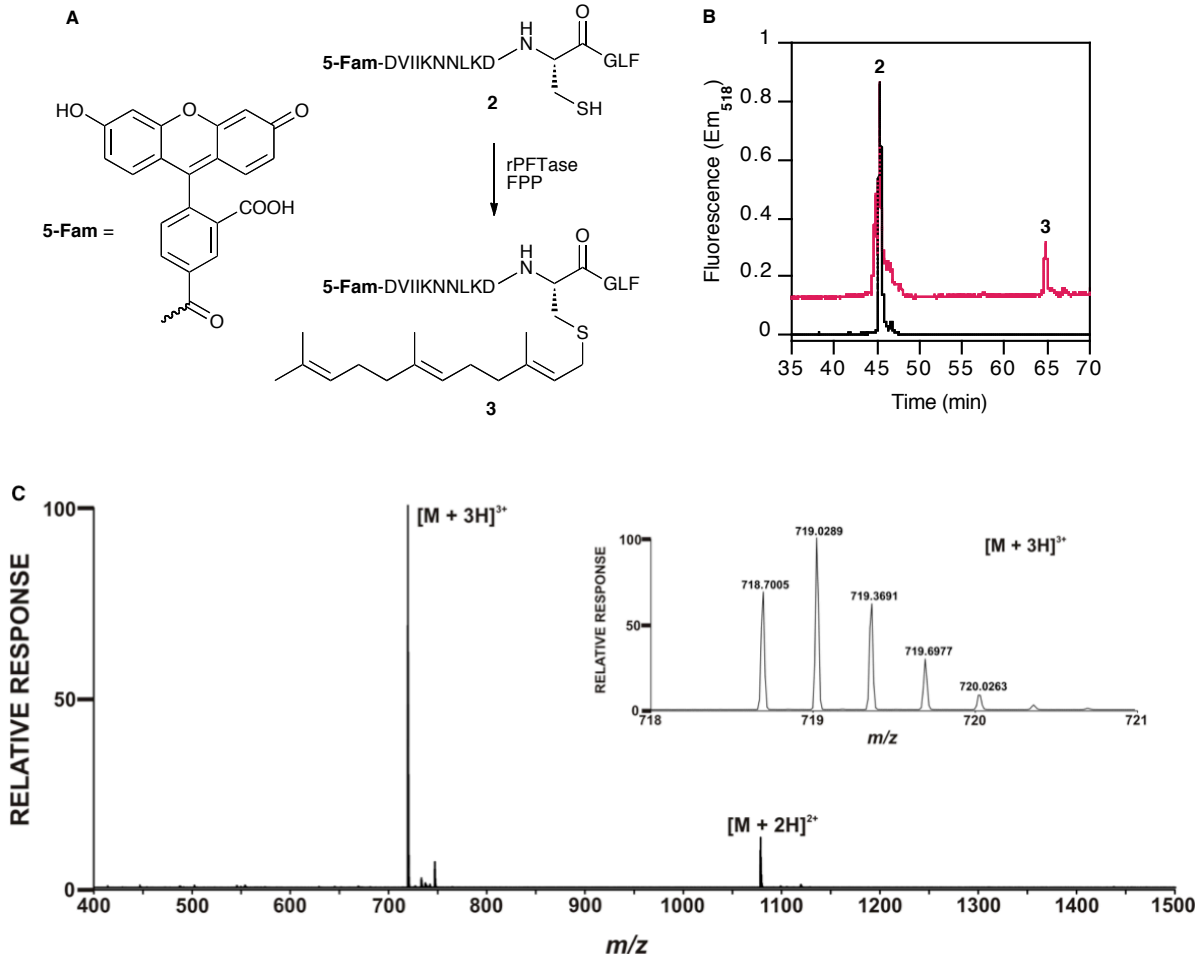

Figure 3.11. Analysis of the farnesylation of a C-terminal peptide derived from GNAI-2. (A) Scheme for rPFTase-catalyzed farnesylation of the peptide, 2; (B) HPLC analysis of peptide 2 before (black) and after farnesylation (red) with rPFTase shows 40% farnesylation of peptide when 2.5 μM peptide 2 was reacted with 10 μM FPP and 100 nM PFTase overnight. (C) Mass spectrum clearly shows the presence of $[M+2H]^{2+}$ (calculated *m/z* = 1077.55, observed *m/z* = 1077.54) and $[M+3H]^{3+}$ (calculated *m/z* = 718.70, observed *m/z* = 718.70) peaks for the farnesylated peptide 3. Inset shows enlarged view of $[M+3H]^{3+}$ peak.

Table 3.2. List of identified proteins containing a possible C-terminal prenylation motif. The upper section of the table lists proteins identified from the whole cell lysate samples, and the bottom section of the table gives proteins identified from the Triton X-114 fractionated samples.

Spot number	Protein	Accession number	Theoretical Mw[a]	Theoretical pI[b]	Number of peptides	% Coverage	C15+FTI/ C15 ratio	Protein identification probability %	Peptides identified[c]	C-terminus	Previously identified in proteomic study[d]
91	Lamin B1	P20700	65961.72	5.11	75	83	-2.37	100	AEHDQLLLNYAK, ALYETELADAR	CAIM	Yes
91	Lamin B2	Q03252	67295.31	5.29	11	22	-2.37	100	EGELTVAQGR, SEVELAAALSDKR	CYVM	Yes
216	HisRS	P12081	57,412.50	5.73	5	13	-1.53	100	ASAELIEEECAK, YDLTVPFAR	LCIC	No
216	PACN-3	Q9UKS6	48,486.70	5.83	3	10	-1.53	100	ADSAVSQEQLR, SPDEVTLTSIVPTR	CVGA	No
362	Lamin A/C	P02545	74139.49	6.57	4	8	-1.79	100	QNGDDPLLTYR, SVGGSGGGSFGDNLVTR	CSIM	Yes
473	Rab 10	P61026	22540.93	8.58	2	11	1.63	100	AFLTLAEDILR, IQIWDTAGQER	SKCC	Yes
473	Rab 1A	P62820	22546.56	5.93	5	41	1.63	100	FADDTYTESYISTIGVDFK, TITSSYYR	GGCC	Yes
473	Rab 22A	Q9UL26	21855.06	8.32	3	29	1.63	100	NAININELFIEISR, GSAAAIIVYDITKEETFSTLK	RSCC	Yes
473	Rab 2A	P61019	23414.36	6.1	4	26	1.63	100	GAAGALLVYDITR, LQIWDTAGQESFR	GGCC	Yes
473	Rab 31	Q13636	21568.78	6.59	4	33	1.63	100	GSAAAVIVYDTITK, NAINIEELFQGISR	RRCC	Yes
473	Rab 7A	P51149	23489.75	6.39	2	13	1.63	100	DPENFPFVVLGNK, EAINVQAFQTIAR	SCSC	Yes
473	Rap 1A	P62834	20647.7	6.39	8	55	1.63	100	LVVLGSGGVGK, SALTVQFVQGIFVEK	CLLL	Yes
473	Cdc42	P60953	21,258.80	6.16	3	20	1.63	100	TPFLLVGTQIDLR, NVFDEAILAALEPPEPK	CVLL	Yes
414	Rab 5A	P20339	23658.68	8.32	3	17	2.39	100	GVDLTEPTQPTR, QASPNIVIALSGNK	CCSN	Yes
414	Rab 5B	P61020	23575.62	8.29	5	33	2.39	100	SEPQNLGGAAGR, GVDLHEQSQQNK	CCSN	Yes
414	Rab 5C	P51148	23482.56	8.64	4	26	2.39	100	GVDLQENNPASR, GAQAAIVVYDITNTDTFAR	CCSN	Yes
11	GNAI-1	P63096	40229.89	5.7	4	14	-10.5	100	LKIDFGDSAR, IAQPNYIPTQQDVLR	CGLF	No
11	GNAI-3	P08754	40401	5.51	6	18	-10.5	100	LKIDFGEAAR, ISQSNYIPTQQDVLR	CGLY	Yes
11	GNAI-2	P04899	40319.71	5.34	7	25	-10.5	100	YDEAASYIQSK, IAQSDYIPTQQDVLR	CGLF	No

[a,b]Theoretical mol wt. and theroretical pI are from ExPasy database. [c]When more than 2 peptides were matched in the MS analysis, 2 representative peptide sequences are listed in the "peptides identified column". [d]Proteins reported by Kho et al.,[76] Nguyen et al.,[132] Chan et al.,[77] Onono et al.,[133] DeGraw et al.,[79] Charron et al.[88]

Table 3.3. Migration pattern and 3D spot view (from DIA analysis) of the spots used for protein identification from the 2D-DIGE gel comparing C15Alk labeling of HeLa cells in presence or absence of an FTI (Analysis without Triton X-114 fractionation).

Spot #	Migration pattern	DIA 3D view
91	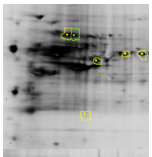	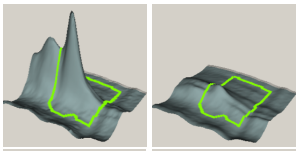
207	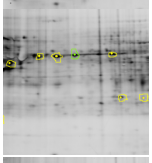	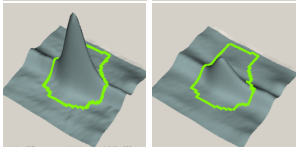
213	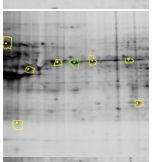	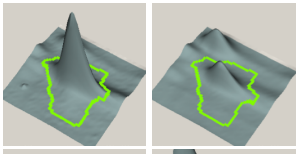
216	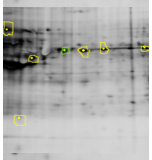	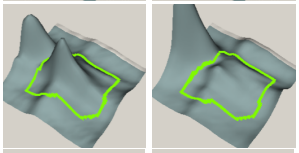
265	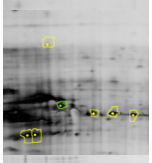	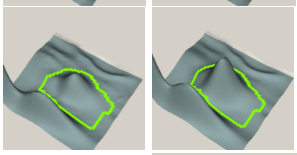
357	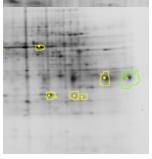	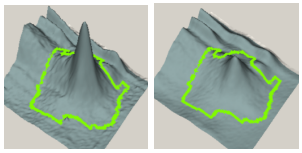
362	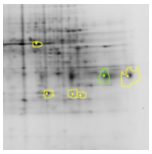	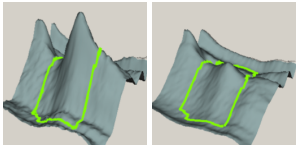
408	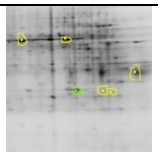	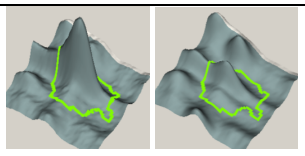

414	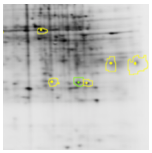	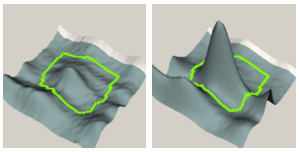
418	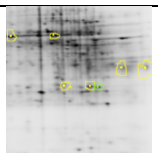	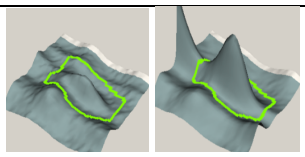
473	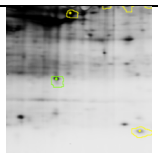	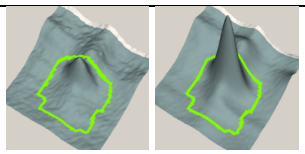
519	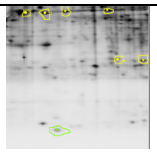	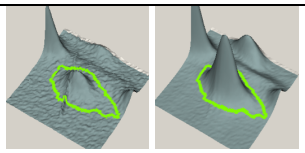

Table 3.4. List of protein spots used for protein identification from the 2D-DIGE gel comparing C15Alk labeling of HeLa cells in presence or absence of an FTI (Analysis with Triton X-114 fractionation).

Spot #	Ratio	Migration pattern	DIA 3D view
2	-93.06	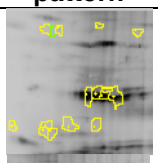	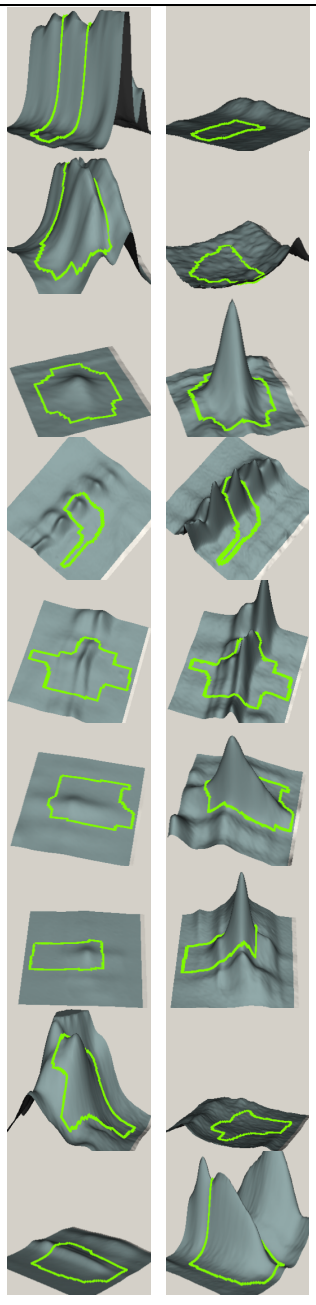
5	-13.18	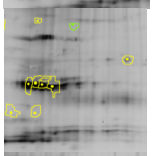	
6	18.78	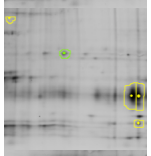	
9	7.96	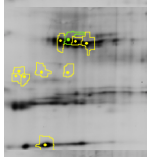	
11	10.50	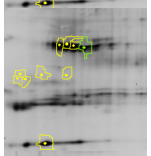	
19	23.97	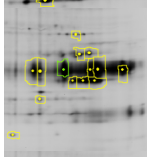	
20	25.82	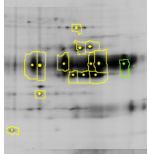	
22	-21.84	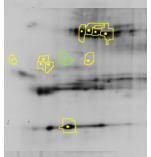	
24	16.36	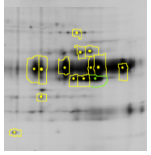	

32	9.12	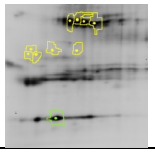	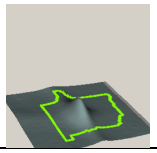	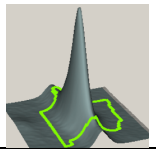

3.3. Discussion

In this study, we describe a strategy for combining metabolic labeling with 2D-DIGE to quantitatively characterize the effects of inhibitors of prenyltransferases on prenylation levels of various proteins. To accomplish this, an alkyne-modified isoprenoid, C15Alk, was employed for metabolic labeling of prenylated proteins in HeLa cells, either in the presence or absence of an FTI. The resulting alkyne-tagged proteins present in these two samples were then conjugated to Cy3-azide and Cy5-azide dyes via Cu(I)-catalyzed click reaction. After mixing equal amounts of the two samples, the proteins were separated via 2D gel electrophoresis and visualized by scanning the gel for Cy3 and Cy5 fluorescence. Fluorescence intensities of a given protein spot in the Cy3 and Cy5 channels correspond to the extent of labeling of the protein with C15Alk in the presence and absence of the FTI. Imaging analysis of the 2D gels using DeCyder software allowed us to identify global changes in the prenylation levels of many proteins that occur in HeLa cells upon treatment with the FTI.

Excision of a subset of the protein spots showing differential labeling in the presence of FTI and subsequent mass spectrometric analysis of these spots identified several prenylated proteins including potentially novel prenylated proteins HisRS, PACN-3, GNAI-1 and GNAI-2 (Table 3.2). We found that FTI treatment decreased labeling of Lamin A/C, Lamin B1 and Lamin B2, which is in

accordance with previous findings. Lamin proteins, components of nuclear lamina, are known FTase substrates and are required for nuclear envelope assembly.[149] Currently, FTIs are being investigated as possible therapeutic agents against Hutchinson-Giford progeria syndrome (HGPS) by inhibiting farnesylation of a mutant form of prelamin A, a precursor to mature lamin A.[149] FTIs are also known to inhibit farnesylation of lamin B1 and lamin B2; however, long-term inhibition of farnesylation of these proteins can have adverse effects of nuclear function.[150] We observed an increase in labeling of several Rab proteins when HeLa cells were treated with the FTI. This is in accordance with the findings by Si et al., that treatment with FTI increased Rab geranylgeranylation in several tissues,[151] and is consistent with the notion that inhibition of farnesylation leads to a larger pool of FPP that can be converted to GGPP resulting in increased geranylgeranylation. FTI treatment was also observed to decrease the labeling of HisRS and PACN-3. These proteins have not been previously reported or predicted to be prenylated, and more analysis is required to establish their prenylation status. We also observed a decrease in labeling of guanine nucleotide-binding proteins GNAI-1, GNAI-2 and GNAI-3 in the presence of FTI. In our previous proteomic analysis of prenylated proteins, we had observed labeling of GNAI-3 with a shorter alkyne-modified FPP analog.[79] In this study, we report GNAI-1 and GNAI-2 as potentially novel substrates of FTase. We show

here that FTase catalyzes *in vitro* farnesylation of a 14 amino acid peptide derived from the C-termini of these proteins. Several protein lacking canonical farnesylation motifs were also identified from some of the protein spots (reported in the supplementary information). One possibility is that these proteins migrate very close to the labeled prenylated proteins on a 2D gel under the conditions used. Alternatively, they could be unanticipated isoprenoid-modified proteins, as observed by Charron et al.[88]

Through the use of 2D-DIGE, we were able to achieve better separation of proteins compared with our earlier work that utilized 1D electrophoresis for detecting labeled prenylated proteins. To further increase the separation, prior pH fractionation and subsequent narrow pH range 2D gel electrophoresis methods could be utilized, as described by Chan et al.[77] The method of DIGE uses mass and charge-matched Cy3- and Cy5- dyes to label two different samples to be compared. This enables multiplexing of the samples on a single gel, eliminating gel-to-gel variations for easy matching of the protein spots from the two samples. In this study, we used Cy3-N_3 and Cy5-N_3, which differ in mass by 26 Da. But this difference causes less than 0.3% difference in Cy3- and Cy5-labeled versions of a protein of a molecular weight of 10 kDa, and is therefore not detectable by gel electrophoresis, consistent with previous reports by Tsolakos et al.[140] Dontsova and co-workers recently reported the synthesis of mass- and

charge-matched Cy3- and Cy5-azide dyes, which can be useful for similar analysis, especially for low molecular weight proteins.[152]

The experiments described here set the stage for future work aimed at identifying improved markers for protein prenylation that may be useful for drug development. In this regard, the alkyne-modified isoprenoid analog used here, C15Alk, has the advantage of being useful for monitoring not only farnesylated but also singly and dually geranylgeranylated proteins, as it is accepted as a substrate by all three prenyltransferase enzymes.[79,80] Overall, the ability to selectively metabolically label prenylated proteins decreases the overall complexity of the samples for analysis and can potentially facilitate the detection of low abundance prenylated proteins that may be relevant top disease.[110] Combining this with 2D DIGE increases resolution and allows facile quantitation of differences due to drug treatment. Such information should be useful for the development of therapeutic strategies based on prenylation inhibition. Moreover, this method could also be applied to studying other post-translation modifications, including S-palmitoylation,[137] N-myristoylation,[137] and glycosylation,[153] which can be studied by similar alkyne-modified reporters.

3.4. Conclusion

In conclusion, we report here a method of combining metabolic labeling of proteins with 2D-DIGE for quantitative detection of the effects of treatment with

FTIs on prenylation levels. This was achieved by using an alkyne-modified isoprenoid analog to tag prenylated proteins, followed by labeling with Cy3-N_3 and Cy5-N_3 dyes via Cu(I)-catalyzed click reaction, and DIGE analysis of labeled proteins. Subsequent mass spectrometry based analysis was used for identification of some of the proteins having altered levels of prenylation, and hence, potential therapeutically significant targets of FTIs. This method could readily be expanded for rapid and comprehensive comparison of the effects of various prenyltransferase inhibitors on prenylation levels of proteins and elucidate differences in the mechanisms of their action.

3.5. Methods

Chemicals and reagents

HeLa cells were generously provided by Dr. Audrey Minden (Department of Chemical Biology, Rutgers University). C15Alk was synthesized as previously described.[154] Cy3-N_3 and Cy5-N_3 were purchased from Lumiprobe. Dulbecco's Modified Eagle Medium (DMEM), fetal bovine serum (FBS), Sypro Ruby protein stain were from Life Technologies. Benzonase (250 units/μL), phenylmethylsulfonyl fluoride (PMSF), protease inhibitor cocktail, Tris(2-carboxyethyl)phosphine (TCEP), tris[(1-benzyl-1H-1,2,3-triazol-4-yl)methyl] amine (TBTA) were purchased from Sigma Aldrich. Detergent Compatible Protein Assay (DC assay), Bradford assay and Criterion™ Tris–HCl gels were obtained

from Bio-Rad. ProteoExtract Protein Precipitation kit and FTI L-744,832 were from Calbiochem. Immobiline™ DryStrips, ampholyte buffer, DeStreak reagent and Deep Purple protein stain solution were purchased from GE Healthcare.

3.5.1. Cell culture and metabolic labeling

HeLa cells were grown in DMEM supplemented with 10% FBS. For metabolic labeling, cell media were supplemented with 50 μM of C15Alk (at 50-70% cell confluence) and cells were grown for 24 h. Where appropriate, 10 μM of FTI was added along with C15Alk into the cell media. After the treatment period, cells were washed twice with ice-cold PBS, suspended in PBS by scraping and pelleted by centrifuging at 1000 x g for 10 min. 200-300 μL of lysis buffer [300 μL PBS containing 0.2% or 1% SDS, 0.64 μL of 1 mM PMSF in ethanol, 0.26 μL of benzonase (250 units/μL) and 5 μL of protease inhibitor cocktail] was added to the pellets and followed by 10 min incubation on ice. Cells were then lysed using a Sonic Dismembrator (Fisher Scientific) at 4 W for 6-10 pulses of 2-10 sec after 20 sec rest periods. The protein concentration in the cell lysate was measured by the DC assay according to the manufacturer's instructions.

3.5.2. Triton X-114 fractionation

Triton X-114 fractionation was performed as previously reported.[145,84,155] Briefly, cells from 100 mm culture plates were lysed in 300-400 μL of 1% Triton X-114 in TBS [50 mM Tris, 150 mM NaCl, pH 7.5] by incubating for 1 h at 4 °C with

rotation. Lysates were centrifuged for 10 min at 10,000 x *g* at 4 °C to remove insoluble debris. An aliquot (~50 μL) of this lysate was stored as total cell lysate. The remaining lysate was subjected to temperature-dependent phase separation by 5 min incubation at 37 °C followed by 10 min centrifugation at 10,000 x *g* at RT. After removal of the aqueous phase (top layer), TBS was added to the detergent phase to reduce the concentration of Triton X-114 to 1%. Cu(I)-catalyzed click reactions of the detergent phase with Cy3- and Cy5-azides were performed as describe below, without estimating the protein concentration. Subsequently, proteins were precipitated by adding 1 volume of 100% trichloroacetic acid (TCA) and 8 volume chilled acetone, and incubating at -20 °C for 1 h. Precipitated proteins were pelleted by centrifugation, and pellets were washed three times with chilled acetone. After resuspending the pellets in IEF rehydration buffer, the protein concentration was estimated using Bradford assay per manufacturer's instructions.

3.5.3. Click reactions

To 50-150 μg (1 mg/mL) of HeLa lysate proteins were added Cy3-N_3 or Cy5-N_3 (final concentration 25 μM), TCEP (final concentration of 1 mM) and TBTA (final concentration of 100 μM). After vortexing, $CuSO_4$ (final concentration of 1 mM) was added and reactions were incubated at RT for 1-2 h, with rotation. Equal quantities of Cy3- and Cy5-labeled proteins were mixed together and

immediately precipitated using a ProteoExtract Protein Precipitation kit to remove excess click reaction reagents.

3.5.4. 2D gel electrophoresis

Protein pellets were resuspended in 250 μL of IEF rehydration buffer [7.0 M urea, 2.0 M thiourea, 2.0% CHAPS, and 1.0% *n*-dodecyl-β-D-maltoside, 12 μM DeStreak reagent, 0.5% v/v ampholyte buffer and 12 mM dithiothreitol (DTT)]. Samples (80 μg protein for Triton X-114-fractionated samples, 125-150 μg protein for other samples) were rehydrated into 13 cm pH 3–10 NL Immobiline™ DryStrips overnight at 30 V for 6 h, 60 V for 7 h, then resolved in an Ettan™ IPGphor™ IEF apparatus per manufacturer's protocol. IEF strips were equilibrated in SDS equilibration buffer (50 mM Tris, pH 8.8, 8.0 M urea, 30% glycerol (v/v), 4.0% SDS, 1.0% DTT) for 0.5 h and resolved on 10-20% polyacrylamide Criterion™ Tris•HCl gels. Cy3- and Cy5-labeled protein spots were visualized with a Typhoon 8610 scanner (GE Healthcare) or a Typhoon FLA 7000 scanner (GE Healthcare). To obtain total protein stain images, gels were stained with either Deep Purple protein stain or Sypro Ruby protein stain and visualized with a Typhoon 8610 scanner or a FX Molecular Imager (Bio-Rad), respectively.

3.5.5. DeCyder analysis

Gel images were cropped with Image Quant v5.2 software (Molecular Dynamics) and imported into DeCyder v5.02 (GE Healthcare) software. Spot detection and quantification of spot intensities (for the gels used for spot excision) was performed using the Differential In-gel Analysis (DIA) module of the DeCyder software, using the double detection algorithm (Cy3 and Cy5 images). The threshold for differential protein labeling to be considered significant was 2 standard deviations. To align and compare spots from three replicates of the FTI-treated samples (without Triton X-114 fractionation), the Biological Variation Analysis (BVA) module was used. The channel pertaining to the C15Alk-treated sample was duplicated and imported as a Cy2 image for normalizing in the BVA analysis.

3.5.6. Spot excision and in-gel tryptic digestion

Gel images were imported into a Genomic Solutions® Investigator ProPicTM instrument (Genomic Solutions, Ann Arbor, MI, USA) for robotic excision. Spots of interest were excised and digested as described by Anderson et al.[138]

3.5.7. MS analysis of protein spots and database search

Lyophilized tryptic peptides were desalted with C_{18} resin according to the "Stage Tip" procedure.[156] Aliquots of ~0.25 µg of total peptide were dissolved in 5.5 µl of

loading solvent (98:2:0.01, H_2O:CH_3CN:HCO_2H) and analyzed using a Velos Orbitrap instrument (Thermo Fisher Scientific) as described previously.[157] The .RAW data files were converted to MzXML format using msconvert (Proteowizard) and then to .MGF files using TINT raw-to-mgf converter. Sequest (version 27) searches were performed against the UniProt *Homo sapiens* (taxon 9606; March 7, 2013 version) database with canonical and isoform sequences (175436 proteins), to which a contaminant database (thegpm.org/crap/index) was appended. Search parameters included variable modifications of methionine oxidation and cysteine iodoacetamide; partial trypsin cleavage (1 missed cleavage); Peptide tolerance 100 ppm, fragment tolerance 0.80 Da; and False Discovery Rate analysis against reversed database.

3.5.8. Synthesis of 5-FAM-DVIIKNNLKDCGLF (2) and Ds-GCGLF (4)

Peptides **2** and **4** (0.05 mmol scale) were synthesized using standard Fmoc solid phase peptide synthesis using an automated peptide synthesizer, following manufacturer's instructions. In brief, Fmoc-Phe-Wang resin (1 eq) was deprotected using piperidine and amino acids (4 eq) were coupled using HCTU (4 eq) and DIEA (1 eq) in DMF solvent. For peptide **4**, 4 eq of Fmoc-dansyl-Gly was used. For peptide **2**, the Fmoc group of the precursor peptide (lacking the 5-FAM group) was deprotected in the automated peptide synthesizer and 5-Carboxyfluorescein (5-Fam) was coupled to it while still on the resin in the

following manner: A solution of 5-FAM-hydroxysuccinimidyl ester (1.1 eq) in 2 mL DMF was added to the peptide on resin. DIEA (2.2 eq) was added and reaction was allowed to proceed overnight on a rotisserie wrapped in aluminum foil. After overnight reaction, resin was treated with 20% piperidine in DMF for 30 min. After washing the resin three times with DMF and three times with CH_2Cl_2, the peptide was cleaved off the resin by treatment with Reagent K for 30 min, precipitated in the presence of Et_2O and pelleted by centrifugation. Pellets of crude peptides **2** and **4** were then dissolved in CH_3OH, and analyzed by HPLC, and purified by preparative HPLC (Buffer A: 0.1% aq TFA, Buffer B: 0.1% TFA in CH_3CN). Purified peptides were analyzed by HPLC and ESI-MS (Figure 3.12, Figure 3.13).

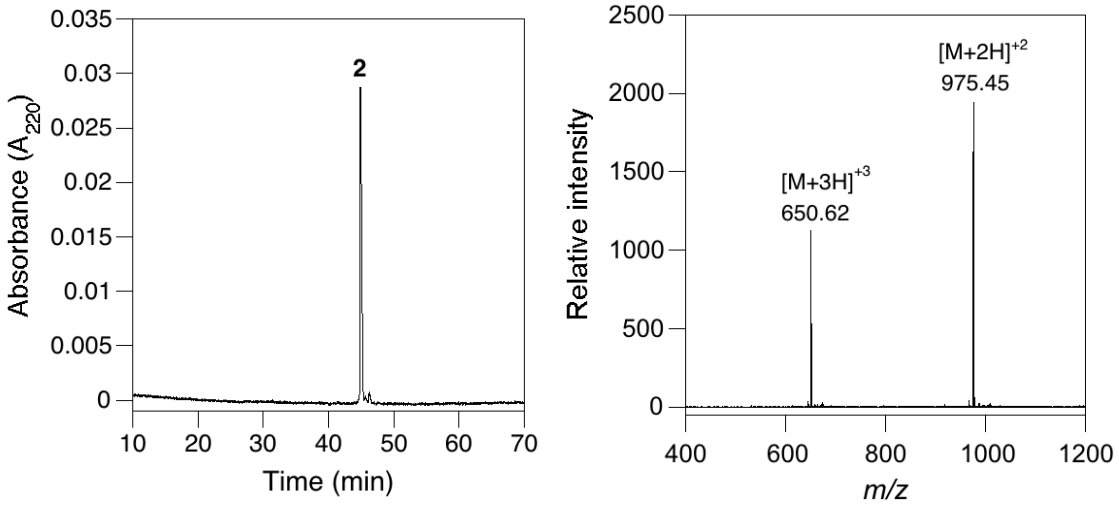

Figure 3.12. Left: HPLC analysis of purified peptide 2 showed 94.5% purity. Right: ESI-MS analysis showed presence of expected peptide. Calculated $[M+2H]^{2+}$ = 975.45, observed $[M+2H]^{2+}$ = 975.43, calculated $[M+3H]^{3+}$ = 650.63, observed $[M+3H]^{3+}$ = 650.62.

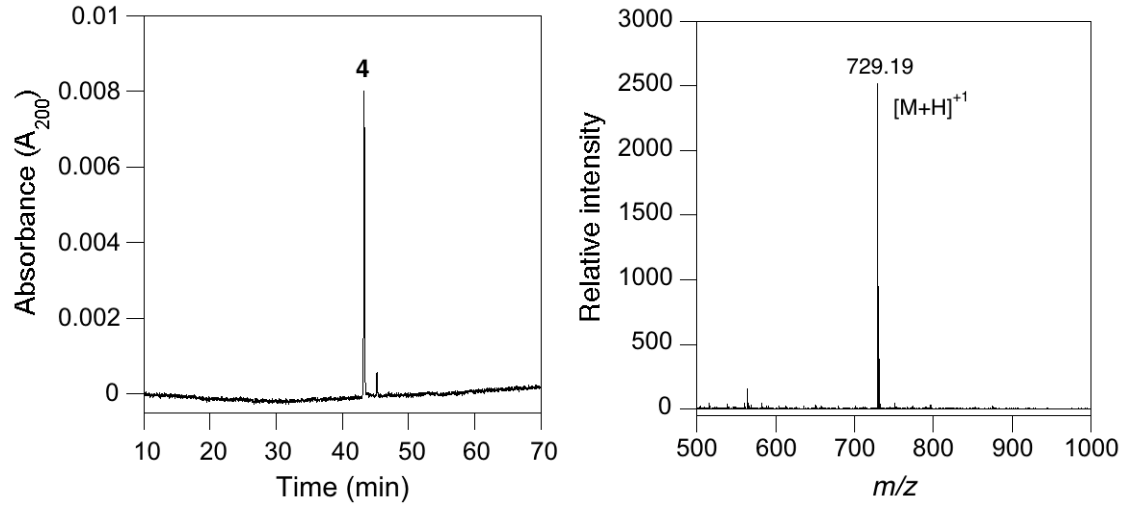

Figure 3.13. Left: HPLC analysis of purified peptide 4 showed 98.5% purity. Right: ESI-MS analysis showed presence of expected peptide. Calculated $[M+H]^{+}$ = 729.27, observed $[M+H]^{+}$ = 729.19.

3.5.9. Enzymatic farnesylation of peptide 2

Enzymatic reactions contained 50 mM Tris, pH 7.4, 25 mM $MgCl_2$, 25 μM $ZnCl_2$, 12.5 mM DTT, 2.5 μM of **2**, 10 μM FPP and 100 nM rat FTase. First, the peptide was incubated with DTT at room temperature for 1 h, in the dark. The reaction was initiated by adding FTase and incubated overnight at room temperature. 100 μL of crude reaction mixture was analyzed by HPLC. For LC-MS analysis, 5 mL of reaction mixture was lyophilized and then resuspended in 250 μL of 20% CH_3CN and 20% MeOH in water. 5 μL of it was analyzed using a Waters Acquity UPLC/Synapt G2 QTOF mass spectrometer.

3.5.10. Continuous fluorescence assay

Assays were performed in 96 well format as described by DeGraw et al.[158] Briefly, the assay solution contained 0.2-25 µM dansyl-GCGLF, and 10 μM FPP in 50 mM Tris, pH 7.5, 5 mM DTT, 5 mM $MgCl_2$, 50 µM $ZnCl_2$, and 0.2 % (*w/v*) *n*-octyl-β-D-glucopyranoside at 25 °C. Peptides were incubated in this buffer for 30 min and the initial fluorescence reading of the dansyl group was recorded (λ_{ex} = 340 nm, λ_{em} = 505 nm) on a DTX880 Multi-mode plate reader (Beckman Coulter). Purified rPFTase was first diluted in a buffer containing BSA (50 mM Tris, pH 7.5, 1 mM DTT, 5 mM $MgCl_2$, 50 µM $ZnCl_2$, 20 μM KCl and 1 mg/mL BSA) and then added to the peptide solution 100 nM concentration to initiate the farnesylation reaction. Fluorescence of dansyl group was measured as a function

of time. The total fluorescence change observed upon reaction completion was divided by the initial concentration of the peptide substrate in a given reaction to yield a conversion from fluorescence units to product concentration (Amp_{conv}). The linear initial rate, V, in fluorescence intensity per minute, was then converted to a velocity (μM product produced per minute) by dividing V with Amp_{conv}.

3.6. Acknowledgements

This work was supported by National Institutes of Health grants GM058842 and GM084152, and a Department of Chemistry Excellence in Graduate Studies fellowship (University of Minnesota). A part of this work was carried out using instruments in the University of Minnesota Center for Mass Spectrometry and Proteomics, and facilities provided by the Minnesota Supercomputing Institute (University of Minnesota). I would like to also acknowledge the following people for their contribution to this work:

Joshua D. Ochocki (Department of Chemistry, University of Minnesota) - Cultured cells and carried out cell treatment with the C15Alk probe and the FTI for some the experiments.

Todd Makrkowski (Center for Mass Spectrometry and Proteomics, University of Minnesota) - Trained me in 2D gel electrophoresis, carried out spot excision, in-gel tryptic digestion, peptide desalting.

LeeAnn Higgins (Center for Mass Spectrometry and Proteomics, University of Minnesota) - Collected MS/MS data for in-gel digested proteomic samples.

Joseph J. Dalluge (Department of Chemistry Mass Spectrometry Laboratory, University of Minnesota) – Acquired LC-MS data for synthetic peptides, assisted in making Figure 3.11.

Chapter 4 Imaging and quantification of the prenylated proteome

4.1. Introduction

As described in Section 1.7, protein prenylation has been the focus of numerous studies since its discovery in the early 1990's because of its connection to cancer, mainly through Ras proteins. Members of the Ras family of proteins are naturally prenylated and mutated forms of Ras, especially K-Ras, are involved in as many as 30% of all human cancers.[159] Inhibition of prenylation using farnesyltransferase inhibitors has been investigated clinically for anti-cancer therapies, with limited success.[160-164] Paradoxically, farnesyltransferase inhibitors have no effect on some patients while they are highly effective in others.[35] These observations underscore the need for better methods of evaluating the cellular and biochemical effects of prenylation inhibitors.[35]

In addition to the cancer association noted above, protein prenylation has also been implicated in other diseases. Recently, changes in isoprenoid metabolism and in the total levels of prenylated proteins have been observed in neurodegenerative diseases like Alzheimer's and Parkinson's disease. For example, the farnesylated protein UCH-L1 is linked to Parkinson's disease and inhibition of farnesylation of this protein has been suggested as a possible therapy for this disease.[165] A potential connection to Alzheimer's disease has been revealed based on the finding that the levels of farnesyl diphosphate (FPP)

and geranylgeranyl diphosphate (GGPP), which are substrates of prenyltransferase enzymes, are elevated in the brains of Alzheimer's patients.[166-168] Furthermore, evidence for the neuroprotective effect of statins on long term potentiation in neurons has recently been attributed to the protein prenylation-dependent molecular pathways downstream of FTase.[169] Importantly, it has also been recently shown that increased prenylation of the RhoA protein leads to progressive neurodegeneration in *Drosophila.*[170]

In spite of the association of protein prenylation with neurodegenerative diseases mentioned above, several studies regarding the implication of inhibition of protein prenylation in such disorders have provided contradicting results. For instance, Hooff and coworkers found that the levels of Aβ abundance did not change upon farnesyltransferase inhibition in an APP695 expressing SH-SY5Y cell line.[171] Several other studies, however, demonstrate that the level of protein prenylation modulates the production of Aβ.[172] For example, Pedrini and coworkers found that use of a farnesyltransferase inhibitor stimulated α-secretase and increased the levels of the α fragment of APP, which precludes the production of Aβ.[173] In several epidemiological and in certain clinical studies, statins have shown some therapeutic benefits in ameliorating the symptoms and pathology of Alzheimer's disease.[174, 175] While there is evidence showing lowering cholesterol favors the above mentioned α-secretase pathway and

decreases Aβ secretion[176], a large number of studies indicate that cholesterol- and Aβ-independent pleiotropic effects of statin are responsible for their beneficial effects in Alzheimer's disease.[174, 175, 177] *In vitro*, acute treatment of mouse brain slices with a statin enhanced long-term potentiation (LTP) in the CA1 region of the hippocampus and LTP enhancement was shown to be caused by FPP depletion and the inhibition of protein farnesylation.[169] *In vivo,* statin treatment to aged beagles, a natural higher mammalian model of Alzheimer's disease, led to antioxidant effects, thereby reducing lipoperoxidation and protein oxidation.[178] Taken together, the studies to date indicate that more work is required to elucidate the cellular mechanisms involved in Alzheimer's disease pathology and the role of protein prenylation in this disease.[179]

One method to study these neurodegenerative diseases and aging phenotypes in a cellular system is to use a model of compromised autophagy. Autophagy is a degradation mechanism for dysfunctional cellular components and aggregated proteins via the lysosome. Autophagy is transcriptionally down-regulated in the brain during normal aging,[180] and dysregulation of autophagy is involved in neurodegenerative diseases including Alzheimer's and Parkinson's disease.[181-183] This is correlated with a decreased abundance of the autophagy-related protein Beclin 1 in the aging human brain.[180] Furthermore, Beclin 1 expression is reduced in early Alzheimer's disease and it is shown to regulate Aβ

accumulation in mice.[182] As more evidence for a connection between autophagy, neurodegenerative disorders, and prenylated proteins emerges, it is crucial to develop tools to better understand precisely what role protein prenylation may play in disease pathology.

Several methods have been recently developed to study various post-translational modifications of proteins using unnatural analogs that exploit metabolic labeling in concert with bioorthogonal chemistry.[137, 184-186] Some of the more commonly studied post-translational modifications (PTMs) studied include glycosylation,[187, 188] palmitoylation,[189-191] myristoylation,[192, 193] and prenylation,[80, 194, 195] which use unnatural substrates to incorporate bioorthogonal functionality onto relevant proteins. These can be derivatized via the 3+2 Huisgen cycloaddition (commonly referred to as Cu(I)-catalyzed click reaction), the strain-promoted alkyne-azide cycloaddition or other bioorthogonal reactions. Despite the numerous reports describing strategies based on metabolic incorporation of unnatural analogs for monitoring PTMs in *ex vivo* cell cultures or animal models, only a small number have ever been reported that allow for the levels of prenylated proteins to be quantified.[196-199]

Historically, the most common method for quantification of prenylated protein levels has been through the use of radioactive assays employing tritiated forms of farnesyl diphosphate, geranylgeranyl diphosphate, or mevalonic acid. Even as

late as 2006, the only method for quantifying prenylated proteins was still a radioactive based assay.[200] The inherent problem with tritium-based radiochemical methods is their low intrinsic sensitivity requiring exposure times as long as several months during autoradiography analysis.[201] In 2009, Nguyen and coworkers developed a mass spectrometry based method to quantify prenylated proteins using an unnatural biotin isoprenoid analog.[132] This approach was able to detect femtomolar levels of prenylated proteins; however, absolute quantitation needed spiking of a ^{15}N labeled protein. Additionally, in order to achieve incorporation of the biotin analog the authors had to perform site directed mutagenesis of FTase and GGTase-I to accept the substrate and thus required the labeling to be performed on cell lysates in lieu of physiologically active cells. Changes in the enzyme binding pocket introduced via site-directed mutagenesis as well as significant perturbation of the isoprenoid substrate structure may result in compensatory changes in protein substrate specificity.[70] Recently, Das and co-workers reported a BODIPY isoprenoid analog, and applied it for flow cytometry and microscopy imaging to analyze its uptake in mammalian cells and zebrafish.[71] While this fluorescent isoprenoid analog provides a direct fluorescence readout, its use is limited to the analysis of the di-geranylgeranylation of Rab proteins. Therefore, methods for quantification and

imaging of overall prenylation (comprising of farnesylation and both forms of geranylgeranylation) in cells are still needed.

Our group and others have previously reported on the development of alkyne isoprenoid analogs[80-82] and employed them in Cu(I)-catalyzed click reactions for identification of prenylated proteins present within cells.[83, 88, 195] Here, we extend the use of one of the alkyne-containing analogs for imaging and quantification of the global prenylome through the use of the click reaction *in situ* (Figure 4.1). This method allows for the localization of prenylated proteins to be visualized, with our results highlighting the distribution of most of the labeled prenylated proteins in the endoplasmic reticulum (ER). Extending the method to flow cytometry, we show quantification of the prenylome in cells is possible and gives similar results as in-gel fluorescence analysis, but represents a more facile and less time-consuming method. The method was applicable to a variety of cell types, including primary astrocytes. Lastly, using a cellular model of compromised autophagy (via siRNA-mediated knockdown of BECN1 gene) as a surrogate to study aging disorders, we show that the levels of prenylated proteins are increased upon autophagy inhibition. This may indicate the potential involvement of protein prenylation in aging disorders such as Alzheimer's and Parkinson's disease, as these diseases have been shown to involve compromised and/or deficient autophagy.[202]

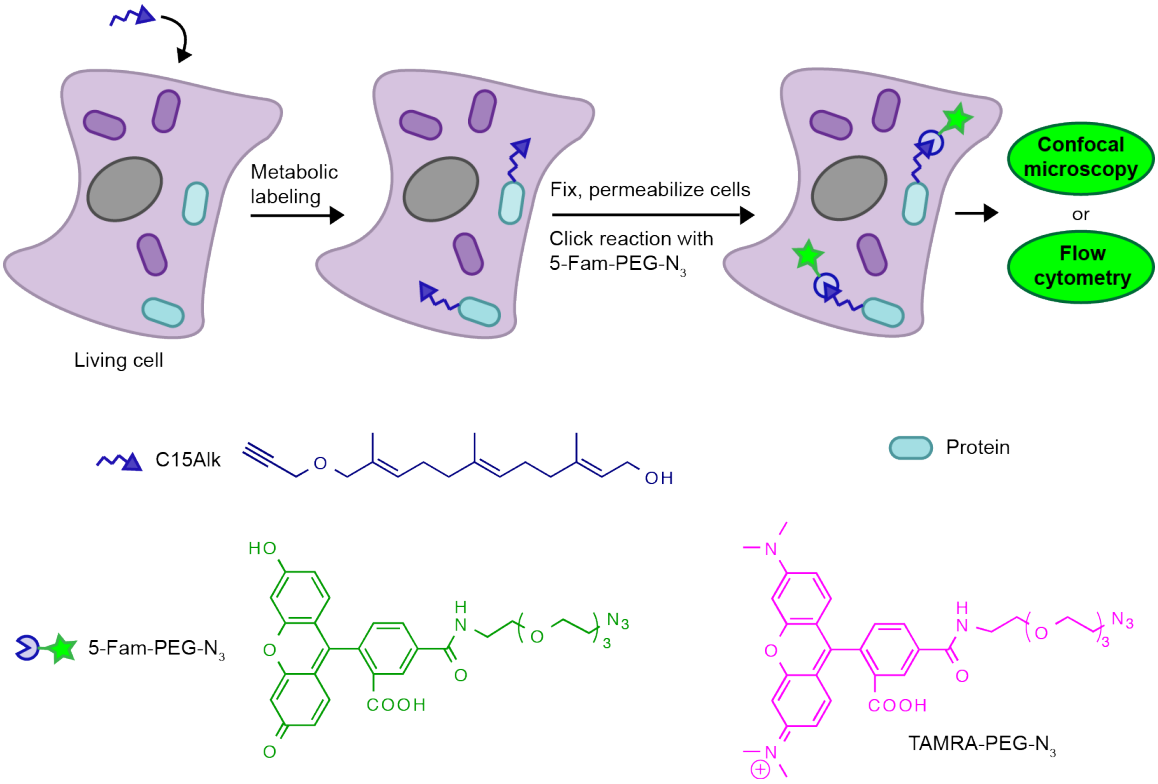

Figure 4.1. Workflow for metabolic incorporation of alkyne-modified isoprenoid analog and subsequent derivatization to a fluorophore for monitoring the global prenylome.

4.2. Research objectives

The aim of this work was to develop a method to quantify the global prenylated proteome by using alkyne-modified isoprenoid analogs. Such methods are expected to enable quantification of total cellular levels of prenylated proteins in different cell types, thereby providing a better understanding of how protein prenylation is modulated in diseases, such as neurodegenerative disorders.

4.3. Results and discussion

4.3.1. Characterization of C15Alk substrate

In our previous work, we established that a diphosphate version of C15Alk (Figure 4.1) is an efficient substrate for yeast FTase and human GGTase using spectrofluorimetric assays.[82] To examine its incorporation efficiency by mammalian FTase, similar experiments were performed using the diphosphate version of C15Alk, as the diphosphate moiety is essential for catalysis. These experiments revealed that C15Alk is a substrate for rat FTase with k_{cat}/K_M value only 3.2-fold lower relative to FPP (Table 4.1, Figure 4.2), indicating that mammalian FTase should readily incorporate it into proteins in living systems.

Table 4.1. Kinetic constants for the rPFTase-catalyzed reaction of FPP and analogues with Ds-GCVLS peptide.

Isoprenoid	k_{cat} (s^{-1})[a]	K_M (μM)[a]	k_{cat}/K_M (rel.)
FPP[b]	0.21 ± 0.01	0.11 ± 0.03	1.0
C15Alk-OPP	0.08 ± 0.004	0.14 ± 0.06	0.31

[a]These values were measured at a single peptide concentration and are hence apparent constants.

[b]These values measured for FPP are comparable to previously published values.[66, 203]

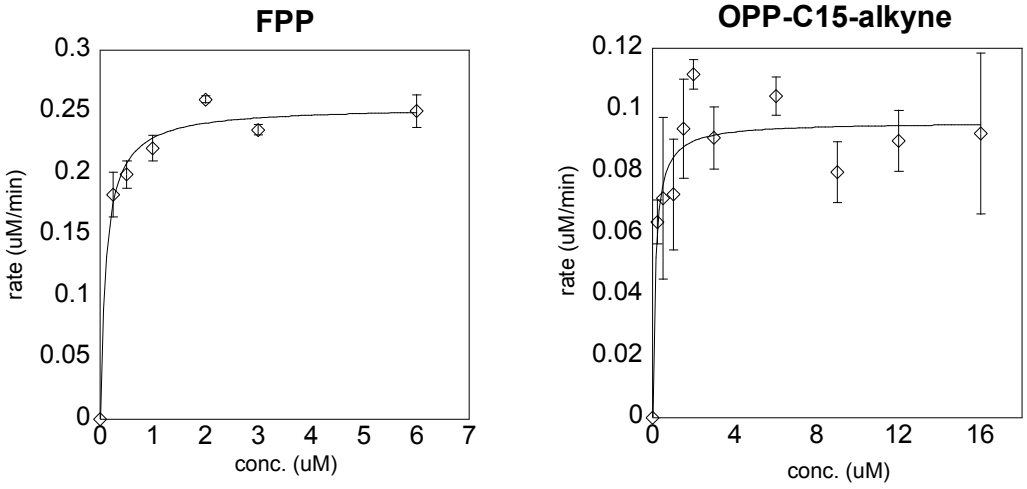

Figure 4.2. Fluorescence-based enzyme assay for prenylation using varying concentrations of FPP and C15Alk-OPP. Experiments were performed using a Varian model Cary Eclipse Fluorescence Spectrophotometer. The fluorescence detector was set at 340 nm and 505 nm for excitation and emission, respectively. Slit widths for excitation and emission were at 10 nm and at 10 nm, respectively.

Next, we sought to determine whether C15Alk could be efficiently incorporated into prenylated proteins in cell culture. For metabolic labeling of cells, we chose to use alcohol form of the analog, which has better cell penetration kinetics compared to the negatively charged diphosphate form. Exogenously provided isoprenols (alcohol forms of isoprenoids) are reported to get converted to corresponding isoprenoid diphosphates inside cells and used for protein prenylation.[204] Consistent with this, our group and others have demonstrated that C15Alk and other unnatural isoprenoid analogs are used incorporated by protein prenyltransferases in mammalian cells.[80, 83, 195] Previous studies have shown that a related isoprenoid azide can be efficiently incorporated into H-Ras, a prototypical farnesylated protein.[76] However, no data was available for the alkyne-modified isoprenoid analogs regarding how well they can get incorporated compared to natural incorporation of FPP. Accordingly, we compared the incorporation of C15Alk and a related analog C10Alk in H-Ras to the incorporation of farnesol, which is a precursor of FPP. COS-1 cells were incubated with lovastatin, an HMG-CoA reductase inhibitor, to deplete the endogenous isoprenoids in the cells. The consequence of this treatment is that prenylated proteins, such as H-Ras, are unable to be processed (prenylated, proteolyzed and methylated) and a shift to unprocessed H-Ras (Figure 4.3, top band 'U') is observed by western blot. Even though a high concentration of

lovastatin was used, the processing of H-Ras could not be completely abolished, but only reduced to approximately 45% of unprocessed protein (Figure 4.3, lane 2), compared to approximately 90% processed under normal conditions (Figure 4.3, lane 1, also Figure S2). When lovastatin was administered in combination with farnesol (FOH), the precursor to the native substrate FPP, H-Ras processing was completely restored (Figure 4.3, lane 3) to the levels seen in the negative control. When giving lovastatin in combination with C10Alk (Figure S2), an analog one isoprenoid unit shorter than the C15Alk, (Figure 4.3, lane 4) or C15Alk (Figure 4.3, lane 5), H-Ras became approximately 60% and 70% processed, respectively (Figure 4.4). This data suggests that while C15Alk cannot completely rescue H-Ras processing, it is incorporated at higher efficiencies than C10Alk in cell culture, at least for H-Ras. Despite being a 3-fold slower substrate compared to FPP (Table 4.1), it is clear that significant amounts of C15Alk gets metabolically incorporated, rendering it suitable for cellular studies of prenylated proteins.

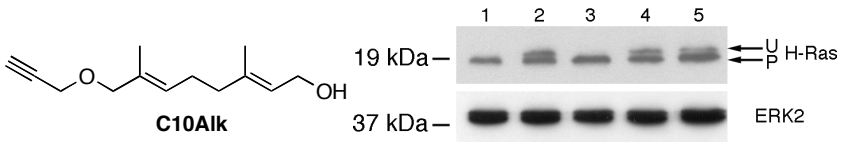

Figure 4.3. Incorporation of C10Alk and C15Alk into H-Ras in COS-1 cells. Left: Structure of C10Alk; Right: COS-1 cells were treated with either DMSO (0.05% v/v, lane 1), 25 μM lovastatin (lane 2), 25 μM lovastatin and 100 μM farnesol (lane 3), 25 μM lovastatin and 100 μM C10Alk (lane 4), or 25 μM lovastatin and 100 μM C15Alk (lane 5). After 24 h, whole cell lysates were prepared and 40 μg of protein was resolved by 15% SDS-PAGE. The proteins were transferred to a PVDF membrane and incubated with an antibody against H-Ras. Note the faster mobility of processed Ras (P) compared with unprocessed Ras (U). Total ERK2 levels were measured as a loading control because they do not change in response to treatment with lovastatin or alkyne isoprenoids.

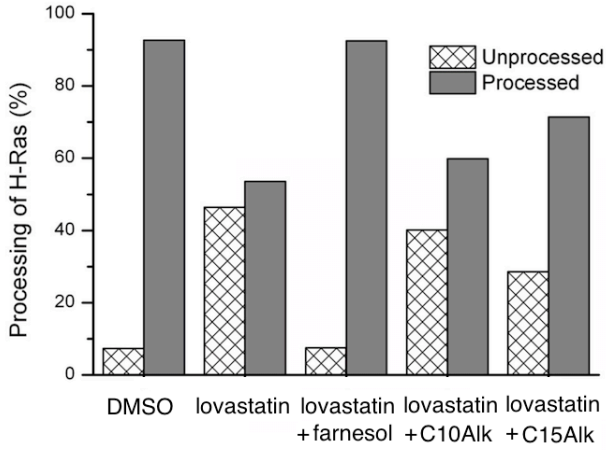

Figure 4.4. Densitometry analysis of western blot bands in Figure 3.3 using ImageJ.

4.3.2. Cellular labeling and visualization of prenylated proteins

After confirming that the alkyne isoprenoids were incorporated into H-Ras, we set out to determine if it was possible to use the click reaction to image the distribution of prenylated proteins in mammalian cells. Upon metabolic incorporation of the alkyne isoprenoid, the cells were fixed and permeabilized in preparation for the click reaction with a fluorophore azide. Following the click reaction, the cells were imaged with confocal microscopy. We used 5-Fam-PEG-N_3, which was synthesized as previously described,[205] for the click reaction. It is important to note that the flexible, hydrophilic PEG linker in the fluorescent azide is critical, as using a less flexible, shorter or more hydrophobic linker results in much higher amounts of background labeling (data not shown).

To investigate the feasibility of this method, we incubated HeLa cells with 10 μM C15Alk for 24 h, in presence or absence of overnight pre-treatment with 25 μM lovastatin. Following the incubation, the cells were fixed, permeabilized, and then washed to remove unincorporated alkyne. Next, the Cu(I)-catalyzed click reaction was performed *in situ* by adding the reagents directly to the cells for 1 h together with 5-Fam-PEG-N_3. The cells were then rinsed several times to remove excess fluorescent reagent and imaged using confocal microscopy. These experiments resulted in a large amount of cellular labeling, with a higher degree of labeling in the presence of the lovastatin pre-treatment (Figure 4.5-B

and -C). Importantly, the background labeling (Figure 4.5-A) was almost non-existent, which is essential to verify that we are not simply imaging nonspecific labeling of the fluorophore azide. The fluorescence observed in the cells appeared to be punctate in nature and clustered around the plasma membrane and the nucleus in specific locations, indicating a large portion of the prenylated proteins were present in these areas. It is known that prenylated proteins receive the isoprenoid modification in the cytosol and are subsequently trafficked to the ER and Golgi for further processing before becoming localized to the plasma membrane (PM).[206] To explore if this was indeed what was being observed, HeLa cells were counterstained with ER Tracker Red to visualize the ER (Figure 4.5-E) and Wheat Germ Aggluitinin conjugated to Alexa Fluor 594 to visualize the PM (Figure 4.5-H). The results show almost complete co-localization between the green and red fluorescence with a Pearson correlation coefficient of 0.901 (Figure 4.5-F). This indicates significant localization of the labeled proteins to the ER, consistent with the established mechanism of prenylated protein transport. Surprisingly, labeled proteins were not localized to the PM (Figure 4.5-I).

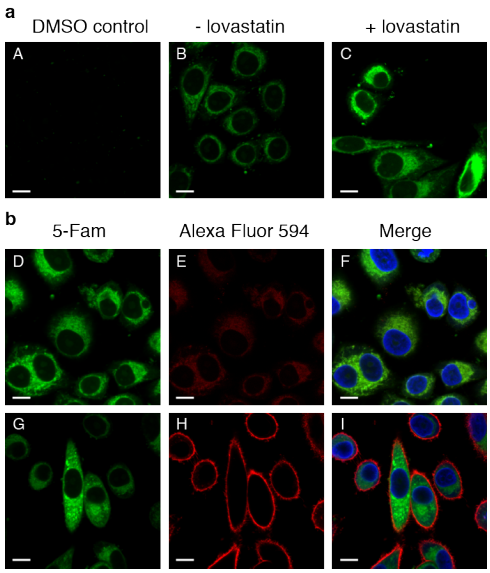

Figure 4.5. Imaging of prenylated proteins in mammalian cells with confocal microscopy indicates C15Alk-labeled proteins localize in ER. Metabolic labeling of HeLa cells was carried out using conditions specified for each panel. Cells were fixed and then after several rinses, the cells were subjected to the click reaction for 1 h with 5-Fam-PEG-N_3 and imaged using a 60x objective. Green channel is showing prenylated proteins 'clicked' to 5-Fam-PEG-N_3, and blue channel is showing cell nucleus stained with Hoescht 34580. A) Control reaction in which HeLa cells were treated with DMSO only. B) HeLa cells were treated with 10 μM C15Alk for 24 h in the absence of any lovastatin pre-treatment. C-I) HeLa cells treated overnight with 25 μM lovastatin, followed by 10 μM C15Alk for 24 h. E) Red channel showing staining of ER by ER Tracker Red. F) Overlay of images from D and E, along with nuclear stain (blue), showing significant colocalization of the green fluorescence with ER. H) Red channel showing staining of PM by Wheat Germ Agglutinin conjugated to Alexa Fluor 594. I) Overlay of images from G and H, along with nuclear stain (blue) indicates green fluorescence does not colocalize with PM. Size bar represents 10 μm.

4.3.3. Quantitative analysis of prenylated protein levels using flow cytometry of whole cells

Having established the ability to label prenylated proteins in cells, we next sought to quantify the total labeling in order to measure dynamic changes in the levels of prenylation. To do this, cells were incubated with C15Alk followed by trypsinization, fixation and permeabilization of cells. The click reaction was performed with 5-Fam-PEG-N_3 for 1 h and the cells were rinsed and analyzed by flow cytometry to measure the fluorescence intensity of each cell. We first optimized the conditions for cell permeabilization (Figure 4.6, left panel) and concentration of 5-Fam-PEG-N_3 for *in situ* click reaction (Figure 4.6, right panel).

While the flow cytometry method for quantifying prenylation levels includes several washing steps to remove unreacted fluorescent azide, it was unclear whether unincorporated alkyne probe present inside cells could react with the azide and remain associated with the cells, leading to false identification of protein labeling. To investigate this, HeLa cells were treated with an alkyne-containing analogue of farnesol, farnesyl alkyne (Figure 4.7), for 24 hours and then subjected to the standard fixation, permeabilization, and click reaction with 5-Fam-PEG-N_3. Importantly, as seen in Figure S4, no cellular labeling was observed above the minimal labeling present in the control sample (cells treated with only DMSO), suggesting that excess alkyne probe is effectively removed in

the washing steps. We also investigated our ability to remove excess alkyne probe that had already been derivatized via click reaction by first reacting the C15Alk analogue with 5-Fam-PEG-N_3 *in vitro* (see 'pre-click' reaction, Figure 4.7), followed by cellular treatment with this complex and flow cytometry. The presence of the large fluorophore covalently linked to the alkyne renders the molecule too large to be incorporated by protein prenyltransferases. Again, no labeling above the DMSO control reaction was observed (Figure 4.7), which suggests that unincorporated probe that has been derivatized via the click reaction can be eliminated using the washing protocol.

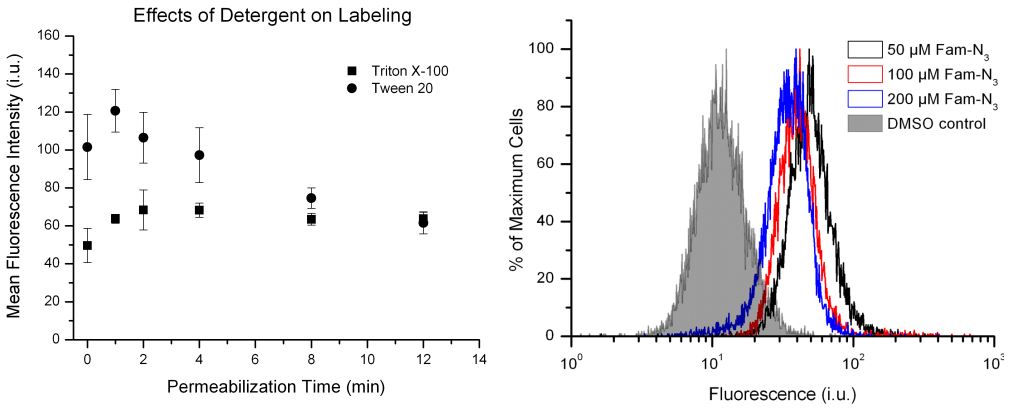

Figure 4.6. Establishing reaction conditions to label the prenylome in cells. HeLa cells were incubated with 50 μM of C15Alk for 24 h and then fixed using paraformaldehyde. Left: Cells were permeabilized using either Triton X-100 or Tween 20 for various lengths of times (0-12 min) and then subjected to the click reaction with 50 μM 5-Fam-PEG-N_3 for 1 h. An incubation time of 2 min with 0.1% Triton X-100 in PBS was found to be optimum. Right: cells were permeabilized using Triton X-100 (2 min at RT) and subjected to click reactions with indicated concentrations of 5-Fam-PEG-N_3 for 1 h. After several additional rinses, the cells were analyzed by flow cytometry and the results are expressed as the percentage of maximum cell count. Data were obtained in triplicate with similar results. 50 μM 5-Fam-PEG-N_3 was found to be sufficient to cause significant labeling over background.

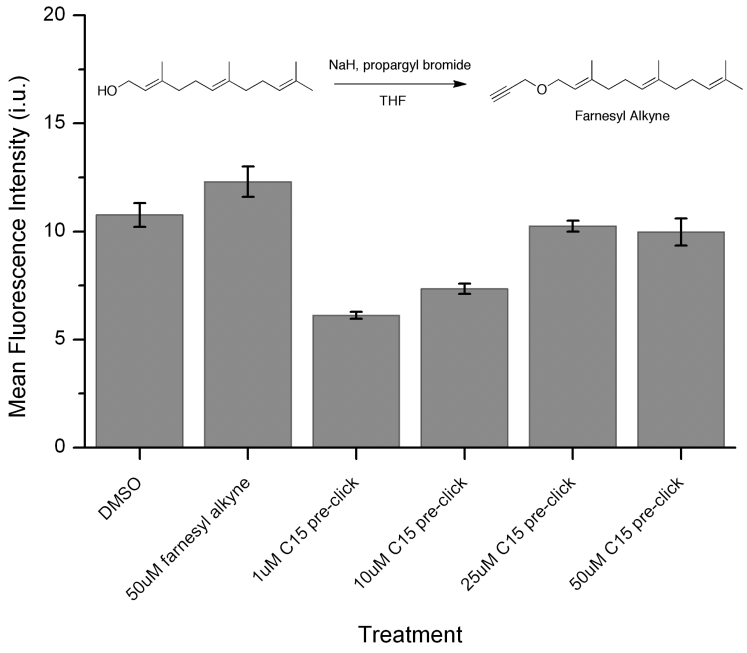

Figure 4.7. Control experiments utilizing a non-reactable farnesyl alkyne analog demonstrate no background labeling. Farnesyl alkyne was incubated with HeLa cells at 50 μM for 24 h followed by fixation, permeabilization, and the click reaction to 5-Fam-PEG-N_3. The extent of the prenylated protein labeling with this analog is not over the DMSO background, as this analog is not capable of being incorporated onto proteins as it lacks the ability to be phosphorylated. Further, C15Alk at various concentrations was incubated with 5-Fam-PEG-N_3 *in vitro* prior to cellular incubation ('C15 pre-click'). This 'pre-clicked' mixture was then added to fixed cells for 1 h, followed by washing and analysis by flow cytometry. The labeling in all cases is less than the DMSO background, indicating that the fluorophore-isoprenoid complex that is formed during the click reaction isn't being trapped or non-specifically attached to the cells and causing background labeling.

4.3.4. Optimizing conditions for metabolic labeling

For optimizing conditions for metabolic labeling of cells with C15Alk, we treated HeLa cells with 10-50 μM of C15Alk for 24 h. We quantified labeling via flow cytometry and observed a concentration dependent increase in labeling (Figure 4.8, left panel: lighter grey columns). We also evaluated labeling at 100 and 200 μM C15Alk (Figure 4.8, right panel), and observed increase in labeling at higher concentration. However, 200 μM C15Alk was found to be toxic to cells. We next sought to compare this method to one previously established[195] that utilized in-gel fluorescence to visualize prenylated proteins. For in-gel analysis, HeLa cells were incubated with 10-50 μM C15Alk for 24 h, followed by lysis and the click reaction of the cellular lysate with TAMRA-PEG-N_3 (Figure 4.1). After removal of excess reagents by protein precipitation, proteins were re-solubilized, and separated on a SDS-PAGE gel, which was scanned to visualize in-gel fluorescence. Consistent with the flow cytometry results, in-gel fluorescence analysis showed a concentration dependent increase in labeling of HeLa cells (Figure 4.9, left panel: lanes 2, 4, 6 and 8; Figure 4.9, right panel: grey columns).

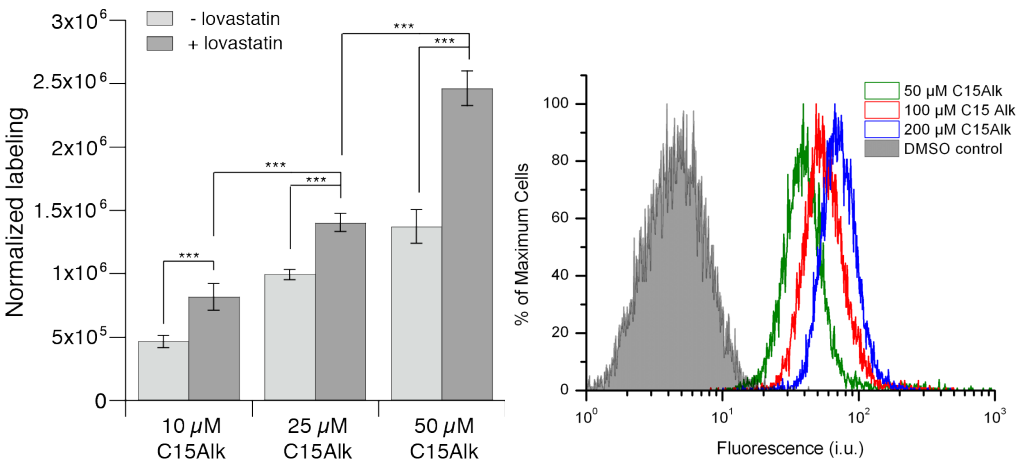

Figure 4.8. Flow cytometry analysis indicates concentration dependent increase in the incorporation of C15Alk. HeLa cells were incubated with C15Alk at indicated concentrations (left panel: 10-50 *μ*M; right panel: 50-100 *μ*M), followed by fixation, permeabilization, and the click reaction to 5-Fam-PEG-N_3 for 1 h to label prenylated proteins. The cells were analyzed via flow cytometry and the results are expressed as the mean fluorescence intensity of 10,000 cells ± standard error of the mean of at least three replicates. For statistical analysis, the Student's *t*-test was performed assuming a two-tailed distribution and samples having equal variance. Results were considered significant if $p < 0.05$ (*), $p < 0.01$ (**), or $p < 0.001$ (***).

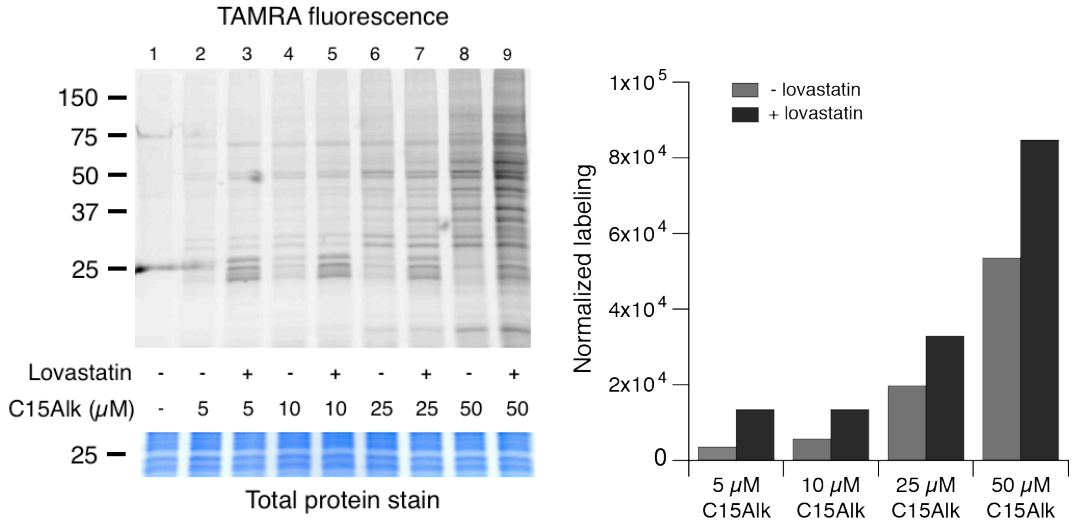

Figure 4.9. In-gel fluorescence analysis demonstrates effects of lovastatin pre-treatment on incorporation of C15Alk at various concentrations. HeLa cells were incubated with C15Alk at indicated concentrations, in the presence or absence of overnight pre-treatment with 25 μM lovastatin. Cells were then lysed, and lysates was subjected to the click reaction to TAMRA-PEG-N_3. Proteins were then separated on a 12% polyacrylamide gel. Gel was scanned for TAMRA fluorescence, and stained with Coomassie Blue for obtaining total protein stain image.

Metabolic labeling of prenylated proteins is often carried out in the presence of a HMG-CoA reductase inhibitor, such as lovastatin, to reduce endogenous levels of FPP and GGPP, and thereby increasing the incorporation of isoprenoid analogs. A recent study also suggests that the metabolism of exogenously added isoprenoid alcohols (conversion to isoprenoid diphosphate and incorporation into prenylated proteins) increases upon inhibition of HMG-CoA reductase.[204] Therefore, we investigated effects of lovastatin treatment on the labeling of prenylated proteins with varying concentrations of C15Alk. Flow cytometry analysis clearly showed an increase in fluorescence labeling in the presence of an overnight pre-treatment with 25 μM lovastatin (Figure 4.8, left panel: dark grey columns). Similar results were also observed via in-gel fluorescence analysis (Figure 4.9, right panel: black columns). Interestingly, in-gel fluorescence revealed differences in labeling patterns in the presence of lovastatin at various concentrations of C15Alk. At 5 μM and 10 μM C15Alk, very little labeling was observed in absence of lovastatin (Figure 4.9, left panel: lanes 2 and 4). However, highly intense bands appeared in the presence of lovastatin (Figure 4.9, left panel: lanes 3 and 5), specifically at 20-25 kDa, which is a region where small molecular weight GTPases are seen. At 25 μM and 50 μM C15Alk, several proteins bands in the 30-75 kDa region were labeled in absence of lovastatin (Figure 4.9, left panel: lanes 6 and 8), and the intensity of these bands

didn't change in the presence of lovastatin (Figure 4.9, left panel: lanes 7 and 9). At these concentrations, the most prominent change in labeling upon lovastatin pre-treatment was again in the 20-25 kDa region. The presence of several bands showing no effect upon lovastatin pre-treatment indicated that high concentrations (25 and 50 μM) of C15Alk could possibly label some proteins in a mechanism independent of protein prenylation.

To determine whether the labeling caused by C15Alk which remained unaffected by lovastatin is relevant to protein prenylation, we first checked whether farnesol (FOH) and geranylgeraniol (GGOH), which are precursors to natural substrates FPP and GGPP, could compete away labeling. Flow cytometry analysis indicated that the presence of 25 μM of FOH and GGOH, did not reduce labeling caused by treatment at 25 μM C15Alk (Figure 4.10, left panel). In-gel fluorescence analysis (Figure 4.10, left panel: lanes 6 and 7) indicated that 25 μM FOH and GGOH reduced labeling in only in the 20-25 kDa region, but slightly increased labeling in the 30-75 kDa region. Mevalonolactone (50-100 μM) alone or in combination with FOH could not compete away labeling caused by 25-50 μM C15alk treatment either, as observed via both flow cytometry and in-gel fluorescence analyses (Figure 4.11). Inside cells, mevalonolactone gets hydrolyzed to mevalonate (Figure 4.11, top left panel), an intermediate of the mevalonate pathway upstream to FPP and GGPP.[207] We next investigated

whether a molecule similar to C15Alk, but lacking a feature required to get catalytically incorporated by prenyltransferase, would cause any labeling in HeLa cells. To this purpose, we synthesized 2,3-dihydro-C15Alk (C15-DH-Alk, Figure 4.12, top), which has isoprenoid backbone and alkyne group present as in C15Alk. However, it cannot act as a substrate for prenyltransferases due to its lack of an allylic diphosphate moiety. Surprisingly, a 50 μM treatment of C15-DH-Alk caused a significant amount of fluorescence labeling of proteins in HeLa cells as observed by in-gel fluorescence analysis (Figure 4.12, bottom left) and flow cytometry (Figure 4.12, bottom right). This labeling was not affected by presence of lovastatin, which is expected given that it is not a substrate of protein prenyltransferases. Overall, our findings suggest that a part of labeling by 25-50 μM C15Alk, which is not affected by presence of lovastatin, occurs by a process independent of protein prenylation. Such off-target labeling of proteins by metabolic cross-talk has been reported for other chemical reporters of post-translational modifications, such as protein glycosylation.[208] This is the first report showing a possibility of alkyne-modified protein prenylation reporters entering isoprenoid metabolism pathways having cross-talk with protein prenylation.

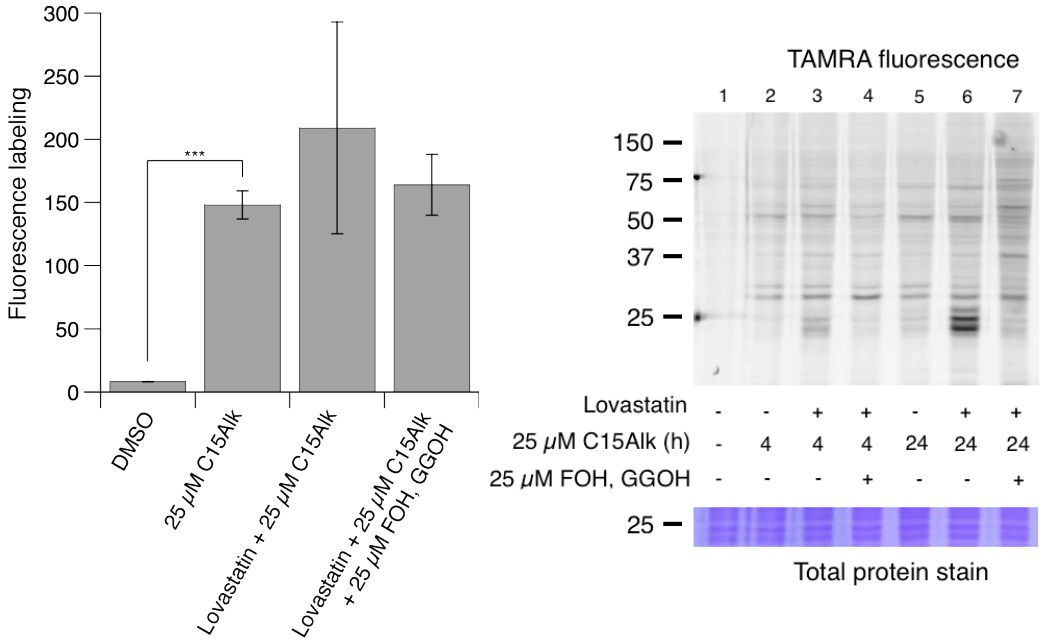

Figure 4.10. Farnesol and geranylgeraniol do not decrease incorporation of 25 or 50 μM C1Alk in HeLa cells. Left: HeLa cells were pre-treated with 25 μM lovastatin for 24 h and then labeled with 25 μM C15Alk for 4 h, in the presence or absence of 25 μM farnesol (FOH) and geranylgeraniol (GGOH); right: HeLa cells were pre-treated with 25 μM lovastatin for 24 h and then labeled with 25 μM C15Alk for 4 h, in the presence or absence of 25 μM farnesol (FOH) and geranylgeraniol (GGOH). Cells were then fixed, permeabilized and subjected to click reactions with the indicated concentrations of 5-Fam-PEG-N_3 for 1 h. The cells were analyzed via flow cytometry and the results are expressed as the mean fluorescence intensity of 10,000 cells ± standard error of the mean of at least three replicates.

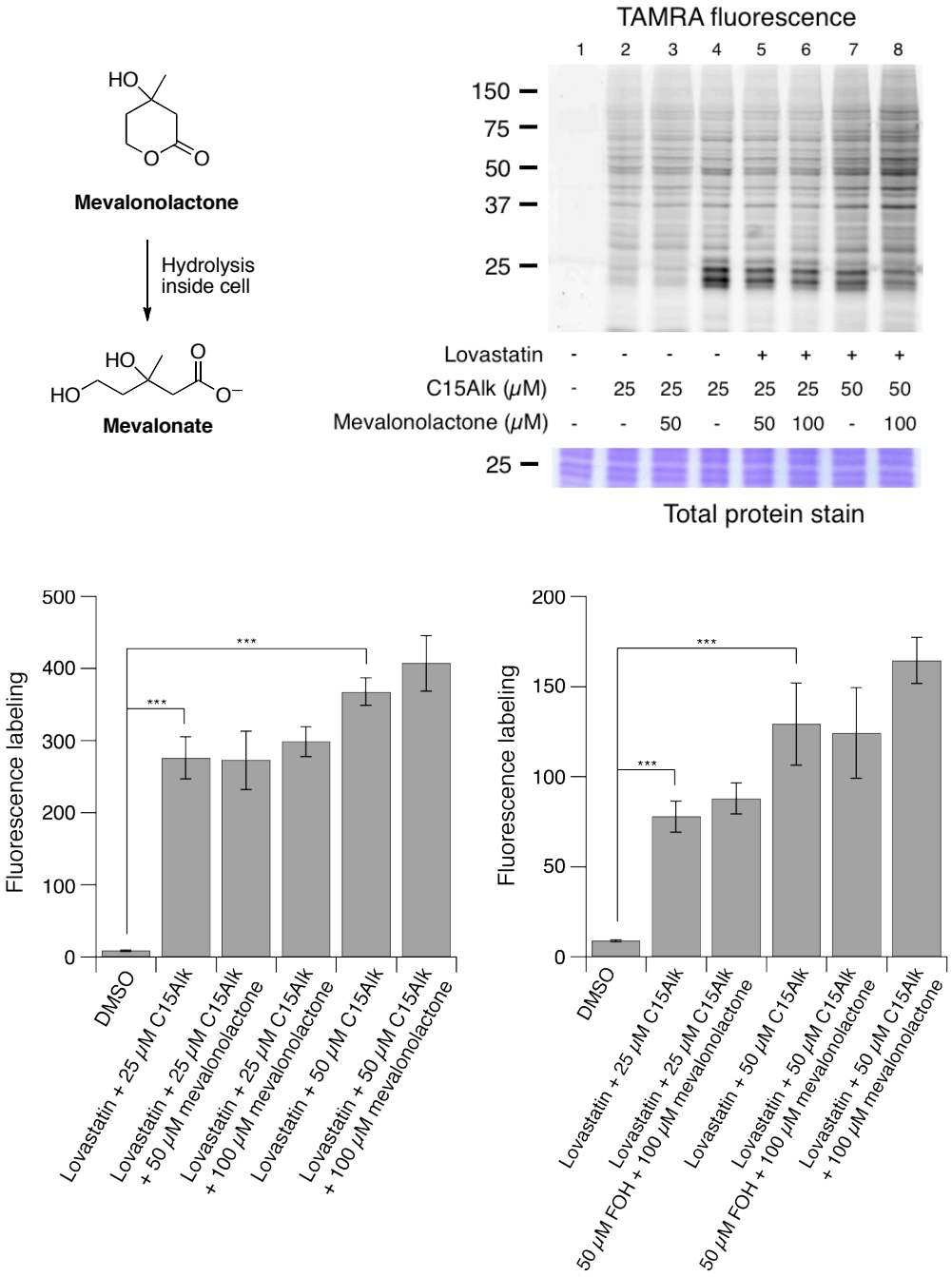

Figure 4.11. Farnesol and mevalonolactone do not decrease the incorporation of 25 or 50 μM C1Alk in HeLa cells. Top left: structure and hydrolysis of mevalonolactone. Top right: HeLa cells were pre-treated with 25 μM lovastatin for 24 h and then labeled with 25 or 50 μM C15Alk for 24 h, in presence or absence of 50-100 μM mevalonolactone. Cell were

lysed, proteins were reacted with TAMRA-PEG-N_3 and separated on a 12% polyacrylamide gel. Bottom left: HeLa cells were pre-treated with 25 μM lovastatin for 24 h and then labeled with 25 or 50 μM C15Alk for 24 h, in presence or absence of 50-100 μM mevalonolactone; bottom right: HeLa cells were pre-treated with 25 μM lovastatin for 24 h and then labeled with 25 or 50 μM C15Alk for 24 h, in presence or absence of 50 μM FOH and 100 μM mevalonolactone. Cells were then fixed, permeabilized and subjected to click reactions with 50 μM of 5-Fam-PEG-N_3 for 1 h. The cells were analyzed via flow cytometry and the results are expressed as the mean fluorescence intensity of 10,000 cells ± standard error of the mean of at least three replicates.

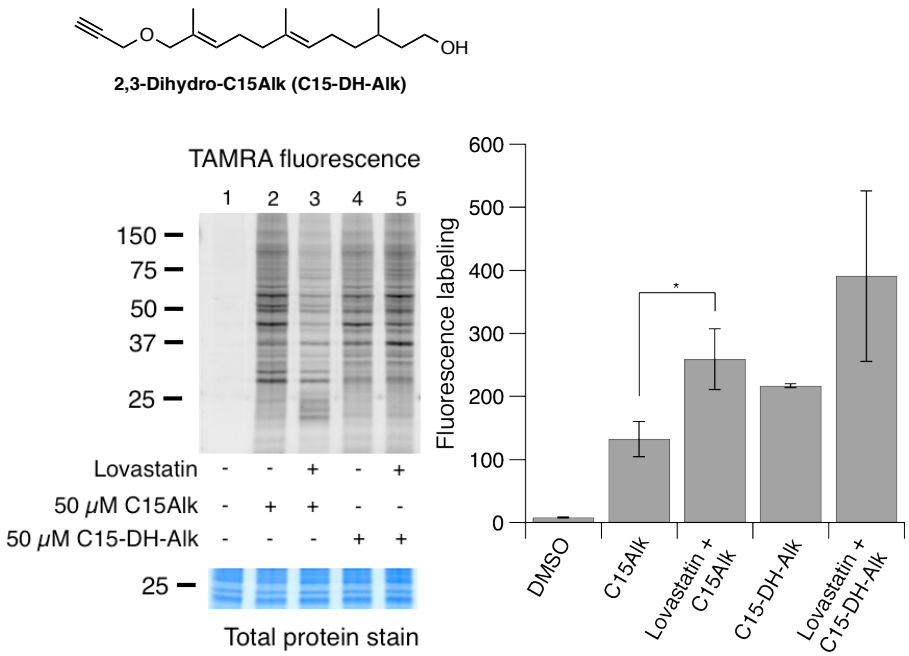

Figure 4.12. Incorporation of C15-DH-Alk in HeLa cells is independent of lovastatin treatment. Top: Structure of C15-DH-Alk, Bottom: HeLa cells were treated with 50 μM of C15Alk or C15-DH-Alk, in presence or absence of pre-treatment with 25 μM lovastatin. Bottom left: Cells were lysed, and lysates were reacted with 25 μM of TAMRA-PEG-N_3 for 1 h and then proteins were separated on a 12% polyacrylamide gel. Bottom right: Cells were then fixed, permeabilized and subjected to click reactions with 50 μM of 5-Fam-PEG-N_3 for 1 h. The cells were analyzed via flow cytometry and the results are expressed as the mean fluorescence intensity of 10,000 cells ± standard error of the mean of at least three replicates.

We next sought to study the labeling of proteins using a lower concentration (10 μM) of C15Alk. Flow cytometry analysis showed that co-treatment of 10-50 μM of FOH and GGOH significantly decreased labeling caused by 10 μM C15Alk treatment (Figure 4.13, grey columns). Increasing concentrations of FOH and GGOH from 10 μM to 25 μM led to increased suppression of labeling from ~75% to ~50%. At 50 μM FOH and GGOH, labeling didn't decrease any further, which we hypothesize is due to the enhanced entry of C15Alk in the presence of high concentrations of the hydrophobic molecules FOH and GGOH. In-gel fluorescence analysis and subsequent densitometry gave similar results (Figure 4.13, black columns), and additionally demonstrated that labeling in 20-25 kDa region of the gel got abolished (Figure 4.14). When HeLa cells were treated overnight with lovastatin and then incubated with 10 μM of C15Alk for varied lengths of time, we observed a time dependent increase in labeling by both flow cytometry and in-gel fluorescence analysis, plateauing at around 24 h (Figure 4.15). Additionally we found that 24 h labeling with 10 μM C15Alk to be comparable to the labeling by 10 μM of the diphosphate version, C15Alk-OPP (Figure 4.16), in terms of both total protein quantification and the in-gel labeling pattern. Taken together, these experiments indicate that the labeling of proteins at 10 μM C15Alk is more prenylation specific as compared to the labeling at 25 μM and 50 μM.

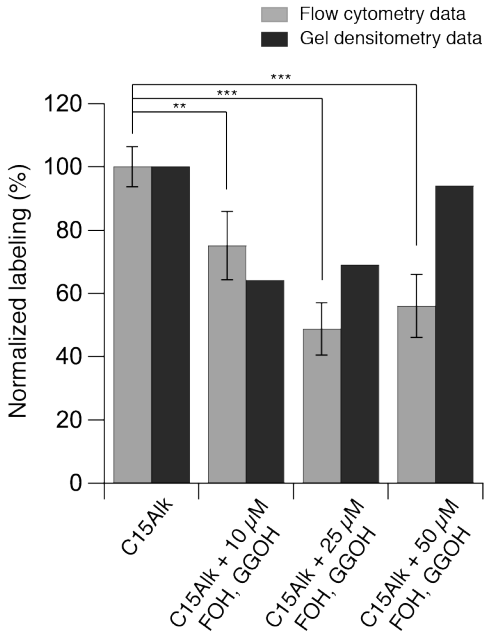

Figure 4.13. Flow cytometry and in-gel fluorescence analysis show that farnesol and geranylgeraniol significantly compete away C15Alk labeling. HeLa cells were treated for 24 h with 10 μM C15Alk, in the presence or absence of 25 μM lovastatin overnight pre-treatment. Various concentration of farnesol and geranylgeraniol (10, 25 or 50 μM) were added simultaneously with C15Alk to compete away cellular labeling of prenylated proteins. Densitometry measurements of in-gel fluorescence images were performed using Image J and graphed against *in situ* analysis via flow cytometry of similarly treated cells, subjected to the flow cytometry quantification method described above. The results are displayed as the normalized maximum fluorescence labeling in which each sample was divided by the maximum value to give a percentage of fluorescent labeling. Both sets of data have been background subtracted and the densitometry data is normalized to the total protein stain.

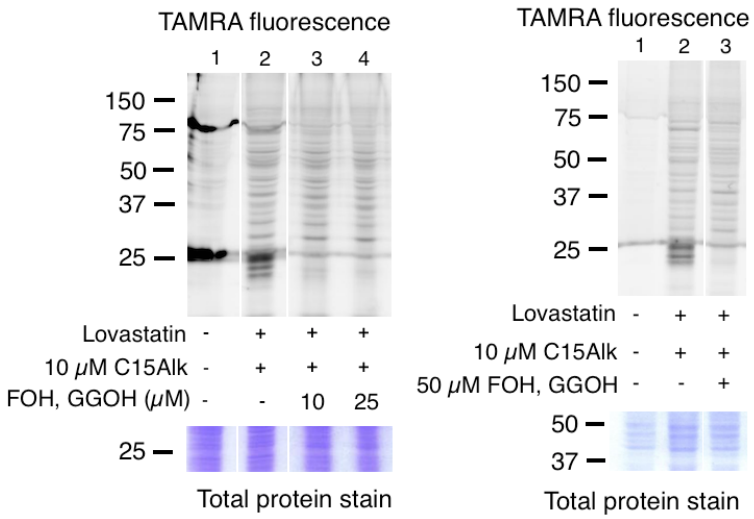

Figure 4.14. 10-50 μM FOH and GGOH significantly compete away labeling caused by 10 μM C15Alk, particularly in 25 kDa region. HeLa cells were treated for 24 h with 10 μM C15, in the presence or absence of 25 μM C15Alk overnight pre-treatment. 10, 25 or 50 μM farnesol and geranylgeraniol, each, were added simultaneously with C15Alk to compete away cellular labeling of prenylated proteins. Cells were lysed, and lysates were reacted with 25 μM of TAMRA-PEG-N_3 for 1 h and then proteins were separated on a 12% polyacrylamide gel. Densitometry analysis of these images included in Figure 4.13.

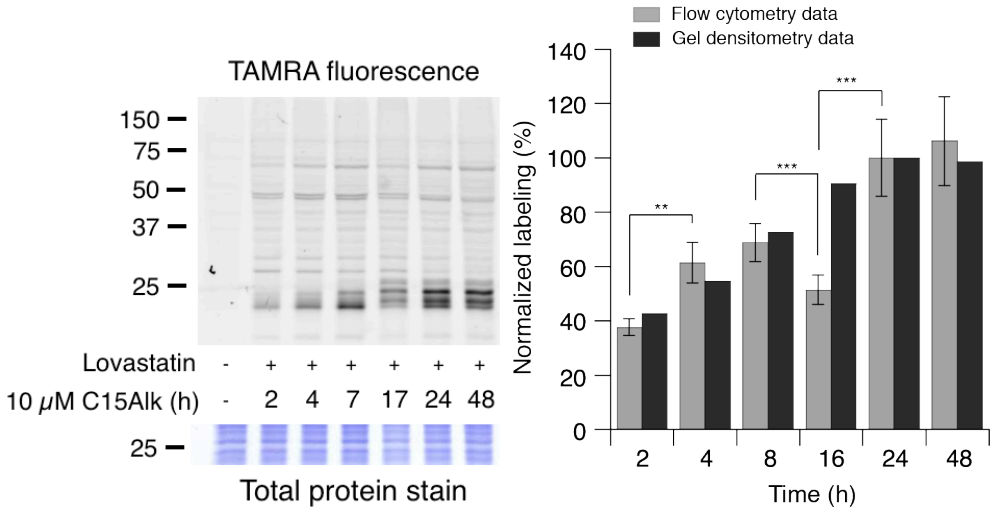

Figure 4.15. Incorporation kinetics of 10 μM C15Alk in HeLa cells studied by flow cytometry and in-gel fluorescence analysis. HeLa cells were treated overnight with 25 μM C15Alk and then incubated with 10 μM C15Alk for the indicated length of time. Densitometry measurements of in-gel fluorescence image were performed using ImageJ and graphed against *in situ* analysis via flow cytometry of similarly treated cells, subjected to the flow cytometry quantification described above. The results are displayed as the normalized maximum fluorescence labeling in which each sample was divided by the maximum value to give a percentage of fluorescent labeling. Both sets of data have been background subtracted and the densitometry data is normalized to the total protein stain.

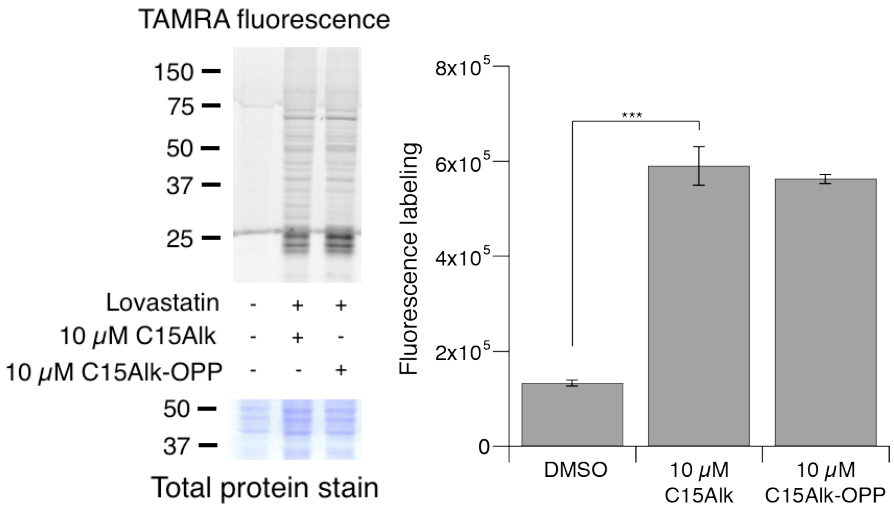

Figure 4.16. Extent and pattern of incorporation of C15Alk-OH and C15Alk-OPP in HeLa cells is similar. HeLa cells were pre-treated with 25 μM lovastatin and then labeled with 10 μM C15Alk or C15Alk-OPP for 24 h. Left: Cells were lysed, and lysates were reacted with μM of TAMRA-PEG-N_3 for 1 h and then proteins were separated on a 12% polyacrylamide gel. Right: Cells were then fixed, permeabilized and subjected to click reactions with 50 μM of 5-Fam-PEG-N_3 for 1 h. The cells were analyzed via flow cytometry and the results are expressed as the mean fluorescence intensity of 10,000 cells ± standard error of the mean of at least three replicates.

It is also important to note that data from our flow cytometry method correlates well with results of a more established in-gel fluorescence method, suggesting that the flow cytometry-based approach reported here provides an accurate measure of protein prenylation levels. An important advantage of the flow cytometry method, however, is that the click reaction is performed *in situ* and the analysis and quantitation can be completed in minutes via whole-cell flow cytometry with fluorescence detection, as compared to the more laborious gel-based technique. Overall, these methods serve complementary purposes. For rapid quantification of global prenylation levels, the flow cytometry procedure is a useful tool; when studying individual prenylated proteins, gel-based techniques are the preferred methods.

4.3.5. Extension of flow cytometry method to other cell types

In addition to quantifying the levels of prenylated proteins in HeLa cells, it was desirable to compare the extent of labeling in a variety of different cell types since differences in tissue type may result in differences in the abundance of prenylated proteins. For example, differences in the levels of various prenylated proteins present in HeLa cells, MCF10A cells and D1 astrocytes were observed in previously reported proteomic experiments.[195] Using the flow cytometry method described here, we found that there are indeed significant differences in the overall levels of prenylated proteins, depending on cell type (Figure 4.17, left

panel; Figure 4.18, left panel). HeLa cells showed the largest extent of labeling, while A549 cells, derived from human lung adenocarcinoma, had a significantly lower amount of labeling than all other cells tested. It is important to consider that the differences in the levels of prenylated proteins between cells could simply reflect a difference in cell size. An analysis of the cell area using confocal microscopy shows that there are only minor differences in the size between these cell types, which indicates that these measurements highlight differences in protein prenylation and not simply cell size (Figure 4.17, right panel). Of particular interest, A549 cells are the same size as HeLa and MCF10A cells but display a more than two-fold lower amount of prenylated proteins.

To further demonstrate the utility of this method, we also explored its application to primary cells; such cells are often superior to immortalized cell lines for studying cellular phenomena. For this, primary astrocytes and glia were isolated from mice and the levels of prenylated proteins in them were quantified using the methods outlined above. These cells demonstrated efficient incorporation of 10 μM C15Alk (Figure 4.18, right panel). Taken together, these results highlight the highly variable nature of protein prenylation in different cell types and the ability of the flow cytometry method reported here to quantify prenylated proteins in a wide spectrum of systems.

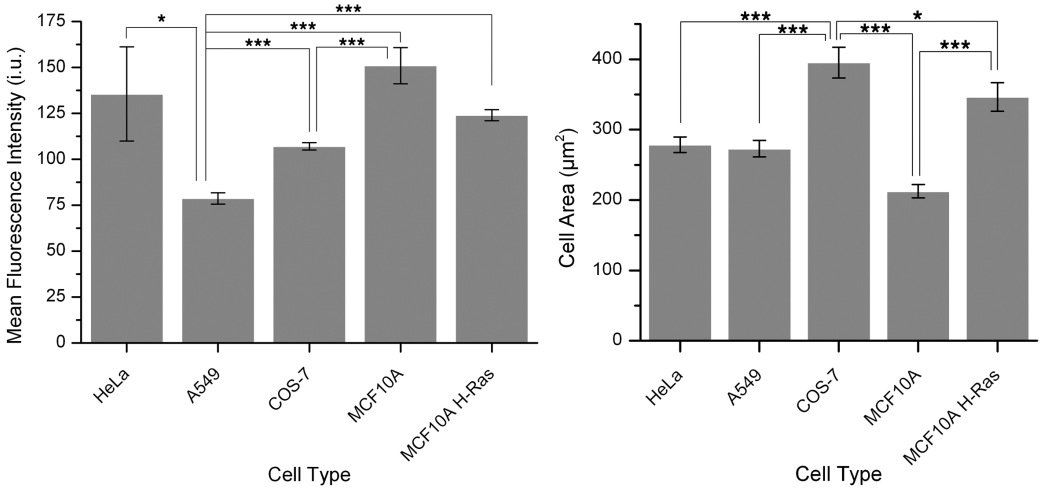

Figure 4.17. Extension of our method to other cell lines. Left: Flow cytometry of various cell types that have been incubated with C15Alk at 50 μM for 24 h, followed by fixation, permeabilization, and the click reaction to 5-Fam-N_3 for 1 h. The results are expressed as the mean fluorescence intensity of 10,000 cells ± standard error of the mean of at least three replicates. Right: The plasma membrane of various types of cells was stained with Wheat Germ Agglutinin-AlexaFluor 594 conjugate (following manufacturers protocols) and the area of the cell was calculated using ImageJ software. The results are expressed as the mean cell area ± standard error of the mean of at least 40 measured cells. For statistical analysis, the Students t-test was performed assuming a one-tailed distribution and samples having equal variance. Results were considered significant if $p < 0.05$ (*), $p < 0.01$ (**), or $p < 0.001$ (***).

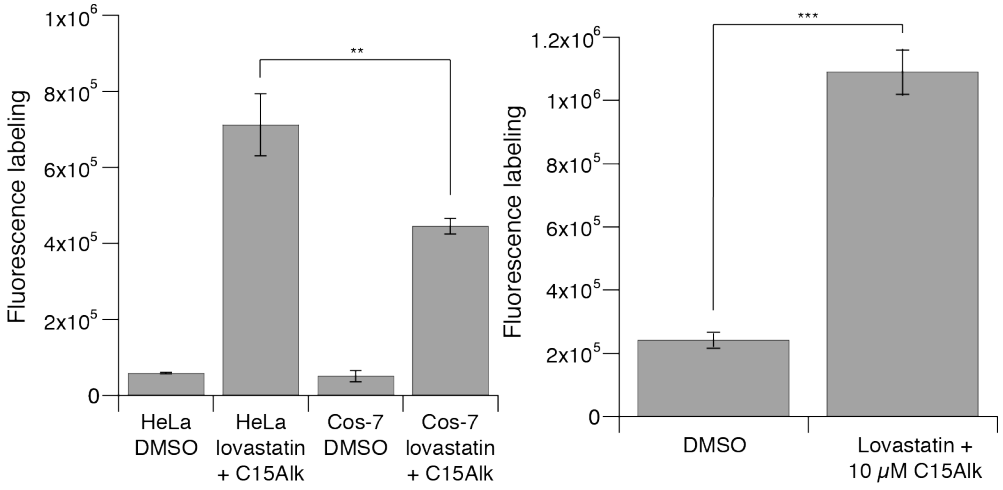

Figure 4.18. Metabolic labeling of prenylated proteins with C15Alk and subsequent click reaction and flow cytometry analysis can be extended to cell lines other than HeLa cells. Left: HeLa and Cos-7 cells were pre-treated overnight with 25 μM lovastatin and then labeled with 10 μM C15Alk. Right: Primary glial astrocyte mixed cells were treated with 25 μM lovastatin and 10 μM C15Alk simultaneously. For both panels: Cells were fixed, permeabilized and subjected to click reactions with 50 μM of 5-Fam-PEG-N_3 for 1 h. The cells were analyzed via flow cytometry and the results are expressed as the mean fluorescence intensity of 10,000 cells ± standard error of the mean of at least three replicates. A. Cos-7 cells, which have higher cell area (see Figure S12), have lesser incorporation of C15Alk compared to HeLa cells. B. There is significant amount incorporation in primary astrocyte cells.

4.3.6. Effects of prenylation inhibitors on the extent of labeling

Having established the ability to measure the levels of prenylated proteins in different cells and showing that this labeling is specific to prenylation, we were interested in quantifying the effects of prenyltransferase inhibitors on total protein labeling. Since C15Alk is a substrate for all three prenyltransferases (FTase, GGTase-I and Rab GGTase), it could be used to evaluate the level of overall protein prenylation in response to treatment of prenyltransferase inhibitors targeting either single or multiple enzymes. The inhibitors employed in this study were L-744,832 (inhibitor of FTase, IC_{50} = 4-18 μM, denoted as FTI in this text)[209], GGTI-286 (inhibitor of GGTase-I, IC_{50} = 2 μM)[210], and 3-PEHPC (inhibitor of Rab GGTase, IC_{50} = 24.1 μM)[211]. We evaluated effects of treatment of individual inhibitor as well as a combination of these inhibitors.

In the flow cytometry experiments we carried out, we found that 10-20 μM of FTI increased the overall labeling of HeLa cell proteins using 10 μM C15Alk (Figure 4.19, top panels). In the presence of a farnesyltransferase inhibitor, some of the farnesylated proteins (such as KRas) are reported to get alternatively geranylgeranylated[35] and dual geranylgeranylation of Rab proteins is hypothesized to be elevated.[151] These phenomena could explain the increase in labeling in the presence of FTI alone. However, what caused labeling to increase when cells were treated with 10-20 μM FTI in the presence of GGTI-286 and/or

3-PEHPC (Figure 4.19, top panels) is currently unclear. Interestingly, a combination of higher concentration of FTI (100 μM) with GGTI-286 and 3-PEHPC resulted in ~30% decrease in labeling of HeLa cells with 10 μM C15alk (Figure 4.19, top left panel). 3-PEHPC and other phosphonocarboxylate inhibitors only inhibit the second geranylgeranylation of Rab proteins.[212] Therefore, 3-PEHPC alone or in combination with an FTI and GGTI-286 is not expected to completely abolish the labeling caused by C15Alk. We also found that in-gel fluorescence and densitometry results in the presence of 10 μM FTI (Figure 4.19, bottom panels) did not correlate with the above mentioned flow cytometry results. Taken together, it is clear that additional experiments are necessary to study the effects of inhibitor treatments on the incorporation of C15Alk in prenylated proteins. In future, it would be necessary to empirically determine what concentrations of various inhibitors to use in the experiments, because the inhibitor concentration required for achieving optimal inhibition of prenyltransferases without causing significant cell toxicity varies depending on the cell type.[133, 209]

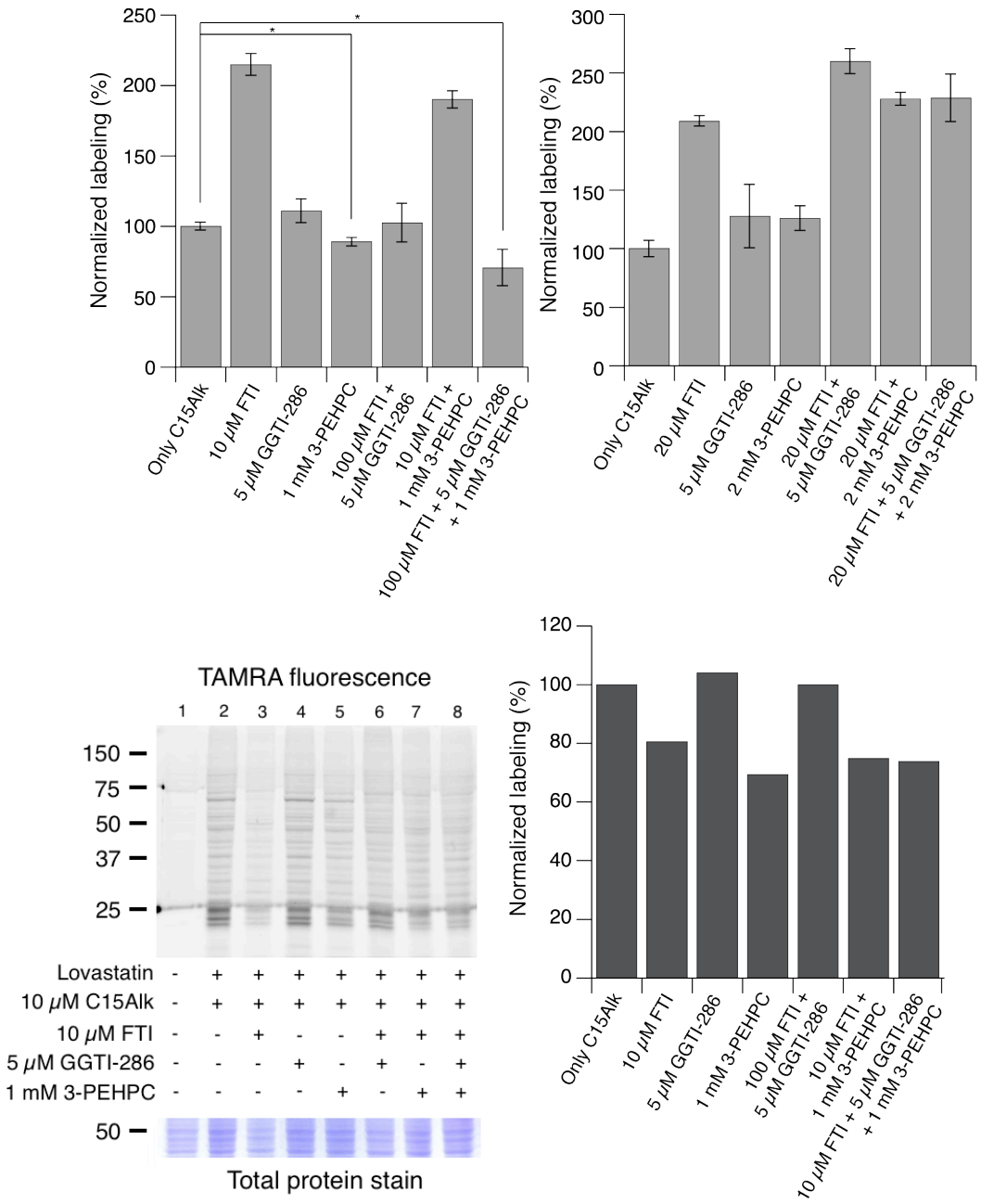

Figure 4.19. Quantitation of the effects of prenyltransferase inhibitors on the metabolic incorporation of C15Alk. HeLa cells were treated overnight with 25 μM lovastatin, and then incubated with indicated concentrations of prenyltransferase inhibitors for 1 h. 10 μM C15Alk was then added to cells and cells were labeled for 24 h (in presence of inhibitors) and then processed for flow cytometry analysis (top panels) or in-gel fluorescence analysis (bottom left). Bottom right: Densitometry analysis of the gel in bottom left panel.

4.3.7. Measurement of prenylation levels in a cellular model of compromised autophagy

Having established a method for determining the levels of prenylated proteins, we next sought to quantify the levels of such proteins in a cellular model of compromised autophagy. We were interested in studying prenylation levels in this system because aging disorders are characterized by deficient autophagy and that protein prenylation has been correlated with Alzheimer's pathology.[170, 180, 213] To study this phenomenon, a model of compromised autophagy was produced by knocking down the BECN1 gene, which is required for autophagy. BECN1 encodes Beclin 1 protein. It is an important gene responsible for autophagy in mammalian cells and it has reduced expression in early Alzheimer's disease.[182] Knockdown of this gene with siRNA is widely used as a model system for having a defective autophagy phenotype.[214-216]

C2C12 mouse myoblast cells were transfected with siRNA against the BECN1 gene for 4 h. After removal of transfection-reagent containing media, cells were incubated for 24 h to maximize gene knockdown. The cells were then treated with 25 μM lovastatin and 10 μM C15Alk for 24 h followed by fixation, permeabilization and the click reaction with 5-Fam-PEG-N_3, at which point the cells were analyzed by flow cytometry to quantify the prenylated proteins. The C2C12 cells in which the BECN1 gene was knocked down showed a 22%

increase in the levels of prenylated proteins (Figure 4.20), compared to cells transfected with a scrambled siRNA. This result indicates that individuals with neurodegenerative disorders may have an increase in the levels of prenylated proteins, possibly because due to an increase in the levels of available FPP or GGPP, because the genes expressing the prenyltransferases are upregulated, or because the activity of the prenyltransferases themselves is amplified.

4.4. Conclusions

The method described here provides a way for the quantification of the total level of prenylated proteins in various types of cells, including primary neurons. We have shown that many of the labeled prenylated proteins localize to the ER and that different types of cells have significant differences in their levels of prenylated proteins. Furthermore, we have shown that the levels of prenylated proteins are increased by about 22% in a cellular model of compromised autophagy. These observations suggest a possible connection between protein prenylation and aging disorders such as Alzheimer's and Parkinson's disease. Additional studies utilizing the method we have developed in mouse models of Alzheimer's disease may help to elucidate the role that isoprenoids and protein prenylation play in neurodegenerative diseases.

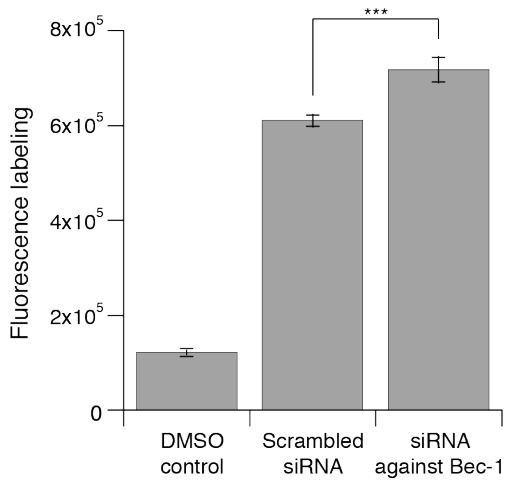

Figure 4.20. In a cellular model of compromised autophagy, a surrogate for studying aging disorders, the levels of prenylated proteins are increased over normal control levels. In the defective autophagy cell model, the BECN1 gene controlling autophagy was knocked down with siRNA for 24 h prior to C15Alk exposure. Normal control cells included transfection of a scrambled siRNA. After 24 h transfection, cells were incubated with 25 μM lovastatin and 10 μM C15Alk for 24 h, followed by fixing, permeabilizing and the click reaction with 5-Fam-PEG-N3 and analysis by flow cytometry. After several additional rinses, the cells were analyzed by flow cytometry and the results are expressed as the mean fluorescence intensity of 10,000 cells ± standard error of the mean of at least three replicates. There is a statistically significant ($p < 0.001$) increase in the amount of prenylated proteins in the model of compromised autophagy.

4.5. Methods

Materials

HeLa cells were the generous gift of Dr. Audrey Minden (Department of Chemical Biology, Rutgers University); all other cell lines were purchased from ATCC. 100 mm tissue culture treated dishes were from Corning Scientific. Petri dishes (35 mm) fitted with microwells (14 mm) and a No. 1.5 coverglass were from MatTek Corporation. Tissue culture treated 6-well multiwell plates and 5mL polystyrene round bottom tubes (12x75mm) were from BD Biosciences. DMEM (Dulbecco's Modified Eagle Medium), ER Tracker Red, wheat germ agglutinin-AlexaFluor 594 conjugate, Lipofectamine 2000, Stealth ATG7 RNAi, Stealth RNAi Universal Negative Control, Opti-MEM, neurobasal medium, B27 supplement, Fetal bovine serum (FBS) and glutamine were from Invitrogen. 3-PEHPC was a generous gift from Dr. David F. Wiemer. GGTI-286 was purchased from CalBioChem and L-744,832 was from Merck. 70 μm cell strainers and SuperSignal West Pico Chemiluminescent Substrate were from ThermoFisher Scientific. Immobilon-P PVDF membranes were from Millipore, Anti-H-ras rabbit polyclonal and anti-ERK2 rabbit polyclonal antibodies were from Santa Cruz Biotechnology. Anti-rabbit IgG horseradish peroxidase-linked secondary antibody was from Cell Signaling. Vydac 218TP54 and 218TP1010 columns were used for analytical and preparative RP-HPLC, respectively. All analytical and preparative RP-HPLC

solvents, water and CH_3CN, contained 0.10% TFA and were of HPLC grade. 5-Carboxyfluorescein succinimidyl ester and TAMRA-succinimidyl ester were from AnaSpec. All other reagents were from Sigma Aldrich, including benzonase nuclease (E1014) and protease inhibitor cocktail (P8340).

4.5.1. General cell culture

Cells were seeded in culture dishes at the following densities prior to experimentation: HeLa 3.1 x 10^4 cells/cm^2, MDCK 2.5 x 10^4 cells/cm^2, A549 3.0 x 10^4 cells/cm^2, NIH/3T3 2.5 x 10^4, MCF10A and MCF10A-HRas 3.3 x 10^4 cells/cm^2, COS-1 and -7 2.0 x 10^4 cells/cm^2, and L6 2.3 x 10^3 cells/cm^2. HeLa, MDCK, NIH/3T3, COS-1, COS-7, and C2C12 were maintained in DMEM supplemented with 10% FBS. A549 were maintained in RPMI supplemented with 10% FBS. MCF10A and MCF10A H-Ras were maintained in DMEM/F12 supplemented with 5% horse serum, 0.5 μg/mL hydrocortisone, 10 μg/mL insulin, 20 ng/mL EGF, and 0.1 μg/mL cholera toxin. All cells were grown at 37°C with 5.0% CO_2.

4.5.2. Imaging Prenylated Proteins

HeLa, A549, MDCK, COS-7, or NIH/3T3 cells were seeded (see above for density) in 35 mm glass bottomed culture dishes and grown to approximately 50% confluence (24 h). The cells were rinsed twice with phosphate buffered

saline (PBS), followed by the addition of 10 μM C15Alk in 2 mL complete DMEM media. After 24 h probe incubation, the cells were rinsed twice with PBS, fixed with 4% paraformaldehyde (PFA) in PBS for 10 min at RT, permeabilized with 0.1% Triton X-100 in PBS for 2 min at RT, and subsequently rinsed three times with PBS. The following reagents were added, in order, at the specified concentration (typically 300 uL total volume in PBS): TAMRA-PEG-N_3 or 5-Fam-PEG-N_3 (0.1 mM), *tris*(2-carboxyethyl)phosphine (TCEP, 1 mM), *tris*[(1-benzyl-1H-1,2,3-triazol-4-yl)methyl] amine (TBTA, 0.2 mM), $CuSO_4$ (1 mM). Following 1 h incubation at RT, the cells were rinsed four times with PBS and Hoescht 34580 nuclear stain was added at a final concentration of 1 μg/mL for 10 min. Additionally, for the colocalization experiments, ER Tracker Red (1 μM for 10 min) or Wheat Germ Agglutinin conjugated to Alexa Fluor 594 (5 μg/mL for 10 min) were added. The cells were rinsed twice with PBS and imaged using an Olympus FluoView FV1000 IX2 Inverted Confocal Microscope with a 60X objective.

4.5.3. Quantifying the Prenylome

Cells were seeded in 6-well culture dishes and grown to approximately 50-60% confluence (24 h). Cell culture media was then supplemented with 25 μM and cells were incubated for 18-24 h. Media from the cells was then replaced with 1 mL fresh media, followed by addition of 10-50 μM C15Alk (or as indicated). Cells

were grown for 24 h in presence of C15Alk, unless otherwise specified. In the inhibitor treatment experiments, 10-100 µM L-744,832, 5 μM GGTI-286 or 1-2 mM 3-PEHPC were added to cells 1 h prior to labeling with 10 μM C15Alk. For competition experiments, 10-50 μM FOH, 10-50 μM GGOH or 50-100 μM mevalonolactone were added immediately following C15Alk addition. After incubation of C15Alk and/or inhibitors for various times (typically 24 h), the cells were rinsed twice with PBS and trypsinized for 5 min. After addition of 4X volume of media to inactivate trypsin, cells were transferred to micro-centrifuge tubes, and pelleted by centrifugation at 100 x g for 5 min. The media was aspirated from the pellet and the cells were fixed with 4% paraformaldehyde in PBS for 10 min at RT, pelleted, and permeabilized with 0.1% Triton X-100 in PBS for 2 min at RT. After permeabilization, cells were pelleted and rinsed twice with 200 μL PBS. Next, the following reagents (at the indicated final concentrations) were mixed immediately prior to use and 100 uL total volume in PBS was added to each cell pellet: 5-Fam-PEG-N_3 (0.5 mM), TCEP (1 mM), TBTA (0.2 mM), $CuSO_4$ (1 mM). Following 1 h incubation at RT, the cells were pelleted, and rinsed three times with 200 μL PBS. Cells were added to a 12 x 75 mm test tube (1.5 mL in PBS) for flow cytometry analysis. A total of 10,000 events (cell counts) for each sample were analyzed using a BD FACSCalibur (BD Biosciences) or a BD Accuri C6 (BD Biosciences).

4.5.4. In-gel fluorescence

HeLa cells were seeded in 60 mm or 100 mm culture dishes at 1.9 x 10^4 cells/cm^2 and grown for approximately 24 h (to approximately 50-60% confluence). Cell media were then supplemented with 25 μM lovastatin (when indicated), cells were grown for 18-24 h. Cell media was then replaced with media containing 10 μM C15Alk (unless specified otherwise) and cells were grown for 24 h (unless specified otherwise). Following this, the cells were rinsed twice with ice-cold PBS and scraped from the plate in 0.6-1.0 mL PBS using a teflon scraper. Cells were pelleted by centrifugation at 100 x g for 5 min. After discarding the supernatant, 200-400 μL of lysis buffer was added to each cell pellet. Lysis buffer consisted of PBS containing 1% SDS, protease inhibitor cocktail (per manufacturers protocols), benzonase (per manufacturers protocols), and 2.4 μM PMSF. Cells were lysed by sonicating with six cycles of 10 seconds on, 20 seconds off on ice. The concentration of protein in the lysate was determined using *DC*™ protein assay (Bio-Rad). To 100 μg (1 mg/mL concentration) of HeLa lysate, click reaction reagents were added at indicated final concentrations: 25 μM TAMRA-PEG-N_3, 1 mM TCEP, and 100 μM TBTA. After vortexing, 1.0 mM $CuSO_4$ (final concentration) was added, and the reaction was allowed to proceed at RT for 1 h. Excess reagents were removed by protein precipitation with a ProteoExtract protein precipitation kit (Calbiochem), following

manufacturers protocols. Protein pellets were dissolved in 1x Laemmli SDS-PAGE loading buffer and boiled for 6 min and 30-50 μg of protein samples were loaded onto 12% polyacrylamide gel. Gel was run at 120 V until dye front reached the bottom of the gel. For in-gel TAMRA fluorescence images, gels were scanned on a BioRad FX Molecular Imager. Gels were stained with Coomassie blue staining solution for total protein stain images.

4.5.5. In-gel fluorescence densitometry

Densitometry was performed using ImageJ. In brief, gel images in the TAMRA channel were converted into 8-bit mode and a region between 150 kDa and 20 kDa was selected for all the lanes. Lane profiles were plotted, bands were defined by drawing vertical lines, and the area under the curve was obtained for various bands in each lane. To remove the background, the area of the band in the DMSO control lane was subtracted from the area of the corresponding band in the other lanes. Proportions of total proteins present in various lanes were determined by densitometry of the total protein stain gel, and intensity of each lane in TAMRA channel was adjusted and normalized to this.

4.5.6. Primary Astrocyte Preparation

The brains were removed from C3H/C57BL/6 mice pups at postnatal day 0-2 and placed in 1x Hanks balanced salt solution (HBSS). Cortices and hippocampi were

dissected out and meninges removed. The tissues were cut into 1 mm^3 pieces with a sterile disposable scalpel, transferred to a conical tube with 1x trypsin in HBSS, and incubated in a 37 °C water bath for 15 minutes. A stop solution, containing 4% FBS and 0.2 mg/ml DNase I in HBSS, was added and the incubation extended for an additional 30 seconds at 37 °C. The tissue mixture was centrifuged at 200 x g for 5 minutes at RT and the supernatant was carefully aspirated from the tube. DMEM containing 10% FBS was added to the cell pellet and the mixture was triturated 20 times with a fire-polished pasteur pipet to dissociate cells. The cell suspension was passed through a 100 μm cell strainer to achieve single-cell suspension. Cells were then plated in T-75 flasks coated with poly-D-lysine, each plate was seeded with approximately 3-5 pups worth of glial cells. Cells were cultured at 37 °C with 5% of CO_2, in DMEM containing 5% FBS, 16 mM Hepes Buffer, 1x non-essential amino acids, 2 mM glutaMAX, 2.5 μg/mL aphotericin-B, and 50 ug/mL gentamicin. Media was changed on days 1, 2, 6, 14 and 21 post-plating to remove cellular debris. At this point, mixed glial/astrocyte cultures were trypsinized and approximately 0.5 x 10^6 cells were plated into each well of a poly-D-lysine (0.1 mg/mL) coated 6-well plate. For purifying astrocytes: 14 days after plating, microglial cells (attached on top of the astrocyte cell monolayer adhered to the culture plate) were harvested by shaking them off the astrocyte monolayer, and media was replaced on astrocyte culture.

Seven days later, this process was performed again. At this time, astrocytes were passaged to a new T-75 flask and allowed to grow for 4 days, at which point they were shaken to remove any residual microglia and passaged again. Four days later, the astrocytes were passaged a third time and the total cell number and viability were determined with a hemacytometer by adding 20 μL of cell suspension and 20 μL of Trypan blue. Approximately 0.5 x 10^6 cells were plated into each well of a 6-well plate, which had been previously coated with 0.1 mg/ml poly-D-lysine. After 3 days in culture, the astrocytes were subjected to isoprenoid labeling reactions (see 'Quantifying the Prenylome' in Methods).

4.5.7. Kinetic Constant Measurement

His-tagged rat FTase (rFTase) was expressed in *E. coli* and purified similarly to previous methods.[82] The rate of farnesylation of purified peptide by rFTase was determined using the time-dependent increase in fluorescence (λ_{ex} 340 nm, λ_{em} 505 nm) upon prenylation of a dansylated form of the peptide. Assays were performed with 2.0 μM dansyl-GlyCysValLeuSer (Ds-GCVLS), 20 nM rFTase, varying concentrations (0.25-16 μM) of FPP/alkyne analogue, 50 mM Tris, pH 7.5, 5 mM DTT, 5 mM $MgCl_2$, 50 μM $ZnCl_2$, and 0.040 % (*w/v*) *n*-dodecyl-β-D-maltoside at 25 °C. Peptides were incubated in reaction buffer for 5 min prior to initiation by the addition of rFTase. Fluorescence was measured as a function of time to define both the initial linear velocity and the reaction end point on a Varian

Cary Eclipse Fluorescence Spectrophotometer. The total fluorescence change observed upon reaction completion was divided by the initial concentration of the peptide substrate in a given reaction to yield a conversion from fluorescence units to product concentration (Amp_{conv}). The linear initial rate, V, in fluorescence intensity per minute, was then converted to a velocity (μM product produced per minute) by dividing V with Amp_{conv}.

4.5.8. Western Blot Analysis

Cell lysates were prepared using the following buffer: 50 mM Tris-HCl, pH 7.4, 1% NP-40, 0.25% Na-deoxycholate, 150 mM NaCl, 1 mM EDTA, 1 mM PMSF, 1 mg/mL aprotinin, 1 mg/mL leupeptin, 1 mM Na_3VO_4, 1 mM NaF, 20 mM b-glycerophosphate. Lysates were cleared by centrifugation (16,000 x g, 10 min, 4 °C) and proteins (40 μg) were resolved using 15% SDS-polyacrylamide mini-gels, and then transferred to Immobilon-P PVDF membrane. After blocking in a TBST/5% milk solution, immunoblots were incubated overnight at 4 °C using the following primary antibodies: anti-H-ras rabbit polyclonal (1:500) and anti-ERK2 rabbit polyclonal (1:2000), see Materials section for manufacturers. Following this, the membranes were incubated with an anti-rabbit IgG horseradish peroxidase-linked secondary antibody. The immunoblots were visualized using the SuperSignal West Pico Chemiluminescent Substrate following manufacturers protocols.

4.5.9. TAMRA-PEG-N_3 synthesis

TAMRA-PEG-N_3 was synthesized similar to a previously described method.[205] TAMRA-succinimidyl ester (25.0 mg, 47.4 µmol) was dissolved in 0.4 mL *N,N*-dimethylformamide (DMF). To this solution, 11-Azido-3,6,9-trioxaundecan-1-amine (14.1 µL, 71.1 µmol) and diisopropylethylamine (4.1 µL, 23.7 µmol) were added. The reaction was stirred overnight at RT in the dark. The reaction was diluted with 10 volumes of 0.1% aqueous TFA, filtered through a 0.2 µm syringe filter, and purified by RP-HPLC on a C_{18} column using a gradient of 1% B per minute (solvent A: 0.1% aqueous trifluoroacetic acid (TFA), solvent B: 0.1% TFA in CH_3CN), affording a dark red solid. Yield: 15.6 mg (52.1%), product eluted at 36% CH_3CN. Deconvoluted ESI-MS calculated for $C_{33}H_{39}N_6O_7$ = 631.3, found 631.3.

4.5.10. Farnesyl alkyne synthesis

Farnesol (3.00 g, 13.5 mmol) was dissolved in dry THF (15.0 mL). The mixture was placed under argon and cooled to 0 ^oC. NaH (0.48 g, 20.2 mmol) was slowly added to the flask. The mixture was stirred at 0 ^oC for 45 min. 80% propargyl bromide in toluene (9.0 mL, 81 mmol) was added to this mixture dropwise and it was stirred at 0 ^oC for 1h. The solution was warmed to room temperature slowly and stirred at room temperature for 16 h, after which point water was added to quench the reaction. The solution was extracted with diethyl ether (3 ×). The

combined organic layers were dried with $MgSO_4$ and concentrated *in vacuo*. The resulting brown oil was purified by flash chromatography (3:1 hexanes/ethyl acetate) to yield farnesyl alkyne as a light brown oil (1.62 g, 46%).

4.6. Acknowledgements

I would like to acknowledge the following people for their contribution to this work:

Joshua Ochocki (Department of Chemistry, University of Minnesota) - Developed the confocal microscopy and flow cytometry methods, optimized conditions for cell fixation and permeabilization. Acquired data and prepared labeled figures for: Figure 4.6, Figure 4.7, Figure 4.8 (right panel), and Figure 4.17.

Michelle Henderson (Department of Chemistry, University of Minnesota) – Cultured and transfected C2C12 cells with siRNA against BECN1 gene.

Yen-Chih Wang (Department of Chemistry, University of Minnesota) - Expression of rat FTase, measurement of kinetic constants for the reaction catalyzed by rat FTase with FPP and C15Alk as isoprenoid substrates.

Janel Warmka (Department of Environmental Health Sciences, University of Minnesota) - H-Ras protein western blots.

Dustin Chernick (Department of Experimental and Clinical Pharmacology, University of Minnesota) - Preparation of primary mouse astrocytes.

Chapter 5 Comparative study of alkyne-modified isoprenoids as chemical reporters of protein prenylation

5.1. Introduction

In Chapter 4, we observed that changing the concentration of alkyne-modified isoprenoid analog C15Alk during the metabolic labeling of HeLa cells caused dramatic effects on the specificity of labeling of prenylated proteins. In the field of prenylation, isoprenoid analogs that cause intense and robust labeling have been typically preferred in proteomic studies.[79, 80, 217] However, whether this labeling is specific to protein prenylation has not yet been investigated in detail. In this study we aim to compare metabolic labeling caused by various alkyne-modified isoprenoid analogs at various concentrations. This analysis is expected to reveal which isoprenoid analog, or combination of which analogs, is the most effective in selectively and efficiently targeting the prenylated proteome.

Several studies have been reported on studying the prenylated proteome using isoprenoid analogs having azide,[76-78] alkyne,[79, 80, 83, 88] anilinogeranyl[133] or biotin[132] functionalities. The biotinylated analog can be incorporated into proteins only by mutant forms of FTase and GGTase-I, whereas the anilinogeranyl-containing analog cannot be easily derivatized for subsequent affinity pull-down. Additionally, it has been noted that using alkyne-modified compounds for metabolic labeling followed by molar excess of azide reagents in the click

reaction results in lower levels of background labeling compared to using the azide-modified counterparts in metabolic labeling.[79, 134] Therefore, in this study, we have focused on comparing various alkyne-modified isoprenoid analogs.

The above-mentioned publications on the prenylated proteome have relied on the use of terminally substituted isoprenoid analogs. The Gibbs laboratory has reported a number of analogs containing a variety of functional groups at the C3 or C7 position of the isoprenoid (Figure 5.1).[218, 219] The investigation by Beese and colleagues revealed that the second "a" residue of the CaaX box (a_2 from Ca_1a_2X) has extensive hydrophobic interactions with methyl group at C7.[220] Therefore, isoprenoid analogs containing substituents at this position are expected to influence CaaX peptide substrate specificity of FTase. Indeed, Gibbs and co-workers found that each of their different FPP analogs having a different substituent at C3 and C7 had a unique pattern of reactivity against a library of CaaX peptides, which differed from the reactivity pattern of the natural FPP substrate.[70, 221] Owing to the distinctly different preferences of FPP and C3- or C7-modified analogs for CaaX sequences, when such analogs are used for the profiling of the prenylated proteome,[217] additional experiments might be required to validate prenylation of identified proteins with the native substrates FPP and GGPP. In the current work, we sought to compare the labeling of proteins in mammalian cells by various isoprenoid analogs containing an alkyne at the

terminal methyl position or at the C7 position by in-gel fluorescence analysis as well as by mass spectrometry based protein identification.

In the prenylated proteome profiling study by Charron and co-workers, a total of 114 proteins (52 with high confidence and 62 with medium confidence) were identified, of which only 22 proteins (17 with high confidence and 5 with medium confidence) contained the consensus sequence required for protein prenylation.[88] While a possible cause for getting non-prenylated protein hits could be non-specific binding and elution of proteins during affinity pull-down, the possibility that the alkyne analog got incorporated into the protein via a pathway other than protein prenylation cannot be ruled out. Recently, Zaro and co-workers reported on such a metabolic cross-talk phenomenon for chemical reporters.[208] They found that a previously published alkyne-containing metabolic chemical reporter of protein glycosylation also got metabolized in cells, becoming involved in modifications that were not glycosylation, such as protein acetylation.[208] These results demonstrated that chemical reporters might not target only a single post-translational modification, but rather have the potential to isolate and discover cross-talk between metabolic pathways in living cells. In this study, we aspired to investigate the off-target labeling caused by alkyne-modified isoprenoid analogs designed to be chemical reporters of protein prenylation.

Metabolic labeling with alkyne-modified analogs, followed by click reaction with fluorescent-azide and in-gel fluorescence analysis provides a relatively fast and inexpensive method to visualize the labeled proteins. It also enables characterization of the specificity of labeling by monitoring the labeling in presence of lovastatin or farnesol and geranylgeraniol. While lovastatin is expected to increase incorporation of isoprenoid analogs into prenylated proteins, farnesol and geranylgeraniol, which are precursors to natural substrates, are expected to compete away labeling. After initial screening of analogs using this method, affinity pull-down and tandem mass spectrometry facilitates determination of the identities of the proteins being labeled and shed light on the similarities and differences in reactivity patterns of analogs in living cells.

5.2. Research objective

The objective of this study was to evaluate the metabolic labeling patterns of various alkyne-modified isoprenoid analogs and compare their efficiency and specificity in labeling prenylated proteins in mammalian cells. The length of isoprenoid analog, the way in which the alkyne reporter group is attached to the isoprenoid backbone, and the concentration used for metabolic labeling could significantly affect (a) their ability to act as substrates for the three different prenyltransferase enzymes, (b) which CAAX box substrates they could modify efficiently, and (c) labeling of non-target proteins. It is essential to choose an

analog capable of providing sensitive and highly prenylation-specific labeling in order to obtain reliable results.

5.3. Results and discussion

5.3.1. In-gel fluorescence analysis of labeling caused by various alkyne-modified isoprenoid analogs

In order to compare incorporation of various alkyne-modified isoprenoids in metabolic labeling process, we treated HeLa cells for 24 hours with analogs shown in Figure 5.2, and then carried out the click reaction of cellular lysates with TAMRA-PEG-N_3 for downstream in-gel fluorescence analysis. Various concentrations of the analogs in the range of 10 μM and 100 μM were used to evaluate whether increasing the concentration affects the intensity and pattern of labeling. Additionally, the effects of lovastatin were characterized by metabolic labeling in the presence and absence of 25 μM lovastatin.

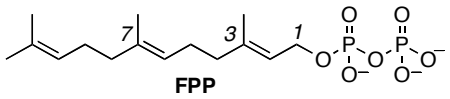

Figure 5.1. Structure of FPP with C1, C3 and C7 positions indicated by corresponding numbers.

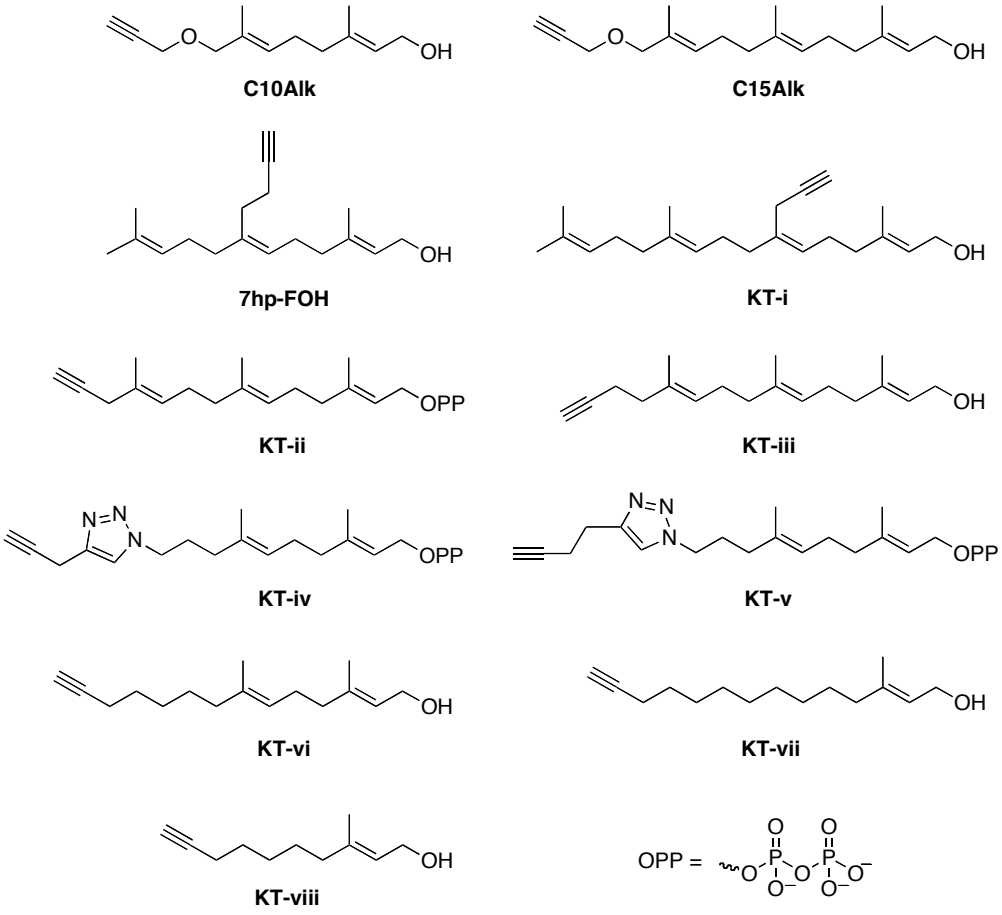

Figure 5.2. Structures of alkyne-modified isoprenoid analogs used in this study.

As reported in Chapter 4, for C15Alk, only marginal labeling was observed in absence of lovastatin at 5 and 10 μM, whereas lovastatin pre-treatment gave intense labeling specifically in 20-25 kDa small GTPases molecular weight region at these concentrations (Figure 5.3, right panel). At 25 μM and 50 μM C15Alk, several proteins bands in 30-75 kDa region were labeled in absence of lovastatin, which remained unaffected in presence of lovastatin. At these higher concentrations, the most prominent change upon lovastatin pre-treatment was again the increase in labeling intensity in the 20-25 kDa region (Figure 5.3, right panel). In Chapter 4 we showed that the part of labeling unaffected by lovastatin was possibly caused via mechanisms independent of protein prenylation. Similar labeling patterns, having specific labeling in the 20-25 kDa region at low probe concentration, and high overall labeling which was only partly affected by lovastatin-treatment, was also observed with probes 7hp-FOH (Figure 5.4, lanes 2-5 in left panel) and KT-vi (Figure 5.4, lanes 4-7 in right panel). Interestingly, C15Alk is known to be utilized by all three prenyltransferases in cells[80, 82] and the diphosphate version of 7hp-FOH is known to act as a substrate for mammalian FTase.[217] However, no knowledge is available regarding whether 7hp-FOH could be incorporated by GGTase-I and GGTase-II, and which of the three prenyltransferases can accept KT-vi as substrate.

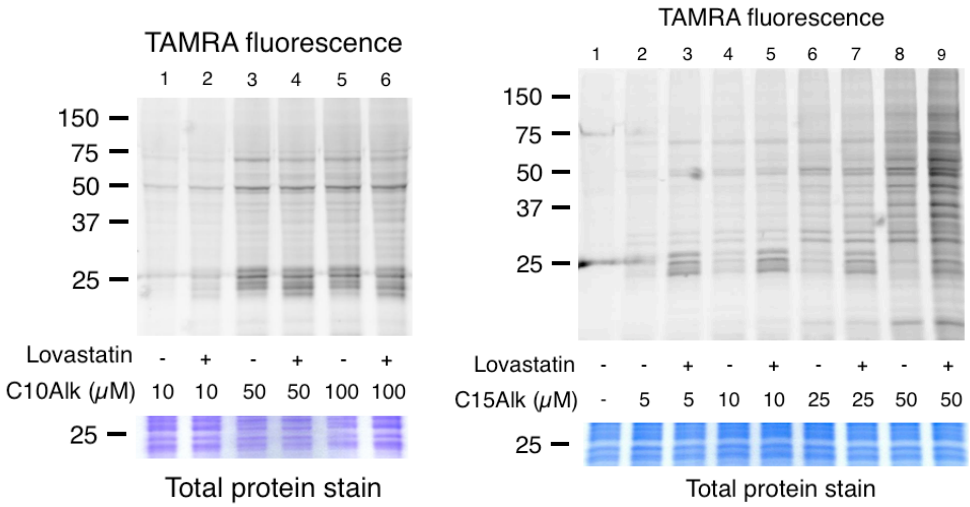

Figure 5.3. In-gel fluorescence analysis of HeLa cells treated with C10Alk and C15Alk. Data indicates that C10Alk (left panel) gives prenylation-specific labeling in the 25 kDa region at 10-100 μM in the presence or absence of lovastatin, whereas C15Alk (right panel) labeling specificity is concentration-dependent.

C10Alk, which is one isoprenoid unit shorter than C15Alk and previously reported to be a substrate of FTase,81 did not produce much labeling at 10 μM (Figure 5.3, lanes 1-2 in left panel). However, at 50 μM and 100 μM, C10Alk gave intense labeling in the 20-25 kDa small GTPases molecular weight region, which slightly increased in presence of lovastatin (Figure 5.3, lanes 3-6 in left panel). This indicated that C10Alk gives prenylation-specific labeling at up to 100 μM concentrations, with low amounts of background labeling. Similarly, highly intense labeling particularly in the 20-25 kDa region independent of concentration was also observed with KT-i (Figure 5.5, lanes 2-5 in left panel), KT-ii (Figure 5.5, lanes 6-9 in right panel) and KT-iii (Figure 5.4, lanes 6-9 in left panel). Notably, KT-i, which mimics the size of GGPP more closely than FPP, was not accepted as a substrate by GGTase-I in an *in vitro* assay using a dansyl-GCVLL substrate.[219] KT-ii and KT-iii showed moderate substrate activity against GGTase-I in the *in vitro* assay[219], whereas, both these compounds were incorporated by FTase in living cells.[80] When comparing the results obtained with probes C10Alk, KT-i, KT-ii and KT-iii to results with C15Alk, 7hp-FOH and KT-vi, we observed that combination of the isoprenoid chain length and the way in which the alkyne-reporter group is attached to the isoprenoid backbone substantially affect the specificity of labeling. The terminal alkyne-containing analogs with chain length comparable to FPP, but slightly shorter than GGPP

(C10Alk, KT-ii, KT-ii), gave selective labeling at all the concentrations tested. On the other hand, the labeling caused by the terminal alkyne-containing analog having a size similar to GGPP (C15Alk) was concentration-dependent. These results contrast with the labeling pattern of C7-modified analogs. In the case of C7-modified analogs, the labeling specificity of the shorter analog (7hp-FPP) depended on concentration used for metabolic labeling, whereas, the longer analog (KT-i) gave specific labeling in 20-25kDa region at multiple concentration used in this study.

Next, KT-iv (Figure 5.5, lanes 2-5 in right panel), KT-v (data not shown) and KT-viii (Figure 5.5, lanes 6-9 in left panel) did not produce any noticeable labeling at up to 100 μM (data at 10-50 μM shown in the indicated figures, data at 100 μM not shown). KT-vii caused intense labeling at 10 μM, which was unaffected by lovastatin pre-treatment and was probably independent of protein prenylation, and the compound was found to be toxic to HeLa cells at concentrations higher than 10 μM. These results suggest that substituting the isoprenoid units in FPP and GGPP by a straight alkyl chain (as in KT-vii and KT-viii) or a triazole moiety (as in KT-iv and KT-v) adversely affects the ability of analogs to be substrates to prenyltransferase enzymes.

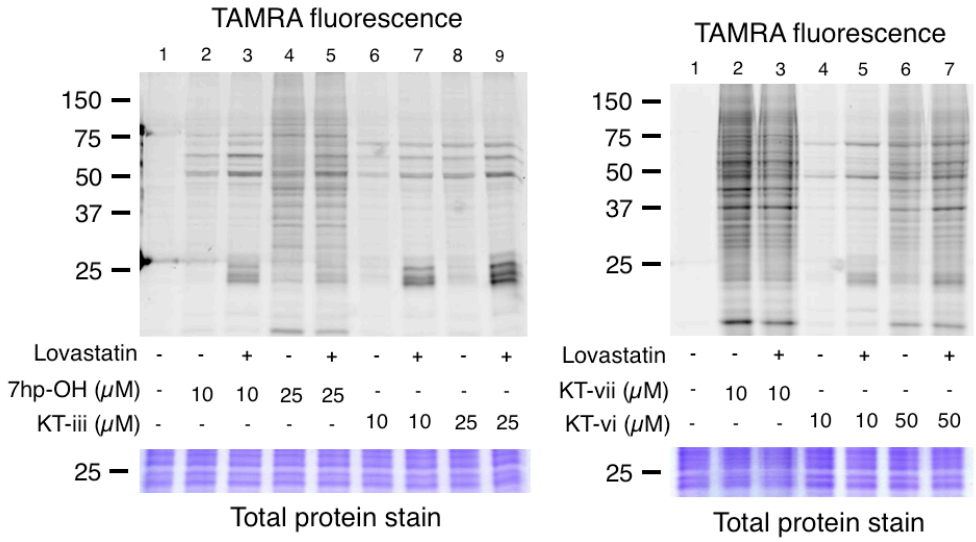

Figure 5.4. In-gel fluorescence analysis indicates differences in the labeling of HeLa cells with various alkyne-modified isoprenoids. Specificity of 7hp-FOH (lanes 2-5 in left panel) and KT-vi (lanes 4-7 in right panel) labeling is concentration-dependent, KT-iii (lanes 6-9, left panel) gives prenylation-specific labeling at 10 and 25 μM, and KT-vii (lanes 2-3, right panel) labeling is not affected by lovastatin indicating that it is not related to protein prenylation.

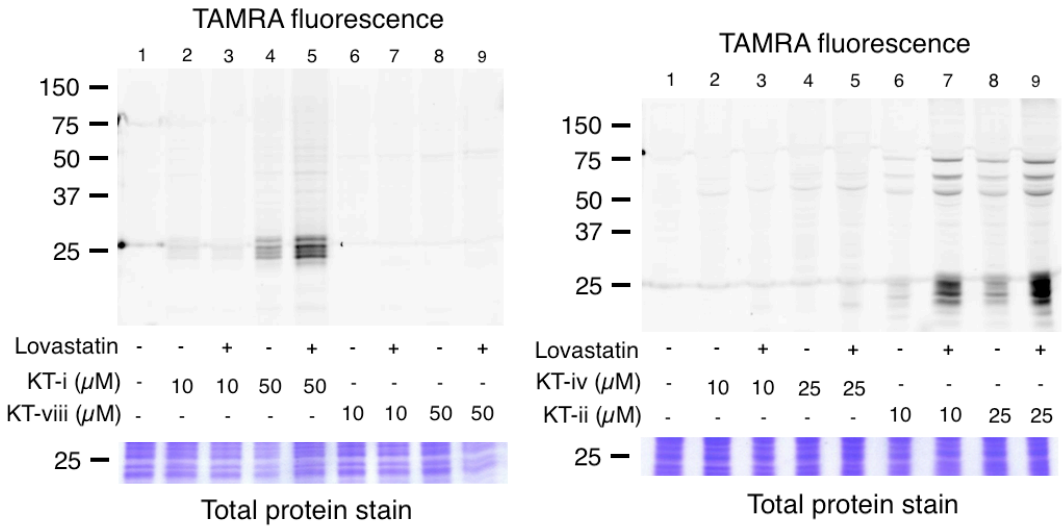

Figure 5.5. In-gel fluorescence analysis indicates differences in labeling of HeLa cells with various alkyne-modified isoprenoids. KT-i (lanes 2-5 in left panel) and KT-ii (lanes 6-9 in right panel) give highly specific labeling in 20-25 kDa small GTPases molecular weight region, which increases in the presence of lovastatin pre-treatment. KT-iv (lanes 2-5 in right panel) and KT-viii (lanes 6-9 in left panel) do not produce any labeling at the multiple concentrations tested.

Taken together, in-gel fluorescence analysis data clearly indicates that it is necessary to characterize isoprenoid analogs for their ability to act as substrates to the three prenyltransferases both *in vitro* and *in vivo*, as well as for specificity of labeling at various probe concentrations before using them for proteomic analysis. Based on the results of the in-gel fluorescence screening, we chose C15Alk, 7hp-FOH and KT-i for further proteomic profiling analysis. 7hp-FOH, which is a C7-modified analog of FPP, and C15Alk, which is a terminal alkyne known to mimic both FPP and GGPP, gave similar labeling patterns and prenylation-specific labeling at low probe concentrations. KT-i, which *in vitro* was not a GGTase-I substrate in spite of mimicking the GGPP size, gave highly specific labeling at multiple concentrations.

5.3.2. Proteomic profiling of COS-7 cells labeled with C15Alk-OPP and 7hp-FPP

In order to achieve the immobilization of alkyne-tagged proteins and subsequent selective release, we synthesized a bifunctional azido linker, biotin-PC-N3 (Figure 5.6), containing an azide site for click reaction, a biotin moiety for streptavidin-based affinity pull-down and a photocleavable o-nitrobenzyl group for selective release of the target proteins from the resin. The o-nitrobenzyl group cleaves upon UV light irradiation (365 nm) in a process depicted in Figure 5.6. Photocleavage of biotin-PC-N_3 was monitored via HPLC by injecting the same

amounts of biotin-PC-N_3 after varied lengths of UV irradiation time. Upon increasing the duration of UV irradiation, intensity of the biotin-PC-N3 peak in the chromatogram decreased, and complete photocleavage was achieved in 3 min (Figure 5.7). Using a recombinant green fluorescent protein containing a C-terminal CaaX motif (GFP-CVIA), we verified that biotin-PC-N_3 could be successfully used in click reactions with alkyne-modified proteins and subsequently for affinity pull-down using Neutravidin resin and elution by UV irradiation (data not shown).

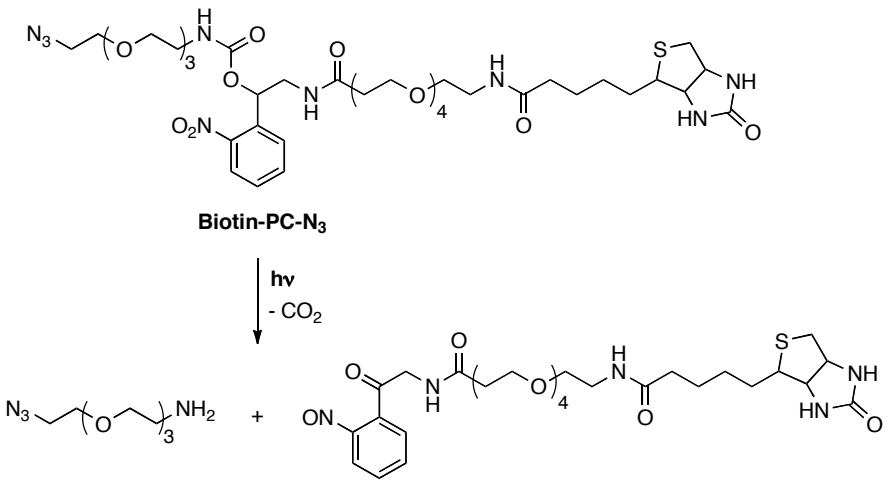

Figure 5.6. Structure and photocleavage reaction of biotin-PC-N_3.

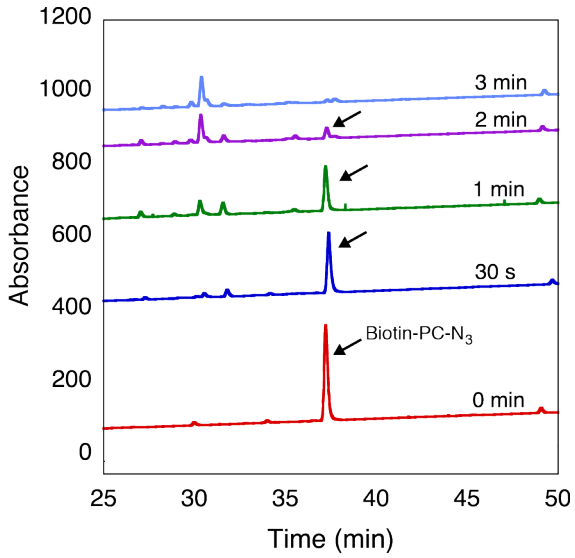

Figure 5.7. Photocleavage of biotin-PC-N3 monitored by the disappearance of its peak in HPLC analysis upon increasing the time of irradiation of 365 nm light.

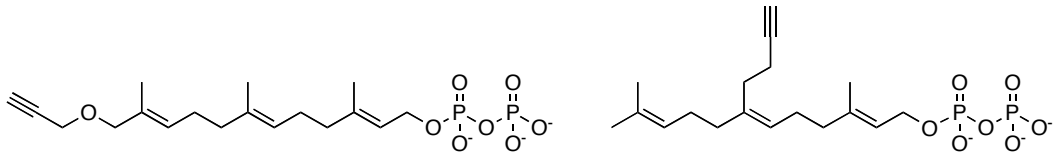

C15Alk-OPP 7hp-FPP

Figure 5.8. Structures of C15Alk-OPP and 7hp-FPP.

Table 5.1. Summary of profiling of prenylated proteins labeled by C15Alk-OPP and 7hp-FPP.

	C15Alk-OPP	7hp-FPP
Total number of proteins containing a potential sequence for protein prenylation	84	98
Number of proteins containing a CaaX motif	54	76
Number of proteins containing CC, CXC or CCXX motif	30	22

Next, we sought to profile the proteins labeled by C15Alk-OPP and 7hp-FPP (Figure 5.8) to compare their selectivity and efficiency of getting incorporated by the three prenyltransferases. For this, COS-7 cells were treated at 10 μM with either C15Alk-OPP or 7hp-FPP in the presence of 20 μM lovastatin. After 24 hour labeling, cells were lysed and the lysates were reacted with biotin-PC-N_3 in a Cu(I)-catalyzed click reaction. The proteins were then incubated with Neutravidin beads for 90 min, unbound proteins were washed off the resin using multiple denaturing buffers and the bound proteins were tryptic digested on-resin. Excess isoprenoids and salts were removed from the tryptic peptide fragments by both an HILIC tip and a C18 cartridge and subjected to LC-MS/MS analysis on an LTQ-Orbitrap Velos mass spectrometer. A large number of proteins containing consensus sequences for protein prenylation (84 labeled with C15Alk-OPP, 98 labeled with 7hp-FPP) were successfully identified from both these analyses (Table 5.1, complete lists of prenylated proteins identified in these analyses are included in tables Table 5.2 and Table 5.3). Importantly, this list of prenylated proteins is significantly more comprehensive (~2.5- to 5-fold larger) than previously published studies based on similar enrichment strategies.[76, 88, 132] In particular, the current analysis using the C15Alk-OPP reporter yielded almost 4-fold more hits than the study reported by Charron and colleagues using an alcohol version of this probe (C15Alk).[88] It should be noted

that the later analysis was carried on a C15Alk-labeled murine macrophage cell line, whereas, the current analysis is based on COS-7 cells, which are kidney fibroblast-like cells derived from the African green monkey. On the other hand, the results obtained with 7hp-FPP are comparable to unpublished results obtained with the same probe and the same cell line by Song and co-workers.[217]

For a more accurate comparison of the C15Alk-OPP and 7hp-FPP incorporation, it is essential to have at least three independent replicates of the proteomic profiling analyses with each probe to verify the reproducibility. Since we only have data from one replicate, additional experimental replicates are needed at this point. However, this preliminary data suggests that the ratio of CaaX proteins (FTase and GGTase-I substrates) to di-geranylgeranylation Rab proteins identified with 7hp-FPP is higher compared to C15Alk-OPP (Table 5.1). Along with the prenylated proteins, a number of proteins lacking the consensus sequence for prenylation were also identified. A total of 628 proteins were identified from the C15Alk-OPP labeled sample, of which 84 proteins are candidates for prenylation; whereas a total of 706 proteins were identified in the 7hp-FPP sample, of which 98 proteins possess the prenylation motif. Having additional replicates of the experiment would also allow for the determination of whether these off-target proteins identified the analysis are non-specific background proteins (getting identified in only one of the replicates) or whether

they are caused by a specific labeling pathway independent of protein prenylation causing them to be reproducibly identified in all the experimental replicates.

5.4. Summary

In summary, we carried out in-gel fluorescence analysis of HeLa cells treated with a panel of 11 isoprenoid analogs and our results indicate that subtle differences in the length of isoprenoid and attachment of the alkyne-reporter group to the isoprenoid backbone have dramatic effects on the pattern and specificity of labeling on prenylated proteins. We also found that analogs containing isoprenoid units substituted with saturated alkyl chain or a triazole moiety are not accepted as substrates by the prenyltransferase enzymes in cells. Proteomic profiling of COS-7 cells labeled with two of the isoprenoid analogs, C15Alk-OPP and 7hp-FPP led to the identification of a large number of prenylated proteins, 84 and 98 prenylated proteins, respectively. These identified proteins were not only CaaX box-containing proteins (substrates of FTase and GGTase-I), but also Rab proteins having a consensus sequence for dual geranylgeranylation by GGTase-II. These results and further experiments suggested in the next section will elucidate the ability of various isoprenoid analogs to efficiently and selectively label the prenylated proteome in living cells. This knowledge will help in choosing the best candidate analog, or a combination of multiple analogs, from the diverse library of available isoprenoid analogs to

use in proteomic profiling. This in turn could allow for the reliable analysis of prenylated proteomes of cultured cells as well as tissues from living animals under normal and diseased states and in response to prenyltransferase inhibitors.

5.5. Future direction

As mentioned in Section 4.3, it is essential to carry out three independent replicates of the proteomic analysis to determine the overlap in identified proteins and their reproducibility. Since only one experimental replicate has been performed so far, we plan to carry out two more replicates for proteomic analysis of COS-7 cells treated with C15Alk-OPP and with 7hp-FPP. While in-gel fluorescence labeling patterns look similar for these analogs, this proteomic analysis will allow us to compare which proteins actually get labeled by these two analogs and evaluate differences in the metabolism of analogs having an alkyne-reporter group at the terminal (for C15Alk-OPP) versus C7 position (for 7hp-FPP). We also plan to carry out proteomic profiling of COS-7 cell proteins labeled by KT-i. This analog is one isoprenoid longer than 7hp-FPP, and comparable in size to C15Alk-OPP. However, during the in-gel fluorescence analysis, it displayed a distinctly specific labeling pattern in the 20-25 kDa region at all the concentrations used for metabolic labeling. This contrasts with the concentration-dependent labeling specificity observed with C15Alk and 7hp-FOH. Proteomic

analysis with this analog and then subsequent comparison of the proteins identified using C15Alk-OPP, 7hp-FPP and KT-i will enable us to determine which one or combination of which isoprenoid analogs is optimal to get comprehensive and selective coverage of the prenylated proteins in proteomic profiling studies.

Another future goal for this study is to detect the site of labeling with these analogs using mass spectrometry. In the current experimental design, alkyne-tagged proteins upon click reaction with biotin-PC-N_3 are incubated on avidin resin. After removal of unbound proteins, bound proteins are tryptic-digested on-resin. After the digestion step, peptides containing the site of modification remain bound to the resin. We plan to use UV irradiation to elute the modified bound peptides from resin via photocleavage reaction shown in Figure 5.6. LC-MS/MS analysis of these eluted peptides is expected to allow for detection of the site of modification as described by Wright and co-workers for protein myristoylation.[222]

5.6. Methods

Compounds KT-i, KT-ii, KT-iii, KT-iv and KT-v were synthesized as described previously.[219] 7hp-OH and 7hp-FPP were synthesized using previously published procedures[217]. C10Alk,[81] C15Alk[82] and C15Alk-OPP[82] were synthesized as previously reported. Benzonase nuclease (E1014) and protease inhibitor cocktail (P8340) were purchased from Sigma Aldrich. ProteoExtract® Protein

Precipitation kit (539180) was from EMD Millipore. *DC*™ Protein Assay kit was obtained from Bio-Rad.

5.6.1. Synthesis of biotin-PC-N_3

Using a precursor synthesized according to a previous report,[223] biotin-PC-N_3 was synthesized as shown in Scheme 5.1.

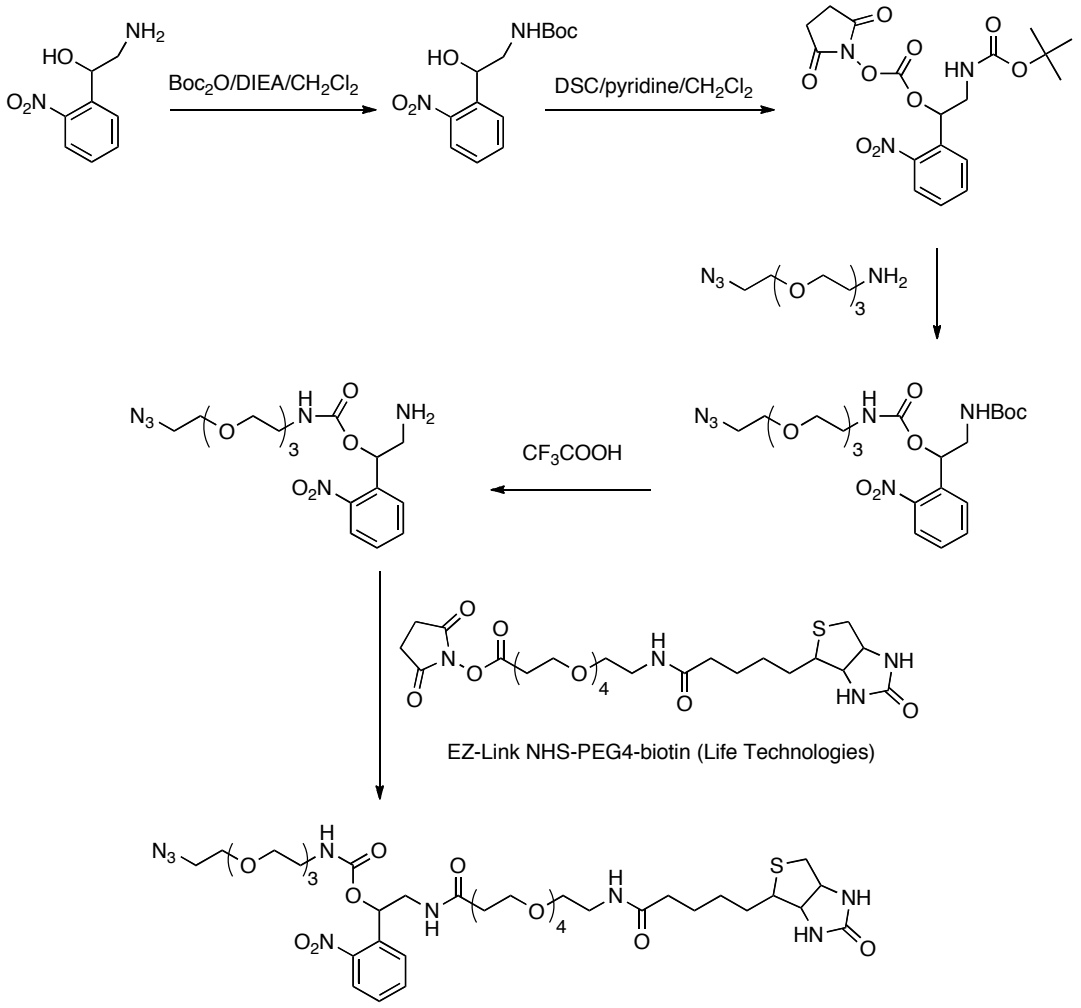

Scheme 5.1. Synthesis of biotin-PC-N_3.

5.6.2. Monitoring photocleavage of biotin-PC-N_3 by HPLC

HPLC analysis was done by injecting 100 μL of a 100μM solution of biotin-PC-N_3, after 0, 0.5, 1, 2, or 3 min irradiation of 365 nm UV light in a standard Rayonet photoreactor, onto a C_{18} analytical HPLC column. A 250 x 4.6 mm C_{18} column (Varian) was used with included 0.1% aqueous trifluoroacetic acid (TFA) as buffer A, and CH_3CN containing 0.1% TFA as buffer B. Buffer B gradient was 0-100% over 100 min and the flow rate was 1 mL/min. Diode array detector was used to monitor absorbance at 214 nm and 260 nm for detecting biotin-PC-N_3 being eluted from the column.

5.6.3. In-gel fluorescence analysis

HeLa cells were maintained in DMEM containing 10% FBS. HeLa cells were seeded in 100 mm culture dishes at 1.9 x 10^4 cells/cm^2 and grown for 24 h (to approximately 50-60% confluence). Cell media was then supplemented with 25 μM lovastatin (when indicated) and cells were incubated for 18-24 h. Cell media was then replaced with fresh media, 10-50 µM of desired isoprenoid analog was added and cells were grown for 24 h. Cells were rinsed twice with ice-cold PBS and scraped from the plate in 1 mL PBS with a teflon scraper (this and the subsequent steps were performed on ice). Cells were placed in 1.5 mL micro-centrifuge tube and pelleted by centrifugation at 100 g for 5 min. After discarding the supernatant, 200-400 µL of lysis buffer (PBS containing 0.10% SDS,

protease inhibitor cocktail (per manufacturers protocols), benzonase (per manufacturers protocols), and 2.4 µM PMSF was added to the cell pellet. Cells were lysed by sonication with six cycles at 4 W of 10 seconds on, 20 seconds off on ice. The concentration of proteins in the lysate was determined using a detergent-compatible protein assay reagent kit. To 100 µg (1 mg/mL) of HeLa lysate was added click reaction reagents at indicated final concentrations: 25 μM TAMRA-PEG-N_3, 1 mM TCEP, and 100 μM TBTA. After vortexing, 1.0 mM $CuSO_4$ was added, and the reaction was allowed to proceed at RT for 1 h. Excess reagents were removed by protein precipitation with a ProteoExtract protein precipitation kit, following manufacturers protocols. Protein pellets were suspended in 1x Laemmli SDS-PAGE loading buffer and sonicated in a water bath for 2 min and heated at 95 °C for 8 min. 30-50 µg of protein was loaded onto 12% polyacrylamide gel and was run at 120 V until dye front reached the bottom (approximately 60-75 min). For in-gel TAMRA fluorescence images, gels were scanned on a Bio-Rad FX Molecular Imager. Gels were stained with Coomassie blue stain solution for total protein stain images.

5.6.4. Enrichment of prenylated proteins

COS-7 were maintained in DMEM containing 10% FBS. Six 100 mm plates were seeded with 800,000 COS-7 cells, each, and grown until they were about 50-60% confluent. Cells were provided with fresh media containing 20 μM lovastatin and

10 μM of either C15Alk-OPP or 7hp-FPP. Cells were incubated for 24 h for metabolic labeling of proteins to occur. Cell were washed twice with cold PBS, harvested in PBS by scraping cells off the plates, and pelleted by centrifugation at 100 x g for 5 min. After removal of the supernatant PBS, cells were lysed in PBS containing 1% SDS, protease inhibitor cocktail and PMSF by sonication. Lysates were centrifuged at 10,000 x g for 5 min and pelleted cell debris were discarded. Protein concentration in lysate was estimated using *DC* protein assay. To cell lysate containing 1-2 mg/mL protein, the click reaction reagents were added to the indicated final concentrations: 100 μM biotin-PC-azide, 1 mM TCEP, 100 μM TBTA and 1 mM CuSO4. After 1 h click reaction at RT, proteins were precipitated to remove excess click reaction reagents by adding 1x volume of chloroform, 4x volume of MeOH and 3x volume of PBS. After 4,500 x g centrifugation for 5 min, the supernatant aqueous layer was discarded. Four times the volume of MeOH was added and proteins were pelleted by centrifuge at 4,500 x g for 5 min. Supernatant was discarded and protein pellets were air-dried.

Protein pellet was dissolved in PBS containing 1% SDS by vortex and sonication to get ~1-2 mg/mL solution. This solution was boiled for 5 min, cooled and then incubated with 300 μL Neutravidin-agarose resin (which was pre-equilibrated in PBS containing 1% SDS) for 90 min at RT. Unbound proteins were

removed by washing the resin 3x with 1% SDS in PBS, 1x with PBS, 3x with 8 M urea, and 3x with 50 mM NH_4HCO_3. Resin was suspended in 300 μL of 50 mM NH_4HCO_3, 6 μg trypsin was added and digestion was carried out overnight at 37 °C. Supernatant peptides were collected and lyophilized.

5.6.5. MS/MS analysis of tryptic peptides

Peptide samples were purified by a Hydrophilic Interaction Chromatography (HILIC) tip (polyLC) and then analyzed on Eksigent Ultra2D HPLC system coupled to a LTQ-Orbitrap Velos mass spectrometer (Thermo Fisher). Buffer A contained 0.1% aqueous formic acid. A linear gradient of 90 min from 0% buffer B (0.1% formic acid in CH_3CN) to 40% buffer B with 300 nL/min flow rate was used for each LC-MS/MS run. Data-dependent acquisition mode was used to collect MS/MS scans on the top 20 most abundant precursor ions (m/z ranges from 300-1700 with resolution of 30,000). Dynamic exclusion time was set to 90 s. The .RAW files were searched against human protein database with no redundant entries using the SEQUEST algorithm on Proteome Discoverer (Version 1.2; Thermo Fisher). Parameters during database search included peptide precursor mass tolerance at 10 ppm, MS/MS tolerance at 0.8 Da, dynamic modification of +15.9949 Da for methionine oxidation, full tryptic digestion with a maximum of two missed cleavages, and data was filtered with 1% false discovery rates (FDR).

Table 5.2. A complete list of prenylated proteins identified in the proteomic profiling of COS-7 cells labeled with C15Alk-OPP

Accession	Description	Caax motif	CC, CXC, CCXX motif	ΣCoverage	Σ# Unique Peptides	Σ# Peptides
Q15907	Ras-related protein Rab-11B OS=Homo sapiens GN=RAB11B PE=1 SV=4 - [RB11B_HUMAN]	√	√	48.62	2	9
P11234	Ras-related protein Ral-B OS=Homo sapiens GN=RALB PE=1 SV=1 - [RALB_HUMAN]	√	√	39.32	3	6
P61812	Transforming growth factor beta-2 OS=Homo sapiens GN=TGFB2 PE=1 SV=1 - [TGFB2_HUMAN]	√	√	5.80	2	2
P01137	Transforming growth factor beta-1 OS=Homo sapiens GN=TGFB1 PE=1 SV=2 - [TGFB1_HUMAN]	√	√	4.87	1	1
Q9Y3L5	Ras-related protein Rap-2c OS=Homo sapiens GN=RAP2C PE=1 SV=1 - [RAP2C_HUMAN]	√		50.82	5	8
P61006	Ras-related protein Rab-8A OS=Homo sapiens GN=RAB8A PE=1 SV=1 - [RAB8A_HUMAN]	√		48.79	3	9
Q9NP72	Ras-related protein Rab-18 OS=Homo sapiens GN=RAB18 PE=1 SV=1 - [RAB18_HUMAN]	√		48.54	9	9
P61225	Ras-related protein Rap-2b OS=Homo sapiens GN=RAP2B PE=1 SV=1 - [RAP2B_HUMAN]	√		45.36	3	6
P20700	Lamin-B1 OS=Homo sapiens GN=LMNB1 PE=1 SV=2 - [LMNB1_HUMAN]	√		42.66	24	27
J9JID7	Lamin B2, isoform CRA_a OS=Homo sapiens GN=LMNB2 PE=1 SV=1 - [J9JID7_HUMAN]	√		40.97	26	29
P62070	Ras-related protein R-Ras2 OS=Homo sapiens GN=RRAS2 PE=1 SV=1 - [RRAS2_HUMAN]	√		40.69	5	7
O75781	Paralemmin-1 OS=Homo sapiens GN=PALM PE=1 SV=2 - [PALM_HUMAN]	√		39.28	8	8
P31689	DnaJ homolog subfamily A member 1 OS=Homo sapiens GN=DNAJA1 PE=1 SV=2 - [DNJA1_HUMAN]	√		39.04	12	12
O60884	DnaJ homolog subfamily A member 2 OS=Homo sapiens GN=DNAJA2 PE=1 SV=1 - [DNJA2_HUMAN]	√		38.83	16	16
P62834	Ras-related protein Rap-1A OS=Homo sapiens GN=RAP1A PE=1 SV=1 - [RAP1A_HUMAN]	√		38.59	1	6
P61224	Ras-related protein Rap-1b OS=Homo sapiens GN=RAP1B PE=1 SV=1 - [RAP1B_HUMAN]	√		38.59	2	7
Q9UBI6	Guanine nucleotide-binding protein G(I)/G(S)/G(O) subunit gamma-12 OS=Homo sapiens GN=GNG12 PE=1 SV=3 - [GBG12_HUMAN]	√		37.50	2	2
P10114	Ras-related protein Rap-2a OS=Homo sapiens GN=RAP2A PE=1 SV=1 - [RAP2A_HUMAN]	√		37.16	2	5
P10301	Ras-related protein R-Ras OS=Homo sapiens GN=RRAS PE=1 SV=1 - [RRAS_HUMAN]	√		37.16	4	6
P63218	Guanine nucleotide-binding protein G(I)/G(S)/G(O) subunit gamma-5 OS=Homo sapiens GN=GNG5 PE=1 SV=3 - [GBG5_HUMAN]	√		32.35	3	3
G3V1B3	60S ribosomal protein L21 OS=Homo sapiens GN=RPL21 PE=1 SV=1 - [G3V1B3_HUMAN]	√		29.89	2	2
P84095	Rho-related GTP-binding protein RhoG OS=Homo sapiens GN=RHOG PE=1 SV=1 - [RHOG_HUMAN]	√		28.80	4	4
O15498	Synaptobrevin homolog YKT6 OS=Homo sapiens GN=YKT6 PE=1 SV=1 - [YKT6_HUMAN]	√		27.78	6	6
Q15382	GTP-binding protein Rheb OS=Homo sapiens GN=RHEB PE=1 SV=1 - [RHEB_HUMAN]	√		26.09	5	5
P63000	Ras-related C3 botulinum toxin substrate 1 OS=Homo sapiens GN=RAC1 PE=1 SV=1 - [RAC1_HUMAN]	√		25.52	5	5
P01111	GTPase NRas OS=Homo sapiens GN=NRAS PE=1 SV=1 - [RASN_HUMAN]	√		24.87	4	5
P02545	Prelamin-A/C OS=Homo sapiens GN=LMNA PE=1 SV=1 - [LMNA_HUMAN]	√		23.64	12	13

F8VVB5	Nucleosome assembly protein 1-like 1 (Fragment) OS=Homo sapiens GN=NAP1L1 PE=1 SV=1 - [F8VVB5_HUMAN]	√		22.98	1	5
P50151	Guanine nucleotide-binding protein G(I)/G(S)/G(O) subunit gamma-10 OS=Homo sapiens GN=GNG10 PE=1 SV=1 - [GBG10_HUMAN]	√		22.06	1	1
P60953	Cell division control protein 42 homolog OS=Homo sapiens GN=CDC42 PE=1 SV=2 - [CDC42_HUMAN]	√		21.47	3	3
P09543	2',3'-cyclic-nucleotide 3'-phosphodiesterase OS=Homo sapiens GN=CNP PE=1 SV=2 - [CN37_HUMAN]	√		21.14	10	10
P01116	GTPase KRas OS=Homo sapiens GN=KRAS PE=1 SV=1 - [RASK_HUMAN]	√		18.52	2	3
B7Z9G5	BRO1 domain-containing protein BROX OS=Homo sapiens GN=BROX PE=1 SV=1 - [B7Z9G5_HUMAN]	√		17.41	5	5
Q9UL25	Ras-related protein Rab-21 OS=Homo sapiens GN=RAB21 PE=1 SV=3 - [RAB21_HUMAN]	√		16.00	4	4
P61586	Transforming protein RhoA OS=Homo sapiens GN=RHOA PE=1 SV=1 - [RHOA_HUMAN]	√		15.03	2	3
P51153	Ras-related protein Rab-13 OS=Homo sapiens GN=RAB13 PE=1 SV=1 - [RAB13_HUMAN]	√		14.78	1	3
K7EM09	Transmembrane protein 205 (Fragment) OS=Homo sapiens GN=TMEM205 PE=1 SV=1 - [K7EM09_HUMAN]	√		14.17	1	1
Q9BVM2	Protein DPCD OS=Homo sapiens GN=DPCD PE=1 SV=2 - [DPCD_HUMAN]	√		13.79	3	3
P62745	Rho-related GTP-binding protein RhoB OS=Homo sapiens GN=RHOB PE=1 SV=1 - [RHOB_HUMAN]	√		12.76	1	2
P51157	Ras-related protein Rab-28 OS=Homo sapiens GN=RAB28 PE=1 SV=2 - [RAB28_HUMAN]	√		12.67	2	2
H0YEI6	WD and tetratricopeptide repeats protein 1 (Fragment) OS=Homo sapiens GN=WDTC1 PE=4 SV=1 - [H0YEI6_HUMAN]	√		11.20	1	1
H0YC77	Annexin (Fragment) OS=Homo sapiens GN=ANXA6 PE=1 SV=1 - [H0YC77_HUMAN]	√		9.89	1	1
P61587	Rho-related GTP-binding protein RhoE OS=Homo sapiens GN=RND3 PE=1 SV=1 - [RND3_HUMAN]	√		9.43	2	2
O14807	Ras-related protein M-Ras OS=Homo sapiens GN=MRAS PE=1 SV=2 - [RASM_HUMAN]	√		5.29	1	1
E5RHS5	Eukaryotic translation initiation factor 3 subunit E (Fragment) OS=Homo sapiens GN=EIF3E PE=1 SV=1 - [E5RHS5_HUMAN]	√		4.42	1	1
Q96EA4	Protein Spindly OS=Homo sapiens GN=SPDL1 PE=1 SV=2 - [SPDLY_HUMAN]	√		4.13	2	2
C9J6P4	Zinc finger CCCH-type antiviral protein 1 OS=Homo sapiens GN=ZC3HAV1 PE=1 SV=1 - [C9J6P4_HUMAN]	√		4.10	3	3
Q32MZ4	Leucine-rich repeat flightless-interacting protein 1 OS=Homo sapiens GN=LRRFIP1 PE=1 SV=2 - [LRRF1_HUMAN]	√		3.96	3	3
G3V3G9	DDB1- and CUL4-associated factor 8 OS=Homo sapiens GN=DCAF8 PE=1 SV=1 - [G3V3G9_HUMAN]	√		2.80	1	2
P49454	Centromere protein F OS=Homo sapiens GN=CENPF PE=1 SV=2 - [CENPF_HUMAN]	√		2.65	6	6
Q8NDI1	EH domain-binding protein 1 OS=Homo sapiens GN=EHBP1 PE=1 SV=3 - [EHBP1_HUMAN]	√		2.11	2	2
Q9Y6Q2	Stonin-1 OS=Homo sapiens GN=STON1 PE=1 SV=2 - [STON1_HUMAN]	√		1.90	1	1
A6NIT2	Phosphorylase b kinase regulatory subunit alpha, skeletal muscle isoform OS=Homo sapiens GN=PHKA1 PE=1 SV=1 - [A6NIT2_HUMAN]	√		0.76	1	1

Q8N3D4	EH domain-binding protein 1-like protein 1 OS=Homo sapiens GN=EHBP1L1 PE=1 SV=2 - [EH1L1_HUMAN]	√		0.59	1	1
P62820	Ras-related protein Rab-1A OS=Homo sapiens GN=RAB1A PE=1 SV=3 - [RAB1A_HUMAN]		√	67.32	5	11
P61106	Ras-related protein Rab-14 OS=Homo sapiens GN=RAB14 PE=1 SV=4 - [RAB14_HUMAN]		√	62.33	10	11
P61019	Ras-related protein Rab-2A OS=Homo sapiens GN=RAB2A PE=1 SV=1 - [RAB2A_HUMAN]		√	62.26	6	11
Q9H0U4	Ras-related protein Rab-1B OS=Homo sapiens GN=RAB1B PE=1 SV=1 - [RAB1B_HUMAN]		√	59.70	3	9
B4DJA5	Ras-related protein Rab-5A OS=Homo sapiens GN=RAB5A PE=1 SV=1 - [B4DJA5_HUMAN]		√	58.21	6	8
H3BSC1	Ras-related protein Rab-11A OS=Homo sapiens GN=RAB11A PE=1 SV=1 - [H3BSC1_HUMAN]		√	51.52	2	9
P20340	Ras-related protein Rab-6A OS=Homo sapiens GN=RAB6A PE=1 SV=3 - [RAB6A_HUMAN]		√	50.48	1	10
P51148	Ras-related protein Rab-5C OS=Homo sapiens GN=RAB5C PE=1 SV=2 - [RAB5C_HUMAN]		√	49.07	6	8
H0YGL6	Ras-related protein Rab-6A (Fragment) OS=Homo sapiens GN=RAB6A PE=1 SV=1 - [H0YGL6_HUMAN]		√	46.77	1	9
P51149	Ras-related protein Rab-7a OS=Homo sapiens GN=RAB7A PE=1 SV=1 - [RAB7A_HUMAN]		√	45.89	8	8
Q8WUD1	Ras-related protein Rab-2B OS=Homo sapiens GN=RAB2B PE=1 SV=1 - [RAB2B_HUMAN]		√	45.83	2	7
P61026	Ras-related protein Rab-10 OS=Homo sapiens GN=RAB10 PE=1 SV=1 - [RAB10_HUMAN]		√	38.50	7	9
P61020	Ras-related protein Rab-5B OS=Homo sapiens GN=RAB5B PE=1 SV=1 - [RAB5B_HUMAN]		√	37.21	4	6
P11233	Ras-related protein Ral-A OS=Homo sapiens GN=RALA PE=1 SV=1 - [RALA_HUMAN]		√	36.89	3	6
Q9UL26	Ras-related protein Rab-22A OS=Homo sapiens GN=RAB22A PE=1 SV=2 - [RB22A_HUMAN]		√	33.51	4	5
Q15286	Ras-related protein Rab-35 OS=Homo sapiens GN=RAB35 PE=1 SV=1 - [RAB35_HUMAN]		√	32.84	5	7
M0R0X1	Ras-related protein Rab-4B (Fragment) OS=Homo sapiens GN=RAB4B PE=1 SV=1 - [M0R0X1_HUMAN]		√	31.25	3	5
P51151	Ras-related protein Rab-9A OS=Homo sapiens GN=RAB9A PE=1 SV=1 - [RAB9A_HUMAN]		√	30.35	5	5
Q13637	Ras-related protein Rab-32 OS=Homo sapiens GN=RAB32 PE=1 SV=3 - [RAB32_HUMAN]		√	30.22	6	6
Q93096	Protein tyrosine phosphatase type IVA 1 OS=Homo sapiens GN=PTP4A1 PE=1 SV=2 - [TP4A1_HUMAN]		√	28.90	5	5
P20338	Ras-related protein Rab-4A OS=Homo sapiens GN=RAB4A PE=1 SV=3 - [RAB4A_HUMAN]		√	27.98	3	5
Q9NRW1	Ras-related protein Rab-6B OS=Homo sapiens GN=RAB6B PE=1 SV=1 - [RAB6B_HUMAN]		√	26.44	1	5
Q13636	Ras-related protein Rab-31 OS=Homo sapiens GN=RAB31 PE=1 SV=1 - [RAB31_HUMAN]		√	21.13	2	3
O95716	Ras-related protein Rab-3D OS=Homo sapiens GN=RAB3D PE=1 SV=1 - [RAB3D_HUMAN]		√	20.55	2	4
Q9BZG1	Ras-related protein Rab-34 OS=Homo sapiens GN=RAB34 PE=1 SV=1 - [RAB34_HUMAN]		√	20.08	4	4
Q9H082	Ras-related protein Rab-33B OS=Homo sapiens GN=RAB33B PE=1 SV=1 - [RB33B_HUMAN]		√	16.16	2	3
Q6IQ22	Ras-related protein Rab-12 OS=Homo sapiens GN=RAB12 PE=1 SV=3 - [RAB12_HUMAN]		√	12.30	2	3
P53004	Biliverdin reductase A OS=Homo sapiens GN=BLVRA PE=1 SV=2 - [BIEA_HUMAN]		√	12.16	3	3
F2Z388	60S ribosomal protein L35 OS=Homo sapiens GN=RPL35 PE=1 SV=1 - [F2Z388_HUMAN]		√	10.42	1	1
E9PJC7	CD82 antigen (Fragment) OS=Homo sapiens GN=CD82 PE=4 SV=1 - [E9PJC7_HUMAN]		√	7.64	1	1

Table 5.3. A complete list of prenylated proteins identified during proteomic profiling of COS-7 cells labeled with 7hp-FPP.

Accession	Description	CAAX motif	CC, CXC motif	ΣCoverage	Σ# Unique Peptides	Σ# Peptides
H3BSC1	Ras-related protein Rab-11A OS=Homo sapiens GN=RAB11A PE=1 SV=1 - [H3BSC1_HUMAN]	√		63.64	2	12
Q15907	Ras-related protein Rab-11B OS=Homo sapiens GN=RAB11B PE=1 SV=4 - [RB11B_HUMAN]	√		62.39	2	12
P10301	Ras-related protein R-Ras OS=Homo sapiens GN=RRAS PE=1 SV=1 - [RRAS_HUMAN]	√		48.62	7	9
P20700	Lamin-B1 OS=Homo sapiens GN=LMNB1 PE=1 SV=2 - [LMNB1_HUMAN]	√		43.69	25	27
Q92930	Ras-related protein Rab-8B OS=Homo sapiens GN=RAB8B PE=1 SV=2 - [RAB8B_HUMAN]	√		41.55	4	9
P62070	Ras-related protein R-Ras2 OS=Homo sapiens GN=RRAS2 PE=1 SV=1 - [RRAS2_HUMAN]	√		40.69	5	7
P51148	Ras-related protein Rab-5C OS=Homo sapiens GN=RAB5C PE=1 SV=2 - [RAB5C_HUMAN]	√		40.28	5	7
J9JID7	Lamin B2, isoform CRA_a OS=Homo sapiens GN=LMNB2 PE=1 SV=1 - [J9JID7_HUMAN]	√		39.84	25	27
P61006	Ras-related protein Rab-8A OS=Homo sapiens GN=RAB8A PE=1 SV=1 - [RAB8A_HUMAN]	√		38.65	4	9
Q9NP72	Ras-related protein Rab-18 OS=Homo sapiens GN=RAB18 PE=1 SV=1 - [RAB18_HUMAN]	√		38.35	7	8
Q9UBI6	Guanine nucleotide-binding protein G(I)/G(S)/G(O) subunit gamma-12 OS=Homo sapiens GN=GNG12 PE=1 SV=3 - [GBG12_HUMAN]	√		37.50	2	2
Q9UL25	Ras-related protein Rab-21 OS=Homo sapiens GN=RAB21 PE=1 SV=3 - [RAB21_HUMAN]	√		36.44	6	6
B4DJA5	Ras-related protein Rab-5A OS=Homo sapiens GN=RAB5A PE=1 SV=1 - [B4DJA5_HUMAN]	√		35.82	4	6
F8VVB5	Nucleosome assembly protein 1-like 1 (Fragment) OS=Homo sapiens GN=NAP1L1 PE=1 SV=1 - [F8VVB5_HUMAN]	√		34.78	2	6
P84095	Rho-related GTP-binding protein RhoG OS=Homo sapiens GN=RHOG PE=1 SV=1 - [RHOG_HUMAN]	√		32.98	5	5
Q93096	Protein tyrosine phosphatase type IVA 1 OS=Homo sapiens GN=PTP4A1 PE=1 SV=2 - [TP4A1_HUMAN]	√		32.95	6	6
P02545	Prelamin-A/C OS=Homo sapiens GN=LMNA PE=1 SV=1 - [LMNA_HUMAN]	√		31.78	19	20
P01111	GTPase NRas OS=Homo sapiens GN=NRAS PE=1 SV=1 - [RASN_HUMAN]	√		31.22	1	6
O95164	Ubiquitin-like protein 3 OS=Homo sapiens GN=UBL3 PE=1 SV=1 - [UBL3_HUMAN]	√		30.77	3	3
P31689	DnaJ homolog subfamily A member 1 OS=Homo sapiens GN=DNAJA1 PE=1 SV=2 - [DNJA1_HUMAN]	√		30.48	10	11
P62834	Ras-related protein Rap-1A OS=Homo sapiens GN=RAP1A PE=1 SV=1 - [RAP1A_HUMAN]	√		30.43	2	6
P61224	Ras-related protein Rap-1b OS=Homo sapiens GN=RAP1B PE=1 SV=1 - [RAP1B_HUMAN]	√		30.43	2	6
G3V1B3	60S ribosomal protein L21 OS=Homo sapiens GN=RPL21 PE=1 SV=1 - [G3V1B3_HUMAN]	√		29.89	2	2
P11233	Ras-related protein Ral-A OS=Homo sapiens GN=RALA PE=1 SV=1 - [RALA_HUMAN]	√		27.67	5	6

O15498	Synaptobrevin homolog YKT6 OS=Homo sapiens GN=YKT6 PE=1 SV=1 - [YKT6_HUMAN]	√		25.76	5	5
P51153	Ras-related protein Rab-13 OS=Homo sapiens GN=RAB13 PE=1 SV=1 - [RAB13_HUMAN]	√		25.12	3	5
P01112	GTPase HRas OS=Homo sapiens GN=HRAS PE=1 SV=1 - [RASH_HUMAN]	√		24.87	1	5
P01116	GTPase KRas OS=Homo sapiens GN=KRAS PE=1 SV=1 - [RASK_HUMAN]	√		24.87	3	5
O60884	DnaJ homolog subfamily A member 2 OS=Homo sapiens GN=DNAJA2 PE=1 SV=1 - [DNJA2_HUMAN]	√		24.27	12	12
Q9Y3L5	Ras-related protein Rap-2c OS=Homo sapiens GN=RAP2C PE=1 SV=1 - [RAP2C_HUMAN]	√		23.50	2	4
O75781	Paralemmin-1 OS=Homo sapiens GN=PALM PE=1 SV=2 - [PALM_HUMAN]	√		21.96	7	7
P61020	Ras-related protein Rab-5B OS=Homo sapiens GN=RAB5B PE=1 SV=1 - [RAB5B_HUMAN]	√		21.86	2	4
P63000	Ras-related C3 botulinum toxin substrate 1 OS=Homo sapiens GN=RAC1 PE=1 SV=1 - [RAC1_HUMAN]	√		18.23	4	4
P61225	Ras-related protein Rap-2b OS=Homo sapiens GN=RAP2B PE=1 SV=1 - [RAP2B_HUMAN]	√		18.03	1	3
Q9BVM2	Protein DPCD OS=Homo sapiens GN=DPCD PE=1 SV=2 - [DPCD_HUMAN]	√		17.73	4	4
P10114	Ras-related protein Rap-2a OS=Homo sapiens GN=RAP2A PE=1 SV=1 - [RAP2A_HUMAN]	√		16.39	1	3
P53004	Biliverdin reductase A OS=Homo sapiens GN=BLVRA PE=1 SV=2 - [BIEA_HUMAN]	√		15.20	4	4
P61586	Transforming protein RhoA OS=Homo sapiens GN=RHOA PE=1 SV=1 - [RHOA_HUMAN]	√		15.03	3	3
P09543	2',3'-cyclic-nucleotide 3'-phosphodiesterase OS=Homo sapiens GN=CNP PE=1 SV=2 - [CN37_HUMAN]	√		14.25	8	8
F8WF48	Translocation protein SEC62 OS=Homo sapiens GN=SEC62 PE=1 SV=1 - [F8WF48_HUMAN]	√		14.12	1	1
Q15382	GTP-binding protein Rheb OS=Homo sapiens GN=RHEB PE=1 SV=1 - [RHEB_HUMAN]	√		13.59	3	3
H0YJ63	Activator of 90 kDa heat shock protein ATPase homolog 1 (Fragment) OS=Homo sapiens GN=AHSA1 PE=1 SV=1 - [H0YJ63_HUMAN]	√		13.33	1	1
P63218	Guanine nucleotide-binding protein G(I)/G(S)/G(O) subunit gamma-5 OS=Homo sapiens GN=GNG5 PE=1 SV=3 - [GBG5_HUMAN]	√		13.24	1	1
P60953	Cell division control protein 42 homolog OS=Homo sapiens GN=CDC42 PE=1 SV=2 - [CDC42_HUMAN]	√		13.09	2	2
P51157	Ras-related protein Rab-28 OS=Homo sapiens GN=RAB28 PE=1 SV=2 - [RAB28_HUMAN]	√		12.67	2	2
P25686	DnaJ homolog subfamily B member 2 OS=Homo sapiens GN=DNAJB2 PE=1 SV=3 - [DNJB2_HUMAN]	√		11.42	3	3
H7BZW2	Centrosomal protein of 85 kDa (Fragment) OS=Homo sapiens GN=CEP85 PE=1 SV=1 - [H7BZW2_HUMAN]	√		11.26	5	5
O14807	Ras-related protein M-Ras OS=Homo sapiens GN=MRAS PE=1 SV=2 - [RASM_HUMAN]	√		10.58	2	2

H0YC77	Annexin (Fragment) OS=Homo sapiens GN=ANXA6 PE=1 SV=1 - [H0YC77_HUMAN]	√		9.89	1	1
Q9BRT3	Migration and invasion enhancer 1 OS=Homo sapiens GN=MIEN1 PE=1 SV=1 - [MIEN1_HUMAN]	√		9.57	1	1
P61587	Rho-related GTP-binding protein RhoE OS=Homo sapiens GN=RND3 PE=1 SV=1 - [RND3_HUMAN]	√		9.43	2	2
B7Z9G5	BRO1 domain-containing protein BROX OS=Homo sapiens GN=BROX PE=1 SV=1 - [B7Z9G5_HUMAN]	√		9.23	3	3
Q9ULC3	Ras-related protein Rab-23 OS=Homo sapiens GN=RAB23 PE=1 SV=1 - [RAB23_HUMAN]	√		8.44	2	2
F6RFD5	Destrin OS=Homo sapiens GN=DSTN PE=1 SV=1 - [F6RFD5_HUMAN]	√		8.15	1	1
F8W8H5	Ras-related protein Rab-24 OS=Homo sapiens GN=RAB24 PE=1 SV=1 - [F8W8H5_HUMAN]	√		8.05	1	1
P04083	Annexin A1 OS=Homo sapiens GN=ANXA1 PE=1 SV=2 - [ANXA1_HUMAN]	√		7.80	2	2
C9JZN1	Guanine nucleotide-binding protein G(I)/G(S)/G(T) subunit beta-2 (Fragment) OS=Homo sapiens GN=GNB2 PE=1 SV=1 - [C9JZN1_HUMAN]	√		7.24	1	1
F5GZL8	Guanine nucleotide-binding protein G(i) subunit alpha-2 OS=Homo sapiens GN=GNAI2 PE=1 SV=1 - [F5GZL8_HUMAN]	√		6.93	2	2
P61812	Transforming growth factor beta-2 OS=Homo sapiens GN=TGFB2 PE=1 SV=1 - [TGFB2_HUMAN]	√		5.80	2	2
B2RAA6	Ras-related protein Rab-26 OS=Homo sapiens GN=RAB26 PE=2 SV=1 - [B2RAA6_HUMAN]	√		5.79	1	1
P01137	Transforming growth factor beta-1 OS=Homo sapiens GN=TGFB1 PE=1 SV=2 - [TGFB1_HUMAN]	√		4.87	1	1
Q8NDI1	EH domain-binding protein 1 OS=Homo sapiens GN=EHBP1 PE=1 SV=3 - [EHBP1_HUMAN]	√		4.55	3	4
P49454	Centromere protein F OS=Homo sapiens GN=CENPF PE=1 SV=2 - [CENPF_HUMAN]	√		4.30	11	11
Q7Z2W4	Zinc finger CCCH-type antiviral protein 1 OS=Homo sapiens GN=ZC3HAV1 PE=1 SV=3 - [ZCCHV_HUMAN]	√		3.99	1	3
C9JA33	Paralemmin-2 OS=Homo sapiens GN=PALM2 PE=4 SV=1 - [C9JA33_HUMAN]	√		3.71	1	1
C9J6P4	Zinc finger CCCH-type antiviral protein 1 OS=Homo sapiens GN=ZC3HAV1 PE=1 SV=1 - [C9J6P4_HUMAN]	√		3.71	2	4
Q9Y6Q2	Stonin-1 OS=Homo sapiens GN=STON1 PE=1 SV=2 - [STON1_HUMAN]	√		3.54	2	2
Q6PHR2	Serine/threonine-protein kinase ULK3 OS=Homo sapiens GN=ULK3 PE=1 SV=2 - [ULK3_HUMAN]	√		2.54	1	1
Q93100	Phosphorylase b kinase regulatory subunit beta OS=Homo sapiens GN=PHKB PE=1 SV=3 - [KPBB_HUMAN]	√		2.38	2	2
Q27J81	Inverted formin-2 OS=Homo sapiens GN=INF2 PE=1 SV=2 - [INF2_HUMAN]	√		2.24	2	2

P32456	Interferon-induced guanylate-binding protein 2 OS=Homo sapiens GN=GBP2 PE=1 SV=3 - [GBP2_HUMAN]	√		2.03	1	1
Q96IG2	F-box/LRR-repeat protein 20 OS=Homo sapiens GN=FBXL20 PE=1 SV=2 - [FXL20_HUMAN]	√		1.83	1	1
Q8N3D4	EH domain-binding protein 1-like protein 1 OS=Homo sapiens GN=EHBP1L1 PE=1 SV=2 - [EH1L1_HUMAN]	√		1.44	1	2
K7EQL6	Ubiquitin carboxyl-terminal hydrolase OS=Homo sapiens GN=USP32 PE=1 SV=1 - [K7EQL6_HUMAN]	√		0.94	1	1
A6NIT2	Phosphorylase b kinase regulatory subunit alpha, skeletal muscle isoform OS=Homo sapiens GN=PHKA1 PE=1 SV=1 - [A6NIT2_HUMAN]	√		0.93	1	1
P46019	Phosphorylase b kinase regulatory subunit alpha, liver isoform OS=Homo sapiens GN=PHKA2 PE=1 SV=1 - [KPB2_HUMAN]	√		0.73	1	1
P62820	Ras-related protein Rab-1A OS=Homo sapiens GN=RAB1A PE=1 SV=3 - [RAB1A_HUMAN]		√	58.54	5	10
Q9H0U4	Ras-related protein Rab-1B OS=Homo sapiens GN=RAB1B PE=1 SV=1 - [RAB1B_HUMAN]		√	57.71	4	9
P51149	Ras-related protein Rab-7a OS=Homo sapiens GN=RAB7A PE=1 SV=1 - [RAB7A_HUMAN]		√	53.62	11	11
H0YGL6	Ras-related protein Rab-6A (Fragment) OS=Homo sapiens GN=RAB6A PE=1 SV=1 - [H0YGL6_HUMAN]		√	51.24	1	10
P61106	Ras-related protein Rab-14 OS=Homo sapiens GN=RAB14 PE=1 SV=4 - [RAB14_HUMAN]		√	46.98	8	9
P61019	Ras-related protein Rab-2A OS=Homo sapiens GN=RAB2A PE=1 SV=1 - [RAB2A_HUMAN]		√	44.81	4	8
P20340	Ras-related protein Rab-6A OS=Homo sapiens GN=RAB6A PE=1 SV=3 - [RAB6A_HUMAN]		√	44.23	1	10
P61026	Ras-related protein Rab-10 OS=Homo sapiens GN=RAB10 PE=1 SV=1 - [RAB10_HUMAN]		√	42.00	7	9
Q8WUD1	Ras-related protein Rab-2B OS=Homo sapiens GN=RAB2B PE=1 SV=1 - [RAB2B_HUMAN]		√	35.19	2	6
M0R1E0	Ras-related protein Rab-4B (Fragment) OS=Homo sapiens GN=RAB4B PE=1 SV=1 - [M0R1E0_HUMAN]		√	31.49	3	5
P51151	Ras-related protein Rab-9A OS=Homo sapiens GN=RAB9A PE=1 SV=1 - [RAB9A_HUMAN]		√	30.35	5	5
Q13636	Ras-related protein Rab-31 OS=Homo sapiens GN=RAB31 PE=1 SV=1 - [RAB31_HUMAN]		√	29.90	4	4
P20338	Ras-related protein Rab-4A OS=Homo sapiens GN=RAB4A PE=1 SV=3 - [RAB4A_HUMAN]		√	28.44	4	6
F5H157	Ras-related protein Rab-35 (Fragment) OS=Homo sapiens GN=RAB35 PE=1 SV=1 - [F5H157_HUMAN]		√	26.49	3	6
Q9BZG1	Ras-related protein Rab-34 OS=Homo sapiens GN=RAB34 PE=1 SV=1 - [RAB34_HUMAN]		√	23.17	5	5
Q9H082	Ras-related protein Rab-33B OS=Homo sapiens GN=RAB33B PE=1 SV=1 - [RB33B_HUMAN]		√	22.71	4	5
O95716	Ras-related protein Rab-3D OS=Homo sapiens GN=RAB3D PE=1 SV=1 - [RAB3D_HUMAN]		√	21.46	2	4

P20337	Ras-related protein Rab-3B OS=Homo sapiens GN=RAB3B PE=1 SV=2 - [RAB3B_HUMAN]		√	14.16	1	3
Q6IQ22	Ras-related protein Rab-12 OS=Homo sapiens GN=RAB12 PE=1 SV=3 - [RAB12_HUMAN]		√	13.52	2	3
Q13637	Ras-related protein Rab-32 OS=Homo sapiens GN=RAB32 PE=1 SV=3 - [RAB32_HUMAN]		√	12.44	3	3
Q86YS6	Ras-related protein Rab-43 OS=Homo sapiens GN=RAB43 PE=1 SV=1 - [RAB43_HUMAN]		√	9.43	1	2
Q9UL26	Ras-related protein Rab-22A OS=Homo sapiens GN=RAB22A PE=1 SV=2 - [RB22A_HUMAN]		√	5.15	1	1

5.7. Acknowledgements

I would like to acknowledge the following people for their contribution to this work:

Kayla Temple (Department of Medicinal Chemistry and Molecular Pharmacology, Purdue University) - Synthesis of compounds KT-i, KT-ii, KT-iii, KT-iv, KT-v, KT-vi, KT-vii and KT-viii, providing 7hp-OH (synthesized by Andrew T. Placzek).

Chuan-Chih Hsu (Department of Biochemistry, Purdue University) - Desalting of proteomic samples, LC-MS/MS data acquisition and protein database search analysis.

Yen-Chih Wang (Department of Chemistry, University of Minnesota) - Synthesis of C10Alk, C15Alk, C15Alk-OPP and biotin-PC-N_3.

Daniel G. Mullen (Department of Chemistry, University of Minnesota) - Synthesis of biotin-PC-N_3.

Jeffrey S. Vervacke (Department of Chemistry, University of Minnesota) - Synthesis of 7hp-FPP from 7hp-OH.

Katie Cornille (Allegheny College) - Preforming independent replicates of some of the in-gel fluorescence experiments to verify reproducibility (data not shown).

Chapter 6 Aldehyde-modified isoprenoid analogs as chemical reporters of protein prenylation

6.1. Introduction

Previous chapters described the use of alkyne-modified isoprenoid analogs for imaging, qunatitation and identification of prenylated proteins. In recent years, our group has developed several isoprenoid analogs containing an aldehyde reporter group, FAPP[224] and **I**[225] (Figure 6.1). These analogs facilitated site-specific protein modifications as well as purification of a protein of interest (containing CaaX genetic tag) from *E. coli* lysate. Aldehyde functionality is rarely present in biomolecules, and reacts selectively with hydrazides and aminooxy compounds to form hydrazones and oximes, respectively.[226] Therefore, aldehydes provide additional bioorthogonal chemistries to use in conjunction with the click reaction for simltaneous dual labeling of proteins.[125] Another unique advantage of aldehydes over other bioorthogonal functional groups is that hydrazone formation can be reversed via transoximization with an excess of aminooxy compounds to form hydrolytically more stable oxime.[225] This transoximization of hydrazones has been exploited by our group for the reversible immobilization of an aldehyde-tagged protein of interest from *E. coli* lysate on hydrazide resin followed by elution using a fluorescent or PEGylated aminooxy to isolate functionalized, purified protein.[225] In this work, we plan to

expand the scope of this method for global labeling and the subsequent selective catch-and-release of prenylated proteins in mammlian cells.

In spite of the inclusion of a reporter group in the isoprenoid moiety, current methods for global analysis of the prenylated proteome (reviewed in section 1.6) identify prenylated proteins based on the detection of unmodified internal peptides and not the C-terminal peptide containing the site of prenylation. This could largely be attributed to the inherent hydrophobicity of the prenylated peptides making chromatographic separation and mass spectrometric analysis challenging.[227] No proteomic study to date has directly detected the prenylated peptides (derived from proteolysis of prenylated proteins). Nonetheless, several studies have described the mass spectrometric detection of an individual prenylated protein or synthetic prenylated peptides. During the analysis of an intact farnesylated transducin γ-subunit via ESI- Q-TOF MS/MS, Takao and co-workers reported on the neutral loss of the farnesyl moiety (204 Da).[228] Hoffman and Kast investigated this phenomenon further by analyzing the neutral loss of farnesyl and the formation of a farnesyl marker ion, $[\text{farnesyl} + H]^{+1}$ from multiple peptides using MALDI and ESI ionization sources.[229] They reported that the neutral loss of farnesyl is predominant in MALDI-TOF-TOF analysis, while the singly charged farnesyl marker ion (m/z = 205) and corresponding fragment ions (m/z = 149 and 135) are preferentially formed in ESI-MS/MS. The authors

suggested that these marker ions/neutral loss could be used as signature characteristic for MS analysis of protein farnesylation. Nishimura and co-workers employed MALDI-QIT-TOF based MS/MS approach for characterizing the prenylation status of CaaX proteins expressed in a cell-free protein synthesis systems.[230] This allowed them to assess the type of prenylation (farnesylation and/or geranylgeranylation) depending on the identity of X residue. Based on extensive study of LC separation and ESI-MS/MS of farnesylated peptides, Wolters and colleagues demonstrated that farnesylated peptides are retained more strongly on reverse phase LC columns than nonfarnesylated peptides.[231] They also achieved detection of 5 pmol (0.12-0.25 μg) of farnesylated peptide spiked into 50 μg of HeLa cell protein digest via ESI-MS/MS analysis, with loss of the neutral farnesyl moiety only occasionally detected. Overall, despite being applicable to analysis of individual proteins, these studies have provided valuable information regarding the behavior of prenylated peptides in chromatography, as well as under various mass spectrometry conditions (ESI-MS/MS and MALDI-MS/MS). This knowledge should help develop mass spectrometric methods applicable on a proteome-wide scale for detecting prenylated peptides.

As mentioned above, the loss of the farnesyl moiety (as a neutral loss of marker ion) occurs during the ionization process. However, it take place inconsistently and to variable extents in various farnesylated peptides. Recently,

Chowdhury and co-workers developed a novel method to enhance the cleavage of the prenyl moiety by oxidizing the thioether linkage between prenyl group and cysteine side chain to a sulfoxide, which is more labile in the gas phase.[227] This resulted in the generation of signature ions to detect and distinguish farnesylation and geranylgeranylation of peptides in MS^2 and acquire MS/MS data on prenylated peptides in MS^3. Moreover, they introduced epoxy groups in the isoprenoid chain via oxidation of C-C double bonds, in order to increase hydrophilicity of prenylated peptides for better chromatographic behavior. While this method could potentially be adapted for analysis of the prenylated proteome, generation of multiple species resulting from epoxidation of C-C double bonds to variable extent, as observed by Chowdhury and colleagues, could complicate MS/MS analysis at the proteomic level. Furthermore, a software tool for searching prenylated proteins in a complex sample based on pattern of cleavage of epoxidized prenyl groups is not available.

Here, we propose to use an aldehyde-modified isoprenoid analog (FAPP) for labeling of prenylated proteins, followed by immobilization to a hydrazide resin and then release and labeling from the resin using aminooxy reagent **II**, in order to reduce the complexity of the proteomic sample (Figure 6.5). Additionally, we plan to introduce a positively charged aminium center on the prenylated peptides and use a less hydrophobic C8 column during LC-MS/MS analysis in order to

improve chromatographic elution and ionization of the hydrophobic prenylated peptides.

6.2. Research objectives

The goal of this project was to develop a mass-spectrometry based method to detect and identify the prenylated peptides from complex proteomic samples. This method envisioned labeling of prenylated proteins using aldehyde-modified isoprenoid analogs, followed by a catch-and-release strategy using hydrazide-functionalized resin and an aminooxy eluting reagent, and attaching a positively charged center to prenylated peptides for enhanced ionization.

6.3. Results and discussion

6.3.1. In-gel fluorescence analysis

In the previous work, Distefano and co-workers demonstrated that the aldehyde-modified isoprenoid analogs FAPP and **I** act as FTase substrates in an *in vitro* assay.[224, 225] In this study, we wanted to investigate whether these analogs could be used for metabolic labeling of prenylated proteins in mammalian cells. To assess this, HeLa cells were treated with 50 μM of FAPP for 4-24 hours in the presence and absence of lovastatin pre-treatment. Cells were then lysed and the oxime ligation reaction with an aminooxy-functionalized Alexa Fluor 488 reagent was carried out in presence of 50 mM aniline catalyst. After removal of the

excess of fluoroscent reagent, proteins were subjected to in-gel fluorescence analysis. Unfortunately, a large degree of background labeling was observed in the control sample, where cells were treated only with DSMO (vehicle) and lacked treatment with FAPP (data not shown). This led us to conclude that this analog is not suitable for metabolic labeling of prenylated proteins in mammalian cells.

Next, we evaluated the use of FAPP for labeling of prenylated proteins in HeLa cell lysate in an *in vitro* reaction. HeLa cells were treated with 25 μM lovastatin to decrease the endogenous pool of isoprenoids, effectively increasing the levels of proteins in the non-prenylated form. Cells were then lysed using a mild non-denaturing buffer and 10 μM of FAPP and 0.2 μM FTase were added to the lysates. Prenylation reactions were stopped after 30 min or 4.5 hours by precipitating the proteins, and the resultant proteins were analyzed by in-gel fluorescence. As seen in Figure 6.2, some background labeling was observed in the control samples lacking FAPP during the prenylation reaction (lanes 6 and 7). However, additional bands, specifically in the 25 kDa region (highlighted in the magenta box), appeared in the presence of both FAPP and FTase. Additionally, this labeling increased in a time-dependent manner (lanes 2 and 3). These bands in 25 kDa region disappeaed when FPP, the natural FTase subatrate, was added to the *in vitro* prenylation reaction (lane 1). In the absence of FTase, a small

amount of labeling was observed, presumably due to reaction with the native FTase present in the lysate (lanes 4 and 5). These results suggest that FAPP is suitable for *in vitro* labeling of prenylated proteins in cell lysates. The aminooxy reagent was found to react with some proteins even in the absece of FAPP. However, in a proteomic experiment, this could be accounted for by employing a control sample lacking FAPP, and then removing the proteins identified in this control sample from the FAPP-containing samples.

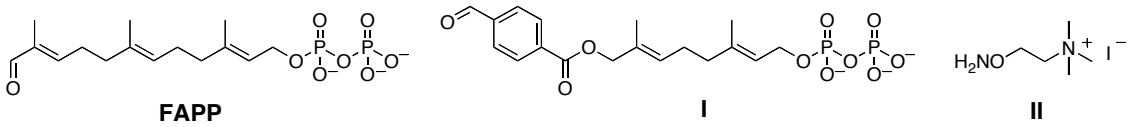

Figure 6.1. Structures of farnesyl aldehyde diphosphate (i), formylbenzoyl-oxy geranyl diphosphate (ii), and 2-aminooxy-*N*,*N*,*N*-trimethylethylaminium iodide (iii).

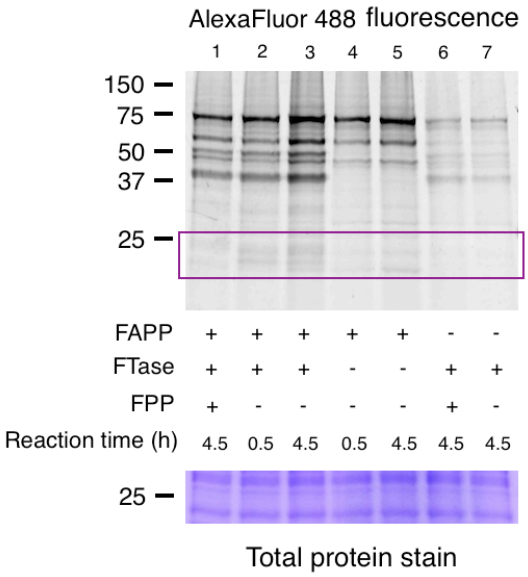

Figure 6.2. In-gel fluorescence analysis of HeLa cells proteins prenylated with FAPP in an *in vitro* reaction. HeLa cells were treated with 25 μM lovastatin for 24 h, and then lysed. Lysates were incubated with FTase and 10 μM FAPP in the presence or absence of 10 μM FPP for the indicated time. Proteins were then conjugated with Alexa Fluor 488 aminooxy reagent and separated on a 12% polyacrylamide gel.

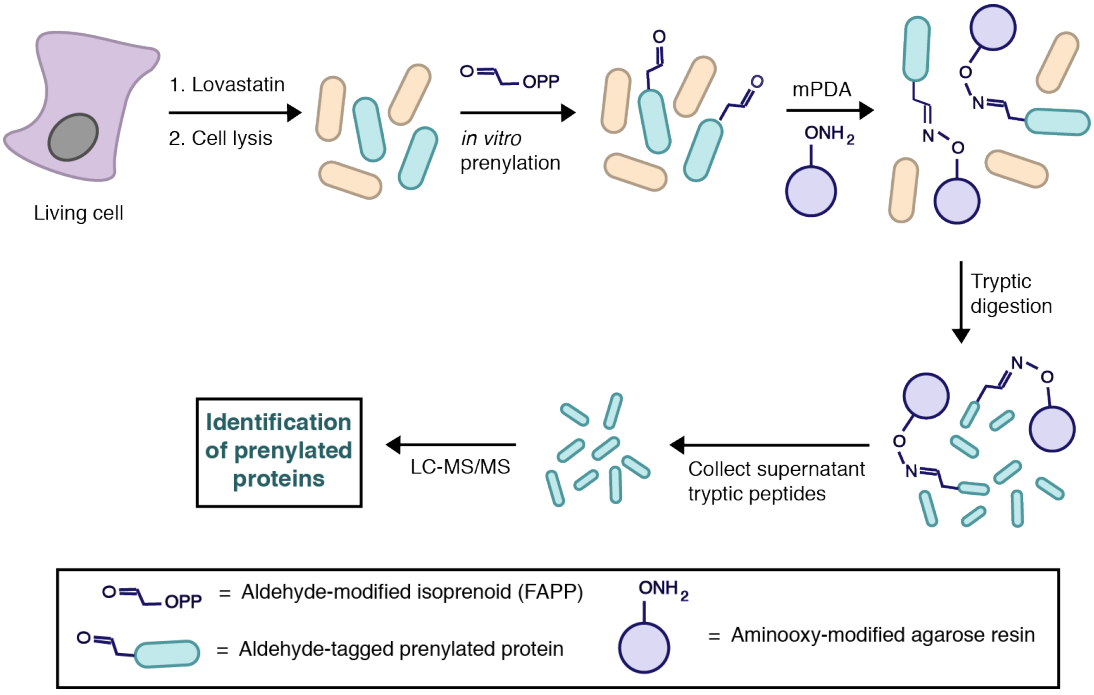

Figure 6.3. Workflow describing enrichment of aldehyde-tagged prenylated proteins using aminooxy-modified agarose resin.

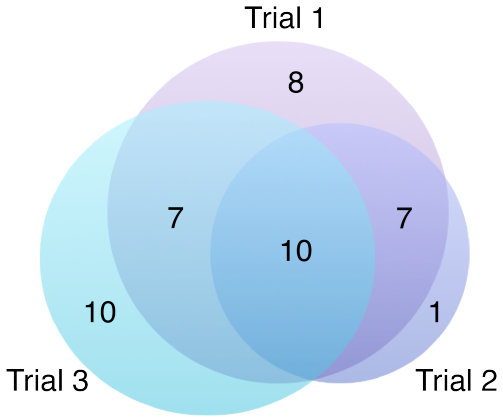

Figure 6.4. Venn diagram showing overlap of prenylated proteins identified in three independent experimental replicates. HeLa cells were treated with 25 *μ*M lovastatin for 24 h, and then the cell lysate was subjected to *in vitro* prenylation with FAPP and FTase. Aldehyde-tagged proteins were captured on aminooxy-modified agarose resin in the presence of mPDA, subjected to on-resin digestion and identified by LC-MS/MS analysis.

6.3.2. Identification of HeLa cell proteins labeled by FAPP

While the in-gel fluorescence experiments described above indicated that FAPP could be used for labeling of prenylated proteins, we wanted to verify this by identifying the labeled proteins. To achieve this, we used a protocol described in Figure 6.3. *In vitro* prenylation of lysate of lovastatin-treated HeLa cells was carried out with FAPP in the presence of FTase. After removal of excess of FAPP, proteins were incubated with aminooxy-modified agarose resin and *m*-phenylene diamine (mPDA) catalyst to capture the aldehyde-tagged proteins via an oxime linkage. After washing off unbound proteins, the captured proteins were tryptic digested on-resin and analyzed by LC-MS/MS on a Velos Orbitrap instrument.

Three independent trials of FAPP-tagged samples were carried out, along with one replicate of a control sample lacking FAPP in the prenylation reaction. A total of 43 prenylated proteins were identified from the three replicates (Figure 6.4 and Table 6.1), of which 24 proteins were identified in at least two of the replicates, and 10 proteins were identified in all three samples. Only one of these 43 prenylated proteins was identified in the control sample, indicating that these proteins indeed get labeled and enriched via FAPP. Interestingly, while we added only FTase in the in vitro reaction, a number of Rab GGTase substrates were identified as well. We attributed this to incorporation of FAPP by endogenous

prenyltransferases in the lysate. We also identified almost 400 additional proteins (combined from the three analyses) lacking any prenylation motif. More than half of these proteins appeared in only one of the analyses, indicating low consistency of their enrichment, suggesting these proteins were non-specifically attached to the aminooxy-functionalized resin. Of the less than 200 nonprenylated proteins identified in at least two of the trials, 42 proteins were also identified in the control sample, indicating that these proteins react with the resin in a manner independent of labeling with FAPP. Carrying out additional trials of the control sample might help to eliminate more nonprenylated proteins from the analysis. Overall, these results confirmed the ability of FAPP to tag prenylated proteins in cell lysate via the *in vitro* prenylation reaction with added enzyme.

Table 6.1. List of prenylated proteins identified from the three replicates of proteomic analyses of HeLa cell proteins labeled with FAPP.

Accession	Protein ID	CaaX box	Trial 1	Trial 2	Trial 3
P31689	DnaJ homolog subfamily A member 1	CQTS	Yes		Yes
P55209	Nucleosome assembly protein 1-like 1	CKQQ	Yes		Yes
P04083	Annexin A1	CGGN	Yes	yes	Yes
Q7Z2W4	Zinc finger CCCH-type antiviral protein 1	CVIS	Yes		Yes
Q93096	Protein tyrosine phosphatase type IVA 1	CCIQ	Yes	yes	Yes
P61586	Transforming protein RhoA	CLVL	Yes	yes	Yes
P01112	GTPase HRas	CVLS	Yes	yes	Yes
Q5VW32	BRO1 domain-containing protein BROX	CYIS	Yes		Yes
P11233	Ras-related protein Ral-A	CCIL	Yes		Yes
P61026	Ras-related protein Rab-10	SKCC	Yes	yes	Yes
Q15382	GTP-binding protein Rheb	CSVM	Yes	yes	Yes
Q9UBI6	Guanine nucleotide-binding protein G(I)/G(S)/G(O) subunit gamma-12	CIIL	Yes	yes	Yes
P60953	Cell division control protein 42 homolog	CCIF	Yes	yes	Yes
P51148	Ras-related protein Rab-5C	CCSN	Yes	yes	Yes
P62491	Ras-related protein Rab-11A	CCQNI	Yes		Yes
P62820	Ras-related protein Rab-1A	GGCC	Yes		Yes
Q27J81	Inverted formin-2	CVIF	Yes		Yes
P02545	Lamin-A/C	CSIM			Yes
P20700	Lamin-B1	CAIM			Yes
O60884	DnaJ homolog subfamily A member 2	CAHQ			Yes
P09543	2',3'-cyclic-nucleotide 3'-phosphodiesterase	CTII			Yes
P40855	Peroxisomal biogenesis factor 19	CLIM			Yes
Q03252	Lamin-B2	CYVM			Yes
P61952	Guanine nucleotide-binding protein G(I)/G(S)/G(O) subunit gamma-11	CVIS			Yes
P30050	60S ribosomal protein L12	CPAS			Yes
Q6P6C2	Probable alpha-ketoglutarate-dependent dioxygenase ABH5	CWHQ			Yes
Q5TAQ9	DDB1- and CUL4-associated factor 8	CMPS			Yes
P20339	Ras-related protein Rab-5A	CCSN	yes	yes	
P51149	Ras-related protein Rab-7a	SCSC	yes	yes	
Q969Q5	Ras-related protein Rab-24	CCHH	yes	yes	
P84095	Rho-related GTP-binding protein RhoG	CILL	yes		
Q15286	Ras-related protein Rab-35	KRCC	yes	yes	
O95164	Ubiquitin-like protein 3	CCVIL	yes	yes	
P61019	Ras-related protein Rab-2A	GGCC	yes		
P62070	Ras-related protein R-Ras2	CVIF	yes	yes	
Q9H0U4	Ras-related protein Rab-1B	GGCC	yes		
P10114	Ras-related protein Rap-2a	CNIQ	yes		
P61006	Ras-related protein Rab-8A	CVLL	yes		
P61020	Ras-related protein Rab-5B	CCSN	yes		
P61106	Ras-related protein Rab-14	GCGC	yes	yes	
P62834	Ras-related protein Rap-1A	CLLL	yes		
Q13636	Ras-related protein Rab-31	RRCC	yes		
P51151	Ras-related protein Rab-9A	SSCC		yes	

6.3.3. Identification of prenylated proteins from mouse brain tissue

With an interest in expanding the utility of FAPP for the labeling of prenyalated proteins in systems other than cultured mammalian cells, we chose to label proteins in mouse brain tissue. Simvastatin (dissolved in 10% DMSO) was administered to a mouse (10 mg/kg) via subcutaneous injecion. After 24 hours, brain tissue was isolated, and homogenized. *In vitro* prenylation with 10 μM FAPP and 0.2 μM FTase was carried out with the clarified brain tissue homogenate. After removal of excess FAPP, proteins were captured on aminooxy resin and tryptic digested on-resin. LC-MS/MS analysis resulted in the identification of 22 prenylated proteins (Table 6.2), out of a total of 228 proteins. Including a control sample in the future experiments should allow for eliminating non-specifically enriched proteins in the analysis. Although more replicates are necessary to improve the coverage and verify the reproducibility, these results point out the applicability of FAPP for the labeling of proteins isolated from the brain tissue of mice via our *in vitro* prenylation strategy. This is the first report of the identification of the prenylated proteins from tissue isolated from a living animal, and this method opens the door for potentially analyzing the prenylated proteome in the brain of a mouse model of Alzheimer's disease and other neurodegenerative disorders.

Table 6.2. List of prenylated protein identified from mouse brain sample subjected to in vitro prenylation with FAPP and then pull-down with aminooxy-modified agarose resin.

Accession	Protein	C-terminal motif	# peptides	% coverage
P18872	Guanine nucleotide-binding protein G(o) subunit alpha	CGLY	8	21
Q9Z0P4	Paralemmin-1	CSVM	5	22
P63011	Ras-related protein Rab-3A	DCAC	4	25
B2RSH2	Guanine nucleotide-binding protein G(i) subunit alpha-1	CGLF	3	9
P16330	2',3'-cyclic-nucleotide 3'-phosphodiesterase	CTII	4	8
Q6PHN9	Ras-related protein Rab-35	KRCC	4	16
P08752	Guanine nucleotide-binding protein G(i) subunit alpha-2	CGLF	2	8
P62835	Ras-related protein Rap-1A	CLLL	2	11
Q9CQD1	Ras-related protein Rab-5A	CCSN	3	18
Q5PR73	GTP-binding protein Di-Ras2	CVVM	3	18
P63321	Ras-related protein Ral-A	CCIL	2	12
P62821	Ras-related protein Rab-1A	GGCC	3	14
Q80ZJ1	Ras-related protein Rap-2a	CNIQ	2	11
P61021	Ras-related protein Rab-5B	CCSN	2	11
Q9D1G1	Ras-related protein Rab-1B	GGCC	2	12
P61027	Ras-related protein Rab-10	SKCC	1	11
P63001	Ras-related C3 botulinum toxin substrate 1	CLLL	1	7
P63216	Guanine nucleotide-binding protein G(I)/G(S)/G(O) subunit gamma-3	CALL	1	20
Q61411	GTPase HRas	CVLS	1	6
Q91V41	Ras-related protein Rab-14	GCGC	1	6
P50153	Guanine nucleotide-binding protein G(I)/G(S)/G(O) subunit gamma-4	CTIL	1	20
Q91Z61	GTP-binding protein Di-Ras1	CALM	1	4

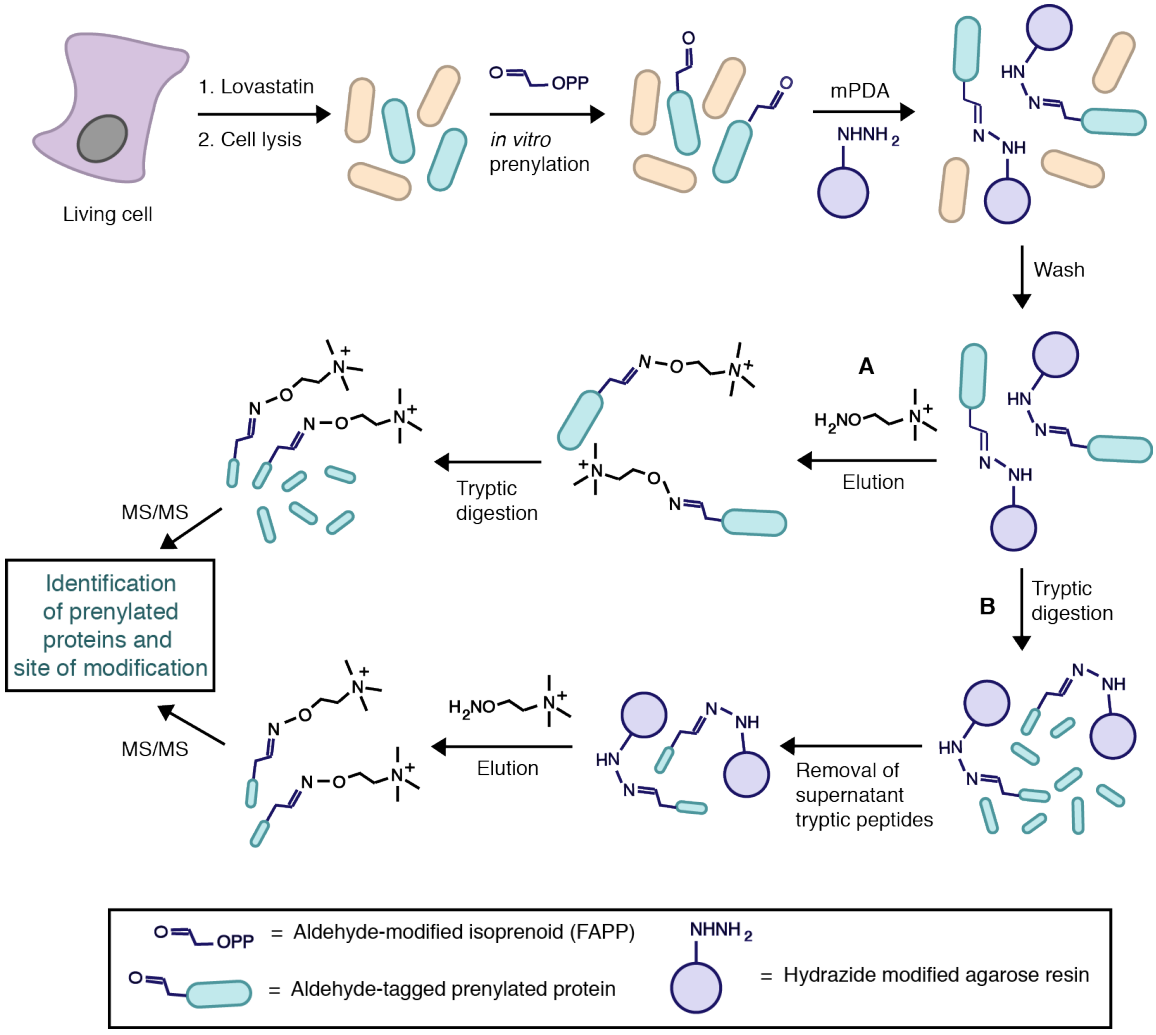

Figure 6.5. Workflow showing our catch-and-release strategy for the mass spectrometry based identification of prenylated proteins and detection of the site of modification.

6.3.4. Catch-and-release strategy: Proof-of-concept experiments

After establishing the use of FAPP for tagging prenylated proteins, we wanted to develop a catch-and-release protocol, wherein, the aldehyde-tagged proteins are captured on a solid support via a reversible hydrazone ligation, and after washing away unbound proteins, the labeled proteins are eluted via transoximization in the presence of an excess of an aminooxy reagent (Figure 6.5). We first performed two proof-of-concept experiments: one with a GFP-CVIA (recombinant green fluorescent protein appended with CVIA sequence at the C-terminus) and the other using synthetic peptides.

We first sought to monitor the immobilization of aldehyde-tagged proteins on the hydrazide resin and its subsequent release. For this purpose, we chose a dansyl-GCVIA peptide and a GFP-CVIA protein, because they can readily be tracked via their fluorescence. We incubated hydrazide resin with nonprenylated and FAPP-prenylated forms of dansyl-GCVIA and GFP-CVIA, in the presence of 50 mM mPDA catalyst. In the case dansyl-GC(FAPP)VIA and GFP-C(FAPP)VIA, upon 3 hour inucubation at room temperature, there was minimal fluorescence in the supernatants, while the resin was highly fluorescent even after multiple washes. This indicated that both these FAPP-tagged molecules immobilized on the resin. The resin incubated with nonprenylated dansyl-GCVIA or GFP-CVIA did not gain any appreciable fluorescence, and the corresponding supernatant

solutions remained fluorescent, suggesting that the protein/peptide lacking an aldehyde tag did not immobilize on the hydrazide resin.

We next evaluated transoximization-mediated elution using acidic pH and an aniline-based catalyst. We monitored the elution of dansyl-GC(FAPP)VIA from the hydrazide resin using 10 mM of **II** in presence of either 1% CH_3COOH, 0.1% TFA or 50 mM mPDA. In all the cases, oximized product of the dansyl-GC(FAPP)VIA was successfully eluted as mointored by LC-MS (data not shown). In order to probe on-resin proteolyis of bound proteins and the subsequent release of C-terminal prenylated peptide (path B in Figure 6.5) from the resin, we subjected the hydrazide resin with immobilized GFP-C(FAPP)VIA to overnight tryptic digestion. After washing away tryptic peptides in the supernatant, the resin was incubated with 10 mM mPDA to release the covalently bound C-terminal tryptic peptide. LC-MS analysis of the eluted material clearly showed the presence of an oxime-modified prenylated C-terminal peptide (data not shown). This released peptide was only four amino acid residues long due to a lysine located immediately upstream to prenylated cysteine. Therefore, this peptide was not used for MS/MS analysis.

Next, we wanted to carry out LC-MS/MS analysis on prenylated peptides conjugated to the aminooxy reagent **II** and use database searching tools to detect the modified peptide. To this end, we synthesized a 14 amino acid peptide

SSPRTQSPQNCSIM (referred to as peptide **III**), derived from the C-terminus of Prelamin-A/C. The peptide was prenylated in an *in vitro* reaction with FAPP and FTase, followed by conjugation with **II** in presence of the mPDA catalyst. The resultant peptide, after desalting, was injected onto a nanoLC system coupled to a hybrid LTQ Orbitrap Velos mass spectrometer. MS/MS data was searched against a human protein database using the SEQUEST algorithm. This led to the identification of the peptide PRTQSPQNC(pren-oxime)SIM containing the desired modification (FAPP prenyl group conjugated to **II**) on the cysteine. Figure 6.6 shows a table containing a list of *b* and *y* ions detected for this peptide as well as the MS/MS spectrum. Notably, the identified peptide was two amino acid residues shorter than compared to the synthetic peptide. This is believed to be due to fragmentation of the peptide at the N-terminus of proline residue, which has been observed for other proline-containing peptides.[232, 233] Furthermore, an intesne singly charged peak at 319.3 was seen in the MS/MS spctrum, which matches with the expected mass of the marker ion, $[\text{prenyl} + H]^{+1}$, corresponding to the loss of prenyl group (the oxime containing modification in this case). This is consistent with the previous literature reporting a similar loss of the farnesyl marker ion.[231]

A point to note here is that, the prenyl modification present on the eluted peptides contain a positively charged aminium center. SEQUEST and other

commonly used database search algorithms are based on an assumption that each positive charge on a peptide originates from the addition of a proton.[233, 234] To account for this, the mass of variable modification used (318.2666) during database analysis was set to be smaller by the mass of one proton, compared to the theoretical mass of the modification (319.2744). In the first trial for the database search of the above mentioned experiment, both 318.2666 and 319.2744 were used as possible cysteine variable modifications, but the expected peptide was identified with the modification have a molecular weight of 318.2666, not 319.2744.

Taken together, these experiments demonstrate that FAPP-tagged proteins and peptides get immobilized on hydrazide resin in the presence of an mPDA catalyst. Bound peptides can be released from the resin using **II** either at acidic pH (1% CH_3COOH or 0.1% TFA) or in the presence of an aniline-based catalyst (50 mM mPDA). Prenylated peptides, containing the isoprenoid conjugated to **II**, can be detected via LC-MS/MS analysis and a subsequent database search.

A

B	B Ions	B+2H	B-NH3	B-H2O	AA	Y Ions	Y+2H	Y-NH3	Y-H2O	Y
1	98.1				P	1,695.9	848.4	1,678.9	1,677.9	12
2	254.2	127.6	237.1		R	1,598.8	799.9	1,581.8	1,580.8	11
3	355.2	178.1	338.2	337.2	T	1,442.7		1,425.7	1,424.7	10
4	483.3	242.1	466.2	465.3	Q	1,341.7		1,324.7	1,323.7	9
5	570.3	285.7	553.3	552.3	S	1,213.6		1,196.6	1,195.6	8
6	667.4	334.2	650.3	649.3	P	1,126.6		1,109.6	1,108.6	7
7	795.4	398.2	778.4	777.4	Q	1,029.5		1,012.5	1,011.5	6
8	909.5	455.2	892.4	891.4	N	901.5		884.5	883.5	5
9	1,330.7	665.9	1,313.7	1,312.7	C+3...	787.4			769.4	4
10	1,417.8	709.4	1,400.7	1,399.8	S	366.2			348.2	3
11	1,530.8	765.9	1,513.8	1,512.8	I	279.1				2
12	1,695.9	848.4	1,678.9	1,677.9	M+16	166.1				1

B

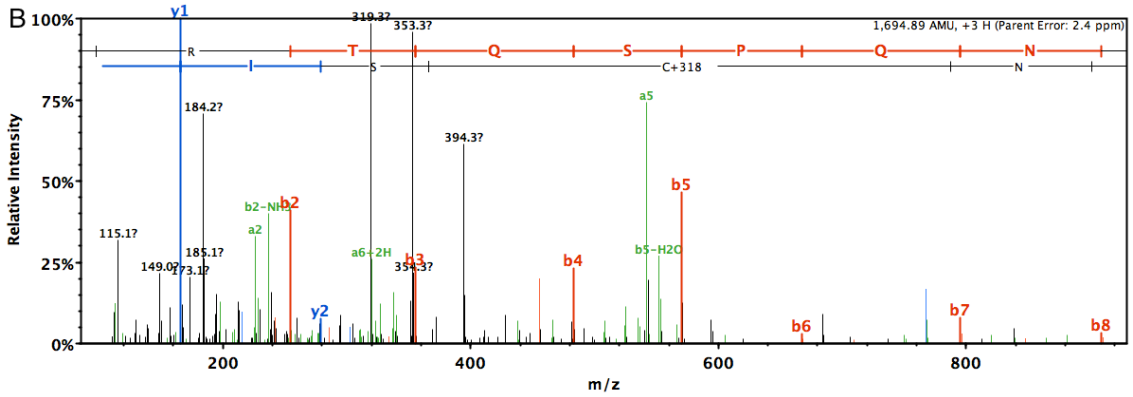

Figure 6.6. Detection of a synthetic prenylated peptide using a SEQUEST database search algorithm. A. Fragmentation table showing a list of all expected *b* and *y* ions from fragmentation of PRTQSPQNC(pren-oxime)SIM, with observed ions highlighted. B. MS/MS spectrum of PRTQSPQNC(pren-oxime)SIM.

6.3.5. Catch-and-release of FAPP-bound proteins in HeLa cells

We next sought to apply this strategy for analysis of the prenylated proteome in HeLa cells. We decided to add GFP-CVIA to the lysate to enable quick monitoring of the capture of proteins on resin, as well as for having a known CaaX protein in the sample for the tracking MS/MS analysis. Since a number of prenylated proteins contain a lysine residue or a poly-lysine sequence upstream of CaaX box (to facilitate plasma membrane anchoring via electrostatic interaction),[235] trypsin is expected to produce very short C-terminal proteolytic peptides. For this reason, we chose to use Glu-C, which is a protease cleaving at the carboxyl side of aspartate and glutamate residues, for digestion.

HeLa cells incubated for 24 hours with 25 μM lovastatin were lysed in a non-denaturing buffer. Lysate was spiked with 2 μM GFP-CVIA, subjected to *in vitro* prenylation with FAPP and FTase, followed by removal of excess FAPP by centrifugal filtration. Proteins were then immobilized on hydrazide resin in the presence of mPDA, and unbound proteins were removed by extensive washing. At this point, resin was found to be fluorescent due to captured GFP-CVIA, indicating successful hydrazone formation with the aldehyde-tagged proteins. Bound proteins were digested on-resin with Glu-C, the resin was washed and then the C-terminal modified peptides were eluted using 10 mM of **II** in presence

of 0.1% TFA. After desalting, the eluted C-terminal peptides were subjected to LC-MS/MS and data was analyzed by SEQUEST.

When the MS/MS data was analyzed against a human protein database, only one CaaX peptide containing the modification, belonging to GNG12 protein, was detected (Figure 6.7). When the same data was searched against a human protein database appended with GFP-CVIA, this GNG12 CaaX peptide was no longer identified. This later analysis identified GFP-CVIA, although not based the C-terminal modified peptide. Moreover, analysis of raw MS^1 data indicated the presence of the intact eluted GFP-C(pren-oxime)VIA protein suggesting that Glu-C digestion did not proceed efficiently. Ineffective protein digestion could explain why only one modified CaaX peptide was detected in this experiment. This indicates that optimization of Glu-C digestion is required prior to further protomic experiments. Additionally, variable protein identification results obtained upon marginally changing the protein database indicates that additional work is required to optimize the parameters used during SEQUEST-based database searching for the prenylated peptides.

A

B	B Ions	B+2H	B-NH3	B-H2O	AA	Y Ions	Y+2H	Y-NH3	Y-H2O	Y
1	138.1	69.5			H	3,324.9	1,663.0	3,307.9	3,306.9	27
2	209.1	105.1			A	3,187.9	1,594.4	3,170.8	3,169.8	26
3	365.2	183.1	348.2		R	3,116.8	1,558.9	3,099.8	3,098.8	25
4	452.2	226.6	435.2	434.2	S	2,960.7	1,480.9	2,943.7	2,942.7	24
5	567.3	284.1	550.2	549.3	D	2,873.7	1,437.3	2,856.7	2,855.7	23
6	664.3	332.7	647.3	646.3	P	2,758.7	1,379.8	2,741.6	2,740.6	22
7	777.4	389.2	760.4	759.4	L	2,661.6	1,331.3	2,644.6	2,643.6	21
8	890.5	445.7	873.5	872.5	L	2,548.5	1,274.8	2,531.5	2,530.5	20
9	1,003.6	502.3	986.5	985.6	I	2,435.4	1,218.2	2,418.4	2,417.4	19
10	1,060.6	530.8	1,043.6	1,042.6	G	2,322.4	1,161.7	2,305.3	2,304.3	18
11	1,173.7	587.3	1,156.6	1,155.7	I	2,265.3	1,133.2	2,248.3	2,247.3	17
12	1,270.7	635.9	1,253.7	1,252.7	P	2,152.2	1,076.6	2,135.2	2,134.2	16
13	1,371.8	686.4	1,354.7	1,353.8	T	2,055.2	1,028.1	2,038.2	2,037.2	15
14	1,458.8	729.9	1,441.8	1,440.8	S	1,954.1	977.6	1,937.1	1,936.1	14
15	1,587.8	794.4	1,570.8	1,569.8	E	1,867.1	934.1	1,850.1	1,849.1	13
16	1,701.9	851.4	1,684.9	1,683.9	N	1,738.1	869.5	1,721.0	1,720.1	12
17	1,798.9	900.0	1,781.9	1,780.9	P	1,624.0	812.5	1,607.0	1,606.0	11
18	1,946.0	973.5	1,929.0	1,928.0	F	1,527.0	764.0	1,509.9	1,509.0	10
19	2,074.1	1,037.6	2,057.1	2,056.1	K	1,379.9	690.5	1,362.9	1,361.9	9
20	2,189.1	1,095.1	2,172.1	2,171.1	D	1,251.8	626.4	1,234.8	1,233.8	8
21	2,317.2	1,159.1	2,300.2	2,299.2	K	1,136.8	568.9	1,119.8	1,118.8	7
22	2,445.3	1,223.2	2,428.3	2,427.3	K	1,008.7	504.8	991.7	990.7	6
23	2,546.4	1,273.7	2,529.3	2,528.4	T	880.6			862.6	5
24	2,967.6	1,484.3	2,950.6	2,949.6	C+3...	779.5				4
25	3,080.7	1,540.9	3,063.7	3,062.7	I	358.3				3
26	3,193.8	1,597.4	3,176.8	3,175.8	I	245.2				2
27	3,324.9	1,663.0	3,307.9	3,306.9	L	132.1				1

B

M S S K T A S T N N I A Q A R R T V Q Q
L R L E A S I E R I K V S K A S A D L M
S Y C E E H A R S D P L L I G I P T S E
N P F K D K K T C I I L

C

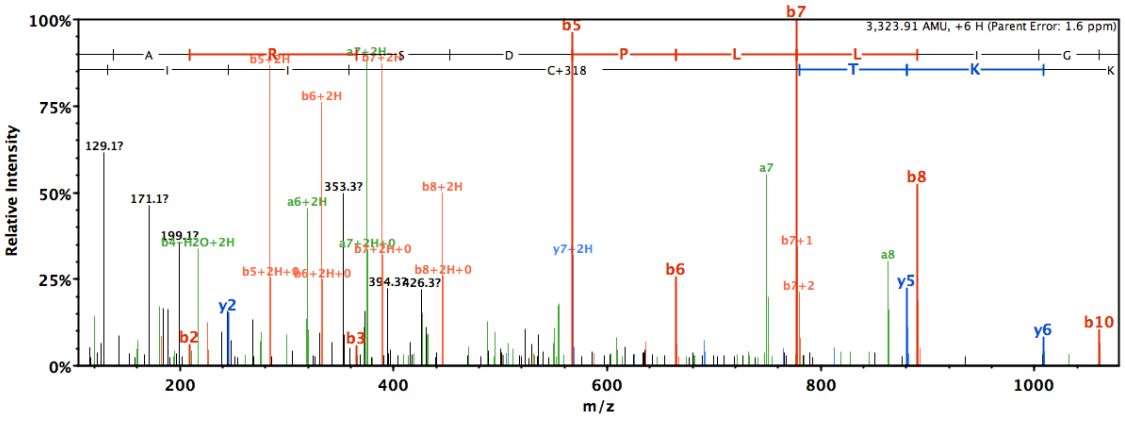

Figure 6.7. Detection of C-terminal prenylated peptide from GNG12 (Uniprot ID: Q9UBI6) using SEQUEST database search algorithm. A. Fragmentation table showing a list of all expected b and y ions, with observed ions highlighted. B. Amino acid sequence of GNG12 protein. Highlighted in yellow is the Glu-C digested peptide, containing the site of modification (Cys residue in green color), detected in the SEQUEST analysis. C. MS/MS spectrum of the indicated peptide.

6.4. Summary

In summary, we demonstrated the use of an aldehyde-modified isoprenoid analog, FAPP, for labeling prenylated proteins via *in vitro* prenylation strategy. By employing aminooxy-modified agarose resin for the enrichment of aldehyde-tagged proteins, we identified several prenylated proteins from HeLa cell lysate as well as from mouse brain tissue homogenates. Furthermore, we developed a catch-and-relase strategy for the enrichement of aldehyde-tagged proteins using hydrazide-functionalized resin and a transoximization reaction in the presence of excess aminooxy reagent. This method allowed for mass spectretric detection of a prenylated peptide from a complex proteomic sample. Results of proteomic experiments indicated the need for optimization of the proteolytic digestion and LC-MS/MS data acquisition and database search. Such experiments are currently underway. Finally, the labeling of prenylated proteins in mouse brain tissue samples indicates that our FAPP-based proteomic method can potentially be employed for prenylated proteome profiling in a mouse model of Alzheimer's diesease and other neurodegerative disorders.

6.5. Future direction

We first plan to carry out experiments to determine the optimal reaction conditions to maximize the efficiency of on-resin protein digestion using Glu-C. Next, we will evaluate the performance of multiple database search engines

(SEQUEST, Mascot and MaxQuant) in their ability to detect prenylated peptides, their capacity for identifying the site of modification and for giving consistent results.

Due to the hydrophobicity of the prenylated peptide, these small molecules are known to be retained strongly on reverse phase matrices.[231] We noted that this was true even for the prenylated peptides conjugated to aminooxy reagent **II**, which contains a positively charged aminium center. This was observed via its solubility properties, elution profile during HPLC, and the fact that prenylated peptides adhered to the C18 nano-LC and kept eluting during wash steps. Therefore, we plan to use a C8 column for LC analysis, instead of the commonly used C18 column. A C8 column is less hydrophobic compared to the C18, and is expected to retain prenylated peptides less strongly. We anticipate that the use of a nano-LC column packed with a C8 chromatography matrix would increase the elution efficiency of prenylated peptides, and thereby increase the identification coverage.

After optimizing all these parameters (digestion protocol, use of C8 column for LC and databse search parameters), we plan to profile the prenylated proteome in brain samples from healthy mice and from a mouse model of Alzheimer's disease. Data would be acquired in at least three independent experimental replicates, as well three replicates of a control sample lacking FAPP

in prenylation reaction. This data is expected to elucidate which prenylated proteins potentially play a role in disease pathology.

6.6. Methods

Farnesyl aldehyde diphosphate (FAPP) and Formylbenzoyl-oxy geranyl diphosphate (**I**) were synthesized as described by Distafeno and co-workers.[224, 225] 2-(aminooxy)-*N*,*N*,*N*-trimethylethylaminium iodide (**II**) was synthesized using a previously reported method.[236] Pierce NHS-activated agarose resin and UltraLink Hydrazide resin were purchased from Pierce, Life Technologies. Sequencing Grade Modified Trypsin and Glu-C were obtained from Promega. Lovastatin was obtained from Cayman Chemicals. All other reagents were from Sigma Aldrich, unless mentioned otherwise. HeLa cells were maintained in DMEM supplemented with 10% FBS.

6.6.1. Synthesis of aminooxy-modified agarose resin

To a 40 mM solution of 1,2-bisaminooxy ethane in 150 mM phosphate buffer, pH 8.0 was added 150-200 mg of dry NHS-activated agarose resin and the solution was incubated overnight at 4 °C. Supernatant was removed and resin was incubated with 0.5 M Tris-HCl, pH 7.2 buffer to block any unreacted NHS ester sites.

6.6.2. Synthesis of SSPRTQSPQNCSIM (III)

The peptide was synthesized by solid phase peptide synthesis using Fmoc-Met-Wang resin (Peptides Internationals), having a loading capacity of 0.57 mmol/g. Resin (175 mg, 0.1 mmol, 1 equiv.) was weighed and transferred to the reaction vessel of an automatic peptide synthesizer (Protein Technologies, Inc.) and washed with DMF to swell the resin. Synthesis of the entire peptide was achieved by loading the required amino acids (4 equiv.) in correct order into the peptide synthesizer. The resin with peptide attached to it was then transferred to a 12 mL syringe using DMF, and subsequently washed thrice with CHCl3. The peptide was cleaved off the resin by Reagent K (TFA/ phenol/ thioanisole/ H2O/ ethanedithiol, 82.5:5:5:5:2.5) for 30 min. The peptide was precipitated by adding Et2O and then pelleted by centrifugation. The peptide was washed 3X with Et2O to remove Reagent K. The crude peptide was analyzed by HPLC (0.1% aqueous TFA as buffer A and 0.1% TFA in CH_3CN as buffer B) and ESI-MS and subsequently purified by preparative-scale HPLC. The peptide eluted at 23% buffer B during a 0 to 100% B in 100 min gradient. Calculated $[M+2H]^{+2}$ = 768.35 , observed $[M+2H]^{+2}$ = 768.38.

6.6.3. Prenylation of III with FAPP and conjugation to II

A solution of peptide **III** dissolved in 0.5 M Tris-HCl, pH 7.5, was incubated with 0.5 M DTT in dark for 1 h. Water (9X volume) was added to adjust the

concentration of peptide to 2.5 μM and the concentration of Tris to 50 mM. $MgCl_2$ and $ZnCl_2$ were added to final concentrations of 10 mM and 10 μM, respectively. Prenylation reaction was intiated by adding FAPP (final concentration 10 μM) and FTase (final concentration 100 nM). After 3 h reaction at 30 °C, peptides were concentrated and desalted using Sep Pak Environmental C18 cartridge (Waters) and lyophilized. Lyophilized prenylated peptide **III** was reconstituted in 100 μL of 10 mM aminooxy aminium solution containing 0.1% TFA and 50 mM mPDA. The conjugation reaction was carried out at RT for 3 h. The peptide was desalted using a Sep Pak C18 cartridge and then lyophilized. Peptide **III** conjugated to **II** was then dissolved in 0.1% TFA in 6:4 H_2O:CH_3CN, and injected onto a nano-LC system coupled to a Velos Orbitrap mass spectrometer (Thermo Scientific).

6.6.4. *In-vitro* prenylation of HeLa cell proteins with FAPP

HeLa cells were seeded in 100 mm culture dishes and grown until ~60% confluence. Cells were then treated with 25 μM lovastatin for 24 h. After 2x washes with ice-cold PBS, cells were harvested in prenylation/lysis buffer (50 mM Hepes, pH 7.2, 50 mM NaCl, 5 mM $MgCl_2$, 10 μM $ZnCl_2$, 5 mM DTT, 0.6 mM PMSF, and protease inhibitor cocktail). Cells were lysed by aspirating 5 times through a 0.55 mm needle. Cell debris was pelleted by 5 min centrifugation at 13,000 x g and clarified lysates were transferred to fresh tubes. If specified, a solution of recombinant green fluorescent protein (GFP) containing a C-terminal

CaaX motif (GFP-CVIA) was spiked in the HeLa cell lysate at a final concentration of 2.5 μM. *In vitro* prenylation was carried out by adding 10 μM of FAPP and 0.2 μM rPFTase, and incubating at room temperature for 3-6 h. To remove excess of isoprenoid, 500 μL or 15 mL Amicon Centrifugal Filters (Merck Millipore) having 10 kDa cutoff were used and buffer was exchanged with fresh lysis buffer by following manufacturer's instructions.

6.6.5. In-gel fluorescence analysis

To 30 μL of 2 μg/μL protein sample *in vitro* prenylated with FAPP**,** 200 μM Alexa Fluor 488-aminooxy (Life Technologies) was added, and the reaction was initiated by adding 50 mM aniline. After 4 h reaction at RT, proteins were precipitated using ProteoExtract protein precipitation kit (Calbiochem) to remove excess dye. Precipitated proteins were pelleted, washed, and then dissolved in 1x Laemli loading buffer. Sample containing 25-30 μg protein were loaded onto 12% polyacrylamide gels and gels were ran at 120 V until dye fronts reached the bottom. Gels were scanned on a Bio-Rad FX Molecular Imager for the Alexa Fluor 488 fluorescence image. Gels were stained with Coomassie blue solution and scanned to obtain total protein stain image.

6.6.6. Pull-down of aldehyde-tagged proteins using aminooxy-modified agarose resin

HeLa cell lysate *in vitro* prenylated with FAPP was incubated with aminooxy-modified agarose resin (~300 μL resin) in the presence of 10 mM mPDA catalyst at RT for 3-4 h. Unbound proteins were washed 1x with PBS, 3x with 4% SDS in PBS, 3x with 8 M urea, and 3x with 50 mM NH_4HCO_3. Resin with aldehyde-tagged proteins immobilized on it was suspended in 150 μL 50 mM NH_4HCO_3 and 2 μg of trypsin was added. Tryptic digestion was performed at 37 °C overnight. Supernatant of the tryptic peptides were recovered and desalted using Thermo Scientific Hyper Sep C18 column. In brief, C18 column was first wetted using 2 mL 0.1% TFA in CH_3CN (buffer B) and the equilibrated in 6 mL of 0.1% aqueous TFA (buffer A). Tryptic peptides were then loaded onto the column and desalted by washing with 8-10 mL of 2% buffer B in buffer A. Peptides were eluted using 1 mL of 30% buffer B in buffer A, 1 mL of 60% buffer B in buffer A and 3 mL of 100% buffer B. Eluted peptides were lyophilized.

6.6.7. Catch-and-release of aldehyde-tagged proteins or peptides

UltraLink Hydrazide resin slurry (200-600 μL) was washed with 400 μL water and equilibrated by washing 3x with prenylation/lysis buffer. HeLa cell proteins spiked with GFP-CVIA that was prenylated *in vitro* with FAPP were added to the resin and incubated for 2-3 h at RT in the presence of mPDA catalyst (final

concetration of 50 mM). Immobilized proteins were subjected to on-resin digestion by adding 2-6 μg trypsin or Glu-C, and incubating overnight at rt. Supernatant digested peptides were collected the next day and the resin was washed 3x with 50 mM NH_4HCO_3 and 3x with 6:4 CH_3CN:H_2O. Bound C-terminal peptides (conatining the site of prenylation) were eluted by 3 h incubation of the resin with 100-300 μL of 10 mM **II** dissolved in 0.1% TFA in 6:4 CH_3CN:H_2O. Eluted peptides were desalted using a C18 cartridge (as described above) and lyophilized.

6.6.8. LC-MS/MS analysis

Digested peptide samples were dissolved in 0.1% TFA in 40:60 CH_3CN:H_2O, and injected on Eksigent Ultra2D HPLC system coupled to a LTQ-Orbitrap Velos mass spectrometer (Thermo Fisher). Buffer A contained 0.1% aqueous formic acid. A linear gradient of 30-75 min from 2% buffer B (0.1% formic acid in CH_3CN) to 90% buffer B with 300 nL/min flow rate was used for LC-MS/MS run. 30 min gradient was used for the sample derived from peptide **III**, whereas 60-75 min gradient was used for HeLa cell proteomic samples. Data-dependent acquisition mode was used to collect MS/MS scans on the top 6 most abundant precursor ions (m/z ranges from 300-1700 with resolution of 30,000).

6.6.9. SEQUEST Database search

The .RAW data files were converted to MzXML format using msconvert (Proteowizard) and then to .MGF files using TINT raw-to-mgf converter. SEQUEST (version 27) searches were performed against the UniProt Homo sapiens (taxon 9606, March 07, 2013) database with canonical and isoform sequences (175 436 proteins), to which a contaminant database (thegpm.org/crap/index) was appended. In some cases, the same database was also appended with an entry for recombinant GFP-CVIA protein. Search parameters included variable modifications of methionine oxidation, and cysteine 318.2671 (for FAPP-oxime modification); partial V-8 cleavage (4 missed cleavage); peptide tolerance 2 ppm, fragment tolerance 0.8 Da; and False Discovery Rate analysis against reversed database. SEQUEST protein identification data was analyzed and visualized by Scaffold (version 3.6.5).

6.7. Acknowledgements

I would like to acknowledge the following people for their contribution to this work:

Mohammad Rashidian (Department of Chemistry, University of Minnesota) - Synthesis of FAPP, **I** and bisaminooxy ethane.

Purushotham Rao Ponugoti (Department of Chemistry, University of Minnesota) - Synthesis of compound **II**.

Peter Villalta (Masonic Cancer Research Center, University of Minnesota) - Acquisition of LC-MS/MS data on Orbitrap Velos mass spectrometer.

Yi Zhang (Department of Chemistry, University of Minnesota) - Expression and purification of GFP-CVIA and FTase.

Shawou Cheng and Kyle J. LeBlanc (Experimental & Clinical Pharmacology, University of Minnesota) - Administration of simvastatin to mice, isolation and homogenization of brain tissue.

Bibliography

1. Kamiya, Y., Sakurai, A., Tamura, S., Takahashi, N., Abe, K., Tsuchiya, E., Fukui, S., Kitada, C., and Fujino, M. (1978) Structure of rhodotorucine-A, a novel lipopeptide, inducing mating tube formation in rhodoporidium-toruloids, *Biochem. Biophys. Res. Commun. 83*, 1077-1083.
2. Wolda, S. L., and Glomset, J. A. (1988) Evidence for modification of Lamin B by a product of mevalonic acid, *J. Biol. Chem. 263*, 5997-6000.
3. Farnsworth, C. C., Wolda, S. L., Gelb, M. H., and Glomset, J. A. (1989) Human Lamin-B contains a farnesylated cysteine residue, *J. Biol. Chem. 264*, 20422-20429.
4. Zhang, F. L., and Casey, P. J. (1996) Protein prenylation: Molecular mechanisms and functional consequences, *Annu. Rev. Biochem. 65*, 241-269.
5. Ghomashchi, F., Zhang, X. H., Liu, L., and Gelb, M. H. (1995) Binding of prenylated and polybasic peptides to membranes - affinities and intervesicle exchange, *Biochem. 34*, 11910-11918.
6. Resh, M. D. (2006) Trafficking and signaling by fatty-acylated and prenylated proteins, *Nat. Chem. Biol. 2*, 584-590.
7. Zhang, H., Seabra, M. C., and Deisenhofer, J. (2000) Crystal structure of Rab geranylgeranyltransferase at 2.0 angstrom resolution, *Structure 8*, 241-251.
8. Taylor, J. S., Reid, T. S., Terry, K. L., Casey, P. J., and Beese, L. S. (2003) Structure of mammalian protein geranylgeranyltransferase type-I, *EMBO J. 22*, 5963-5974.
9. Pompliano, D. L., Schaber, M. D., Mosser, S. D., Omer, C. A., Shafer, J. A., and Gibbs, J. B. (1993) Isoprenoid diphosphate utilization by recombinant human farnesyl-protein transferase - interactive binding between substrates and a preferred kinetic pathway, *Biochem. 32*, 8341-8347.
10. Dolence, J. M., Cassidy, P. B., Mathis, J. R., and Poulter, C. D. (1995) Yeast protein farnesyltransferase: Steady-state kinetic studies of substrate binding, *Biochem. 34*, 16687-16694.
11. Long, S. B., Casey, P. J., and Beese, L. S. (2002) Reaction path of protein farnesyltransferase at atomic resolution, *Nature 419*, 645-650.
12. Pickett, J. S., Bowers, K. E., Hartman, H. L., Fu, H. W., Embry, A. C., Casey, P. J., and Fierke, C. A. (2003) Kinetic studies of protein farnesyltransferase mutants establish active substrate conformation, *Biochem. 42*, 9741-9748.

13. Yang, Y., Wang, B., Ucisik, M. N., Cui, G., Fierke, C. A., and Merz, K. M., Jr. (2012) Insights into the mechanistic dichotomy of the protein farnesyltransferase peptide substrates CVIM and CVLS, *J. Am. Chem. Soc. 134*, 820-823.
14. Mu, Y. Q., Omer, C. A., and Gibbs, R. A. (1996) On the stereochemical course of human protein-farnesyl transferase, *J. Am. Chem. Soc. 118*, 117-123.
15. Edelstein, R. L., Weller, V. A., Distefano, M. D., and Tung, J. S. (1998) Stereochemical Analysis of the Reaction Catalyzed by Yeast Protein Farnesyltransferase, *J. Org. Chem. 63*, 5298-5299.
16. Dolence, J. M., and Poulter, C. D. (1995) A Mechanism for Posttranslational Modifications of Proteins by Yeast Protein Farnesyltransferase, *Proc. Nat. Acad. Sci. USA 92*, 5008-5011.
17. Mu, Y. Q., Gibbs, R. A., Eubanks, L. M., and Poulter, C. D. (1996) Cuprate-mediated synthesis and biological evaluation of cyclopropyl- and tert-butylfarnesyl diphosphate analogs, *J. Org. Chem. 61*, 8010-8015.
18. Weller, V. A., and Distefano, M. D. (1998) Measurement of the alpha-secondary kinetic isotope effect for a prenyltransferase by MALDI mass spectrometry, *J. Am. Chem. Soc. 120*, 7975-7976.
19. Pais, J. E., Bowers, K. E., and Fierke, C. A. (2006) Measurement of the alpha-secondary kinetic isotope effect for the reaction catalyzed by mammalian protein farnesyltransferase, *J. Am. Chem. Soc. 128*, 15086-15087.
20. Lenevich, S., Xu, J., Hosokawa, A., Cramer, C. J., and Distefano, M. D. (2007) Transition state analysis of model and enzymatic prenylation reactions, *J. Am. Chem. Soc. 129*, 5796-+.
21. Ho, M.-H., Vivo, M. D., Peraro, M. D., and Klein, M. L. (2009) Unraveling the Catalytic Pathway of Metalloenzyme Farnesyltransferase through QM/MM Computation, *J. Chem. Theory Comput. 5*, 1657-1666.
22. Huang, C. C., Casey, P. J., and Fierke, C. A. (1997) Evidence for a catalytic role of zinc in protein farnesyltransferase - Spectroscopy of Co^{2+}-farnesyltransferase indicates metal coordination of the substrate thiolate, *J. Biol. Chem. 272*, 20-23.
23. Rozema, D. B., and Poulter, C. D. (1999) Yeast protein farnesyltransferase. pK(a)s of peptide substrates bound as zinc thiolates, *Biochem. 38*, 13138-13146.
24. Tobin, D. A., Pickett, J. S., Hartman, H. L., Fierke, C. A., and Penner-Hahn, J. E. (2003) Structural Characterization of the Zinc Site in Protein Farnesyltransferase, *J. Am. Chem. Soc. 125*, 9962-9969.

25. Yokoyama, K., McGeady, P., and Gelb, M. H. (1995) Mammalian protein geranylgeranyltransferase-I: Substrate specificity, kinetic mechanism, metal requirements, and affinity labeling, *Biochem. 34*, 1344-1354.
26. Clausen, V. A., Edelstein, R. L., and Distefano, M. D. (2001) Stereochemical analysis of the reaction catalyzed by human protein geranylgeranyl transferase, *Biochem. 40*, 3920-3930.
27. Hartman, H. L., Bowers, K. E., and Fierke, C. A. (2004) Lysine b311 of Protein Geranylgeranyltransferase Type I Partially Replaces Magnesium, *J. Biol. Chem. 279*, 30546-30553.
28. Terry, K. L., Casey, P. J., and Beese, L. S. (2006) Conversion of protein farnesyltransferase to a geranylgeranyltransferase, *Biochem. 45*, 9746-9755.
29. Desnoyers, L., Anant, J. S., and Seabra, M. C. (1996) Geranylgeranylation of Rab proteins, *Biochem. Soc. Trans. 24*, 699-703.
30. Witter, D. J., and Poulter, C. D. (1996) Yeast geranylgeranyltransferase type-II: Steady state kinetic studies of the recombinant enzyme, *Biochem. 35*, 10454-10463.
31. Zhang, H., Seabra, M. C., and Deisenhofer, J. (2000) Crystal Structure of Rab geranylgeranyltransferase at 2.0 A resolution, *Structure 8*, 241-251.
32. Guo, Z., Wu, Y.-W., Das, D., Delon, C., Cramer, J., Yu, S., Thuns, S., Lupilova, N., Waldmann, H., Brunsveld, L., Goody, R. S., Alexandrov, K., and Blankenfeldt, W. (2008) Structures of RabGGTase-substrate/product complexes provide insights into the evolution of protein prenylation, *EMBO J. 27*, 2444-2456.
33. Schuld, N. J., Vervacke, J. S., Lorimer, E. L., Simon, N. C., Hauser, A. D., Barbieri, J. T., Distefano, M. D., and Williams, C. L. (2014) The chaperone protein SmgGDS interacts with small GTPases entering the prenylation pathway by recognizing the last amino acid in the CAAX motif, *J. Biol. Chem. 289*, 6862-6876.
34. Ochocki, J. D., and Distefano, M. D. (2013) Prenyltransferase inhibitors: treating human ailments from cancer to parasitic infections, *MedChemComm 4*, 476-492.
35. Berndt, N., Hamilton, A. D., and Sebti, S. M. (2011) Targeting protein prenylation for cancer therapy, *Nat. Rev. Cancer 11*, 775-791.
36. London, N., Lamphear, C. L., Hougland, J. L., Fierke, C. A., and Schueler-Furman, O. (2011) Identification of a novel class of farnesylation targets by structure-based modeling of binding specificity, *Plos Comput. Biol. 7*, e1002170.

37. Maurer-Stroh, S., Koranda, M., Benetka, W., Schneider, G., Sirota, F. L., and Eisenhaber, F. (2007) Towards complete sets of farnesylated and geranylgeranylated proteins, *Plos Comput. Biol. 3*, 634-648.
38. Maurer-Stroh, S., and Eisenhaber, F. (2005) Refinement and prediction of protein prenylation motifs, *Genome Biol. 6*, R55.
39. Hougland, J. L., Hicks, K. A., Hartman, H. L., Kelly, R. A., Watt, T. J., and Fierke, C. A. (2010) Identification of Novel Peptide Substrates for Protein Farnesyltransferase Reveals Two Substrate Classes with Distinct Sequence Selectivities, *J. Mol. Biol. 395*, 176-190.
40. Reiss, Y., Stradley, S. J., Gierasch, L. M., Brown, M. S., and Goldstein, J. L. (1991) Sequence requirement for peptide recognition by rat-brain P21Ras protein farnesyltransferase, *Proc. Natl. Acad. Sci. U. S. A. 88*, 732-736.
41. Hightower, K. E., Huang, C. C., Casey, P. J., and Fierke, C. A. (1998) H-Ras peptide and protein substrates bind protein farnesyltransferase as an ionized thiolate, *Biochem. 37*, 15555-15562.
42. Pompliano, D. L., Gomez, R. P., and Anthony, N. J. (1992) Intramolecular fluorescence enhancement- A continuous assay of Ras farnesyl-protein transferase, *J. Am. Chem. Soc. 114*, 7945-7946.
43. Stirtan, W. G., and Poulter, C. D. (1995) Yeast protein geranylgeranyltransferase type-I - Overproduction, purification, and characterization, *Arch. Biochem. Biophys. 321*, 182-190.
44. Boutin, J. A., Marande, W., Petit, L., Loynel, A., Desmet, C., Canet, E., and Fauchére, J. L. (1999) Investigation of S-farnesyl transferase substrate specificity with combinatorial tetrapeptide libraries, *Cell. Signal. 11*, 59-69.
45. Krzysiak, A. J., Scott, S. A., Hicks, K. A., Fierke, C. A., and Gibbs, R. A. (2007) Evaluation of protein farnesyltransferase substrate specificity using synthetic peptide libraries, *Bioorg. Med. Chem. Lett. 17*, 5548-5551.
46. Krzysiak, A. J., Aditya, A. V., Hougland, J. L., Fierke, C. A., and Gibbs, R. A. (2010) Synthesis and screening of a CaaL peptide library versus FTase reveals a surprising number of substrates, *Bioorg. Med. Chem. Lett. 20*, 767-770.
47. Hougland, J. L., Lamphear, C. L., Scott, S. A., Gibbs, R. A., and Fierke, C. A. (2009) Context-dependent substrate recognition by protein farnesyltransferase, *Biochem. 48*, 1691-1701.
48. Lamphear, C. L., Zverina, E. A., Hougland, J. L., and Fierke, C. A. (2011) Global identification of protein prenyltransferase substrates: defining the prenylated proteome, *Enzymes 29*, 207-234.

49. Wang, Y.-C., and Distefano, M. D. (2012) Solid-phase synthesis of C-terminal peptide libraries for studying the specificity of enzymatic protein prenylation, *Chem. Comm. 48*, 8228-8230.
50. Wang, Y.-C., Dozier, J. K., Beese, L. S., and Distefano, M. D. (2014) Rapid analysis of protein farnesyltransferase substrate specificity using peptide libraries and isoprenoid diphosphate analogues, *ACS Chem. Biol. 9*, 1726-1735.
51. Omer, C. A., Kral, A. M., Diehl, R. E., Prendergast, G. C., Powers, S., Allen, C. M., Gibbs, J. B., and Kohl, N. E. (1993) Characterization of recombinant human farnesyl-protein transferase: Cloning, expression, farnesyl diphosphate binding, and functional homology with yeast prenyl-protein transferases, *Biochem. 32*, 5167-5176.
52. Bukhtiyarov, Y. E., Omer, C. A., and Allen, C. M. (1995) Photoreactive analogs of prenyl diphosphates as inhibitors and probes of human protein farnesyltransferase and geranylgeranyltransferase type-I, *J. Biol. Chem. 270*, 19035-19040.
53. Edelstein, R. L., and Distefano, M. D. (1997) Photoaffinity labeling of yeast farnesyl protein transferase and enzymatic synthesis of a Ras protein incorporating a photoactive isoprenoid, *Biochem. Biophys. Res. Commun. 235*, 377-382.
54. Gaon, I., Turek, T. C., and Distefano, M. D. (1996) Farnesyl and geranylgeranyl pyrophosphate analogs incorporating benzoylbenzyl ethers: synthesis and inhibition of yeast protein farnesyltransferase, *Tetrahedron Lett. 37*, 8833-8836.
55. Gaon, I., Turek, T. C., Weller, V. A., Edelstein, R. L., Singh, S. K., and Distefano, M. D. (1996) Photoactive Analogs of Farnesyl Pyrophosphate Containing Benzoylbenzoate Esters: Synthesis and Application to Photoaffinity Labeling of Yeast Farnesyltransferase, *J. Org. Chem. 61*, 7738-7745.
56. Turek, T. C., Gaon, I., and Distefano, M. D. (1996) Analogs of farnesyl pyrophosphate incorporating internal benzoylbenzoate esters: Synthesis, inhibition kinetics and photoinactivation of yeast protein farnesyltransferase, *Tetrahedron Lett. 37*, 4845-4848.
57. Turek, T. C., Gaon, I., Distefano, M. D., and Strickland, C. L. (2001) Synthesis of Farnesyl Diphosphate Analogues Containing Ether-Linked Photoactive Benzophenones and Their Application in Studies of Protein Prenyltransferases, *J. Org. Chem. 66*, 3253-3264.
58. Turek, T. C., Gaon, I., Gamache, D., and Distefano, M. D. (1997) Synthesis and evaluation of benzophenone-based photoaffinity labeling

analogs of prenyl pyrophosphates containing stable amide linkages, *Bioorg. Med. Chem. Lett. 7*, 2125-2130.
59. Quellhorst, G. J., Allen, C. M., and Wessling-Resnick, M. (2001) Modification of Rab5 with a photoactivatable analog of geranylgeranyl diphosphate, *J. Biol. Chem. 276*, 40727-40733.
60. Turek-Etienne, T. C., Strickland, C. L., and Distefano, M. D. (2003) Biochemical and structural studies with prenyl diphosphate analogues provide insights into isoprenoid recognition by protein farnesyl transferase, *Biochem. 42*, 3716-3724.
61. Hovlid, M. L., Edelstein, R. L., Henry, O., Ochocki, J., DeGraw, A., Lenevich, S., Talbot, T., Young, V. G., Hruza, A. W., Lopez-Gallego, F., Labello, N. P., Strickland, C. L., Schmidt-Dannert, C., and Distefano, M. D. (2010) Synthesis, properties, and applications of diazotrifluropropanoyl-containing photoactive analogs of farnesyl diphosphate containing modified linkages for enhanced stability, *Chem. Biol. Drug Des. 75*, 51-67.
62. Vervacke, J. S., Funk, A. L., Wang, Y.-C., Strom, M., Hrycyna, C. A., and Distefano, M. D. (2014) Diazirine-containing photoactivatable isoprenoid: synthesis and application in studies with isoprenylcysteine carboxyl methyltransferase, *J. Org. Chem. 79*, 1971-1978.
63. DeGraw, A. J., Zhao, Z., Hsieh, J., Jefferies, M., Distefano, M. D., Strickland, C. L., Shintani, D., Nural, H., McMahan, C., and Xie, W. (2007) A photoactive isoprenoid diphosphate analogue containing a stable phosphonate linkage: synthesis and structural biochemical studies with prenyltransferases, *J. Org. Chem. 72*, 4587 - 4595.
64. Strickland, C. L., Windsor, W. T., Syto, R., Wang, L., Bond, R., Wu, Z., Schwartz, J., Le, H. V., Beese, L. S., and Weber, P. C. (1998) Crystal structure of farnesyl protein transferase complexed with a CaaX peptide and farnesyl diphosphate analogue, *Biochem. 37*, 16601-16611.
65. Zahn, T. J., Whitney, J., Weinbaum, C., and Gibbs, R. A. (2001) Synthesis and evaluation of GGPP geometric isomers: Divergent substrate specificities of FTase and GGTase I, *Bioorg. Med. Chem. Lett. 11*, 1605-1608.
66. Subramanian, T., Pais, J. E., Liu, S., Troutman, J. M., Suzuki, Y., Subramanian, K. L., Fierke, C. A., Andres, D. A., and Spielmann, H. P. (2012) Farnesyl Diphosphate Analogues with Aryl Moieties Are Efficient Alternate Substrates for Protein Farnesyltransferase, *Biochem. 51*, 8307-8319.
67. Roberts, M. J., Troutman, J. M., Chehade, K. A. H., Cha, H. C., Kao, J. P. Y., Huang, X., Zhan, C.-G., Peterson, Y. K., Subramanian, T., Kamalakkannan, S., Andres, D. A., and Spielmann, H. P. (2006)

Hydrophilic anilinogeranyl diphosphate prenyl analogues are Ras function inhibitors, *Biochem. 45*, 15862-15872.
68. Troutman, J. M., Subramanian, T., Andres, D. A., and Spielmann, H. P. (2007) Selective modification of CaaX peptides with ortho-substituted anilinogeranyl lipids by protein farnesyl transferase: Competitive substrates and potent inhibitors from a library of farnesyl diphosphate analogues, *Biochem. 46*, 11310-11321.
69. Gibbs, B. S., Zahn, T. J., Mu, Y. Q., Sebolt-Leopold, J. S., and Gibbs, R. A. (1999) Novel farnesol and geranylgeraniol analogues: A potential new class of anticancer agents directed against protein prenylation, *J. Med. Chem. 42*, 3800-3808.
70. Krzysiak, A. J., Rawat, D. S., Scott, S. A., Pais, J. E., Handley, M., Harrison, M. L., Fierke, C. A., and Gibbs, R. A. (2007) Combinatorial Modulation of Protein Prenylation, *ACS Chem. Biol. 2*, 385-389.
71. Das, D., Tnimov, Z., Nguyen, U. n. T. T., Thimmaiah, G., Lo, H., Abankwa, D., Wu, Y., Goody, R. S., Waldmann, H., and Alexandrov, K. (2012) Flexible and general synthesis of functionalized phosphoisoprenoids for the study of prenylation in vivo and in vitro, *ChemBioChem 13*, 674-683.
72. Dozier, J. K., Khatwani, S. L., Wollack, J. W., Wang, Y.-C., Schmidt-Dannert, C., and Distefano, M. D. (2014) Engineering protein farnesyltransferase for enzymatic protein labeling applications, *Bioconjugate Chem. 25*, 1203-1212.
73. Kim, M. K., Kleckley, T. S., Wiemer, A. J., Holstein, S. A., Hohl, R. J., and Wiemer, D. F. (2004) Synthesis and activity of fluorescent isoprenoid pyrophosphate analogues, *J. Org. Chem. 69*, 8186-8193.
74. Placzek, A. T., Krzysiak, A. J., and Gibbs, R. A. (2011) Chemical probes of protein prenylation, *Enzymes, Vol 30: Protein Prenylation, Pt B 30*, 91-127.
75. Patel, D. V., Schmidt, R. J., Biller, S. A., Gordon, E. M., Robinson, S. S., and Manne, V. (1995) Farnesyl Diphosphate-Based Inhibitors of Ras Farnesyl Protein Transferase, *J. Med. Chem. 38*, 2906-2921.
76. Kho, Y., Kim, S. C., Jiang, C., Barma, D., Kwon, S. W., Cheng, J., Jaunbergs, J., Weinbaum, C., Tamanoi, F., Falck, J., and Zhao, Y. (2004) A tagging-via-substrate technology for detection and proteomics of farnesylated proteins, *Proc. Natl. Acad. Sci. U. S. A. 101*, 12479-12484.
77. Chan, L. N., Hart, C., Guo, L., Nyberg, T., Davies, B. S. J., Fong, L. G., Young, S. G., Agnew, B. J., and Tamanoi, F. (2009) A novel approach to tag and identify geranylgeranylated proteins, *Electrophoresis 30*, 3598-3606.

78. Berry, A. F. H., Heal, W. P., Tarafder, A. K., Tolmachova, T., Baron, R. A., Seabra, M. C., and Tate, E. W. (2010) Rapid multilabel detection of geranylgeranylated proteins by using bioorthogonal ligation chemistry, *ChemBioChem 11*, 771-773.
79. DeGraw, A. J., Palsuledesai, C., Ochocki, J. D., Dozier, J. K., Lenevich, S., Rashidian, M., and Distefano, M. D. (2010) Evaluation of Alkyne-Modified Isoprenoids as Chemical Reporters of Protein Prenylation, *Chem. Biol. Drug Des. 76*, 460-471.
80. Charron, G., Tsou, L. K., Maguire, W., Yount, J. S., and Hang, H. C. (2011) Alkynyl-farnesol reporters for detection of protein S-prenylation in cells, *Mol. BioSyst. 7*, 67-73.
81. Duckworth, B. P., Zhang, Z., Hosokawa, A., and Distefano, M. D. (2007) Selective labeling of proteins by using protein farnesyltransferase, *ChemBioChem 8*, 98-105.
82. Hosokawa, A., Wollack, J. W., Zhang, Z. Y., Chen, L., Barany, G., and Distefano, M. D. (2007) Evaluation of an alkyne-containing analogue of farnesyl diphosphate as a dual substrate for protein-prenyltransferases, *Int. J. Pept. Res. Ther. 13*, 345-354.
83. Palsuledesai, C. C., Ochocki, J. D., Markowski, T. W., and Distefano, M. D. (2014) A combination of metabolic labeling and 2D-DIGE analysis in response to a farnesyltransferase inhibitor facilitates the discovery of new prenylated proteins, *Mol. Biosyst. 10*, 1094-1103.
84. Reinicke, A. T., Hutchinson, J. L., Magee, A. I., Mastroeni, P., Trowsdale, J., and Kelly, A. P. (2005) A Salmonella typhimurium effector protein SifA is modified by host cell prenylation and S-acylation machinery, *J. Biol. Chem. 280*, 14620-14627.
85. Price, C. T. D., Al-Quadan, T., Santic, M., Jones, S. C., and Abu Kwaik, Y. (2010) Exploitation of conserved eukaryotic host cell farnesylation machinery by an F-box effector of Legionella pneumophila, *J. Exp. Med. 207*, 1712-1725.
86. Ivanov, S. S., Charron, G., Hang, H. C., and Roy, C. R. (2010) Lipidation by the host prenyltransferase machinery facilitates membrane localization of legionella pneumophila effector proteins, *J. Biol. Chem. 285*, 34686-34698.
87. Marakasova, E. S., Akhmatova, N. K., Amaya, M., Eisenhaber, B., Eisenhaber, F., van Hoek, M. L., and Baranova, A. V. (2013) Prenylation: From bacteria to eukaryotes, *Mol. Biol. 47*, 622-633.
88. Charron, G., Li, M. M. H., MacDonald, M. R., and Hang, H. C. (2013) Prenylome profiling reveals S-farnesylation is crucial for membrane

targeting and antiviral activity of ZAP long-isoform, *Proc. Natl. Acad. Sci. U. S. A. 110*, 11085-11090.
89. Nguyen, U. T. T., Guo, Z., Delon, C., Wu, Y., Deraeve, C., Fraenzel, B., Bon, R. S., Blankenfeldt, W., Goody, R. S., Waldmann, H., Wolters, D., and Alexandrov, K. (2009) Analysis of the eukaryotic prenylome by isoprenoid affinity tagging, *Nat. Chem. Biol. 5*, 227-235.
90. Onono, F. O., Morgan, M. A., Spielmann, H. P., Andres, D. A., Subramanian, T., Ganser, A., and Reuter, C. W. M. (2010) A tagging-via-substrate approach to detect the farnesylated proteome using two-dimensional electrophoresis coupled with Western blotting, *Mol. Cell. Proteomics 9*, 742-751.
91. Porcu, G., Wilson, C., Di Giandomenico, D., and Ragnini-Wilson, A. (2010) A yeast-based genomic strategy highlights the cell protein networks altered by FTase inhibitor peptidomimetics, *Mol Cancer 9*, 197.
92. Schafer, W. R., Kim, R., Sterne, R., Thorner, J., Kim, S. H., and Rine, J. (1989) Genetic and pharmacological suppression of oncogenic mutations in Ras genes of yeast and humans, *Science 245*, 379-385.
93. Reiss, Y., Goldstein, J. L., Seabra, M. C., Casey, P. J., and Brown, M. S. (1990) Inhibition of purified p21ras farnesyl:protein transferase by Cys-AAX tetrapeptides, *Cell 62*, 81-88.
94. Bishop, W. R., Doll, R., and Kirschmeier, P. (2011) Farnesyl transferase inhibitors: From targeted cancer therapeutic to a potential treatment for progeria, *Enzymes 29*, 275-303.
95. Bos, J. L. (1989) Ras oncogenes in human cancer - a review, *Cancer Res. 49*, 4682-4689.
96. Lerner, E. C., Zhang, T. T., Knowles, D. B., Qian, Y. M., Hamilton, A. D., and Sebti, S. M. (1997) Inhibition of the prenylation of K-Ras, but not H- or N-Ras, is highly resistant to CAAX peptidomimetics and requires both a farnesyltransferase and a geranylgeranyltransferase I inhibitor in human tumor cell lines, *Oncogene 15*, 1283-1288.
97. Raponi, M., Lancet, J. E., Fan, H., Dossey, L., Lee, G., Gojo, I., Feldman, E. J., Gotlib, J., Morris, L. E., Greenberg, P. L., Wright, J. J., Harousseau, J.-L., Loewenberg, B., Stone, R. M., De Porre, P., Wang, Y., and Karp, J. E. (2008) A 2-gene classifier for predicting response to the famesyltransferase inhibitor tipifarnib in acute myeloid leukemia, *Blood 111*, 2589-2596.
98. Abate-Pella, D., Zeliadt, N. A., Ochocki, J. D., Warmka, J. K., Dore, T. M., Blank, D. A., Wattenberg, E. V., and Distefano, M. D. (2012) Photochemical Modulation of Ras-Mediated Signal Transduction using

Caged Farnesyltransferase Inhibitors: Activation via One- and Two-Photon Excitation, *ChemBioChem 13*, 1009-1016.
99. Yang, S. H., Bergo, M. O., Toth, J. I., Qiao, X., Hu, Y., Sandoval, S., Meta, M., Bendale, P., Gelb, M. H., Young, S. G., and Fong, L. G. (2005) Blocking protein farnesyltransferase improves nuclear blebbing in mouse fibroblasts with a targeted Hutchinson-Gilford progeria syndrome mutation, *Proc. Natl. Acad. Sci. U. S. A. 102*, 10291-10296.
100. Fong, L. G., Frost, D., Meta, M., Qiao, X., Yang, S. H., Coffinier, C., and Young, S. G. (2006) A protein farnesyltransferase inhibitor ameliorates disease in a mouse model of progeria, *Science 311*, 1621-1623.
101. Gordon, L. B., Kleinman, M. E., Miller, D. T., Neuberg, D. S., Giobbie-Hurder, A., Gerhard-Herman, M., Smoot, L. B., Gordon, C. M., Cleveland, R., Snyder, B. D., Fligor, B., Bishop, W. R., Statkevich, P., Regen, A., Sonis, A., Riley, S., Ploski, C., Correia, A., Quinn, N., Ullrich, N. J., Nazarian, A., Liang, M. G., Huh, S. Y., Schwartzman, A., and Kieran, M. W. (2012) Clinical trial of a farnesyltransferase inhibitor in children with Hutchinson-Gilford progeria syndrome, *Proc. Natl. Acad. Sci. U. S. A. 109*, 16666-16671.
102. Boston, C. s. H. (2009) Study of zoledronic acid, pravastatin and lonafarnib for patients with progeria, US National Institute of Health, http://clinicaltrials.gov/ct2/show/record/NCT00916747.
103. Kraus, J. M., Tatipaka, H. B., McGuffin, S. A., Chennamaneni, N. K., Karimi, M., Arif, J., Verlinde, C. L. M. J., Buckner, F. S., and Gelb, M. l. H. (2010) Second generation analogues of the cancer drug clinical candidate tipifarnib for anti-Chagas disease drug discovery, *J. Med. Chem. 53*, 3887-3898.
104. Carrico, D., Ohkanda, J., Kendrick, H., Yokoyama, K., Blaskovich, M. A., Bucher, C. J., Buckner, F. S., Van Voorhis, W. C., Chakrabarti, D., Croft, S. L., Gelb, M. H., Sebti, S. M., and Hamilton, A. D. (2004) In vitro and in vivo antimalarial activity of peptidomimetic protein farnesyltransferase inhibitors with improved membrane permeability, *Bioorg. Med. Chem. 12*, 6517-6526.
105. Yokoyama, K., Trobridge, P., Buckner, F. S., Scholten, J., Stuart, K. D., Van Voorhis, W. C., and Gelb, M. H. (1998) The effects of protein farnesyltransferase inhibitors on trypanosomatids: inhibition of protein farnesylation and cell growth, *Mol. Biochem. Parasitol. 94*, 87-97.
106. Fletcher, S., Cummings, C. G., Rivas, K., Katt, W. P., Horney, C., Buckner, F. S., Chakrabarti, D., Sebti, S. M., Gelb, M. 1. H., Van Voorhis, W. C., and Hamilton, A. D. (2008) Potent, plasmodium-selective farnesyltransferase inhibitors that arrest the growth of malaria parasites:

Structure-activity relationships of ethylenediamine-analogue scaffolds and homology model validation. *J. Med. Chem. 51*, 5176-5197.

107. Walters, C. E., Pryce, G., Hankey, D. J. R., Sebti, S. M., Hamilton, A. D., Baker, D., Greenwood, J., and Adamson, P. (2002) Inhibition of Rho GTPases with protein prenyltransferase inhibitors prevents leukocyte recruitment to the central nervous system and attenuates clinical signs of disease in an animal model of multiple sclerosis, *J. Immun. 168*, 4087-4094.
108. Coxon, F. P., Helfrich, M. H., Van't Hof, R., Sebti, S., Ralston, S. H., Hamilton, A., and Rogers, M. J. (2000) Protein geranylgeranylation is required for osteoclast formation, function, and survival: Inhibition by bisphosphonates and GGTI-298, *J. Bone Mineral Res. 15*, 1467-1476.
109. Bordier, B. B., Marion, P. L., Ohashi, K., Kay, M. A., Greenberg, H. B., Casey, J. L., and Glenn, J. S. (2002) A prenylation inhibitor prevents production of infectious hepatitis delta virus particles, *J. Virol. 76*, 10465-10472.
110. Liu, Z., Meray, R. K., Grammatopoulos, T. N., Fredenburg, R. A., Cookson, M. R., Liu, Y., Logan, T., and Lansbury, P. T., Jr. (2009) Membrane-associated farnesylated UCH-L1 promotes alpha-synuclein neurotoxicity and is a therapeutic target for Parkinson's disease, *Proc. Natl. Acad. Sci. U. S. A. 106*, 4635-4640.
111. Duckworth, B. P., Xu, J., Taton, T. A., Guo, A., and Distefano, M. D. (2006) Site-specific, covalent attachment of proteins to a solid surface, *Bioconjugate Chem. 17*, 967-974.
112. Gauchet, C., Labadie, G. R., and Poulter, C. D. (2006) Regio- and chemoselective covalent immobilization of proteins through unnatural amino acids, *J. Am. Chem. Soc. 128*, 9274-9275.
113. Duckworth, B. P., Zhang, Z. Y., Hosokawa, A., and Distefano, M. D. (2007) Selective labeling of proteins by using protein farnesyltransferase, *Chembiochem 8*, 98-105.
114. Xu, J., DeGraw, A. J., Duckworth, B. P., Lenevich, S., Tann, C.-M., Jenson, E. C., Gruber, S. J., Barany, G., and Distefano, M. D. (2006) Synthesis and reactivity of 6,7-dihydrogeranylazides: Reagents for primary azide incorporation into peptides and subsequent Staudinger ligation, *Chem. Biol. Drug Des. 68*, 85-96.
115. Tolstyka, Z. P., Richardson, W., Bat, E., Stevens, C. J., Parra, D. P., Dozier, J. K., Distefano, M. D., Dunn, B., and Maynard, H. D. (2013) Chemoselective Immobilization of Proteins by Microcontact Printing and Bio-orthogonal Click Reactions, *ChemBioChem 14*, 2464-2471.

116. Weinrich, D., Lin, P.-C., Jonkheijm, P., Nguyen, U. T. T., Schroeder, H., Niemeyer, C. M., Alexandrov, K., Goody, R., and Waldmann, H. (2010) Oriented Immobilization of Farnesylated Proteins by the Thiol-Ene Reaction, *Angew. Chem. Int. Ed. 49*, 1252-1257.
117. Choi, S.-r., Seo, J.-s., Bohaty, R. F. H., and Poulter, C. D. (2014) Regio- and chemoselective immobilization of proteins on gold surfaces, *Bioconjugate Chem. 25*, 269-275.
118. Seo, J.-s., and Poulter, C. D. (2014) Sandwich antibody arrays using recombinant antibody-binding Protein L, *Langmuir 30*, 6629-6635.
119. Dursina, B.-E., Reents, R., Niculae, A., Veligodsky, A., Breitling, R., Pyatkov, K., Waldmann, H., Goody, R. S., and Alexandrov, K. (2005) A genetically encodable microtag for chemo-enzymatic derivatization and purification of recombinant proteins, *Protein Expression Purif. 39*, 71-81.
120. Mahmoodi, M. M., Rashidian, M., Dozier, J. K., and Distefano, M. D. (2013) Chemoenzymatic site-specific reversible immobilization and labeling of proteins from crude cellular extract without prior purification using oxime and hydrazine ligation, *Curr. Protoc. Chem. Biol. 5*, 89-109.
121. Duckworth, B. P., Chen, Y., Wollack, J. W., Sham, Y., Mueller, J. D., Taton, T. A., and Distefano, M. D. (2007) A universal method for the preparation of covalent protein-DNA conjugates for use in creating protein nanostructures, *Angew. Chem., Int. Ed. 46*, 8819-8822.
122. Khatwani, S. L., Kang, J. S., Mullen, D. G., Hast, M. A., Beese, L. S., Distefano, M. D., and Taton, T. A. (2012) Covalent protein-oligonucleotide conjugates by copper-free click reaction, *Bioorg. Med. Chem. 20*, 4532-4539.
123. Yeo, J. E., Wickramaratne, S., Khatwani, S., Wang, Y.-C., Vervacke, J., Distefano, M. D., and Tretyakova, N. Y. (2014) Synthesis of Site-Specific DNA–Protein Conjugates and Their Effects on DNA Replication, *ACS Chem. Biol. 9*, 1860-1868.
124. Rashidian, M., Mahmoodi, M. M., Shah, R., Dozier, J. K., Wagner, C. R., and Distefano, M. D. (2013) A Highly Efficient Catalyst for Oxime Ligation and Hydrazone–Oxime Exchange Suitable for Bioconjugation, *Bioconjugate Chem. 24*, 333-342.
125. Rashidian, M., Kumarapperuma, S. C., Gabrielse, K., Fegan, A., Wagner, C. R., and Distefano, M. D. (2013) Simultaneous Dual Protein Labeling Using a Triorthogonal Reagent, *J. Am. Chem. Soc. 135*, 16388-16396.
126. Prendergast, G. C. (2001) Actin' up: RhoB in cancer and apoptosis, *Nat. Rev. Cancer 1*, 162-168.
127. Sebti, S. M., and Der, C. J. (2003) Searching for the elusive targets of farnesyltransferase inhibitors, *Nat. Rev. Cancer 3*, 945-951.

128. Sebti, S. M. (2005) Protein farnesylation: Implications for normal physiology, malignant transformation, and cancer therapy, *Cancer Cell 7*, 297-300.
129. Rix, U., and Superti-Furga, G. (2009) Target profiling of small molecules by chemical proteomics, *Nat. Chem. Biol. 5*, 616-624.
130. Heal, W. P., Wickramasinghe, S. R., and Tate, E. W. (2008) Activity based chemical proteomics: profiling proteases as drug targets, *Curr. Drug Discov. Technol. 5*, 200-212.
131. Sletten, E. M., and Bertozzi, C. R. (2009) Bioorthogonal Chemistry: Fishing for Selectivity in a Sea of Functionality, *Angew. Chem. Intl. Ed. 48*, 6974-6998.
132. Nguyen, U. T. T., Guo, Z., Delon, C., Wu, Y., Deraeve, C., Fraenzel, B., Bon, R. S., Blankenfeldt, W., Goody, R. S., Waldmann, H., Wolters, D., and Alexandrov, K. (2009) Analysis of the eukaryotic prenylome by isoprenoid affinity tagging, *Nat. Chem. Biol. 5*, 227-235.
133. Onono, F. O., Morgan, M. A., Spielmann, H. P., Andres, D. A., Subramanian, T., Ganser, A., and Reuter, C. W. M. (2010) A tagging-via-substrate approach to detect the farnesylated proteome using two-dimensional electrophoresis coupled with Western blotting, *Mol. Cell. Proteomics 9*, 742-751.
134. Speers, A. E., and Cravatt, B. F. (2004) Profiling enzyme activities in vivo using click chemistry methods, *Chem. Biol. 11*, 535-546.
135. Labadie, G. R., Viswanathan, R., and Poulter, C. D. (2007) Farnesyl diphosphate analogues with omega-bioorthogonal azide and alkyne functional groups for protein farnesyl transferase-catalyzed Ligation reactions, *J. Org. Chem. 72*, 9291-9297.
136. Hannoush, R. N., and Arenas-Ramirez, N. (2009) Imaging the lipidome: omega-alkynyl fatty acids for detection and cellular visualization of lipid-modified proteins, *ACS Chem. Biol. 4*, 581-587.
137. Hannoush, R. N., and Sun, J. (2010) The chemical toolbox for monitoring protein fatty acylation and prenylation, *Nat. Chem. Biol. 6*, 498-506.
138. Andersen, J. D., Boylan, K. L. M., Xue, F. S., Anderson, L. B., Witthuhn, B. A., Markowski, T. W., Higgins, L., and Skubitz, A. P. N. (2010) Identification of candidate biomarkers in ovarian cancer serum by depletion of highly abundant proteins and differential in-gel electrophoresis, *Electrophoresis 31*, 599-610.
139. Chan, L. N., and Tamanoi, F. (2011) Global Analysis of Prenylated Proteins by the Use of a Tagging via Substrate Approach, *Enzymes, Vol 29: Protein Prenylation, Pt A 29*, 195-206.

140. Tsolakos, N., Techanukul, T., Wallington, A., Zhao, Y., Jones, C., Nagy, J., and Wheeler, J. X. (2009) Comparison of two combinations of cyanine dyes for prelabelling and gel electrophoresis, *Proteomics 9*, 1727-1730.
141. Nørgaard, P., Law, B., Joseph, H., Page, D. L., Shyr, Y., Mays, D., Pietenpol, J. A., Kohl, N. E., Oliff, A., Coffey, R. J., Poulsen, H. S., and Moses, H. L. (1999) Treatment with farnesyl-protein transferase inhibitor induces regression of mammary tumors in transforming growth factor (TGF) alpha and TGF alpha/neu transgenic mice by inhibition of mitogenic activity and induction of apoptosis, *Clin. Cancer Res. 5*, 35-42.
142. Węsierska-Gądek, J., Kramer, M. P., and Schmid, G. (2008) A Combined Treatment of HeLa Cells With the Farnesyl Protein Transferase Inhibitor L-744,832 and Cisplatin Significantly Increases the Therapeutic Effect as Compared to Cisplatin Monotherapy, *J. Cell. Biochem. 104*, 189-201.
143. Maurer-Stroh, S., and Eisenhaber, F. (2005) Refinement and prediction of protein prenylation motifs, *Genome Biol. 6*.
144. Trueblood, C. E., Boyartchuk, V. L., Picologlou, E. A., Rozema, D., Poulter, C. D., and Rine, J. (2000) The CaaX proteases, Afc1p and Rce1p, have overlapping but distinct substrate specificities, *Mol. Cell. Biol. 20*, 4381-4392.
145. Coxon, F. P., Ebetino, F. H., Mules, E. H., Seabra, M. C., McKenna, C. E., and Rogers, M. J. (2005) Phosphonocarboxylate inhibitors of Rab geranylgeranyl transferase disrupt the prenylation and membrane localization of Rab proteins in osteoclasts in vitro and in vivo, *Bone 37*, 349-358.
146. Cassidy, P. B., Dolence, J. M., and Poulter, C. D. (1995) Continuous Fluorescence Assay for Protein Prenyltransferases, *Methods Enzymol. 250*, 30-43.
147. DeGraw, A. J., Hast, M. A., Xu, J., Mullen, D., Beese, L. S., Barany, G., and Distefano, M. D. (2008) Caged protein prenyltransferase substrates: Tools for understanding protein prenylation, *Chem. Biol. Drug Des. 72*, 171-181.
148. Hicks, K. A., Hartman, H. L., and Fierke, C. A. (2005) Upstream polybasic region in peptides enhances dual specificity for prenylation by both farnesyltransferase and geranylgeranyltransferase type I, *Biochem. 44*, 15325-15333.
149. Bishop, W. R., Doll, R., and Kirschmeier, P. (2011) Farnesyl Transferase Inhibitors: From Targeted Cancer Therapeutic to a Potential Treatment for Progeria, *Enzymes, Vol 29: Protein Prenylation, Pt A 29*, 275-303.

150. Adam, S. A., Butin-Israeli, V., Cleland, M. M., Shimi, T., and Goldman, R. D. (2013) Disruption of lamin B1 and lamin B2 processing and localization by farnesyltransferase inhibitors, *Nucleus 4*, 142-150.
151. Si, X. N., Zeng, Q., Ng, C. H., Hong, W. J., and Pallen, C. J. (2001) Interaction of farnesylated PRL-2, a protein-tyrosine phosphatase, with the beta-subunit of geranylgeranyltransferase II, *J. Biol. Chem. 276*, 32875-32882.
152. Osterman, I. A., Ustinov, A. V., Evdokimov, D. V., Korshun, V. A., Sergiev, P. V., Serebryakova, M. V., Demina, I. A., Galyamina, M. A., Govorun, V. M., and Dontsova, O. A. (2013) A nascent proteome study combining click chemistry with 2DE, *Proteomics 13*, 17-21.
153. Agard, N. J., and Bertozzi, C. R. (2009) Chemical Approaches To Perturb, Profile, and Perceive Glycans, *Acc. Chem. Res. 42*, 788-797.
154. Hosokawa, A., Wollack, J. W., Zhang, Z., Chen, L., Barany, G., and Distefano, M. D. (2007) Evaluation of an alkyne-containing analogue of farnesyl diphosphate as a dual substrate for protein-prenyltransferases, *Int. J. Pept. Res. Ther. 13*, 345-354.
155. Berg, T. J., Gastonguay, A. J., Lorimer, E. L., Kuhnmuench, J. R., Li, R., Fields, A. P., and Williams, C. L. (2010) Splice Variants of SmgGDS Control Small GTPase Prenylation and Membrane Localization, *J. Biol. Chem. 285*, 35255-35266.
156. Rappsilber, J., Ishihama, Y., and Mann, M. (2003) Stop and go extraction tips for matrix-assisted laser desorption/ionization, nanoelectrospray, and LC/MS sample pretreatment in proteomics, *Anal. Chem. 75*, 663-670.
157. Lin-Moshier, Y., Sebastian, P. J., Higgins, L., Sampson, N. D., Hewitt, J. E., and Marchant, J. S. (2013) Re-evaluation of the Role of Calcium Homeostasis Endoplasmic Reticulum Protein (CHERP) in Cellular Calcium Signaling, *J. Biol. Chem. 288*, 355-367.
158. DeGraw, A. J., Keiser, M. J., Ochocki, J. D., Shoichet, B. K., and Distefano, M. D. (2010) Prediction and Evaluation of Protein Farnesyltransferase Inhibition by Commercial Drugs, *J. Med. Chem. 53*, 2464-2471.
159. Saxena, N., Lahiri, S. S., Hambarde, S., and Tripathi, R. P. (2008) RAS: target for cancer therapy, *Cancer Invest. 26*, 948-955.
160. Agrawal, A. G., and Somani, R. R. (2009) Farnesyltransferase inhibitor as anticancer agent, *Mini-Rev. Med. Chem. 9*, 638-652.
161. Brunner, T. B., Hahn, S. M., Gupta, A. K., Muschel, R. J., McKenna, W. G., and Bernhard, E. J. (2003) Farnesyltransferase inhibitors: an overview of the results of preclinical and clinical investigations, *Cancer Res. 63*, 5656-5668.

162. Dangle, P. P., Zaharieva, B., Jia, H., and Pohar, K. S. (2009) Ras-MAPK pathway as a therapeutic target in cancer--emphasis on bladder cancer, *Recent Pat. Anticancer Drug Discov. 4*, 125-136.
163. Konstantinopoulos, P. A., Karamouzis, M. V., and Papavassiliou, A. G. (2007) Post-translational modifications and regulation of the RAS superfamily of GTPases as anticancer targets, *Nat. Rev. Drug Discovery 6*, 541-555.
164. Le, M. S., Loriot, Y., and Soria, J. C. (2009) Targeting the KRAS pathway in NSCLC therapy, *Bull. Cancer 96*, S69-S74.
165. Liu, Z., Meray, R. K., Grammatopoulos, T. N., Fredenburg, R. A., Cookson, M. R., Liu, Y., Logan, T., and Lansbury, P. T., Jr. (2009) Membrane-associated farnesylated UCH-L1 promotes α-synuclein neurotoxicity and is a therapeutic target for Parkinson's disease, *Proc. Natl. Acad. Sci. U. S. A. 106*, 4635-4640.
166. Eckert, G. P., Hooff, G. P., Strandjord, D. M., Igbavboa, U., Volmer, D. A., Mueller, W. E., and Wood, W. G. (2009) Regulation of the brain isoprenoids farnesyl- and geranylgeranylpyrophosphate is altered in male Alzheimer patients, *Neurobiol. Dis. 35*, 251-257.
167. Hooff, G. P., Patel, N., Wood, W. G., Mueller, W. E., Eckert, G. P., and Volmer, D. A. (2010) A rapid and sensitive assay for determining human brain levels of farnesyl-(FPP) and geranylgeranylpyrophosphate (GGPP) and transferase activities using UHPLC-MS/MS, *Anal. Bioanal. Chem. 398*, 1801-1808.
168. Hooff, G. P., Volmer, D. A., Wood, W. G., Mueller, W. E., and Eckert, G. P. (2008) Isoprenoid quantitation in human brain tissue: a validated HPLC-fluorescence detection method for endogenous farnesyl- (FPP) and geranylgeranylpyrophosphate (GGPP), *Anal. Bioanal. Chem. 392*, 673-680.
169. Mans, R. A., McMahon, L. L., and Li, L. (2012) Simvastatin-mediated enhancement of long-term potentiation is driven by farnesyl-pyrophosphate depletion and inhibition of farnesylation, *Neurosci. 202*, 1-9.
170. Cook, M., Mani, P., Wentzell, J. S., and Kretzschmar, D. (2012) Increased RhoA Prenylation in the *loechrig (loe)* Mutant Leads to Progressive Neurodegeneration, *PLoS ONE 7*, e44440.
171. Hooff, G. P., Peters, I., Wood, W. G., Muller, W. E., and Eckert, G. P. (2010) Modulation of cholesterol, farnesylpyrophosphate, and geranylgeranylpyrophosphate in neuroblastoma SH-SY5Y-APP695 cells: impact on amyloid beta-protein production, *Mol. Neurobiol. 41*, 341-350.

172. Cole, S. L., and Vassar, R. (2006) Isoprenoids and Alzheimer's disease: a complex relationship, *Neurobiol. Dis. 22*, 209-222.
173. Pedrini, S., Carter, T. L., Prendergast, G., Petanceska, S., Ehrlich, M. E., and Gandy, S. (2005) Modulation of statin-activated shedding of Alzheimer APP ectodomain by ROCK, *PLoS Med. 2*, e18.
174. Fonseca, A. C., Resende, R., Oliveira, C. R., and Pereira, C. M. (2010) Cholesterol and statins in Alzheimer's disease: current controversies, *Exp. Neurol. 223*, 282-293.
175. Barone, E., Di Domenico, F., and Butterfield, D. A. (2014) Statins more than cholesterol lowering agents in Alzheimer disease: Their pleiotropic functions as potential therapeutic targets, *Biochem. Pharmacol. 88*, 605-616.
176. Cole, S. L., Grudzien, A., Manhart, I. O., Kelly, B. L., Oakley, H., and Vassar, R. (2005) Statins cause intracellular accumulation of amyloid precursor protein, beta-secretase-cleaved fragments, and amyloid beta-peptide via an isoprenoid-dependent mechanism, *J. Biol. Chem. 280*, 18755-18770.
177. Butterfield, D. A., Barone, E., and Mancuso, C. (2011) Cholesterol-independent neuroprotective and neurotoxic activities of statins: perspectives for statin use in Alzheimer disease and other age-related neurodegenerative disorders, *Pharmacol. Res. 64*, 180-186.
178. Barone, E., Cenini, G., Di Domenico, F., Martin, S., Sultana, R., Mancuso, C., Murphy, M. P., Head, E., and Butterfield, D. A. (2011) Long-term high-dose atorvastatin decreases brain oxidative and nitrosative stress in a preclinical model of Alzheimer disease: a novel mechanism of action, *Pharmacol. Res. 63*, 172-180.
179. Hottman, D. A., and Li, L. (2014) Protein prenylation and synaptic plasticity: implications for Alzheimer's disease, *Mol. Neurobiol. 50*, 177-185.
180. Lipinski, M. M., Zheng, B., Lu, T., Yan, Z., Py, B. F., Ng, A., Xavier, R. J., Li, C., Yankner, B. A., Scherzer, C. R., and Yuan, J. (2010) Genome-wide analysis reveals mechanisms modulating autophagy in normal brain aging and in Alzheimer's disease, *Proc. Natl. Acad. Sci. U. S. A. 107*, 14164-14169.
181. Janda, E., Isidoro, C., Carresi, C., and Mollace, V. (2012) Defective autophagy in Parkinson's disease: role of oxidative stress, *Mol. Neurobiol. 46*, 639-661.
182. Pickford, F., Masliah, E., Britschgi, M., Lucin, K., Narasimhan, R., Jaeger, P. A., Small, S., Spencer, B., Rockenstein, E., Levine, B., and Wyss-Coray, T. (2008) The autophagy-related protein beclin 1 shows reduced

expression in early Alzheimer disease and regulates amyloid-β accumulation in mice, *J. Clin. Invest. 118*, 2190-2199.
183. Rubinsztein, D. C., DiFiglia, M., Heintz, N., Nixon, R. A., Qin, Z. H., Ravikumar, B., Stefanis, L., and Tolkovsky, A. (2005) Autophagy and its possible roles in nervous system diseases, damage and repair, *Autophagy 1*, 11-22.
184. Bertozzi, C. R. (2011) A decade of bioorthogonal chemistry, *Acc. Chem. Res. 44*, 651-653.
185. Boyce, M., and Bertozzi, C. R. (2011) Bringing chemistry to life, *Nat. Methods 8*, 638-642.
186. Hang, H. C., and Linder, M. E. (2011) Exploring protein lipidation with chemical biology, *Chem. Rev. 111*, 6341-6358.
187. Hanson, S. R., Hsu, T. L., Weerapana, E., Kishikawa, K., Simon, G. M., Cravatt, B. F., and Wong, C. H. (2007) Tailored glycoproteomics and glycan site mapping using saccharide-selective bioorthogonal probes, *J. Am. Chem. Soc. 129*, 7266-7267.
188. Wu, C. Y., and Wong, C. H. (2011) Chemistry and glycobiology, *Chem. Commun. 47*, 6201-6207.
189. Kostiuk, M. A., Keller, B. O., and Berthiaume, L. G. (2009) Non-radioactive detection of palmitoylated mitochondrial proteins using an azido-palmitate analogue, *Methods Enzymol. 457*, 149-165.
190. Martin, B. R., and Cravatt, B. F. (2009) Large-scale profiling of protein palmitoylation in mammalian cells, *Nat. Methods 6*, 135-138.
191. Yount, J. S., Charron, G., and Hang, H. C. (2012) Bioorthogonal proteomics of 15-hexadecynyloxyacetic acid chemical reporter reveals preferential targeting of fatty acid modified proteins and biosynthetic enzymes, *Bioorgan. Med. Chem. 20*, 650-654.
192. Hannoush, R. N. (2012) Profiling cellular myristoylation and palmitoylation using omega-alkynyl fatty acids, *Methods Mol. Biol. 800*, 85-94.
193. Hannoush, R. N., and Arenas-Ramirez, N. (2009) Imaging the Lipidome: ω-Alkynyl Fatty Acids for Detection and Cellular Visualization of Lipid-Modified Proteins, *ACS Chem. Biol. 4*, 581-587.
194. Berry, A. F. H., Heal, W. P., Tarafder, A. K., Tolmachova, T., Baron, R. A., Seabra, M. C., and Tate, E. W. (2010) Rapid Multilabel Detection of Geranylgeranylated Proteins by Using Bioorthogonal Ligation Chemistry, *ChemBioChem 11*, 771-773.
195. DeGraw, A. J., Palsuledesai, C., Ochocki, J. D., Dozier, J. K., Lenevich, S., Rashidian, M., and Distefano, M. D. (2010) Evaluation of alkyne-modified isoprenoids as chemical reporters of protein prenylation, *Chem. Biol. Drug Des. 76*, 460-471.

196. Chang, P. V., Prescher, J. A., Sletten, E. M., Baskin, J. M., Miller, I. A., Agard, N. J., Lo, A., and Bertozzi, C. R. (2010) Copper-free click chemistry in living animals, *Proc. Natl. Acad. Sci. U. S. A. 107*, 1821-1826, S1821/1821-S1821/1826.
197. Dehnert, K. W., Beahm, B. J., Huynh, T. T., Baskin, J. M., Laughlin, S. T., Wang, W., Wu, P., Amacher, S. L., and Bertozzi, C. R. (2011) Metabolic labeling of fucosylated glycans in developing zebrafish, *ACS Chem. Biol. 6*, 547-552.
198. Sletten, E. M., and Bertozzi, C. R. (2011) From mechanism to mouse: a tale of two bioorthogonal reactions, *Acc. Chem. Res. 44*, 666-676.
199. Andersen, K. A., Aronoff, M. R., McGrath, N. A., and Raines, R. T. (2015) Diazo groups endure metabolism and enable chemoselectivity in cellulo, *J. Am. Chem. Soc. 137*, 2412-2415.
200. Benetka, W., Koranda, M., Maurer-Stroh, S., Pittner, F., and Eisenhaber, F. (2006) Farnesylation or geranylgeranylation? Efficient assays for testing protein prenylation in vitro and in vivo, *BMC Biochem. 7*, 6.
201. Berndt, N., and Sebti, S. M. (2011) Measurement of protein farnesylation and geranylgeranylation in vitro, in cultured cells and in biopsies, and the effects of prenyl transferase inhibitors, *Nat. Protoc. 6*, 1775-1791.
202. Cuervo, A. M., Bergamini, E., Brunk, U. T., Droge, W., Ffrench, M., and Terman, A. (2005) Autophagy and aging: the importance of maintaining "clean" cells, *Autophagy 1*, 131-140.
203. Rawat, D. S., Krzysiak, A. J., and Gibbs, R. A. (2008) Synthesis and biochemical evaluation of 3,7-disubstituted farnesyl diphosphate analogues, *J. Org. Chem. 73*, 1881-1887.
204. Onono, F., Subramanian, T., Sunkara, M., Subramanian, K. L., Spielmann, H. P., and Morris, A. J. (2013) Efficient use of exogenous isoprenols for protein isoprenylation by MDA-MB-231 cells Is regulated independently of the mevalonate pathway, *J. Biol. Chem. 288*, 27444-27455.
205. Ochocki, J. D., Mullen, D. G., Wattenberg, E. V., and Distefano, M. D. (2011) Evaluation of a cell penetrating prenylated peptide lacking an intrinsic fluorophore via in situ click reaction, *Bioorg. Med. Chem. Lett. 21*, 4998-5001.
206. Wright, L. P., and Philips, M. R. (2006) Thematic review series: lipid posttranslational modifications. CAAX modification and membrane targeting of Ras, *J. Lipid Res. 47*, 883-891.
207. Roelofs, A. J., Hulley, P. A., Meijer, A., Ebetino, F. H., Graham, R., Russell, G., and Shipman, C. M. (2006) Selective inhibition of Rab prenylation by a phosphonocarboxylate analogue of risedronate induces

apoptosis, but not S-phase arrest, in human myeloma cells, *Intl. J. Cancer 119*, 1254-1261.
208. Zaro, B. W., Chuh, K. N., and Pratt, M. R. (2014) Chemical Reporter for Visualizing Metabolic Cross-Talk between Carbohydrate Metabolism and Protein Modification, *ACS Chem. Biol. 9*, 1991-1996.
209. Feldkamp, M. M., Lau, N., and Guha, A. (1999) Growth inhibition of astrocytoma cells by farnesyl transferase inhibitors is mediated by a combination of anti-proliferative, pro-apoptotic and anti-angiogenic effects, *Oncogene 18*, 7514-7526.
210. Lerner, E. C., Qian, Y., Hamilton, A. D., and Sebti, S. M. (1995) Disruption of oncogenic K-Ras4B processing and signaling by a potent geranylgeranyltransferase I inhibitor, *J. Biol. Chem. 270*, 26770-26773.
211. Marma, M. S., Xia, Z., Stewart, C., Coxon, F., Dunford, J. E., Baron, R., Kashemirov, B. A., Ebetino, F. H., Triffitt, J. T., Russell, R. G., and McKenna, C. E. (2007) Synthesis and biological evaluation of alpha-halogenated bisphosphonate and phosphonocarboxylate analogues of risedronate, *J. Med. Chem. 50*, 5967-5975.
212. Baron, R. A., Tavare, R., Figueiredo, A. C., Blazewska, K. M., Kashemirov, B. A., McKenna, C. E., Ebetino, F. H., Taylor, A., Rogers, M. J., Coxon, F. P., and Seabra, M. C. (2009) Phosphonocarboxylates inhibit the second geranylgeranyl addition by Rab geranylgeranyl transferase, *J. Biol. Chem. 284*, 6861-6868.
213. Hung, S.-Y., Huang, W.-P., Liou, H.-C., and Fu, W.-M. (2009) Autophagy protects neuron from Aβ-induced cytotoxicity, *Autophagy 5*, 502-510.
214. Parr, C., Carzaniga, R., Gentleman, S. M., Van Leuven, F., Walter, J., and Sastre, M. (2012) Glycogen synthase kinase 3 inhibition promotes lysosomal biogenesis and autophagic degradation of the amyloid-beta precursor protein, *Mol. Cell. Biol. 32*, 4410-4418.
215. Mizushima, N., and Levine, B. (2010) Autophagy in mammalian development and differentiation, *Nat. Cell Biol. 12*, 823-830.
216. Xing, S., Zhang, Y., Li, J., Zhang, J., Li, Y., Dang, C., Li, C., Fan, Y., Yu, J., Pei, Z., and Zeng, J. (2012) Beclin 1 knockdown inhibits autophagic activation and prevents the secondary neurodegenerative damage in the ipsilateral thalamus following focal cerebral infarction, *Autophagy 8*, 63-76.
217. Song, J. (2010) Development of mass spectrometric tools for the cellular characterization of protein prenylation, p 172, Purdue University, Ann Arbor.
218. Placzek, A. T., and Gibbs, R. A. (2011) New synthetic methodology for the construction of 7-substituted farnesyl diphosphate analogs, *Org. Lett. 13*, 3576-3579.

219. Temple, K. J. (2013) Synthesis of novel isoprenoid diphosphate analogs as chemical tools to investigate protein geranylgeranylation, p 350, Purdue University, Ann Arbor.
220. Lane, K. T., and Beese, L. S. (2006) Thematic review series: lipid posttranslational modifications. Structural biology of protein farnesyltransferase and geranylgeranyltransferase type I, *J. Lipid Res. 47*, 681-699.
221. Reigard, S. A., Zahn, T. J., Haworth, K. B., Hicks, K. A., Fierke, C. A., and Gibbs, R. A. (2005) Interplay of isoprenoid and peptide substrate specificity in protein farnesyltransferase, *Biochem. 44*, 11214-11223.
222. Wright, M. H., Clough, B., Rackham, M. D., Rangachari, K., Brannigan, J. A., Grainger, M., Moss, D. K., Bottrill, A. R., Heal, W. P., Broncel, M., Serwa, R. A., Brady, D., Mann, D. J., Leatherbarrow, R. J., Tewari, R., Wilkinson, A. J., Holder, A. A., and Tate, E. W. (2014) Validation of N-myristoyltransferase as an antimalarial drug target using an integrated chemical biology approach, *Nat. Chem. 6*, 112-121.
223. Wang, Y.-C., and Distefano, M. D. (2012) Solid-phase synthesis of C-terminal peptide libraries for studying the specificity of enzymatic protein prenylation, *Chem. Commun. 48*, 8228-8230.
224. Rashidian, M., Dozier, J. K., Lenevich, S., and Distefano, M. D. (2010) Selective labeling of polypeptides using protein farnesyltransferase via rapid oxime ligation, *Chem. Commun. 46*, 8998-9000.
225. Rashidian, M., Song, J. M., Pricer, R. E., and Distefano, M. D. (2012) Chemoenzymatic reversible immobilization and labeling of proteins without prior purification, *J. Am. Chem. Soc. 134*, 8455-8467.
226. Patterson, D. M., Nazarova, L. A., and Prescher, J. A. (2014) Finding the right (bioorthogonal) chemistry, *ACS Chem. Biol. 9*, 592-605.
227. Bhawal, R. P., Sadananda, S. C., Bugarin, A., Laposa, B., and Chowdhury, S. M. (2015) Mass spectrometry cleavable strategy for identification and differentiation of prenylated peptides, *Anal. Chem. 87*, 2178-2186.
228. Kassai, H., Satomi, Y., Fukada, Y., and Takao, T. (2005) Top-down analysis of protein isoprenylation by electrospray ionization hybrid quadrupole time-of-flight tandem mass spectrometry; the mouse Tgamma protein, *Rapid Commun. Mass Spectrom. 19*, 269-274.
229. Hoffman, M. D., and Kast, J. (2006) Mass spectrometric characterization of lipid-modified peptides for the analysis of acylated proteins, *J. Mass Spectrom. 41*, 229-241.
230. Suzuki, T., Ito, M., Ezure, T., Shikata, M., Ando, E., Utsumi, T., Tsunasawa, S., and Nishimura, O. (2007) Protein prenylation in an insect

cell-free protein synthesis system and identification of products by mass spectrometry, *Proteomics 7*, 1942-1950.
231. Wotske, M., Wu, Y., and Wolters, D. A. (2012) Liquid chromatographic analysis and mass spectrometric identification of farnesylated peptides, *Anal. Chem. 84*, 6848-6855.
232. Dong, N.-p., Zhang, L.-x., and Liang, Y.-z. (2011) A comprehensive investigation of proline fragmentation behavior in low-energy collision-induced dissociation peptide mass spectra, *Intl. J. Mass Spectrom. 308*, 89-97.
233. Frank, A. M. (2009) Predicting intensity ranks of peptide fragment ions, *J. Proteome Res. 8*, 2226-2240.
234. Yates III, J. R., Eng, J. K., Clauser, K. R., and Burlingame, A. L. (1996) Search of sequence databases with uninterpreted high-energy collision-induced dissociation spectra of peptides, *J. Am. Soc. Mass Spectrom. 7*, 1089-1098.
235. Gelb, M. H., Brunsveld, L., Hrycyna, C. A., Michaelis, S., Tamanoi, F., Van Voorhis, W. C., and Waldmann, H. (2006) Therapeutic intervention based on protein prenylation and associated modifications, *Nat. Chem. Biol. 2*, 518-528.
236. Biswas, S., Huang, X., Badger, W. R., and Nantz, M. H. (2010) Nucleophilic cationization reagents, *Tetrahedron Lett. 51*, 1727-1729.